BIOCONJUGATION OF ENZYMES AND PROTEINS ON MULTIFUNCTIONAL AND NANOSTRUCTURED SOLID SUPPORTS FOR BIOMOLECULAR INTERACTIONS MONITORING

Jane Politi

Dottorato in Scienze Biotecnologiche – XXVIII ciclo

Indirizzo Biotecnologie Industriale e Molecolare

Università di Napoli Federico II

Dottorato in Scienze Biotecnologiche – XXVIII ciclo

Indirizzo Biotecnologie Industriali e Molecolari

Università di Napoli Federico II

BIOCONJUGATION OF ENZYMES AND PROTEINS ON MULTIFUNCTIONAL AND NANOSTRUCTURED SOLID SUPPORTS FOR BIOMOLECULAR INTERACTIONS MONITORING

Jane Politi

Dottorando: Jane Politi

Relatore: Paola Giardina, Luca De Stefano

Coordinatore: Prof. Giovanni Sannia

...All'amor...

che move il sole e l'altre stelle...

INDICE/INDEX

Riassunto

A. Introduzione

I biosensori destano notevole interesse in diversi campi biotecnologici, grazie alla loro versatilità d'utilizzo come la diagnostica, lo sviluppo di dispositivi biomedicali ed il monitoraggio di inquinanti in acque potabili (Ligler and Rowe, 2004). I biosensori sono costituiti da un trasduttore ottico (o elettrico, meccanico, ecc.), che costituisce l'elemento sensibile, ed una sonda biomolecolare, che dona specificità al dispositivo, perchè capace di legare selettivamente le molecole target. Entrambi gli elementi sono oggetto del presente lavoro di tesi, che studia le proprietà di diversi materiali per poi sviluppare dispositivi biosensoristici.

B. Trasduttori ottici adoperati

I materiali nanostrutturati possiedono proprietà fisiche e chimiche da cui scaturiscono interessanti peculiarità (fotoluminescenza, riflettività, etc.) che li rendono i mattoni fondamentali per lo sviluppo della prossima generazione di strumenti e dispositivi per applicazioni biotecnologiche. In particolare nel presente lavoro di tesi, i seguenti due tipi di materiale nanostrutturato verranno presi in considerazione:

- silicio poroso (PSi),
- nanoparticelle d'oro (AuNPs).

Il Silicio poroso (PSi) è un materiale nanostrutturato di notevole interesse, perchè ideale per l'immobilizzazione di biomolecole, data la sua peculiare caratteristica di matrice a struttura simile ad una spugna con un'area superficiale dell'ordine di centinaia di metri quadrati per centimetri cubici (Sailor, 2012). Il PSi viene fabbricato tramite attacco elettrochimico (Figure 1 A-B) di silicio cristallino drogato in acido fluidrico (HF) (Laurell et al. 1996). Le proprietà ottiche di questo affascinante materiale, proprio in virtù delle cavità che lo caratterizzano, dipendono dal vuoto contenuto e possono essere accuratamente controllate modificando i parametri del processo (tempo di attacco, concentrazione di HF, livello di drogaggio del silicio, e così via), in modo da ottenere diverse strutture fotoniche (Fabry Perot, specchio di Bragg, microcavità ottica, sequenza multistrato aperiodica, etc. visibili in Figura 1 C), con elevata qualità ottica (Letant and Sailor 2000, Moretti et al. 2006).
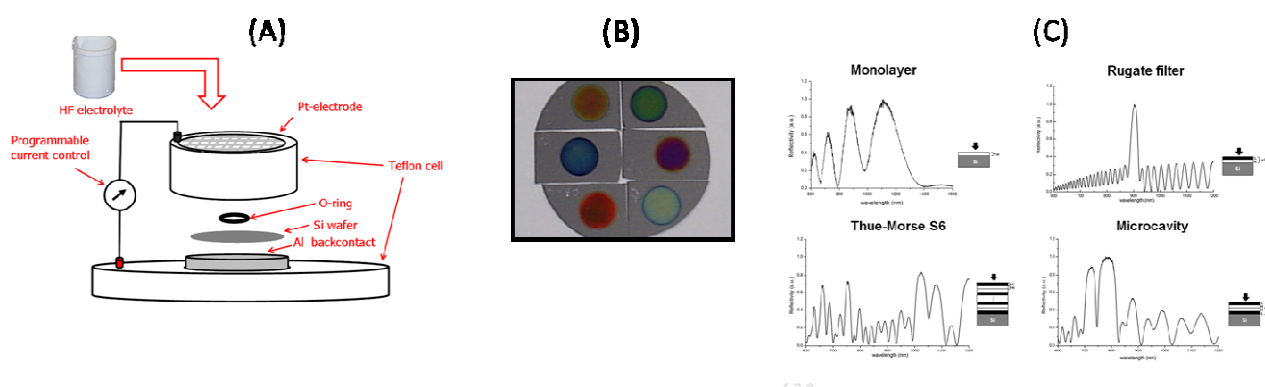

Figure 1. Rappresentazione schematica della cella elettrochimica adoperata per la fabbricazione di chip in PSi (A); immaggine macroscopica dei chip in PSi (B); esempi di strutture ottiche in PSi (C).

L'inconveniente principale di questo materiale è la sua instabilità chimica, infatti il PSi appena fabbricato si degrada rapidamente se esposto all'azione dell'ossigeno

atmosferico provocando una sostituzione dei legami Si-H con quelli Si-O-Si (Ouyang, 2005). Per queste motivazioni, come dimostrato di seguito in questo lavoro, una corretta procedura di passivazione deve essere studiata, ottenuta ad applicata.

Le nanoparticelle d'oro (AuNPs) sono tra i materiali nanostrutturati più utilizzati per applicazioni che vanno dall'ambito medico al monitoraggio ambientale grazie alle loro uniche caratteristiche ottiche. Il metodo più popolare per la preparazione di AuNPs in acqua utilizza citrato per ridurre acido cloroaurico ($HAuCl_4$) in condizioni di ebollizione, ma diversi nuovi approcci sono stati sviluppati per ridurre i sali di Au (III) in acqua in presenza di diversi ligandi stabilizzatori delle particelle colloidali (Li et al. 2011). Gli stabilizzatori sono importanti elementi che proteggono dall'aggregazione delle particelle e ne controllano le proprietà funzionali, ma d'altro canto, va considerata la loro tossicità che ne è il principale svantaggio (Huo et al. 2008). Per questi motivi, queste molecole organiche pericolose potrebbero essere sostituite da molecole amfifiliche come il polietilenglicole (PEG) per preparare soluzioni biocompatibili di AuNPs (Li et al. 2014, Spadavecchia et al. 2014, Doane et al. 2010, Manson et al. 2011). Recentemente, grandi progressi sono stati compiuti nell'uso di nanoparticelle di oro, per applicazioni biomediche, grazie alla loro stabilità, la reattività chimica, la natura non tossica e forte assorbimento e proprietà dispersive (Manson et al. 2011, Tian et al. 2013). Per esempio biomolecule- e / o biopolimeri coniugati con AuNPs sono largamente utilizzati come marcatori o veicoli per il rilascio di farmaci, nonché per prodotti cosmetici, come componenti anti-invecchiamento per la protezione della pelle (Zenhai et al. 2011, Parab et al. 2011). Le nanoparticelle modificate mostrano anche cariche elettrostatiche che consentono forti interazioni con proteine ed enzimi. Tali interazioni giocano un ruolo fondamentale nello sviluppo di dispositivi biosensoristici. Una schematizzazione delle fasi necessarie per lo sviluppo di un dispositivo per applicazioni biotecnologiche basato su nanoparticelle d'oro è rappresentato in Figura 2.
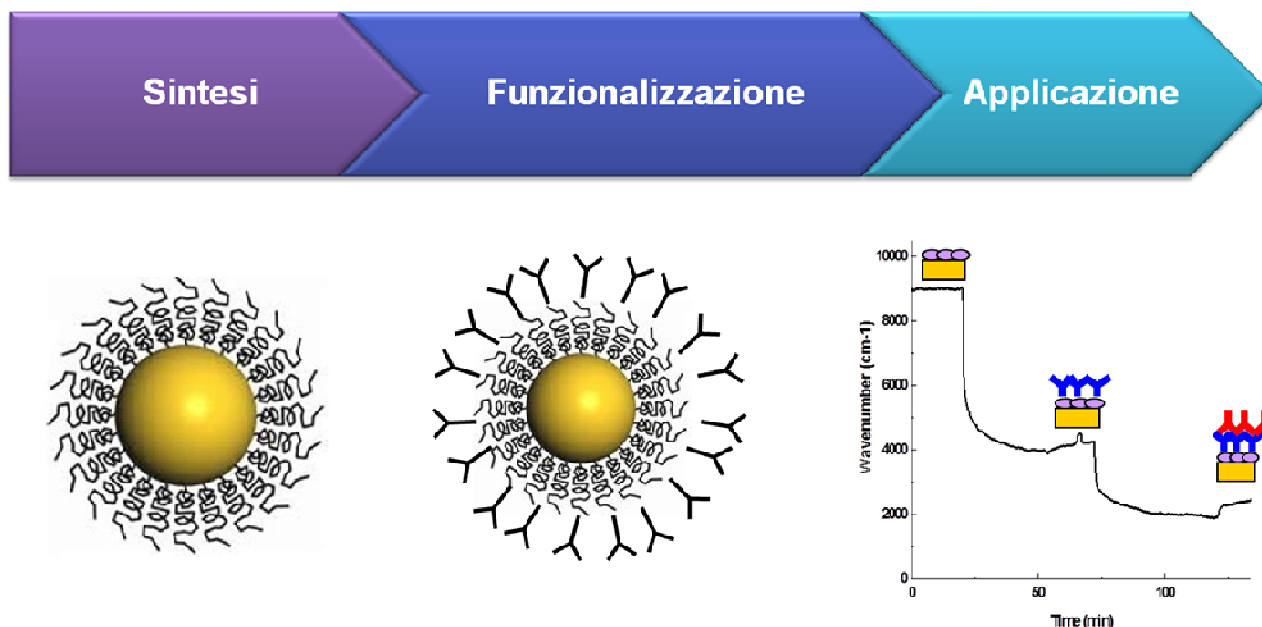
Figure 2. Rappresentazione schematica delle tre fasi necessarie allo sviluppo di un sistema stabile basato su nanoparticelle d'oro per appliaczioni biotecnologiche.

C. Sonde biomolecolari scelte

La bioconiugazione delle sonde molecolari costituisce un ulteriore argomento oggetto di studio di questo progetto di tesi. Diversi sono i metodi di bioconiugazione dei materiali nanostrutturati utili nello sviluppo di nano-biosistemi per applicazioni

sensoristiche. Materiali auto-assemblanti, presenti anche in natura, sono estremamente interessanti come interfacce funzionali tra i trasduttori artificiali e il mondo vivente (De Stefano et al. 2007). Le suddette interfacce non richiedono alcuna procedura chimica, né strumentazione speciale per la loro deposizione. Insieme ai materiali auto-assemblanti, fondamentale è lo studio dell'utilizzo di amminosilani e crosslinker (Zhang et al. 2010).

Obiettivi di questo progetto di dottorato sono:

• Studio delle condizioni di bioconiugazione su materiali nanostrutturati tramite due strategie:

    o immobilizzazione di biosonde tramite approccio covalente (utilizzando amminosilani e reticolanti);

    o immobilizzazione di biosonde tramite approccio non covalente (sfruttando le proprietà di auto-assemblaggio di proteine);

• Sviluppo di biosensori per applicazioni biomediche ed ambientali.

Molti tipi di biomolecole possono essere utilizzate nello sviluppo dei biosensori. Proteine ed anticorpi sono da molto tempo ormai considerate come biomolecole di interesse primario in questa area di applicazione. Le suddette molecole contengono un ricco numero di catene laterali utili per l'immobilizzazione su supporti solidi e siti attivi utili per il monitoraggio delle interazioni molecolari.

Le Fitochelatine sono proteine citoplasmatiche a basso peso molecolare ricche in cisteina appartenenti alla III classe della famiglia delle metallotioneine. Sono oligopeptidi costituiti da (y-glutammil-cisteinil)$_n$-glicina, dove n sta per un numero variabile di ripetizioni del dìpeptide y-glutammil-cisteina; tali ripetizioni, da 2 a 11 (da PC$_2$ a PC$_{11}$) sono più frequentemente da 2 a 5. I gruppi sulfidrilici (o tiolici) -SH della cisteina permettono la chelazione dei metalli pesanti e ne prevengono quindi l'interazione con i componenti cellulari. Le fitochelatine possono infatti formare complessi molecolari con vari metalli pesanti, i quali non possono esercitare effetti tossici perché sottratti alla libera circolazione all'interno del citoplasma cellulare (Sigel et al. 2009). Le fitochelatine si rinvengono nelle piante, nei funghi e in tutti i gruppi di alghe tra cui cianobatteri e licheni. La sintesi delle fitochelatine avviene direttamente a partire dal glutatione oppure da un'altra fitochelatina a più basso grado di polimerizzazione per mezzo dell'enzima Glutatione γ-glutammilcisteiniltransferasi (Cobbett et al. 2000). Tali organismi, a differenza degli animali, traggono nutrienti (per esempio, rame e zinco) e metalli potenzialmente tossici (per es. cadmio, piombo o mercurio) dall'ambiente acquatico o terrestre. Le concentrazioni di questi elementi, sia quelli essenziali che i non essenziali, possono variare per cause naturali o antropiche. È pertanto importante per le piante possedere meccanismi che ne mantengano le concentrazioni entro limiti di sicurezza; la sintesi delle fitochelatine è attivabile nell'arco di pochi minuti e costituisce pertanto un'importante risposta fisiologica per il mantenimento dell'omeostasi cellulare e per la detossificazione. In questo studio sono state utilizzate Fitochelatine di tipo 6 (PC$_6$), con la seguente struttura generale (γ-Glu-Cys)$_6$Gly acquistate dall'azienda AnaSpec S.p.A. per lo studio dell'interazione molecolare con ioni piombo in seguito alla loro coniugazione su AuNPs e su PSi.

Le idrofobine sono piccole proteine (circa 100 residui amminoacidici) ad alta attività superficiale, note da circa 10 anni per le loro peculiari proprietà. Prodotte da funghi filamentosi, sono bio-surfattanti e auto-assemblano in membrane anfifiliche alle interfacce solido-liquido o aria-liquido. Per le loro proprietà, le idrofobine hanno diversi ruoli biologici, ad esempio sono coinvolte nella formazione e nel rivestimento di ife aeree, spore, corpi fruttiferi e nell'adesione delle ife a superfici idrofobiche durante le interazioni simbiotiche o patogene (Wösten et al. 2001). La famiglia delle idrofobine fungine è stata divisa in due classi in base a caratteristiche strutturali e funzionali: le idrofobine di classe I formano un film estremamente robusto costituito da strutture di tipo amiloide chiamate "*rodlet*" che

possono essere depolimerizzate solo in acidi forti (i.e. TFA 100%), mentre i polimeri formati dalle idrofobine di classe II sono non fibrillari e meno stabili, possono essere sciolti in etanolo o soluzioni acquose di sodio dodecil solfato (SDS) (Zampieri et al. 2010). Le principali caratteristiche dei film d'idrofobine rispetto agli altri film proteici sono la loro maggiore resistenza chimica e l'abilità di modificare sensibilmente la bagnabilità della superficie dei materiali (Hou et. al 2009), Infatti, per la loro natura amfifilica, il rivestimento di idrofobine converte superfici idrofobiche in idrofiliche e vice versa. In questo progetto, si dimostrerà che le idrofbine potranno essere adoperate sia come stabilizzanti/passivanti dei materiali nanostrutturati e sia come sonda biomolecolare in grado di interagire quantitativamente con gli analiti target.

Infine, la rivelazione di arsenico data la domanda mondiale diffusa per rilevarne e quantificarne l'inquinamento, sia naturale che di origine antropica, è stata oggetto di ricerca. Per questa rilevante e crescente domanda di dispositivi semplici da usare a basso costo, soprattutto nei paesi in via di sviluppo, enzimi estratti da interessanti forme di batteri sono state oggetto del presente studio. *Thermus thermophilus HB27* è un organismo estremofilo capace di vivere in ambienti geotermici ricchi di arsenico: questo batterio ha sviluppato capacità sia ossidante che riducente nei confronti dell'arsenico, svolgendo così un ruolo importante nella sua speciazione e biodisponibilità (Paez-Espino et al 2001, Girhing et al 2009). Meccanismi di riduzione dell'arsenato (Jackson et al 2003, Macy et al., 2000) possono essere individuati su tre famiglie: la prima famiglia è stata caratterizzata come ArsC glutatione glutaredossina dipendente (ArsC-GSH / GRX) ed è stata identificata nei batteri enterici (per esempio *Escherichia coli*); il secondo è noto come ArsC tioredossina dipendente (ArsC-Trx) ed è stato trovato in batteri Gram-positivi (ad esempio Staphylococcus). L'ultima famiglia, che comprende il gene ars2, è stato amplificato da Saccharomyces cerevisiae (Mukhopadhyay et al. 2002). Attività microbiche giocano un ruolo critico nel ciclo geochimico dell'arsenico, perché possono promuovere o inibire la sua produzione da parte di materiali sedimentari, principalmente da reazioni ossidoreduttive (Reyes et al.2008, Oremland et al., 2005, Bartolucci et al. 2013). La riduzione di arsenico pentavalente, As (V), a arsenico trivalente, As (III), è la principale reazione che causa il rilascio di arsenico dalle superfici minerarie nelle acque sotterranee; infatti, oltre ad essere più tossico, l'arsenito è la forma più comune di arsenico trovato in falde contaminate (Murphy et al. 2009). Entrambi gli stati di ossidazione di As verranno rivelati tramite un saggio a occhio nudo che sfrutta l'enzima derivante da *Thermus thermophilus HB27* ArsC (*TtArsC*).

D. Dispositivi ottici per applicazioni biosensoristiche sviluppati

Le interazioni molecolari monitorate nel presente studio di tesi hanno trovato applicazione in ambito biomedicale ed ambientale.

a. Monitoraggio di oligosaccaridi in soluzioni acquose

Studi di monitoraggio di oligosaccaridi in soluzioni acquose sono stati effettuati tramite l'utilizzo di silicio poroso e nanoparticelle d'oro, con le caratteristiche interfacciali modificate tramite l'utilizzo di idrofobine come biosonde stabilizzanti. In entrambi i casi è stata verificata la presenza di glucosio in fase solida ed in soluzione acquosa. In particolare, nel caso del silicio poroso è stato in primis verificata la capacità delle idrofobine di stabilizzare le superfici di PSi e proteggerlo da soluzioni acide contenenti acido fluoridrico. Inoltre, le suddette superfici, nonostante il riassemblaggio delle idrofobine (indotto per favorire la suddetta passivazione del dispositivo) sono state caratterizzate come ancora capaci di interagire con il D-glucosio. Mentre nel caso delle nanoparticelle d'oro, è stata provata l'abilità delle idrofobine di agire da tensioattivi e da biosonde attive in

soluzione. Le idrofobine infatti sono capaci di stabilizzare le soluzioni colloidali di oro e contemporaneamente restare attive nei confronti delle biomolecole presenti nell'ambiente circostante. La caratterizzazione del nuovo sistema sviluppato ha rivelato un'affinità di legame di 7.3 ± 0.3 mg/mL ed una sensibilità di 0.13 ± 0.06 a.u./mg mL^{-1} per il D-glucosio in soluzione.

b. Monitoraggio dell'interazione molecolare PSA-Anti/PSA

Il presente studio ha sfruttato un procedimento chimico semplice e riproducibile per l'immobilizzazione su superficie d'oro di nanobastoncelli di oro opportunamente funzionalizzati. Lo scopo è stato di ottenere una superficie quasi-ordinata di nanobastoncelli di oro legati covalentemente ad una superficie d'oro che può essere utilizzata, per esempio, per il bioriconoscimento antigene/anticorpo tramite risonanza plasmonica di superficie (SPR). Come esperimento per provare il concetto, abbiamo scelto di quantificare l'antigene prostatico specifico (PSA), che è il marcatore del cancro alla prostata tramite SPR in trasformata di Fourier, rivelando una sensibilità di 37±2 cm^{-1}/mgL^{-1}.

c. Rivelazione a occhio nudo di ioni di arsenico

Un interessante saggio ad occhio nudo per la rivelazione di ioni di arseniato ed arsenito è stato sviluppato tramite l'utilizzo di nanoparticelle d'oro. Grazie alle capacità di aggregazione delle nanoparticelle in seguito all'esposizione a sali di metalli pesanti quali arsenico pentavalente e arsenico trivalente, si distinguono nettamente dalle analisi ad occhio nudo anche basse concentrazioni (85 μM). Infine, lo studio basato sullo spostamento del plasmone superficiale localizzato in presenza di ioni metallici che non sono substrati (Cd^{2+}, Pb^{2+} e Hg^{2+}) dell'enzima ha indicato che il bioriconoscimento è altamente specifico, ma non completamente selettivo.

d. Rivelazione label-free di ioni piombo

Monitoraggio di ioni piombo in soluzioni acquose sono state portate a termine tramite metodiche ottiche e gravimetriche. In particolare, sono state ottenute costanti di affinità di 3.5±0.6 ppb e 10±2 ppb e sensibilità di 0.18±0.03 ppb/nm e 0.07 ± 0.03 ppb/Hz nel caso del PSi e di risuonatori in quarzo, rispettivamente. E' stato verificato inoltre che questo sistema è reversibile, con un massimo di sei cicli di rigenerazione. Il lavoro fornisce un buon punto di partenza per lo sviluppo di un biosensore nanostrutturati reversibili per realizzare un futuro dispositivo Lab-on-Chip (LoC) per il rilevamento in situ di metalli pesanti.

Summary

Biosensors are interesting tools in various biotechnological fields, because of their versatility in fields such as diagnostics, development of biomedical devices and monitoring of pollutants in drinking water (Ligler and Rowe, 2004). Biosensors are constituted by an optical (or electrical, mechanical, etc.) transducer, which constitutes the sensitive element, and a biomolecular probe, which gives specificity to the device, because it is able to selectively bind target molecules. Both elements are the subject of this thesis, that studies the properties of different materials and characterization techniques for biosensing devices development.

Nanostructured materials have physical and chemical properties arising interesting peculiarities (such as photoluminescence, reflectivity, etc.) that make them the fundamental building blocks for the development of the next generation of tools and devices for biotechnological applications. In particular, the following two types of nanostructured material were studied:
- porous silicon (PSi);
- gold nanoparticles (AuNPs).

Further item of the present thesis is the bioconjugation of molecular bioprobes. It is well known that there are several methods of bioconjugation useful in the development of nano-bio-systems for sensor applications. Self-assembling materials, found in nature, are extremely interesting as functional interfaces between the artificial transducers and the living world (De Stefano et al. 2007). These interfaces do not require any chemical procedure, nor special equipment for their deposition. Along with the self-assembling materials, essential is the study of the use of aminosilanes and crosslinker (Zhang et al. 2010). Moreover, it is well known that an optimization study of bioprobes immobilization is a hot topic in biosensors study. Therefore, objectives of this PhD project are:
- ❖ Study of spotting conditions of bioconjugation onto nanostructured materials by two strategies:
  - o immobilization of biomolecules by covalent approach (using aminosilane and crosslinker);
  - o immobilization by non-covalent approach due to self-assembling of proteins;
- ❖ Development of biosensors for biomedical and environmental applications.

Molecular interactions monitored by label-free optical techniques performed onto different nanostructured materials found application in both biomedical and environmental monitoring fields. Interesting devices were finally obtained:

- ✓ glucose interaction monitoring with an affinity constant of about 40mM;
- ✓ PSA-Anti/PSA interaction monitoring witha a sensitivity of 37 ± 2 cm^{-1}/mgL^{-1};
- ✓ reversible device for lead ions detection in aqueous environment were developed, with a LOD of 2ppb (5 times lower then World Health Organization legal limit for drinking water);
- ✓ naked eye assay for arsenic ions speciation (also at 85µM).

ABBREVIATIONS

AuNPs: Gold Nanoparticles

AuNRs: Gold Nanorods

DLS: Dynamic Light Scattering

FT-IR: Fourier Trasform Infrared (Spectroscopy)

FT-SPR: Fourier Trasform Surface Plasmon Resonance

LoC: Lab-On-a-Chip

LSP: Localised Surface Plasmon

LSPR: Localised Surface Plasmon Resonance

PM-IRRAS: Polarization Modulation Infrared Reflection Absorption Spectroscopy

PSi: Porous Silicon

QCM: Quartz Crystal Microbalance

SPR: Surface Plasmon Resonance

SR: Spectroscopic Reflectometry

TtArsC: Thermus Thermophilus Hb27 Encodes Chromosomal Arsenate Reductase

ZnO NWs: Zinc Oxide Nanowires

1. Introduction to Nanostructured Materials: Properties and Biomodifications

The PhD entitled "BIOCONJUGATION OF ENZYMES AND PROTEINS ON MULTIFUNCTIONAL AND NANOSTRUCTURED SOLID SUPPORTS FOR BIOMOLECULAR INTERACTIONS MONITORING" was performed at National Research Council - Institute for Microelectronics and Microsystems, in collaboration with Department of Chemical Sciences, University of Naples under the co-tutoring of Dr. Luca De Stefano and Prof. Paola Giardina.

Nanostructured materials denomination is referred to materials with delicate structures of "small" sizes, in the range between 1 and 100 nm, and with specific properties and functions related to the "size effect" (Niemer 2001, Cui et al. 2003, Whitesides et al. 2003). These materials, thanks to their unique properties, have the capability to be adapted and integrated into biomedical devices. In the last twenty years, medicine, biology, engineering and biotechnology (discipline able to cross all the fields cited) are among the most promising and challenging fields involved in the application of nanostructured materials (Safarik et al. 2009). Rapid advancements of nanostructured materials have been made in a wide variety of biomedical applications, including novel tissue engineered scaffolds and devices, site-specific drug delivery systems, non-viral gene carriers, biosensor and screening systems, and clinical bio-analytical diagnostics and therapeutics (Bauer et al. 2004). Noticeable examples could be done: nanocomposites have been used to stabilize and regenerate bone matrices (Kikuchi et al. 2004, Bradt et al. 1999); biosensing of nanotubes and nanowires has demonstrated unprecedented sensitivity for biomolecule detection (Alivisatos et al. 2004, Penn et al. 2003, Drummond et al. 2003) and nanoscale assemblies/particles have been used to deliver high concentrations of therapeutic drugs and/or biomolecules, possessing high bio-affinity to specific host sites for precise drug administration (Moghimi et al. 2003, Takeuchi et al. 2001, Muller et al. 2001).

In the present section will be discussed the main characteristics of the two nanostructured materials adoperated in this PhD thesis: Porous Silicon and Gold Nanoparticles. Both materials will be biomodified by different approaches here introduced and widely discussed and applied in section 2 and 3.

1.1 Porous silicon for biomolecular interactions monitoring

As a general introduction to porous silicon material and devices for biomolecular interaction monitoring, the proceeding published in 2013 conference "Fotonica" helded in

Milano on "*Porous silicon based photonic structures for optical monitoring of biochemical interactions*" is reported below.

POROUS SILICON BASED PHOTONIC STRUCTURS FOR OPTICAL MONITORING OF BIOCHEMICAL INTERACTIONS

I. Rea, A. Caliò, M. Terracciano, J. Politi. L. De Stefano, I. Rendina

CNR-IMM, Unit of Naples, via P. Castellino 111, 80131, Napoli

Porous silicon based optical biosensors are moving from academic laboratories to market applications, especially in the field of medical diagnosis and prognosis. One of the most important issues is the interface between the photonic transducer and the biomolecules that is used as very specific and selective probe against analytical targets. In this work, we present our achievements in developing optical integrated devices for genomic, proteomic, and medical applications.

1. Introduction

The development of biochips is a major thrust of the rapidly growing biotechnology industry, which encompasses a very diverse range of research efforts including genomics, proteomics, computational biology, and pharmaceuticals, among other activities. Advances in these areas are giving scientists new methods for unraveling the complex biochemical processes occurring inside cells, with the larger goal of understanding and treating human diseases. At the same time, the semiconductor industry has been steadily perfecting the science of microminiaturization. The merging of these two fields in recent years has enabled biotechnologists to begin packing their traditionally bulky sensing tools into smaller and smaller spaces, onto so-called biochips. These chips are essentially miniaturized laboratories that can perform hundreds or thousands of simultaneous biochemical reactions. Biochips enable researchers to quickly screen large numbers of biological analytes for a variety of purposes, from disease diagnosis to detection of bioterrorism agents. In Figure 1, the schematic of a porous silicon based biosensor is presented: the support is fabricated by electrochemical etching of silicon that makes spongy the bulk material; molecular bioprobes are attached on its surface, and, finally, molecular interactions with their biological counterparts are monitored by optical signals.
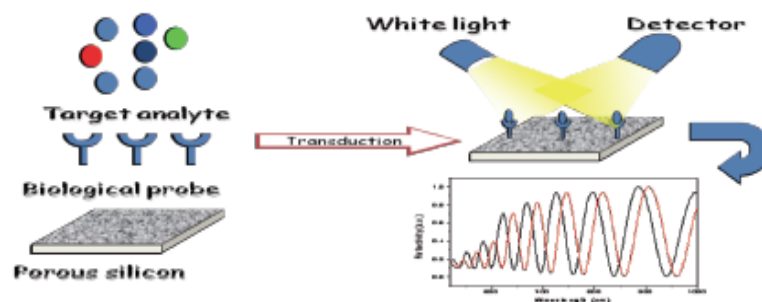
Figure 1 - Schematic of a porous silicon based biosensor.

2. Optical detection

Optical transduction is more and more used since photonic devices could be small, lightweight and thus portable due to the integrability of all optical components. Furthermore, optical devices do not require electric contacts. Fluorescence is by far the most used optical signaling method but a wide-use sensor can not be limited by the labeling of the probe nor the analyte, since this step is not always possible.

Reagentless optical biosensors are monitoring devices, which can detect a target analyte in a heterogeneous solution without the addition of anything than the sample. In the fields of

genomics and proteomics this is a straightforward advantage since it allows real-time readouts and, thus, very high throughoutputs analysis. A label free optical biosensor can be realized by integrating the biological probe with a signaling material, which directly transduces the molecular recognition event into an optical signal.

There are many advantages of optical sensing. Optical sensing schemes are sensitive. By measuring differences in wavelengths or times, optical signals can be readily multiplexed. Some optical techniques, such as fluorescence, have intrinsic amplification in which a single label can lead to a million photons. In addition, some optical techniques are zero or "black" background in which the only source of signal is due to the presence of the species being measured, thereby enabling high sensitivity measurements. Finally, optical signals travel in an open path—no wires or other transmitting conduits are necessary. This feature enables remote measurements to be made.

There are a variety of optical sensing transduction mechanisms including:

- Luminescence
- Fluorescence—intensity, lifetime, polarization
- Phosphorescence
- Fluorescence resonance energy transfer
- Absorbance
- Scattering
- Raman-surface enhanced, resonance
- Surface plasmon resonance
- Interference

3.   Porous silicon based photonic structures

Another rubric for classifying optical sensors revolves around the categories of materials, surfaces, and arrays. In the materials field, there is a burgeoning effort in developing new materials for performing optical sensing. Such materials encompass work in the fields of polymers, ceramics, and semiconductors as well as more conventional inorganic and organic materials. These materials can be used as new recognition agents, as supports for immobilizing sensing materials, as materials for concentrating analytes, and as intrinsic optical sensors with integrated functionality including binding and signal transduction. This latter goal of creating materials that integrate binding with optical signal transduction is a major area of interest and investigation.

The current interest in porous silicon (PSi) results from the demonstration of efficient visible photoluminescence of this material, first reported by Prof. Canham in 1990. However, PSi is not a new material: it was first reported over 40 years ago by Uhlir. During studies of the electropolishing of silicon in aqueous hydrofluoric acid (HF), he observed that the surface often became black, brown or red. More detailed studies were performed by Turner and Archer, but these films were not recognized as being PSi. It was Watanabe et al. who first reported their porous nature. Porous silicon, then, has been investigated for applications in microelectronics, optoelectronics, chemical and biological sensors, and biomedical devices.

The in vivo use of porous silicon was first promoted by Leigh Canham, who demonstrated its resorbability and biocompatibility in the mid 1990s. Subsequently, PSi or porous SiO2 (prepared from PSi by oxidation) host matrices have been employed to demonstrate in vitro release of the steroid dexamethasone, ibuprofen and many other drugs. The first report of drug delivery from PSi across a cellular barrier was performed with insulin, delivered across monolayers of Caco-2 cells. An excellent review of the potential for use of PSi in various drug delivery applications has recently appeared.

The basic method to fabricate PSi is electrochemical dissolution of single crystalline silicon wafer in a hydrofluoridic acid electrolyte solution. This is obtained by monitoring either the anodic current (galvanostatic) or voltage (potentiostatic). Today, the electrochemical etching is a standard method to fabricate nanostructured porous silicon: a proper choice of the applied current density, the electrolyte composition, and the silicon doping allow precise control over the morphology and, consequently, on the physical and chemical properties of

the porous silicon structure. Computer controlled electrochemical etching processes are exploited for the realization of porous silicon films of controlled thickness and porosity (defined as the percentage of void in the silicon volume).

Nanoporous, mesoporous and macroporous structures can be achieved, with pore size ranging from few nanometers up to microns. Moreover, since the etching process is self-stopping, it is possible to fabricate with a single run process multilayer stacks made of single layers of different porosity. The dielectric properties of each PSi layer, and in particular its refractive index n, can be namely modulated between those of crystalline silicon (n = 3.54, porosity = 0) and air (n= 1, porosity = 100 %); so that alternating high and low porosity layers, lot of photonic structures, such as Fabry-Perot interferometers, omni-directional Bragg reflectors, optical filters based on microcavities, and even complicated quasi-periodic sequences (Thue-Morse) can be simply realized, as it is shown in Figure 2.
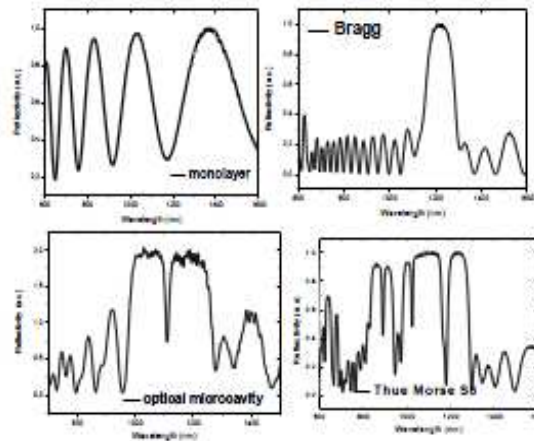

Figure 2. Experimental reflectivity spectra of different PSi optical structures.

4.   Surface functionalization

a PSi sensor cannot discriminate the components of a complex mixture because the sensing mechanism is not selective. Some researchers have chemically or physically modified the Si–H surface sites in order to enhance the sensor selectivity through specific interactions. The common approach is to create a covalent bond between the PSi surface and the biomolecules which specifically recognize the target analytes. The reliability of a biosensor strongly depends on the functionalization process: how fast, simple, homogenous and repeatable it is. This step is also very important for the stability of the sensor: it is well known that 'as-etched' PSi has a Si–H terminated surface due to the Si dissolution process which is very reactive. The substitution of the Si–H bonds with Si–C ones guarantees a much more stable surface from the thermodynamic point of view. Three different PSi surface modification strategies in order to realize an optical biosensor are here reported: the target is the fabrication of sensitive label-free biosensors, which are highly requested for applications in high throughput drug monitoring and disease diagnostics; unlabelled analytes require in fact easier and faster analytical procedures.

FT-IR spectroscopy (Thermo - Nicholet NEXUS) has been used to compare the different passivation procedures: a pure chemical process based on Grignard Reactives; a photoinduced chemical modification based on the undecenoic organic acid and a passivation method simultaneous to the etching process. In each case the carboxyl-terminated monolayer covering the PSi surface acts as a substrate for the chemistry of the subsequent attachment of the DNA sequences.

Before the functionalization process the PSi substrate has been immersed in an aqueous ethanol solution, containing millimolar concentration of KOH, for 15 min. This alkaline treatment produces an increase in the porosity of about 15-20% so improving the infiltration of the biomolecular probes into the pores. The process removes also most of the Si-H bonds from the PSi surface that can be restored by rinsing the PSi device in a low concentration HF-based solution (5 mM) for 30 s. Results of the second passivation method are shown in Figure 3 as example.
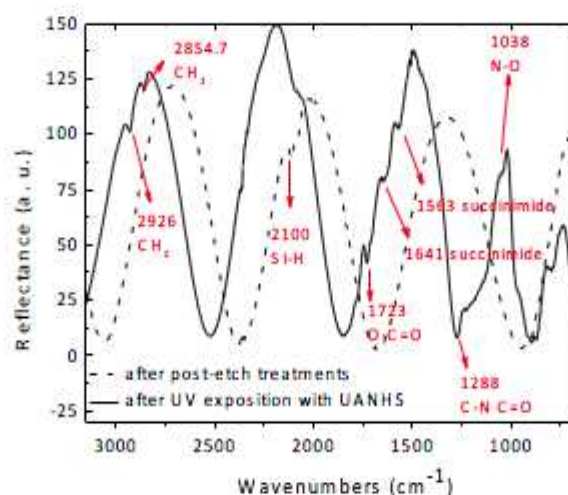

Figure 3. FT-IR spectra of the porous silicon monolayer before and after the photoinduced functionalization process based on UV exposure.

5. Conclusion

This paper represents our main achievements in developing optical integrated devices for genomic, proteomic, and medical applications: starting from crystalline silicon, the most used material in consumer electronic, we fabricate photonic structures that are properly functionalized and bioconjugated with different molecular bioprobes which selectively recognize target analytes of interest in the biomedical field.

Acknowledgements

Authors would like to thank AEIT and SIOF for the patronage of Fotonica 2013.

Bibliography

[1] L. De Stefano, L. Rotiroti, I. Rea, I. Rendina, P. Arcari, A. Lamberti, C. Sanges, "DNA optical detection based on porous silicon technology: from biosensors to biochips" Sensors 2007, 7, 214-221.

[2] L. De Stefano, L. Rotiroti, I. Rendina, A.M. Rossi, M. Rossi, S. D'Auria, "Biochips at work: porous silicon microbiosensor for proteomic diagnostic", J. Phys.: Condens. Matter 19 (2007) 395007.

[3] L. De Stefano, S. D'Auria, "Confocal imaging of proteins distribution in porous silicon optical structures", J. Phys.: Condens. Matter 19 (2007) 395009.

[4] Moretti, L. De Stefano, I. Rea, I. Rendina, "Periodic versus aperiodic: enhancing the sensitivity of porous silicon based optical sensor", Appl. Phys. Lett. 90, 191112 (3 pages) 2007, (selected paper for the May 15, 2007 issue of Virtual Journal of Biological Physics Research).

1.1.1 Characterization and optimization of bioprobes bioconjugation by covalent approach

Crucial point in porous silicon based device development is the bioprobe immobilization that should be a process that both avoids the affection of bioprobe functionality and passivate the surface.

The immobilization procedures studied in the present PhD thesis to passivate the surfaces used two principal strategies:

- covalent approach;
- non-covalent approach.

The first approach take advantage by using several intermediate molecule (silanes and cross-linker molecules) in order to passivate the surfaces and to allow the bioprobe rearrangement onto passivated surfaces thanks to appropriated spacer arms adoperated. Immobilization procedures of bioprobes onto transducer are performed by a chemical derivatization of the material. In literature very used procedures involves aminosilane and crosslinker molecules in order to passivate the surfaces. The bioprobes, in these approaches, can be attached by primary amines given by amino-terminal silane. If primary amines are used as the biomolecule's reactive group, homobifunctional cross-linker are then employed. In past, the most common methods for immobilizing biomolecules onto amino silane surfaces employs glutaraldehyde, but several studies (Walt and Agayan 1994) have demonstrated that the commercial aqueous solutions of glutharaledehyde are a mixture of mono and multimer structures. These different structures all react with proteins in different ways which may affect the degree and type of immobilizzation. Moreover, glutaraldheyde molecules exhibits a strong fluorescence with an emission in green part of visible light. This emission could hide an eventual fluorescence emission due to biomolecules immobilization or biomelecular recognition mechanism.

Since the use of amino-terminal silane and crosslinker molecules is very important and useful in bioprobes immobilization, the first part of this PhD thesis section was focused on optimization of parameters (time of interaction, temperature of reaction, molecules concentration, etc.) used during immobilization procedure. The preliminary study was effectuated on cristalline silicon matrices (chemically reactive as PSi) using a generic bioprobe as Protein A. The entire functionalization study and characterization is reported in the following section.

Optical characterization of aminosilane-modified silicon dioxide surface for biosensing

M. Terracciano
Institute for Microelectronics and Microsystems, National Council of Research, Via P. Castellino 111, I-80131 Naples, Italy
Dept. of Pharmacy, University of Naples Federico II, Naples, Italy

I. Rea
ilaria.rea@na.imm.cnr.it
Institute for Microelectronics and Microsystems, National Council of Research, Via P. Castellino 111, I-80131 Naples, Italy

J. Politi
Institute for Microelectronics and Microsystems, National Council of Research, Via P. Castellino 111, I-80131 Naples, Italy
Dept. of Chemical Sciences - "Federico II" University of Naples, Naples Italy

L. De Stefano
Institute for Microelectronics and Microsystems, National Council of Research, Via P. Castellino 111, I-80131 Naples, Italy

Silicon dioxide surfaces, functionalized by two aminosilane compounds (3-amino-propyl-triethoxysilane, APTES; 3-amino-propyl-dimethyl-ethoxysilane, APDMES) both dissolved in different solvents (dry ethanol and toluene), have been investigated by standard techniques such as spectroscopic ellipsometry (SE), water contact angle (WCA), and atomic force microscopy (AFM). Silane thicknesses between 5 and 80 Å have been found, depending on deposition conditions; surface wettabilities change, accordingly. These organic-inorganic interfaces have also been modified by a cross-linker (bis-sulfosuccinimidyl suberate) in order to covalently bind a fluorescein labeled protein A. The amount of protein linked to functional surfaces has been quantified by SE and fluorescence microscopy. These results could be very useful in developing new platforms for optical biosensing.
[DOI: http://dx.doi.org/10.2971/jeos.2013.13075]

Keywords: Surface functionalization, biomaterials, ellipsometry, water contact angle, atomic force microscopy

1 INTRODUCTION

Bioconjugation chemistry is a key issue not only for fabrication of sensitive and selective biosensors, but also for many technological devices, which can be used in biomedical diagnostics and even in fundamental scientific studies. In the last few years, multifunctional lab-on-chip platforms for biomolecular interactions monitoring have been proposed [1]–[3], as well as new single molecule spectroscopy methodologies [4, 5], all based on specific passivation protocols of support surfaces. The aim of these treatments is immobilization on a solid support of biological molecules, preserving their specific functionalities through a good control of their orientation and organization. Even if glass [6] and gold [7] have been classically used, and therefore their passivation chemistries deeply studied in these kinds of application, on the other hand, silicon, and silicon related materials, are attracting growing interest, due to widespread diffusion of microfabrication technologies, well developed in the frame of consumer electronics. The most common route of silicon surfaces functionalization is to attach alkylsilanes layers through the formation of Si-O-Si bonds between the silanol groups present on oxidized silicon surface and the hydrolyzed organosilane molecules [8]. Recently, the interaction mechanism between silane layers and silicon surfaces have been deeply characterized, up to molecular level [9]–[11]. Although wet deposition by solution immersion is the most common method to prepare these samples, mono-functional and tri-functional aminosilane molecules, like 3-amino-propyl-triethoxysilane, APTES, and 3-amino-propyl-dimethyl-ethoxysilane, APDMES, respectively have been deposited on dehydrated silicon support also by chemical vapour deposition, which is a robust process, currently used in semiconductors industry [12]. APTES and APDMES have structural differences, as schematized in Figure 1. APTES has three attachment points to the surface or other silane molecules, therefore it can polymerize. Conversely, APDMES has only one attachment point and it cannot polymerize. In this work, we have experimentally characterized amino-
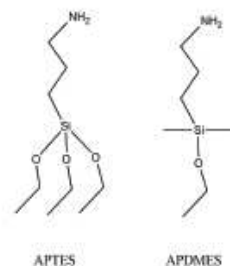

FIG. 1 Structures of 3-aminopropyltriethoxysilane (APTES) and 3-aminopropyl-dimethylethoxysilane (APDMES).
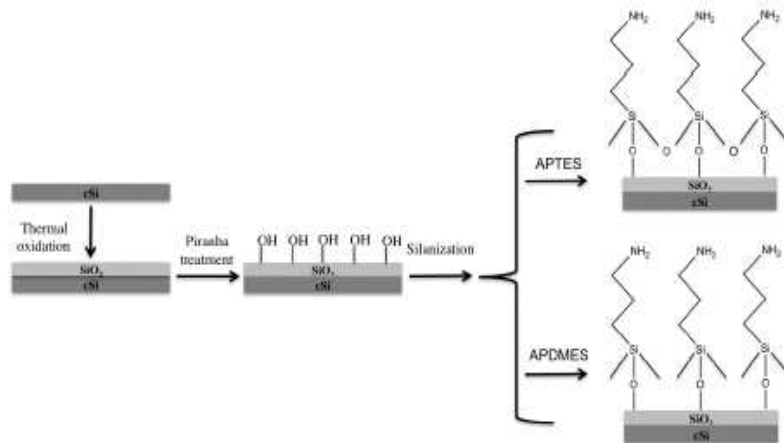
FIG. 2 Scheme of silicon surface modification by APTES and APDMES.

Sample	Silane	Solvent	Incubation time (min)
S1	Aptes 5%	Ethanol	30
S2	Aptes 5%	Ethanol	60
S3	Aptes 5%	Toluene	30
S4	Aptes 5%	Toluene	60
S5	Apdmes 5%	Ethanol	30
S6	Apdmes 5%	Ethanol	60
S7	Apdmes 5%	Toluene	30
S8	Apdmes 5%	Toluene	60

TABLE 1 Sample preparation conditions.

modified silicon dioxide surfaces by several techniques, such as spectroscopic ellipsometry (SE), water contact angle (WCA), and atomic force microscopy (AFM). Data highlight some important features of these surface passivation strategies useful in realization of immune-arrays or, in general, bioconjugated devices.

2 MATERIAL AND METHODS

2.1 Silane surface modifications

Highly doped p$^+$ silicon wafer, <100> oriented, 0.003 Ω-cm resistivity, 400 μm thick, was cut into 10 mm × 10 mm square pieces. After cleaning by means of standard RCA process [13], silicon substrates were thermally oxidized at 1050°C for 5 hours. Chips were, then, immersed in piranha solution (H$_2$SO$_4$:H$_2$O$_2$=4:1) at room temperature for 30 min so as to create Si-OH groups on silicon surface, extensively washed in milli Q water, and dried in a stream of nitrogen gas. Eight different silane films, namely S1-S8, were obtained by incubating the silicon substrates at room temperature, for 30 or 60 min, into 5% silane solutions prepared by direct dissolution of silane, APTES or APDMES, in ethanol or anhydrous toluene, as summarized in Table 1. After silanization, silicon chips were rinsed three times in the solvent used for the process for 2 min so as to remove silane excess. The last step is

silane curing on heater at 100°C for 10 min. The scheme of silanization process performed on silicon surface is reported in Figure 2. The experiment has been performed on two sets of identical samples to confirm results.

2.2 Biofunctionalization

Chemicals and solvents were purchased from Sigma-Aldrich. Protein A labeled with -FITC (PrA*) was immobilized on silane modified silicon surface using bis(sulfosuccinimidyl)suberate (BS^3) crosslinker. The scheme of functionalization process is reported in Figure 3. Each chip was incubated with 150 μl of 1.6 mM BS^3 in PBS solution (0.1 M; pH=7.4) at 4°C for 5 hours. N-hydroxysulfosuccinimide (NHS) ester reacts (through SN$_2$) with primary amines of silanized surface forming stable amine bonds and releasing a NHS group. The functionalized substrate was then incubated overnight (ON) at 4°C with 150 μl of 2 mg/ml PrA* in PBS (0.1 M; pH=7.4) buffer. NHS ester reacts with primary amines in the side chain of lysine residues of PrA* forming stable amine bonds and releasing an other one NHS group.

2.3 Spectroscopic ellipsometry

Spectroscopic ellipsometry (SE) measurements were performed by a Jobin Yvon UVISEL-NIR phase modulated spectroscopic ellipsometer apparatus, at an angle of incidence of 65° over the range 300–1600 nm with a resolution of 5 nm. The instrument measures the spectral variation of the ellipsometric angles Ψ and Δ defined through the relation:

$$tg\Psi e^{i\Delta} = \frac{R_p}{R_s} \qquad (1)$$

where R_p and R_s are the complex reflection coefficients of the light polarized parallel and perpendicular to plane of incidence. Thickness of films present on silicon surface was determined from the ellipsometric data analysis using Delta Psi software [14].
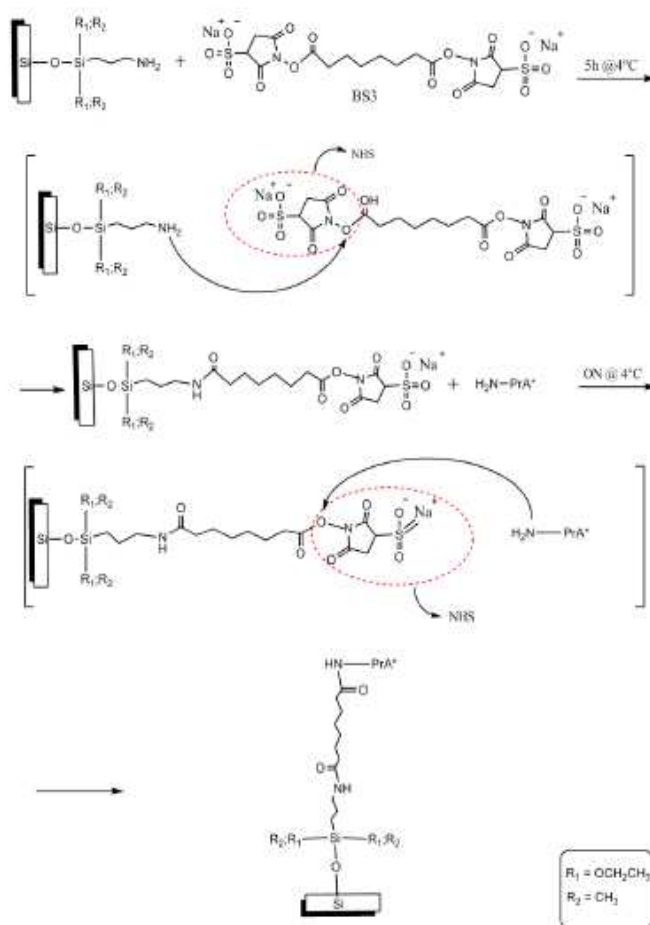
FIG. 3 Functionalization of silane modified cSi surface with PrA*.

2.4 Water contact angle measurements

Sessile drop technique has been used for water contact angle (WCA) measurements on a First Ten Angstroms FTA 1000 C Class coupled with drop shape analysis software. The WCA values reported in this work are the average of at least three measurements.

2.5 Atomic Force Microscopy

A XE-100 AFM (Park Systems) was used for the imaging of biofilms. Surface imaging was obtained in non-contact mode using Silicon/aluminum coated cantilevers (PPP-NCHR 10M; Park Systems) 125 µm long with a resonance frequency of 200 to 400 kHz and nominal force constant of 42 N/m. The scan frequency was typically 1 Hz per line. Roughness has been calculated on 3 µm × 3 µm images.

2.6 Fluorescence microscopy

Fluorescence analysis was performed by means of a Leica Z16 APO fluorescence macroscope equipped with a camera Leica

DFC300. I3 filter was used for image acquisition consists in a 450–490 nm band-pass excitation filter, a 510 nm dichromatic mirror, and a 515 nm suppression filter. Fluorescence intensity values reported in the work are averaged on three measurements.

3 RESULTS AND DISCUSSION

A precise estimation of silane layers thickness requires the ellipsometric analysis of samples before and after silanization processes. The measure performed on bare silicon dioxide (before silanization) allows an exact determination of its thickness (95.46 ± 0.03 nm) and a consequence certain estimation of silane layer. Refractive index of silicon dioxide as function of wavelength is taken from reference [15].

Spectroscopic ellipsometry data, reported in Table 2 together with water contact angle variations (i.e., the difference between the WCA of sample after and before silanization process. WCA of bare silicon dioxide surface is $(60.8 \pm 0.8)°$, reveal a common trend for all characterized samples: the esti-
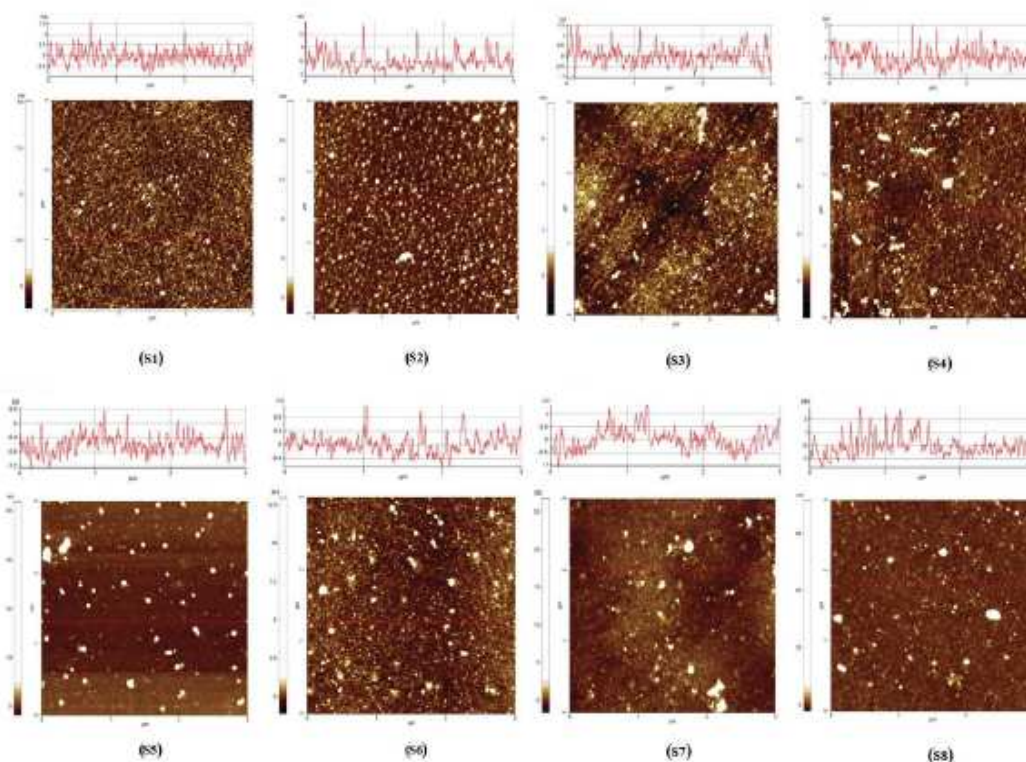
25

FIG. 5 3 μm wide AFM images of aminosilane modified cSi surfaces after PrA* functionalization.
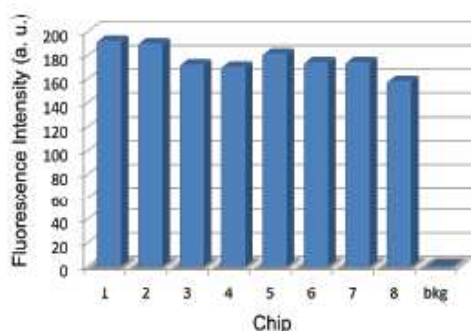

FIG. 4 Fluorescence intensity measured on the chips functionalized with PrA* and on background (silane modified cSi surface + BS³).

Sample	Fluorescence intensity (a. u.)
S1	192±2
S2	190±6
S3	172±1
S4	170±5
S5	181±2
S6	174±2
S7	174±2
S8	158±3

TABLE 6 Fluorescence intensity measured on the chips functionalized with PrA*. The values have been obtained as average of three different measurements on the same sample.

that less cross-linker is better than too much. This conclusion is also supported by fluorescence data (Figure 4), summarized in details in Table 6. Fluorescence intensity is an integrated density calculated on an area of 100×100 μm² using a freeware software, ImageJ. Each value reported in Table 6 is the average of three independent measurements on same sample. Fluorescence intensity of bare silicon dioxide is (7±2) a. u.

The fluorescence intensity of odd samples (which has been incubated for 30 min) is always greater than that of even ones (incubated 60 min), independently of considered silane. Anyway, absolute values of fluorescent intensities are very close each other, so that all samples have been effectively functionalized.

Quite differently, AFM images and characterization highlight some distinctions between PrA* surfaces on APTES and APDMES modified supports (see Figure 5). Quantitative measurements are expressed in terms of roughness, which values are reported for all samples in Table 7. Roughness of thermally grown silicon dioxide is 0.250 nm.

M. Terracciano, et al.

Sample	Roughness (nm)
S1	0.353
S2	0.605
S3	0.416
S4	0.550
S5	0.264
S6	0.294
S7	0.353
S8	0.776

TABLE 7 Root mean square roughness values of sample surfaces after PtA* functionalization measured using an AFM (3 × 3 µm²)

By examining both series (S1-S4; S5-S8) of number, it is evident that APDMES samples are smoother than APTES ones, except for sample S8 that is quite always very different from S5-S7. Moreover, in case of APTES samples, the thinner is the protein layer, the greater is the roughness, probably because of vertical inhomogeneity of APTES layer and PrA* film are very similar. APTES treated surfaces seem more crowded than APDMES ones, and again we believe that this is also due to self-assembling nature of APTES with respect to APDMES.

4 CONCLUSIONS

We have successfully functionalized silane modified flat oxidized silicon surfaces by ordinary chemical procedure, and we have studied how different solvents and incubation times can affect the quality of the protein layer on top. Quantitative measurements based on SE, WCA and AFM reveal that smoother and homogeneous film can be obtained using APDMES in toluene incubated for 30 min. Anyway, all other samples show good functionalization degree as it can be seen by fluorescence characterization.

5 ACKNOWLEDGEMENTS

References

[1] F. F. Bier, and S. Schumacher, "Integration in Bioanalysis: Technologies for Point-of-Care Testing," Adv. Biochem. Eng. Biotechnol. 133, 1–14 (2013).

[2] A. L. Washburn, and R. C. Bailey, "Photonics-on-a-chip: recent advances in integrated waveguides as enabling detection elements for real-world, lab-on-a-chip biosensing applications," Analyst 136, 227–236 (2011).

[3] S. Schumacher, J. Nestler, T. Otto, M. Wegener, E. Ehrentreich-Förster, D. Michel, K. Wunderlich, et al., "Highly-integrated lab-on-chip system for point-of-care multiparameter analysis," Lab. Chip. 12, 464–473 (2012).

[4] S.J. Attwood, A. M. C. Simpson, R. Stone, S. W. Hamaia, D. Roy, R. W. Farndale, M. Ouberai, and M. E. Welland, "A Simple Bioconjugate Attachment Protocol for Use in Single Molecule Force Spectroscopy Experiments Based on Mixed Self-Assembled Monolayers," Int. J. Mol. Sci. 13, 13521–13541 (2012).

[5] V. K. Yadavalli, J. G. Forbes, and K. Wang, "Functionalized self-assembled monolayers on ultraflat gold as platforms for single molecule force spectroscopy and imaging," Langmuir 22, 6969–6976 (2006).

[6] Z. Yang, Y. Chevolot, T. Géhin, V. Dugas, N. Xanthopoulos, V. Laporte, T. Delair, et al., "Characterization of three amino-functionalized surfaces and evaluation of antibody immobilization for the multiples detection of tumor markers involved in colorectal cancer," Langmuir 29, 1498–1509 (2013).

[7] R. K. DeLong, C. M. Reynolds, Y. Malcolm, A. Schaeffer, T. Severs, and A. Wanekays, "Functionalized gold nanoparticles for the binding, stabilization, and delivery of therapeutic DNA, RNA, and other biological macromolecules," Nanotechnol. Sci. Appl. 3, 53–63 (2013).

[8] J. J. Gooding, and S. Ciampi, "The molecular level modification of surfaces: From self-assembled monolayers to complex molecular assemblies," Chem. Soc. Rev. 40, 2704–2718 (2011).

[9] M. Zhu, M. Z. Lerum, and W. Chen, "How to prepare reproducible, homogeneous, and hydrolytically stable aminosilane-derived layers on silica," Langmuir 28, 416–423 (2013).

[10] N. Aissaoui, L. Bergaoui, J. Landoulsi, J. F. Lambert, and S. Boujday, "Silane layers on silicon surface: mechanism of interaction, stability, and influence on protein adsorption," Langmuir 28, 656–665 (2012).

[11] L. De Stefano, G. Oliviero, J. Amato, N. Borbone, G. Piccialli, L. Mayol, I. Rendina, et al. "Aminosilane functionalizations of mesoporous oxidized silicon for oligonucleotides synthesis and detection," J. R. Soc. Interface 10, 20130160 (2013).

[12] F. Zhang, K. Sautter, A. M. Larsen, D. A. Findley, R. C. Davis, H. Samha, and M. R. Lindford, "Chemical Vapor Deposition of three aminosilanes on silicon dioxide: surface characterization, stability, effects of silane concentration, and cyanine dye adsorption," Langmuir 26, 14648–14654 (2010).

[13] W. Kern, Handbook of semiconductor wafer cleaning technology: science, technology, and applications (William Andrew Publishing/Noyes, Norwich, 1993).

[14] Horiba Jobin Yvon DELTA PSI Software manual, ver. 2.4.3 158. (Horiba Scientific, 2011).

[15] E. D. Palik (ed.), Handbook of optical constants of solids (Academic Press, San Diego, 1985).

[16] P. Brocos, A. Piñeiro, R. Bravo, and A. Amigo, "Refractive indices, molar volumes and molar refractions of binary liquid mixtures: concepts and correlations," Phys. Chem. Chem. Phys. 5, 550–557 (2003).

[17] P. A. Cuypers, J. W. Corsel, M. P. Janssen, J. M. Kop, W. T. Hermens, and H. C. Hemker, "The adsorption of prothrombin to phosphatidylserine multilayers quantitated by ellipsometry," J. Biol. Chem. 258, 2426–2431 (1983).

[18] P. Déjardin (ed.), Proteins at solid-liquid interfaces (Springer-Verlag, Berlin, 2006).

[19] U. Jönsson, M. Malmqvist, I. Rönnberg, "Absorption of immunoglobulin G, protein A, and fibronectin in the submonolayer region evaluated by a combined Study of ellipsometry and radiotracer techniques," J. Colloid Interface Sci. 103, 360–372 (1985).

1.2 Gold nanoparticles properties and characterizations

One of the most commonly used metal-based nanoparticles in biosensing, nanomedicine, etc. are the gold nanoparticles (AuNPs). These are available in the range from 1 to more than 120 nm and they disclose considerable applications in optics, catalysis, materials science and nanotechnology also including biology and nanomedicine (Bosselier and Astruc 2009).

While there is a large number of ways to synthesize AuNPs, the most common is to start from $HAuCl_4$ (Figure 1.1). The first reported synthesis was performed by Michael Faraday in 1857, where he described the formation of deep red solutions of colloidal gold (the so called "activated gold") by reduction of an aqueous solution of chloroaurate ($AuCl_4^-$) using phosphorus in CS2 (a two-phase system) (Daniel and Astruc 2004). Through the years many other methods were investigated in order to obtain colloidal gold suspensions: one of the most important was the Turkevich method, introduced in 1951, where the reduction of Au^{3+} to Au^0, obtained with a small amount of sodium citrate, evolved in a single water phase (Turkevich et al. 1951). In this synthesis, the growth of the NPs is controlled by varying the citrate/gold ratios: the citrate ions form a double layer around the particles, stabilizing them electrostatically. Generally, smaller amount of citrate yields larger nanospheres.
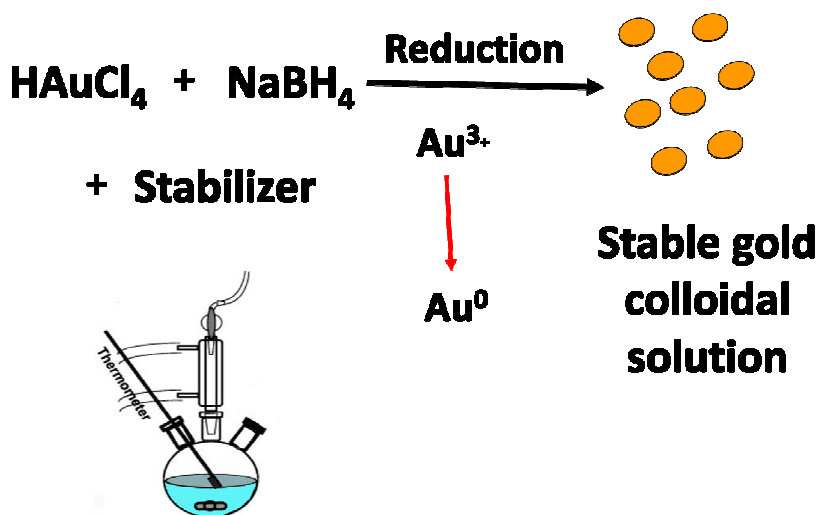

Figure 1.1. Schematization of gold nanoparticles synthesis starting from $HAuCl_4$ solution.

Even if it is possible to produce nearly monodisperse gold nanospheres, the major limitations of this method are the low yield and the restriction of using water as solvent. As already mentioned, every nanostructure used for medical purposes needs to be water-soluble and biocompatible, and AuNPs are not an exception. They are turned to water-soluble NPs typically by using water soluble thiol ligands, which can be divided into three groups:

❖ thiols terminated with a polyethylene glycol (PEG) moiety that are employed to form "inert surfaces" which resist to nonspecific adsorption of biomolecules;

❖ simple alkyl-thiols with a polar end group such as a carboxylate or an ammonium ion;

❖ biomolecules such as peptides, glycosides, DNA sequences, containing a thiol group or linked to a short alkyl thiol.

In particular, the last two categories may display some possibilities of functional groups at the interface and can be exploited to create medical diagnostic and therapeutic nanostructures (Gentilini et al. 2008, Pengo et al. 2003, Simard et al. 2000). Another way to functionalize gold NPs surface with specific organic molecules is through ligand-exchange reactions. Ligand-exchange reactions are mainly used for two reasons: to achieve more monodisperse, homogeneously coated NPs and to obtain multi-functionalized gold NPs, in such a way the final NPs are characterized by various properties deriving from a mixed ligand shell (Daglar and Aydogan 2013).

Between all the advantages, offered by differently functionalized AuNPs, the most interesting property derives from the Au core. In fact, the great interest to AuNPs is due to the electronic properties of Au. According to the Mie theory, an electromagnetic frequency induces a resonant coherent oscillation of the free electrons on the surface of a spherical nanoparticles, called surface plasmon resonance (SPR), only if the particle size is much smaller than the light wavelength (Ghosh and Pal 2007) (Figure 1.2). For metal nanoparticles, the localized SPR (LSPR) results in an enhanced electromagnetic field at the metal nanoparticle surface (Link and El-Sayed 2009). For AuNPs the plasmon resonance is observed down to 3 nm diameters, below which the NP can no longer be considered as a "normal metal" with a conduction band (Bosselier and Astruc 2009). As a result, an enhanced electromagnetic field appears at the AuNP surface above this size allowing surface-enhanced optical properties revealed using spectroscopic techniques. Thus, the signal intensity of the SPR bands is several orders of magnitude larger than those of all the organic dyes. Therefore, from a biomedical point of view, plasmon absorbance is an important feature for gold nanoparticles. Gold exhibits size-tunable plasmon absorption due to electrons confinement, in both the ground and excited state, to dimensions smaller than the electron mean free path (≈20 nm for gold). If the nanoparticle size is further reduced, confinement of the free electrons reaches a second critical size scale called the electron Fermi wavelength. This starts to happen at a size lower than 3 nm and should result in discrete, quantum-confined electronic transitions that heavily affect the plasmon absorption properties (Zheng et al. 2004).
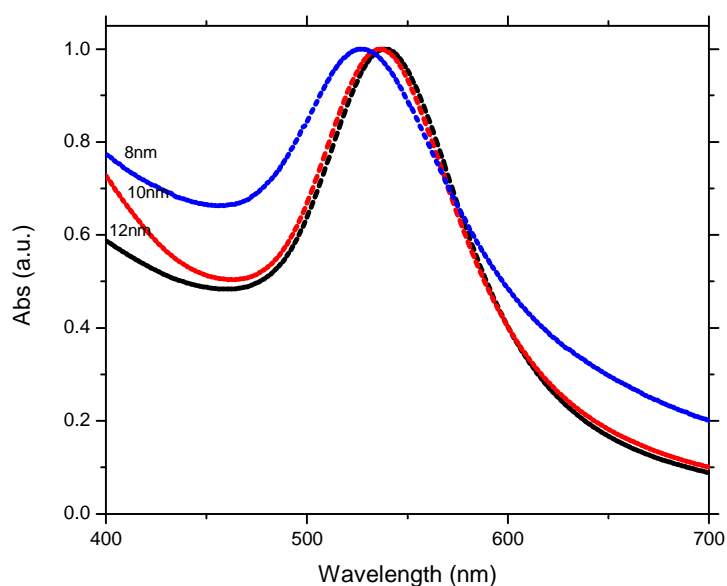

Figure 1.2. LSPR absorption of three different gold nanoparticles solutions.

Gold nanostructures could be the perfect tool for diagnostic and therapy, due to their versatility. Some techniques, as NIR fluorescence imaging and photothermal therapy, take advantage of the specific signals given by tailored shapes of gold complexes. Nanorods, as said before, present two characteristic plasmonic peaks in the UV-Vis-NIR spectrum (Figure 1.3). These techniques employ longitudinal oscillation of electrons, which gives rise to a strong long wavelength band in the NIR part of the spectrum. These peaks can be tuned properly to have the maximum of longitudinal absorption peak of the surface plasmon resonance in the range of 700 - 900 nm. Despite nanorods, gold nanoparticles present just one characteristic surface plasmon resonance peak in the UV-Vis spectra, around 520-540 nm depending on their dimension and shape. Also with NPs, SPR can be used to have a very peculiar signal for imaging. It is possible, for example, to enhance a signal due to the very intense electric field that is created around the AuNPs. This is the case of surface enhanced Raman spectroscopy (SERS), which takes advantage of Raman effect: when a photon is scattered by an atom or a molecule, it could be scattered elastically (Rayleigh scattering) or inelastically (Raman scattering). Due to their unique optical properties, this interesting materials is very useful in biosensing and biomedical applications.
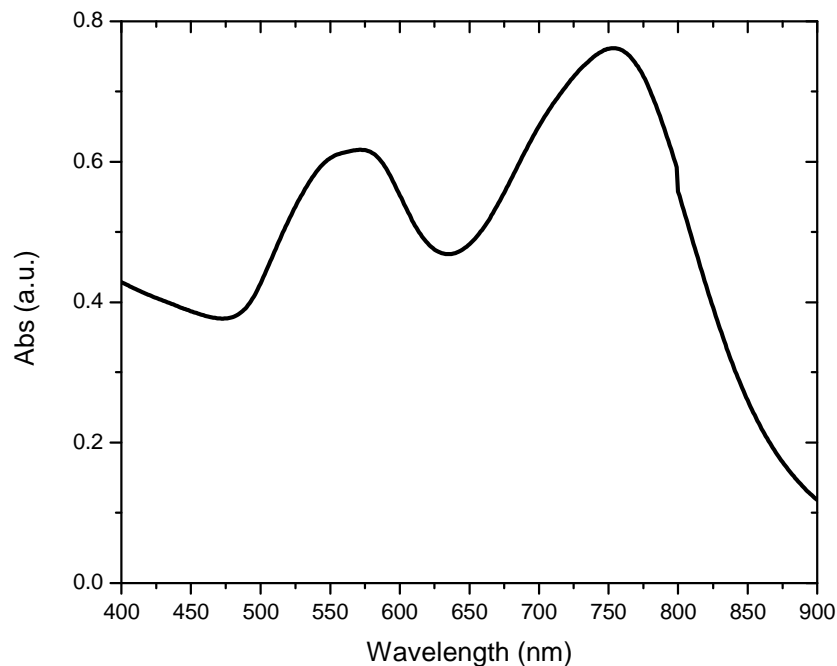
Figure 1.3. LSP absorption of gold nanorods solution shows a transversal plasmon oscillation (at 560nm) and a longitudinal plasmon oscillation (at 760nm).

1.3 Aims of the project

Within the scenario offered by the unique properties of nanostructured materials as Porous Silicon and Gold Nanoparticles, this work focused in particular on the applications of these nanostructures as biosensing tools for environmental and biomedical applications. Consequently, this thesis is now split in two macroareas:

- o **section 2** is focused on label-free devices developed for biomedical applications;

- o **section 3** is focused on characterizations of heavy metals detection in aqueous solutions for environmental monitoring applications.

2. Porous Silicon and Gold nanoparticles based devices for biomedical applications

Biomedical devices development concerns the preliminar study of biomolecular interaction between bioprobes and target analytes. The bioprobe should be efficiently immobilized onto the tranducer. Transducers are fundamental components in biosensing devices for biomedical application; in fact, they are deputed to transduce a signal that vary as function of biomolecular recognition. Since nanostructured materials have physical and chemical properties (such as photoluminescence, reflectivity, etc.), in last twenty years they easily became fundamental building blocks as tranducer element in development of the next generation of tools and devices. Therefore, a study of bioconjugation optimization should be evaluated.

In the present PhD thesis the following two types of nanostructured material were studied:

- o porous silicon (PSi);
- o gold nanoparticles (AuNPs).

The following sections will be focused on the description of different bioconjugation approaches performed onto PSi (**section 2.1**) and AuNPs (**section 2.2**).

2.1 Porous silicon based device development

2.1.1 Hydrophobin-based porous silicon passivation for glucose interaction monitoring

The study of interfaces plays a key role in hybrid bio/non-bio devices development: the need to integrate biological molecules into devices with inorganic transducers without denaturating or simply affecting the functionalities of the biological molecule became a hot topic. In past studies, Vmh2 Class I Hydrophobins was used to functionalize the silicon surfaces. The film of Vmh2 nanometer thick, deposited on crystalline silicon, has proved an efficient protection for the etching with KOH in the liquid phase leaving unaltered the optical properties (De Stefano et al., 2007; De Stefano et al., 2008); moreover, Vmh2 was found able to interact with sugars both in solution and on silicon surfaces (Rea et al. 2012).

In the following study, it will be presented the double effect of Vmh2 as both passivating and active layer onto porous silicon surfaces. Hydrophobins proteins were used to passivate three different optical structures based porous silicon:

- Microcavity;
- Rugate Filters;
- Thue Morse structures.

Onto each optical structure object of study the interaction monitoring with glucose aqueous solution at 1.2 mg/mL concentration was performed. Characterization as spectroscopic reflectometry, water contact angle and fluorescence microscopy investigation were performed.

Hybrid bio/non-bio interfaces for protein-glucose interaction monitoring

Alessandro Caliò,[1,2] Ilaria Rea,[1] Jane Politi,[1,3] Paola Giardina,[3] Sara Longobardi,[3] and Luca De Stefano[1,a]

[1]IMM-CNR, Via P. Castellino 111, 80131 Napoli, Italy
[2]Department of Physical Sciences, University of Naples "Federico II," Via Cinthia, 80100 Napoli, Italy
[3]Department of Chemical Sciences, University of Naples "Federico II," Via Cinthia, 80100 Napoli, Italy

Amphiphilic proteins, which self-assemble at solid-liquid interface in nanometric biolayer, such as hydrophobins, can be used as multifunctional film to passivate porous silicon dioxide and also sense glucose. Several porous silicon dioxide optical transducers (rugate filter, Thue-Morse sequence, and microcavity) have been protein-modified and tested in monitoring hydrophobins-glucose binding. A simple, easy-to-integrate technique, such as water contact angle, is able to reveal sugar presence at 1.2 mg/ml, whereas spectroscopic reflectometry fails. Fluorescence measurements confirm protein layer-glucose interaction. This proof-of-concept measurement could be the starting point for small analytes porous silicon based optical sensors. © 2013 AIP Publishing LLC. [http://dx.doi.org/10.1063/1.4824379]

I. INTRODUCTION

Interfaces play a key role in optical biosensor fabrication: biological molecules need to be integrated with inorganic transducers, both electrical and optical, preserving their functions and specificity. Single DNA strands, proteins, enzymes, and antibodies must be blocked on surface by absorption or covalently, depending on different chemistry used. In case of proteins and antibodies, also orientation of biological molecules is very important, since biological interactions with their ligands are strongly dependent on spatial arrangement: binding sites and variable portion should be properly exposed in order to form stable molecular complexes.[1–3]

Hydrophobins (HFBs) are small proteins of about 100 amino acid residues, produced by fungi, self-assembling into an amphipathic membrane at an interface, such as water-air or solid-water. HFBs have been classified into two groups, namely class I and class II, based on differences in their hydropathy patterns, spacing of amino acids between the cysteine residues and properties of the aggregates they form. Class I HFBs generate very insoluble assemblies, which can only be dissolved in strong acids, like 100% trifluoroacetic acid (TFA). Assemblies of class II can be more easily dissolved in ethanol or sodium dodecyl sulfate (SDS). The intriguing properties of these proteins make them of great interest to biotechnologists, as they have potentialities for numerous applications.[4,5] When synthetized by the fungus, these proteins grow together with some glucans, which are oligo- and poly-saccharides that are found in the culture medium. In particular, what we have found, in case of HFBs from *Pleurotus ostreatus*, an edible fungus that is common in Mediterranean diet, is that these proteins link also to simple sugars, i.e., glucose and maltose, when mixed in aqueous solutions. This bond strongly affects structure and behavior of HFBs, both in solution and on solid surface, even if they seem to have not a specific binding site for these small molecules.[6,7]

Porous silicon (PSi) has by far emerged as ideal support material for immobilization of biomolecules, since exhibits a sponge-like morphology characterized by specific surface area of the order of hundreds of square meters per cubic centimetres.[8] PSi can be fabricated by electrochemical etching of doped crystalline silicon in hydrofluoric acid (HF).[9] Since PSi is a network of air holes in a silicon matrix, its dielectric properties depend on voids content and can be accurately controlled by tuning the process parameters (etch time, HF concentration, doping level, and so on), so that different photonic structures (Fabry Perot interferometer, Bragg mirror, optical microcavity, aperiodic multilayered sequence, and optical waveguide), showing high quality optical responses, can be obtained.[10–13] Main drawback of this fascinating material is its chemical instability: as-etched PSi quickly degrades on exposure to atmosphere since Si-H bonds tend to be substituted by Si-O-Si ones, but also oxidised PSi can be corroded in aqueous environments. Lot of chemical procedures have been proposed to overcome this limit.[14–17] On the other hand, self-assembling materials, both organic and biological in nature, are extremely interesting as functional interfaces between man-made, artificial transducers, and the living realm: they do not require any specific or complex chemical procedure, nor special instrumentation for their deposition, such as high vacuum chambers, and so on.[18] When deposited in similar condition, HFBs also assure formation of layers of very close thicknesses, so that their use could be of real concern about inorganic surface passivation.[19] We have already demonstrated in recent papers how HFB can protect planar crystalline silicon surface and PSi multilayers on exposure to KOH and NaOH, respectively.[20,21]

In this work, we present our results on monitoring HFB interactions with glucose by several porous silicon based photonic devices, when the proteins are already self-assembled on PSi surface. A biological passivation

[a]Author to whom correspondence should be addressed. Electronic mail: luca.destefano@cnr.it

procedure of porous silicon oxidized surface by low vacuum drop casting deposition of hydrophobins is proposed.

II. MATERIALS AND METHODS

A. Fabrication of porous silicon photonic structures

Porous silicon photonic structures were fabricated by electrochemical etching of p^+ crystalline silicon (0.001 Ω cm resistivity, $\langle 100 \rangle$ oriented, 500 μm thick) in hydrofluoric acid (HF, 50% in volume), water, and ethanol solution (1:1:1) in dark and at room temperature. Before anodization dissolution, each silicon substrate was immersed in HF solution for 2 min in order to remove native oxide layer. Rugate filter was made by 20 pairs, each one alternating low (L) and high (H) refractive index couples.[22] Explicit layers sequence is: LH-($LH \times 18$)-LH. Current density, used for rugate filter fabrication, had sinusoidal profile and varied between 170 mA/cm^2 and 200 mA/cm^2. Each sinusoidal period was approximated by step-functions (40 sinusoidal periods, 12 steps for each period). Low porosity layers had high refractive index $n_H = 1.58$, while high porosity layers had low refractive index $n_L = 1.52$; values of refractive indexes were calculated at $\lambda = 902$ nm. Thue-Morse structure is generated following the substitution rules $H \to HL$ and $L \to LH$, so that a 64 layers sequence can be expressly written as $LHHLHLLHHLLHLHHLHLLHLHHLLHHHLHLLHHLLHLH$ $HLLHHHLHLLHLHHHLHLLHHHLLHLHHL$. Low refractive index was obtained applying current density equal to 100 mA/cm^2 for 1.6 s, while high refractive index layer required 200 mA/cm^2 for 1.2 s, corresponding to $n_L = 1.53$ and $n_H = 1.79$, and thicknesses $d_L = 156$ nm and $d_H = 120$ nm, respectively. Values of refractive indexes were calculated at $\lambda = 753$ nm. Microcavity is constituted by a $\lambda/2$ layer (optical thickness) sandwiched between two 9.5 period Bragg reflectors (BRs), and the sequence is: LH-($LH \times 8$)-$L(HH)L$ -($HL \times 8$)-HL. The thicknesses, d_H and d_L, of the layers constituting the BRs satisfy the relation $n_H d_H + n_L d_L = m\lambda_B/2$, where n_H and n_L are high and low refractive indexes, m is an integer, and λ_B is the Bragg wavelength. High porosity layers were obtained applying a current density of 200 mA/cm^2 for 1.2 s ($n_L = 1.53$; $d_L = 156$ nm); low porosity layers were obtained applying a current density of 100 mA/cm^2 for 1.4 s ($n_H = 1.79$; $d_H = 105$ nm). Values of refractive indexes were calculated at $\lambda = 745$ nm. For all structures, time breaks of 5 s were used during etching process in order to recover HF concentration at dissolution edge and start next layer formation with zero current density, so that variation current is always the same for each layer. The etching area is 0.98 cm^2. After the electrochemical process, pores dimension was increased by rinsing the "as-etched" porous silicon structures in KOH-ethanol solution (1.5 mM) for 15 min.[23] Devices were then thermally oxidized against uncontrolled environmental aging and corrosion in alkaline solutions.[24] Oxidation has been performed in pure O$_2$ by applying a two-step process: 30 min at 400 °C followed by 15 min at 900 °C. Even if PSi stacks are made of several tenths of porous layers, the reflectivity spectra are of very good quality in a wide range of wavelengths, as it is shown in Figure 1 in case of rugate filter (Fig. 1(a)), Thue-Morse sequence (Fig. 1(b)), and optical

FIG. 1. (A) Reflectivity spectrum of the PSi rugate filter made alternating low (L) and high (H) refractive index layers. (B) Reflectivity spectrum of aperiodic PSi Thue-Morse structure. (C) Reflectivity spectrum of 40 layers PSi optical microcavity.

micro-cavity (Fig. 1(c)). Schemes of explicit layers sequences are shown in Figure S1, in Supplemental Materials, for all PSi structures.[25]

B. Protein purification

Class I hydrophobin Vmh2 secreted by basidiomycete fungus *P. ostreatus* was purified and identified in previous work.[6] Briefly, pure hydrophobins were dissolved with TFA treatment in 70% acetonitrile aqueous solution. Vmh2 concentration was evaluated using PIERCE 660 nm Protein Assay kit, since it is compatible with organic solvents and is equal to 0.2 mg/ml.

C. Protein infiltration

Differently from our previous work, in the present case, deposition of hydrophobins was performed by drop casting in low vacuum (see deposition chamber in Figure 2), a technique we used for liquid crystal infiltration in PSi matrix.[26] Deposition can be outlined as follows: (1) place sample in the center of vacuum chamber; (2) insert syringe, through

FIG. 2. Deposition chamber used for in vacuum HFBs infiltration into PSi photonic structures.

plastic cap, into chamber; (3) connect vacuum pump to chamber; (4) turn on vacuum, which allows air release from PSi pores, and simultaneously extracts the solution with hydrophobins from syringe to sample; (5) turn off vacuum; (6) leave the sample in chamber for 1 h, so that hydrophobins penetrate into pores; (7) place sample on hot plate at 80 °C for 10 min; (8) wash sample by 70% acetonitrile aqueous solution; (9) dry sample with nitrogen; (10) repeat steps from (1) to (9). Steps (1)-(7) produce a hydrophobins compact biofilm in PSi pores, while eighth step removes excess of hydrophobins not bound to PSi surface.

D. Spectroscopic reflectometry

Reflectivity spectra of PSi photonic structures have been acquired using a simple experimental setup: a white light was sent on PSi samples by means of a Y optical reflection probe (Avantes). Same probe was used to guide output signal to optical spectrum analyzer (Ando AQ6315A). Spectra were acquired at normal incidence with resolution of 0.2 nm. At least three measurements have been recorded to have average spectrum of the sample.

E. Water contact angle (WCA) measurements

Sessile drop technique has been used for WCA measurements on a First Ten Angstroms FTA 1000 C Class coupled with drop shape analysis software. The WCA values reported in this work are average of at least three measurements.

F. Fluorescence microscopy

Fluorescence analysis was performed by means of Leica Z16 APO fluorescence macroscope equipped with a camera Leica DFC300. Optics used for acquisition was a 450–490 nm band-pass excitation filter, a 510 nm dichromatic mirror, and

TABLE I. Reflectivity peak measurements performed on the PSi structures "as etched," after KOH treatment, and after oxidation.

Structure	$\lambda_{AS\ ETCHED}$ (nm)	λ_{KOH} (nm)	λ_{OX} (nm)
Rugate filter	902.8 ± 0.7	878 ± 1	775.81 ± 0.04
Thue-Morse filter	753.9 ± 0.9	730.6 ± 0.3	631.4 ± 0.4
Microcavity	746 ± 1	721 ± 1	636.1 ± 0.4

a 515 nm suppression filter. Fluorescence values reported in the work are averages of three measurements.

G. Chemical stability

Oxidised PSi multilayer have been coated by HFB and exposed to diluted HF in order to check the effectiveness of proteins surface coverage. After HFB deposition, samples have been immersed in aqueous solution of HF (1% V/V) for 80 s, recording the reflectivity spectrum every 20 s.

III. RESULTS AND DISCUSSION

Since PSi based optical transducers have to be infiltrated by biological matter, we slightly enlarge pores dimension by KOH treatment and passivate PSi surface by thermal oxidation: in Table I are reported values of wavelengths resonances before and after these modifications for each device. In particular, thermal oxidation stabilises PSi surface by substituting Si-H bonds with Si-O-Si, but also strongly changes its wettability: Figure 3 documents the huge variation of water contact angle, from 130° to 4°, in case of fresh PSi and oxidised PSi, respectively.

HFB aqueous solutions have infiltrated in PSi structures in low vacuum conditions: this procedure minimizes hydrostatic pressure due to air presence in pores. The HFB self-assembled biolayer partially substitutes air in PSi pores, so that the average refractive index increases and the reflectivity spectrum undergoes a red-shift proportional to the protein film thickness. Figure 4 shows red-shift of reflectivity spectra for each photonic structure: since the red-shift is the biggest (Fig. 4(b)), Thue-Morse sequence is the most permeable of three, as we have already demonstrated in case of volatile substances in our previous work.[27] Furthermore, red-shifts of both Thue-Morse and micro-cavity are mainly due to HFB penetrated in the so-called defects (i.e., layers that disrupt periodicity along the direction of stratification); while in case of rugate filter, shift is due to HFB distribution along all the PSi layers, which implies less sensitivity. HFB infiltration in PSi

FIG. 3. Water contact angle measurements before (A) and after (B) thermal oxidation of PSi structure.

pores turns the highly hydrophilic surfaces of oxidised PSi devices into very much less hydrophilic ones, as demonstrated by images reported in Figure 4: rugate surface exhibited a change in WCA of about 65° (Fig. 5(a)), Thue-Morse of 50° (Fig. 5(b)), and microcavity of 77° (Fig. 5(c)).

The presence of a HFB proteins layer inside PSi not only changes wettability of oxidised multilayers but also protects the oxide against corrosion by hydrofluoric acid water solution. Since HF is very strong acid, dipping protein modified PSi samples into such a solution is a severe test for HFB passivation film. Results are summarised in Figure 6 for a rugate device: while a protein-coated sample reflectivity spectrum shows a blue shift of about 70 nm (Fig. 6(a)), but its shape is still of very good optical quality, the uncoated

FIG. 5. (A) Water contact angle measurements performed on the PSi rugate filter before and after the HFBs deposition. (B) Water contact angle measurements performed on the Thue-Morse structure before and after the HFBs deposition. (C) Water contact angle measurements performed on the PSi optical microcavity before and after the HFBs deposition.

FIG. 4. (A) Reflectivity spectra of the PSi rugate filter before (solid line) and after (dotted line) the HFBs deposition; (B) reflectivity spectra of the PSi Thue-Morse structure before (solid line) and after (dotted line) the HFBs deposition; (C) reflectivity spectra of the Psi optical microcavity before (solid line) and after (dotted line) the HFBs deposition.

one is completely corroded and the optical signal is not more meaningful (Fig. 6(b) dotted line).

HFB complex with glucans, naturally available oligomers of glucose, in water solution,[6] and these aggregates are still able to self-assemble in nanometric biofilms on solid surfaces.[7] Unfortunately, since the crystalline model of HFB is not yet available, the interaction between protein and sugars is not completely understood: from biological consideration, HFB is not a sugar binding protein, so that the presence of a specific binding site cannot be hypothesized, but it selectively binds glucose with respect to other sugars,[28] at least in solutions. One of the aims of this work is to verify if the self-assembled biolayer of hydrophobins is still able to interact with glucose. The detection of very small molecules is always challenging, since they only slightly changes average refractive index. Glucose is a very small molecule (about 180 Da) with respect to HFB (about 10 kDa) and our previous results indicate that each HFB molecule co-ordinates to about 200 glucose molecules in solution, while only to 20, or less, when assembled in biofilm on surface.[6,7,28] In particular, we have verified that spectroscopic reflectometry is not so sensitive to allow optical detection of glucose (see Figures S2 and S3, and their comments, in Supplemental Materials)[25] when protein modified PSi photonic transducers are exposed to sugar solution, at least for concentration up to 1.2 mg/ml. WCA technique instead can be used in sugar
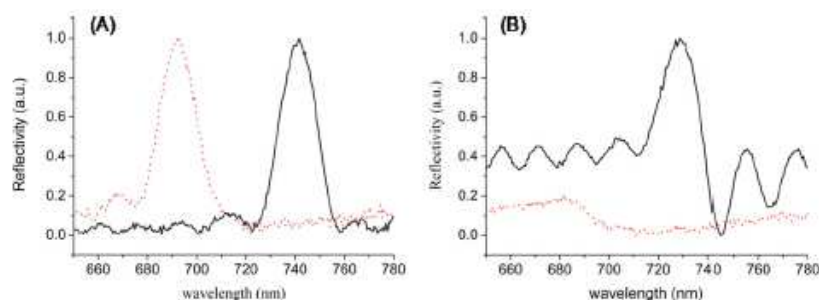
FIG. 6. (A) Reflectivity spectra of a protein coated rugate filter at $t=0$ s (straight line) and after 80 s (dotted line) exposure to diluted HF. (B) Reflectivity spectra of a bare rugate at $t=0$ s (straight line) and after 80 s (dotted line) exposure to diluted HF.
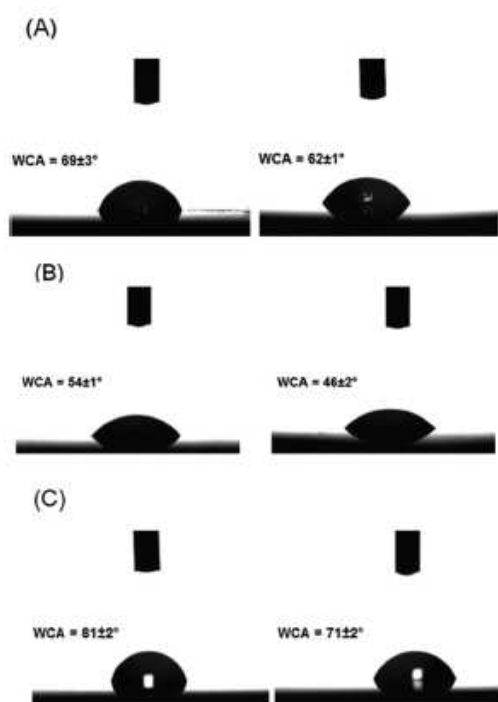
FIG. 7. (A) Water contact angle measurements performed on the PSi rugate filter before and after the deposition of aqueous glucose solution 1.2 mg/ml. (B) Water contact angle measurements performed on the Thue-Morse structure before and after the deposition of aqueous glucose solution 1.2 mg/ml. (C) Water contact angle measurements performed on the PSi optical microcavity before and after the deposition of aqueous glucose solution 1.2 mg/ml.
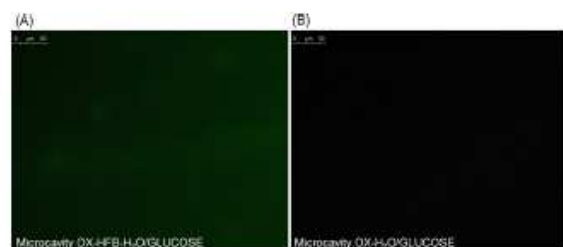
FIG. 8. (A) Fluorescence image of HFBs modified oxidized PSi microcavity after Fluo-glucose incubation. (B) Fluorescence image of bare oxidized PSi microcavity after Fluo-glucose incubation.

monitoring: as we report in Figure 7, values of contact angles vary of 7° (Fig. 7(a), rugate), 8° (Fig. 7(b), Thue-Morse), and 10° (Fig. 7(c), microcavity), after glucose deposition and extensive water rinsing. WCA decrease can be explained since glucose binding on HFB layer increases overall surface polarity, making it more hydrophilic. A further evidence of biofilm-glucose interaction is that obtained by fluorescence imaging in case of labelled sugar molecules: we have deposited, by drop casting, on HFB-PSi ((A) sample), and on bare PSi as control ((B) sample), aliquots of fluorescein-modified glucose (same concentration as before) and acquired images after washing. In Figure 8(a), fluorescence is well evident and quite homogeneous on the entire surface, whereas the control sample is totally black (Fig. 8(b)).

IV. CONCLUSIONS

Different optical techniques have been used in monitoring interaction between a self-assembled biofilm of hydrophobin proteins, infiltrated in PSi, and glucose. Even if spectroscopic reflectometry does not reveal any red shift ($\Delta\lambda < 1$ nm) of HFB-PSi optical spectra on exposure to glucose solution (1.2 mg/ml), water contact angle measurements and fluorescence microscopy highlight the presence of sugar in HFB-PSi without any doubts. Moreover, the stable and compact protein biofilm is able to penetrate the intricate, sponge-like matrix of different PSi multilayers and to protect them against corrosion on exposure to diluted HF (1% V/V). On these bases, we believe that HFB could be used as a biological, functional layer that adds useful features to well-known and high-performances PSi based optical transducers.

[1]M. Dekker, *Physical Chemistry of Biological Interfaces*, edited by A. Baszkin and W. Norde (CRC Press - Taylor & Francis Group, New York, 1999).
[2]J. Voros, Biophys. J. **87**, 553 (2004).
[3]W. Norde, Colloids Surf., B **61**, 1 (2008).
[4]H. A. Wösten, Ann. Rev. Microbiol. **55**, 625 (2001).
[5]H. J. Hektor and K. Scholtmeijer, Curr. Opin. Biotechnol. **16**, 434 (2005).
[6]A. Armenante, S. Longobardi, I. Rea, L. De Stefano, M. Giocondo, A. Silipo, A. Molinaro, and P. Giardina, Glycobiology **20**, 594 (2010).
[7]I. Rea, P. Giardina, S. Longobardi, V. Casuscelli, F. Porro, I. Rendina, and L. De Stefano, J. R. Soc., Interface **9**, 2450 (2012).
[8]M. J. Sailor, *Porous Silicon in Practice: Preparation, Characterization and Applications* (Wiley-VCH Verlag GmbH & Co. KGaA, 2012).
[9]T. Laurell, J. Drott, L. Rosengren, and K. Lindström, Sens. Actuators B **31**, 161 (1996).
[10]S. Létant and M. J. Sailor, Adv. Mater. **12**, 355 (2000).
[11]P. A. Snow, E. K. Squire, P. S. J. Russell, and L. T. Canham, J. Appl. Phys. **86**, 1781 (1999).

[12]L. Pavesi, Riv. Nuovo Cimento **20**, 1 (1997).

[13]L. Moretti, I. Rea, L. Rotiroti, I. Rendina, G. Abbate, A. Marino, and L. De Stefano, Opt. Express **14**, 6264 (2006).

[14]M. P. Stewart and J. M. Buriak, Adv. Mater. **12**, 859 (2000).

[15]J. Salonen, V. P. Lehto, and E. Laine, Appl. Phys. Lett. **70**, 637 (1997).

[16]B. Gelloz, T. Nakagawa, and N. Koshida, Appl. Phys. Lett. **73**, 2021 (1998).

[17]L. De Stefano, G. Oliviero, J. Amato, N. Borbone, G. Piccialli, L. Mayol, I. Rendina, M. Terracciano, and I. Rea, J. R. Soc. Interface **10**, 20130160 (2013).

[18]G. M. Whitesides, Sci. Am. **273**, 114 (1995).

[19]L. De Stefano, I. Rea, E. De Tommasi, P. Giardina, A. Armenante, S. Longobardi, M. Giocondo, and I. Rendina, J. Nanophoton. **3**, 031985 (2009).

[20]L. De Stefano, I. Rea, P. Giardina, A. Armenante, M. Giocondo, and I. Rendina, Langmuir **23**, 7920 (2007).

[21]L. De Stefano, I. Rea, P. Giardina, A. Armenante, and I. Rendina, Adv. Mater. **20**, 1529 (2008).

[22]T. A. Schmedake, F. Cunin, J. R. Link, and M. J. Sailor, Adv. Mater. **14**, 1270 (2002).

[23]R. Herino, G. Bomchil, K. Barla, C. Bertrand, and J. L. Ginoux, J. Electrochem. Soc. **134**, 1994 (1987).

[24]V. Chamard, G. Dolino, and F. Muller, J. Appl. Phys. **84**, 6659 (1998).

[25]See supplementary material at http://dx.doi.org/10.1063/1.4824379 for schematic of PSi structures and their optical spectra before and after exposure to glucose solution.

[26]G. V. Tkachenko, V. Tkachenko, L. De Stefano, and I. A. Sukhoivanov, J. Opt. A, Pure Appl. Opt. **11**, 105106 (2009).

[27]L. Moretti, I. Rea, L. De Stefano, and I. Rendina, Appl. Phys. Lett. **90**, 191112 (2007).

[28]S. Longobardi, D. Picone, C. Ercole, R. Spadaccini, L. De Stefano, I. Rea, and P. Giardina, Biomacromolecules **13**, 743 (2012).

2.2 Gold Nanoparticles based interaction monitoring

Despite the considerable variety of AuNPs properties and contributions, the present PhD thesis will focus as first on synthesis and stabilization of gold colloidal solutions using innovative stabilizers (such as PEG diacid and Hydrophobins proteins) alone and in competition; then, standard seed-growth synthesis in presence of CTAB as stabilizer was also studied for gold nanorods synthesis.

2.2.1 HFB as co-stabilizer in gold nanospheres synthesis

The utilization of biomolecules to tune the surface properties and assembly of AuNPs is a very attractive approach that has received considerable attention. For instance, (1) biomolecule and/or biopolymer-conjugated AuNPs are largely used as biomarkers and biodelivery vehicles in the medicine/pharmacy, and in cosmetic products (Song et al. 1997). In the past decades, though many synthetic strategies have been developed to prepare AuNPs in organic or aqueous solvent (Cui et al. 2008).

The surfactant-like properties of hydrophobins from Pleorotus ostreatus were studied at the air-water interface, at surfaces, and in solution. They can form a highly stable coating which can be used to promote biocompatibility, to improve stability and particle size of suspension and emulsions, or to preserve the activity at a surface or a solid material. On the surface of the folded molecule, there is a coherent hydrophobic patch which makes the molecule amphiphilic. The amphiphilicity gives the protein the ability to strongly stick to hydrophobic surfaces, which makes HFB suitable, for surface immobilization. In this work we used HFB class I, extracted from basidiomycete Pleurotus Ostreatus to synthesize three types of hybrid gold nanoparticles in which HFB molecules plays a double role as surfactant and reagent in the synthetic process of AuNPs.

Bioconjugation of Enzymes and Proteins on Multifunctional and Nanostructured Solid Supports for Biomolecular Interactions Monitoring
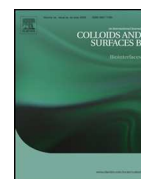
The amphiphilic hydrophobin Vmh2 plays a key role in one step synthesis of hybrid protein–gold nanoparticles

Jane Politi [a,c,d], Luca De Stefano [c,*], Sara Longobardi [d], Paola Giardina [d], Ilaria Rea [c], Christophe Methivier [a,b], Claire-Marie Pradier [a,b], Sandra Casale [a,b], Jolanda Spadavecchia [a,b]

[a] Sorbonne Universités, UPMC Paris 06, Laboratoire de Réactivité de Surface, 4 place Jussieu, Paris F-75005, France
[b] CNRS, UMR 7197, Laboratoire de Réactivité de Surface, Paris F-75005, France
[c] Institute for Microelectronics and Microsystems, Unit of Naples-National Research Council, Via P. Castellino 111, 80127 Italy
[d] Department of Chemical Sciences, University of Naples "Federico II", Via Cinthia, Naples 80126 Italy

ARTICLE INFO

ABSTRACT

We report a simple and original method to synthesize gold nanoparticles in which a fungal protein, the hydrophobin Vmh2 from Pleurotus ostreatus and dicarboxylic acid-terminated polyethylene-glycol (PEG) has been used as additional components in a one step process, leading to hybrid protein–metal nanoparticles (NPs). The nanoparticles have been characterized by ultra-violet/visible, infrared and X-ray photoelectron spectroscopies, dynamic light scattering and also by electron microscopy imaging. The results of these analytical techniques highlight nanometric sized, stable, hybrid complexes of about 12 nm, with outer surface rich in functional chemical groups. Interaction with protein and antibodies has also been exploited.

© 2015 Elsevier B.V. All rights reserved.

1. Introduction

Gold Nanoparticles (AuNPs) have been used in the last decade in many popular fields of investigation such as nanomedicine, imaging, environmental monitoring and biomolecular sensing, due to their unique physical and chemical properties [1,2], which can be tailored for any specific application.

The utilization of biomolecules to tune the surface properties and the assembly of AuNPs is a very attractive approach that has received considerable attention: this technology combines the advantages of green chemistry, since harmless biological substances are used instead of some aggressive chemical compounds, with the unique properties of biological probes, leading to the next generation of nanometric complexes. Biomolecules and/or biopolymer-conjugated AuNPs have been used as biomarkers in diseases early diagnosis and as in vivo drug delivery vehicles in medicine/pharmacy applications, and also in cosmetic products [3,4].

Ionic detergents can be usefully exploited as stabilizing agents during the synthesis of nanoparticles, since they not only prevent particles aggregation but also help in tuning composition, shape and size. To date, a variety of stabilizers have been employed in the synthesis of AuNPs [1,5,6]. Even if surfactants play an important role in contemporary pharmaceutical biotechnology, since can control wetting, stability and bioavailability of drugs [7,8], most of them are toxic, and the removal of excess stabilizer causes unwanted effects, such as aggregation of the particles, which is a matter of concern in various clinical applications. Moreover, lyophobic colloids, such as polymers, which require energy for their formation, are quite unstable from the thermodynamic point of view, and frequently form large aggregates. Colloids association such as micelles, on the other hand, can form spontaneously self-assemblies under certain conditions, and are thermodynamically more stable towards both dissociation and aggregation [9]. Organic molecules exploited in AuNPs synthesis can be substituted by polyethylene glycol (PEG) in order to obtain biocompatible PEG-stabilized gold nanoparticles [10]. Recently, Spadavecchia et al. have reported a one-solution synthesis approach to prepare polymer modified gold nanoparticles using dicarboxylic PEG as stabilizer agent which demonstrated high stability under realistic biomedical conditions [11]. Moreover, gold nanoparticles synthesis was demonstrated by using

* Corresponding author. Fax: +39 0816132598.
E-mail address: luca.destefano@cnr.it (L. De Stefano).

a mixture of a protein, namely collagen, and surfactants [12]. Collagen and Hydrophobins can be considered useful biological agents as co-surfactants in one-pot gold nanoparticles synthesis. Collagen is one of the most important and abundant structural protein in the extracellular matrix, largely used in biomedical and biomaterials applications [13,14]. Hydrophobins (HFB) are small (about 100 amino acid residues) proteins produced by filamentous fungi. They are highly surface-active, and self-assemble at hydrophilic/hydrophobic interfaces into an amphipathic nanometric layer at interfaces between different phases (air–liquid, solid–liquid). HFB are classified in class I (highly insoluble layer) and class II (easily soluble layer). Both types of hydrophobins have been used to disperse hydrophobic materials; to stabilize foam in food products; to immobilize enzymes, peptides, antibodies, and cells, on surfaces [15–18]. Hybrid nanoparticles made of collagen or hydrophobins proteins as co-stabilizers could be of interest in many fields, from biotechnological to biomedical applications.

The biological functions of HFB are linked to the reduction of the water surface tension, and to their ability to self-assemble into an amphipatic membrane when they reach an interface, thus allowing fungi to escape from aqueous environment and to facilitate air dispersal of the spores [19,20]. On the surface of the folded molecules, there is a coherent hydrophobic patch, which makes the molecule amphiphilic. The amphiphilicity gives the protein the ability to strongly stick to hydrophobic surfaces [21], forming a highly stable coating which can be used to promote biocompatibility [22], and to act as an intermediate layer for cells, proteins, or other type of molecules binding. Previous studies [23,24] demonstrated the ability of class II HFB from Trichoderma reesei to effcently coat thermally-hydrocarbonized porous silicon nanoparticles and to synthesize beclomethasone dipropionate/protein-coated nanoparticles for drug delivery purposes. The HFB Vmh2 purified from Pleurotus ostreatus was used in the present work: Vmh2 aggregates in very stable nanometric layer and its peculiar properties at the air–water interface, on surfaces, and in solution have been recently studied [25,26].

Hybrid biological–organic–metal nanoparticles have been synthesized in which Vmh2 molecules played a double role in the formation of AuNPs, as a "natural" surfactant and additive reagent. We also engineered hybrid nanoparticles in which Vmh2 protein was coupled with non-ionic surfactants, namely PEG diacid, in the synthesis, thus changing chemical and optical properties of AuNPs. The resulting hybrid PEG–HFB–AuNPs are very interesting since they expose chemical groups with non fouling characteristics and also ensure a satisfying accessibility of HFB for biomolecular interaction.

2. Experimental

2.1. Materials

All chemicals were reagent grade or higher and were used as received unless otherwise specified. Tetrachloroauric acid ($HAuCl_4$), sodium borohydride ($NaBH_4$), Polyethylene glycol 600 Diacid (PEG), N-hydroxysuccinimide (NHS), 1-(3-dimethylaminopropyl)-N -ethylcarbodiimide hydrochloride (EDC), Bovine Serum Albumine (BSA), phosphate buffered saline (PBS, 0.1 M, pH 1.68, 7, 12), trifluoroacetic acid (TFA), Sodium Dodecyl Sulfate (SDS), methanol (CH_3OH), chloroform ($CHCl_3$) and ethanol (C_2H_5OH) were purchased from Sigma–Aldrich.

2.2. Purification and extraction of HFB

White-rot fungus, P. ostreatus (Jacq.: Fr.) Kummer (type: Florida; ATCC No. MYA-2306) was maintained at 4 °C through periodic

transfer on potato dextrose agar (Difco) plates in the presence of 0.5% yeast extract. Mycelia were inoculated in 1 L flasks containing 500 mL of potato-dextrose broth (24 g/L) supplemented with 0.5% yeast extract, grown at 28 °C in shaken mode (150 rpm). After 10 days of fungal growth, mycelia were separated by filtration through gauze, treated twice with 2% SDS in a boiling water bath for 10 min, washed several times with water and once with 60% ethanol to completely remove the detergent. The residue was dried under nitrogen, grinded and treated with 100% TFA in a water bath sonicator (Elmasonic S30, Elma) for 30 min, and centrifuged (10 min at 3200 × g). The supernatant was dried, dissolved in 60% ethanol and centrifuged (20 min at 3200 × g) obtaining a raw extract solution. The ethanol was removed from the raw extract under vacuum at 40 °C using rotavapor and the material was freeze-dried, then lipids were extracted in a mixture of water–methanol–chloroform 2:2:1 v/v (5 min in bath sonicator). After centrifugation, proteins appeared as a solid aggregate at the interface between the water–methanol and the chloroform phases. They were recovered by removal of liquid phases. The aggregated protein was dried, treated with TFA for 30 min in bath sonicator, re-dried and dissolved in 80% ethanol. The sample was centrifuged (90 min at 12000 × g) and the supernatant dried, treated with TFA as above-described and re-dissolved in 60% ethanol [20].

2.3. Synthesis procedures

2.3.1. Synthesis of hybrid hydrophobin gold nanoparticles (HFB–AuNPs)

HFB–AuNPs (Schemes 1 a and 2) were prepared by a well assessed chemical reduction process [27]. Briefly, 5 mL of HFB solution (150 g/mL) was mixed with 5 mL of 0.0001 M aqueous $HAuCl_4$ solution for 10 min. 600 L of 0.01 M $NaBH_4$ was added drop-wise to the resulting solution, followed by rapid stirring. After 1 h without agitation, the solution became purple, the characteristic color of AuNPs. The product was centrifuged at 15000 rpm for 25 min and the pellet was recovered and purified by washing with milliQ water for three times.

2.3.2. Synthesis of hybrid PEG–hydrophobin gold nanoparticles (PEG–HFB–AuNPs)

PEG–HFB–AuNPs (Schemes 1 b and 2) were prepared under the same conditions as HFB–AuNPs. 2 mL of Polyethylene glycol 600 Diacid (PEG) with a hydrodynamic diameter of 6 nm measured by TEM (Fig. S1 in supplementary materials) solution was mixed with 5 mL of HFB solution and 5 mL of 0.0001 M aqueous $HAuCl_4$ solution under stirring at room temperature. After 10 min, 1.2 mL of $NaBH_4$ (0.01 M) was added drop-wise followed by rapid stirring and kept without agitation for 2 h. The resulting red-rose solution was centrifuged and purified at the same conditions.

2.4. PM-IRRAS measurements

Polarization Modulation-Infrared reflection absorption spectroscopy (PM-IRRAS) spectra were recorded on a commercial Thermo (Les Ulis, France) Nexus spectrometer. The external beam was focused on the sample with a mirror, at an optimal incident angle of 80°. PM-IRRAS technique requires that samples to be analyzed should be covalently bound to a gold plated glass slide. A ZnSe grid polarizer and a ZnSe photoelastic modulator, modulating the incident beam between p- and s-polarizations (HINDS Instruments, PEM 90, modulation frequency = 37 kHz), were placed before the sample. The light reflected from the sample was then focused onto a nitrogen-cooled MCT detector. The presented spectra result from the sum of 128 scans recorded at 8 cm^{-1} resolution. Spectra were acquired after each step of the gold substrate functionalization.
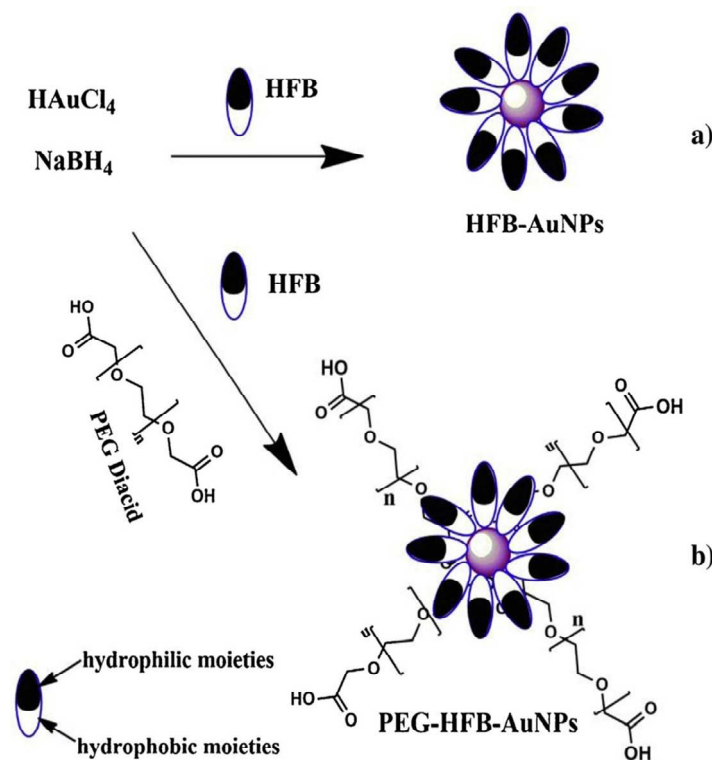
Scheme 1. Representation of one-step synthesis of hybrid hydrophobin gold nanoparticles without surfactants (a), and with PEG Diacid as surfactant (b) (dimensions of molecules are not in scale).
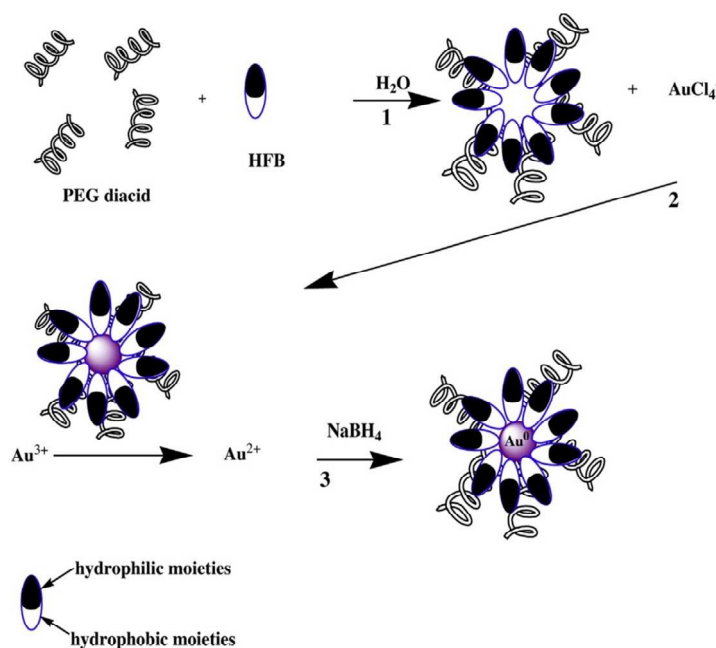
Scheme 2. Representation of proposed mechanism of AuCl$_4^-$ reduction and particle formation in the presence of PEG diacid and HFB as surfactants (dimensions of molecules are not in scale).

Each spectrum shown represents the average of three measurements.

Chemical procedures of gold–glass substrate functionalization, based on self-assembling monolayers (SAMs) of cysteamine in

absolute ethanol, have been previously optimized [28]. Briefly, the freshly cleaned gold substrate was immersed in an unstirred 10 mM ethanol solution of -mercaptoethylamine (cysteamine) at room temperature, in the dark, for 6 h. The gold substrates were then washed with ethanol and milliQ water to remove the excess of thiols. Two series of glass slides were prepared by using 2 mL of PEG–HFB–AuNPs and PEG–AuNPs at 2×10^{-6} M [11] dissolved in 2 mL of buffer solution (PBS pH 7), in which ½ Eq. of EDC/NHS was added, and stirred for 2 h (activation) to form an amide link between COOH groups of both HFB protein and PEG diacid, and NH_2 end groups of the cysteamine on gold surface. The colloidal solution was spotted on cysteamine–gold-coated surface for 12 h at room temperature. Vmh2 solution (150 g/mL) was deposited on gold surfaces functionalized by PEG–AuNPs (same procedures and concentrations for 2 h), then washed in milliQ water and dried under nitrogen flow. Study of interaction with BSA was achieved according to the following procedure: BSA (5 mg/L in PBS pH 7) was drop deposited on the nanostructured surfaces; after 1 h, BSA solution was removed, and the surface was rinsed with a buffer solution then milliQ water and dried under nitrogen for 10 min. A similar protocol was used for anti-Immunoglobulin G/Immunoglobulin G (anti-IgG/IgG) interaction.

2.5. X-ray photoelectron spectroscopy (XPS) measurements

XPS analyses were performed using a SPECS spectrometer (SPECS, Germany) equipped by a monochromatized Al X-ray source (h = 1486.6 eV) and a Phoibos 150 hemispherical energy analyzer. Pass energies of 20 eV was used, and 10 eV, for the survey and narrow scans respectively. Gold nanoparticles were deposited on gold surface and analyzed after rinsing and drying. Each spectrum shown represents the average of three measurements.

2.6. UV/vis measurements

Absorption spectra were recorded using a Jasco V-570 UV/VIS/NIR Spectrophotometer from Jasco Int. Co., Ltd., Tokyo, Japan. 1 mL of each nanoparticles solution were acquired in the range between 200 and 800 nm after 30 min from synthesis; moreover 1 mL PEG–HFB–AuNPs were dissolved in PBS solution 0.1 M at different pH (pH 1.68, 7, 12) during 18 h.

2.7. TEM measurements

Transmission electron microscopy (TEM) measurements were recorded on a JEOL JEM 1011 microscope operating at an accelerating voltage of 100 KV. The TEM images were collected after separating the surfactant from the metal particles by centrifugation. Typically 1 mL of the sample was centrifuged for 20 min at a speed of 14000 rpm/min. The upper part of the colorless solution was removed and the solid portion was re-dispersed in 1 mL of water. 2 L of this re-dispersed particle suspension was placed on a carbon coated copper grid and dried at room temperature.

2.8. Dynamic light scattering (DLS) measurements

The size and surface charge measurements were performed by dynamic light scattering (DLS) using a Zetasizer Nano ZS (Malvern Instruments, Malvern, UK) equipped with a He–Ne laser (633 nm, fixed scattering angle of 173°, room temperature 25 °C).

3. Results and discussion

Combination of inorganic nanoparticles with organic materials to form hybrids nanocomposites reveals unique physical, chemical, optical and electrical properties which make them different

and more applicable than macroscopic materials [29]. Amphiphilic proteins, such as hydrophobins, could be suitable for both stabilization of colloidal solutions and active self-assembled layer for biosensing applications. Biointerfacial properties of gold nanoparticles were already improved by coating them with a bifunctional PEG linker carrying two carboxylic groups. As example, the synthesis of PEG-capped gold nanoparticles (PEG–AuNPs) was achieved by reducing tetrachloroauric acid ($HAuCl_4$) with sodium borohydride ($NaBH_4$) in the presence of PEG-diacid as a capping agent [30]. In the case of PEG–AuNPs, PEG-diacid is used for the stabilization of the particles through electrostatic interactions between the carboxylic acid groups and the gold surface in the same way as the citrate normally works.

Some authors have synthesized spherical PEG–AuNPs with uniform size distribution by a simple one step synthesis by using a non-toxic stabilizer [31]. Other groups have reported the mechanism of gold nanoparticle formations in the presence of poly(ethylene oxide)–poly(propylene oxide)–poly(ethylene oxide) block copolymers (PEO–PPO–PEO) varying temperature and solvent [32]. These block copolymers form cavities (pseudo-crown ether structure) that can bind metal ions [33] and reduction of bound $AuCl_4^-$ ions can proceed via oxidation of the oxyethylene and oxypropylene segments [34]. In the case under study, the synthesis of PEG–HFB–AuNPs was carried out by reducing tetraclororoauric acid ($HAuCl_4$) in presence of HFB and PEG-diacid, as stabilizers and bland reducer, also adding sodium borohydride ($NaBH_4$) as strong reducing agent. The formation of gold nanoparticles from $AuCl_4^-$ can be summarized in three main steps (see Scheme 2): (1) formation of HFB–PEG diacid mixture (see also Supplementary Materials); (2) reduction of metal ions (Au^{3+} to Au^{2+}) promoted by HFB–PEG diacid mixture, which leads to the formation of preliminary HFB–PEG–gold complex; (3) further reduction of Au^{2+} to Au^0 due to $NaBH_4$ reducer and growth of gold particles and colloidal stabilization by molecules of PEG polymer. In this process, interactions between $AuCl_4^-$ ions and mixture of HFB–PEG diacid molecules (attractive ion–dipole interactions vs repulsive interactions due to hydrophobicity) are crucial in controlling the reduction of $AuCl_4^-$ which governs the final particle size. Metal salt reactivity is of extreme importance both in the bulk solution, where causes the nucleation of the first gold seeds, and on the surface of the fresh formed gold particles, thus mastering the growth rate.

In order to determine the shape and the size distribution of the hybrid nanoparticles obtained by HFB as stabilizer, with and without PEG diacid, TEM images have been analyzed by measuring the diameter of at least 100 nanoparticles. The average size of particles of HFB–AuNPs was found to be 7.0 nm ± 0.5 nm (Fig. 1a). TEM image of PEG–HFB–AuNPs shows nanoparticles with an average size of 12.0 nm ± 0.7 nm (Fig. 1b). Some particles display a somehow faceted shape as a result of their nanocrystalline nature. In previous studies [11,35], we evaluated the diameter of PEG–AuNPs as 7.0 nm ± 0.2 nm. Further investigation on size distribution and surface charge of nanoparticles in aqueous solution were performed by dynamic light scattering (DLS) and reported in Fig. 2. The size distribution of PEG–HFB–AuNPs in aqueous solution highlights two ranges of NPs size: 16 ± 5 nm, close to that found by TEM images, and 140 ± 80 nm (by intensity of scattering). Volume particles size distribution calculation (made by Zetasizer Nano ZS software) reveals that the smallest NPs represent 84% of the total, while numbers distribution calculation (made by Zetasizer Nano ZS software) evaluates the 100% presence of nanoparticles as 10 ± 4 nm size distribution. Moreover, zeta-potential measurements quantifies a surface charge of 30 ± 4 mV, related to the positive charges of Vmh2 hydrophilic moieties, and confirms that PEG–HFB–AuNPs form a stable colloidal aqueous solution. The polydispersion index,
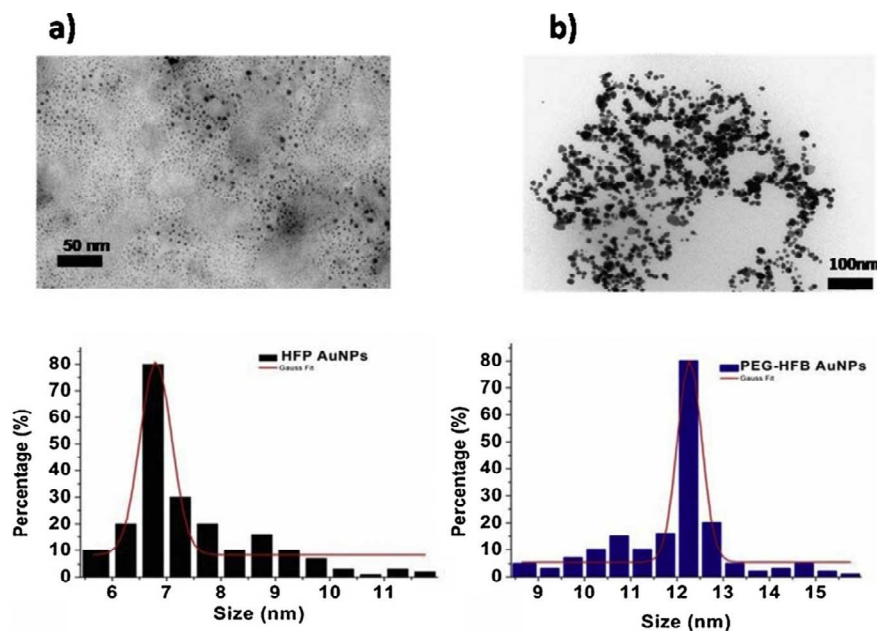
Fig. 1. TEM images and size distribution histograms of HFB–AuNPs (a) and PEG–HFB–AuNPs (b).
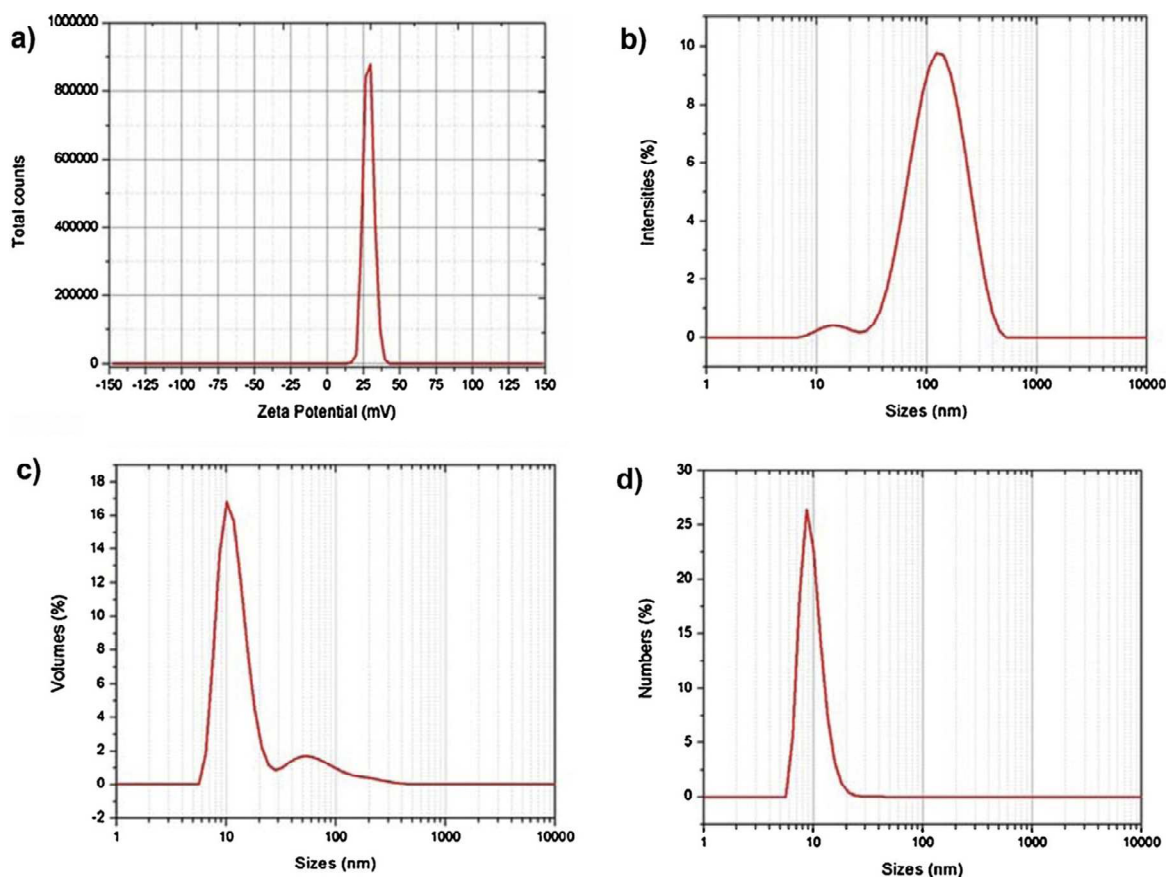

Fig. 2. Zeta potential (a) and size distributions of PEG–HFB–AuNPs in water (pH 7) evaluations of intensity (b), volume (c) and numbers (d) by DLS measurements.
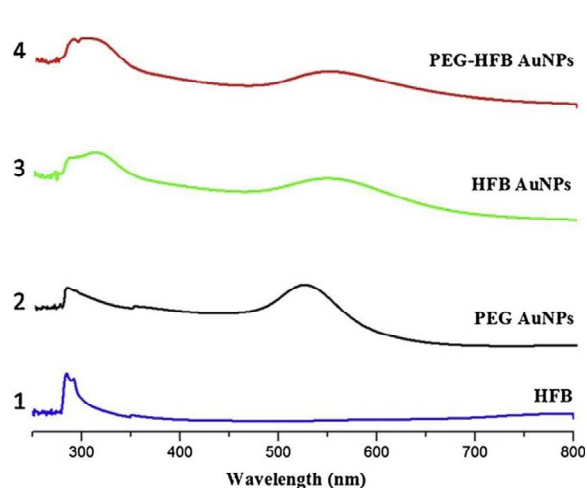
Fig. 3. UV–vis absorption spectra of (1) HFB, (2) PEG–AuNPs, (3) HFB–AuNPs and (4) PEG–HFB–AuNPs.

Fig. 4. PM-IRRAS spectra of (1) HFB, (2) PEG–AuNPs, (3) HFB–AuNPs and (4) PEG–HFB–AuNPs. Note that spectra 1–3 are four times enhanced with respect to spectrum 4.

Fig. 5. UV–vis spectra of PEG–HFB–AuNPs in buffer solutions at pH 1.68 (A), 7 (B) and 12.45 (C).

i.e., a measurement of nanoparticles size dispersion, has the value of 0.35 ± 0.01, which means quite a uniform dimensional distribution.

Characterization of localized surface plasmon (LSP) resonances by UV–vis absorbance measurements is also a topical point in the study of gold nanoparticles. Fig. 3, curve 1, shows UV–vis absorption spectra of HFB molecules characterized by a small peak at 280 nm due to the single aromatic residue in the protein. Fig. 3, curves 2, 3 and 4 report absorption spectra of hybrid AuNPs, all characterized by a small peak at 300 nm and a large band in the 530–550 nm range. The small shift of the visible band position depends on the ratio of the gold salt to the capping materials during the reaction processes. In particular, PEG–AuNPs (Fig. 3 curve 2) shows a plasmon peak at 520 nm; HFB–AuNPs (Fig. 3 curve 3) shows a plasmon peak at 549 nm; this peak is generally ascribed to collective oscillation, known as the surface plasmon oscillation of the metal electrons in the conduction band [36,37]. The absorption peak of PEG–HFB–AuNPs is centered at 545 nm (see Fig. 3 curve 4). Organic and biological complexes adsorbed on surface allow a better dispersion of Au ions, which were reduced to form single AuNPs of quite uniform size. UV–vis spectra remain unaltered after storage for more than three months at room temperature, proving the formation of a very stable particle suspension.

The nanoparticles were also characterized by PM-IRRAS spectroscopy, after deposition on a flat gold surface (see Fig. 4).

The infrared spectra in Fig. 4, curves 2 and 4, show absorption bands at around $1660 \, \text{cm}^{-1}$ ascribed to amide I ($_{C=O}$), and $1550 \, \text{cm}^{-1}$ for amideII ($_{C-N} + 1_{N-H}$), absorption is found in HFB, HFB–AuNPs and PEG–HFB–AuNPs (curve 1, 3, 4, respectively); moreover, PEG AuNPs and PEG–HFB–AuNPs present a characteristic broadband at about $1100 \, \text{cm}^{-1}$ in the ($_{C-O}$) region. Peaks at $1400–1450 \, \text{cm}^{-1}$ clearly evidences PEG-carboxylic groups, which can be available for further covalent links with proteins via their amino groups. PM-IRRAS results clearly support the formation of hybrid protein–gold nanoparticles with free chemical groups.

PEG–HFB AuNPs could be considered a promising system for biological applications, in particular for their well-known biocompatibility, and pH stability. Physical and chemical properties of AuNPs are also monitored by UV–vis absorbance changes. Fig. 5 displays UV–vis spectra of PEG–HFB–AuNPs registered after buffer exposure that still show the HFB typical peak at 280 nm and the nanoparticles characteristic peak at 545 nm. This investigation supports the ability of PEG–HFB–AuNPs to interact from acid to basic pH solutions maintaining unchanged absorbance and consequently also unchanged structure and physical–chemical properties. These
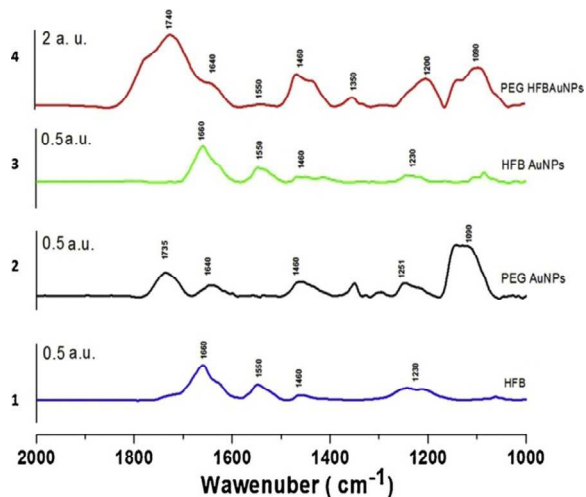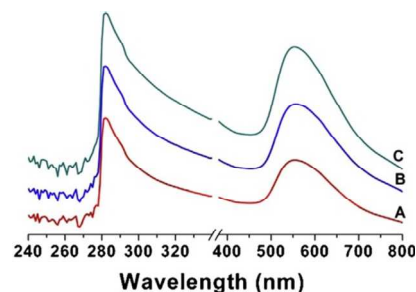
indications have been completed by XPS analysis, which is useful to understand the chemical differences of organic–inorganic complexes, by comparing PEG–AuNPs [11] and PEG–HFB–AuNPs. The XPS spectra of the PEG–AuNPs and PEG–HFB–AuNPs are displayed in Fig. 6. The PEG–AuNPs C 1s peak was decomposed into three contributions, a main one at 286.6 eV and two weaker ones at 284.9 and 289.2 eV; those last ascribed to carbon atoms in C—O—C, C—H and COOH respectively, thus in good agreement with main PEG chemical groups. The O 1s peak was decomposed into two contributions at 532.9 and 533.9 eV: those are attributed to oxygen in the C—O—C PEG chains, and in water molecules, which could be trapped inside the PEG chains. Note that the Au 4f peaks were very intense, indicating that the PEG polymer is either inside a hybrid gold–PEG nanostructure or, constituting a very thin or discontinuous layer around the nanoparticles.

The spectra of the PEG–HFB–AuNPs display significant differences, namely the appearance of a strong N 1s peak, an almost full attenuation of the gold signal, together with some changes in the C 1s and O 1s profiles. The C 1s peak is again dominated by the contribution at 286.5 eV but the contribution at 289.2 eV (289.4 eV on the Au–PEG spectrum) is increased, obviously due to the amide and carboxyl groups of proteins; the O 1s peak is now best fitted with three peaks, the additional contribution, at 532.0 eV, can be ascribed to the oxygen in C&9552;O bonds, present in the protein. The N 1s peak, centered at 400.1 eV, is that of the protein amino groups. Eventually, the Au 4f peak is now hardly detected, suggesting the dominating presence of proteins around the nanoparticles.

Bioconjugation of Enzymes and Proteins on Multifunctional and Nanostructured Solid
Supports for Biomolecular Interactions Monitoring

221   J. Politi et al. / Colloids and Surfaces B: Biointerfaces 136 (2015) 214–221   221

with biomolecules. In conclusion, this last investigation reveals the ability of PEG–HFB–AuNPs to interact with biological molecules better than the original constituents, making them suitable for biomedical applications.

4. Conclusions

In the present work, we showed that hybrid HFB–AuNPs can be synthesized via a simple one step method. The key role of the HFB molecules during the growth process of nanoparticles was investigated by mixing it with dicarboxylic acid-terminated polyethylene-glycol (PEG), as standard surfactants in the synthesis. Stable nanometric hybrid protein–organic–metal NPs have been obtained, with average diameter of 12 nm for PEG. XPS showed that Vmh2 strongly bind to Au core whereas surfactants act as outer shells. Even if engaged within the hybrid complex, HFB can interact with a model protein, BSA, more than a standard organic–metal NP can do. Moreover, interaction of nanoparticles with immunoglobulins wa salso demonstrated. These results open a route to simple, effective, and also green chemistry synthesis of a new class of hybrid multipurpose NPs which will be tailored for different biomedical application, such as sensing, drugs targeting and delivering.

Appendix A. Supplementary data

Supplementary data associated with this article can be found, in the online version, at http://dx.doi.org/10.1016/j.colsurfb.2015.09.021.

References

[1] Y. Xia, Y. Xiong, B. Lim, S.E. Skrabalak, Angew. Chem. Int. Ed. 48 (1) (2009) 60.
[2] E.E. Bedford, J. Spadavecchia, C.-M. Pradier, F.X. Gu, Macromol. Biosci. 12 (2012) 724.
[3] C.X. Song, V. Labhasetwar, H. Murphy, X. Qu, W.R. Humphrey, R.J. Shebuski, R.J. Levy, J. Controlled Release 43 (1997) 197.
[4] N. Reum, C. Fink-Straube, T. Klein, R.W. Hartmann, C.M. Lehr, M. Schneider, Langmuir 26 (22) (2010) 16901.
[5] N. Li, P. Zhao, D. Astruc, Angew. Chem. Int. Ed. 53 (7) (2014) 1756.
[6] T. Sakai, P. Alexandridis, Langmuir 21 (17) (2005) 8019.
[7] C.A. Smith, C.A. Simpson, K. Ganghyeok, C.J. Carter, D.L. Feldheim, ACS Nano 7 (5) (2013) 3991.
[8] R.K. Gangwar, V.A. Dhumale, D. Kumari, U.T. Nakate, S.W. Gosavi, R.B. Sharma, S.N. Kale, S. Datar, Mat. Sci. Eng. 32 (8) (2012) 2659.
[9] B.G. Yu, T. Okano, K. Kataoka, G. Kwon, J. Controlled Release 53 (1–3) (1998) 131.
[10] G. Park, D. Seo, I.S. Chung, H. Song, Langmuir 29 (44) (2013) 13518.
[11] J. Spadavecchia, R. Perumal, A. Barras, J. Lyskawa, P. Woisel, W. Laure, C.M. Pradier, R. Boukherroub, S. Szunerits, Analyst 139 (2014) 157.
[12] J. Spadavecchia, E. Apchain, M. Albéric, E. Fontan, I. Reiche, Angew. Chem. Int. Ed. 53 (2014) 1–5.
[13] J. Vuola, H. Gçransson, T. Bçhling, S. Asko-Seljavaara, Biomaterials 17 (1996) 1761–1766.
[14] X. Duan, H. Sheardown, Biomaterials 27 (2006) 4608–4617.
[15] H.A. Wösten, K. Scholtmeijer, Appl. Microbiol. Biotechnol. 99 (4) (2015) 1587–1597.
[16] I. Rea, P. Giardina, S. Longobardi, F. Porro, V. Casuscelli, I. Rendina, L. De Stefano, J. R. Soc. Interface 9 (75) (2012) 2450.
[17] H.A. Wösten, M.L. de Vocht, Biochim. Biophys. Acta (BBA)-Rev. Biomembr. 1469 (2) (2000) 79–86.
[18] M.B. Linder, Curr. Opin. Colloid. Interface Sci. 14 (5) (2009) 356–363.
[19] A. Calio, I. Rea, J. Politi, P. Giardina, S. Longobardi, L. De Stefano, J. Appl. Phys. 114 (13) (2013) 134904.
[20] A. Armenante, S. Longobardi, I. Rea, L. De Stefano, M. Giocondo, A. Silipo, A. Molinaro, P. Giardina, Glycobiology 20 (5) (2010) 594.
[21] M. Ballero, E. Mascia, A. Rescigno, E.S. Teulada, Micol. Ital. 19 (1990) 39.
[22] M.I. Janssen, M.B.M. van Leeuwen, T.G. van Kooten, J. de Vries, L. Dijkhuizen, H.A.B. Wösten, Biomaterials 25 (14) (2004) 2731.
[23] L.M. Bimbo, E. Mäkilä, J. Raula, T. Laaksonen, P. Laaksonen, K. Strommer, E.I. Kauppinen, J. Salonen, M.B. Linder, J. Hirvonen, H.A. Santos, Biomaterials 32 (34) (2011) 9089–9099.
[24] H.K. Valo, P.H. Laaksonen, L.J. Peltonen, M.B. Linder, J.T. Hirvonen, T.J. Laaksonen, ACS Nano 4 (3) (2010) 1750–1758.
[25] X. Chen, D. Zhao, L.Z. Zhao, Y.L. An, R.J. Ma, L.Q. Shi, Q.J. He, L. Chen, Sci. China Ser. B Chem. 52 (9) (2009) 1372.
[26] K. Holmberg, B. Jonson, B. Kronberg, B. Lindman, Surfactants and Polymers in Aqueous Solution, John Wiley & Sons Ltd. Book, 2002, ISBN: 0-471-49883-1.
[27] L. Castaneda, J. Valle, N. Yang, S. Pluskat, K. Slowinska, Biomacromolecules 9 (12) (2008) 3383.
[28] J. Spadavecchia, J. Moreau, J. Hottin, M. Canva, Sens. Act. B: Chem. 143 (1) (2009) 139.
[29] A.K. Khan, R. Rashid, G. Murtaza, A. Zahra, J. Trop, Pharm. Res. 13 (7) (2014) 1169.
[30] K.G. Neoh, E.T. Kang, Polym. Chem. 2 (2011) 747.
[31] M.S. Yavuz, Y. Cheng, J. Chen, C.M. Cobley, Q. Zhang, M. Rycenga, J. Xie, C. Kim, K.H. Song, A.G. Schwartz, L.V. Wang, Y. Xia, Nat. Mater. 8 (12) (2009) 935–939.
[32] P. Khullar, A. Mahal, V. Singh, T.S. Banipal, G. Kaur, M.S. Bakshi, Langmuir 6 (13 2010) 11363.
[33] S. Hong, K.L. Shuford, S. Park, Chem. Mater. 23 (8) (2011) 2011.
[34] D. Ray, V.K. Aswal, J. Kohlbrecher, Langmuir 27 (7) (2011) 4048.
[35] J. Politi, J. Spadavecchia, M. Iodice, L. De Stefano, Analyst 140 (1) (2015) 149–155.
[36] S. Eustis, M.A. El-Sayed, Chem. Soc. Rev. 35 (2006) 209.
[37] P. Mulvaney, Langmuir 12 (1996) 788.

2.2.2 Glucose interaction monitoring by PEG-HFB AuNPs

The glucose in blood is commonly used as the marker in clinical diagnosis, and its monitoring is important to evaluate the human health condition. In recent years, determination of glucose with nanoparticles has attracted great interest because of their optical properties (Kang et al. 2008). However, most of these methods involving nanoparticles, are also based on enzymes, that can be easily denatured by environmental changes or digested proteases (Moatsou et al. 2008), though some instrumental methods for the detection of glucose with non-enzymatic methods have been developed (Adhikari et al. 2015).

In this work, we exploited the peculiar properties of Vmh2 in order to use it both as stabilizer in one step synthesis and also as active biomolecular probe for glucose interaction monitoring.

Bioconjugation of Enzymes and Proteins on Multifunctional and Nanostructured Solid Supports for Biomolecular Interactions Monitoring

Page 1 of 17   CONFIDENTIAL - AUTHOR SUBMITTED MANUSCRIPT draft

One-Pot Synthesis of Gold Nanoparticles-Vmh2 Hydrophobin Nanobiocomplex for Glucose Monitoring

Jane Politi[1,3,4*], Luca De Stefano[3], Ilaria Rea[3], Alfredo Maria Gravagnuolo[4], Paola Giardina[4], Christophe Methivier[1], Sandra Casale[1,2], Jolanda Spadavecchia[1,2*]

[1]Sorbonne Universités, UPMC Paris 06, Laboratoire de Réactivité de Surface, 4 place Jussieu, F-75005 Paris, France.

[2] CNRS, UMR 7244, CSPBAT, Laboratoire de Chimie, Structures et Propriétés de Biomateriaux et d'Agents Therapeutiques Université Paris 13, Sorbonne Paris Cité, Bobigny, France CNRS, Paris, France

[3]Institute for Microelectronics and Microsystems, Unit of Naples-National Research Council, Via P. Castellino 111, 80127 Italy.

[4]Department of Chemical Sciences, University of Naples « Federico II », Via Cinthia, 80126 Naples Italy.

KEYWORDS

Class I Hydrophobins, Gold nanoparticles, One-step synthesis, Glucose monitoring

Corresponding Authors

* Jane Politi,Via P. Castellino 111, 80127, Naples, Italy,tel +390816132490, fax +390816132598, jane.politi@na.imm.cnr.it

* Jolanda Spadavecchia, 99 avenue Jean-baptiste Clément, 93430, Villetaneuse, tel 33 (0)1 49 40 33 52, fax 33 (0)1 49 40 20 36, jolanda.spadavecchia@univ-paris13.fr

ABSTRACT

The hydrophobinVmh2 is a small amphiphilic protein, which self-assembles on different surfaces and naturally interacts with glucose. Here, we report on the synthesis of a nanobiocomplex made of

polyethylene glycol, Vmh2 and gold nanoparticles by one-step process and on its ability to

recognise glucose in aqueous solution at 0.3-0.6-1.2 mg/mL concentrations. Even though the Vmh2

proteins are intrinsically bonded to the gold core, an effective glucose interaction monitoring was

demonstrated by using Dynamic Light Scattering (DLS), ultraviolet-visible (UV-Vis), Polarization-

Modulated Infrared Reflection–Absorption (PM-IRRAS) and X-ray Photoelectron (XPS)

Spectroscopies. Experimental results highlighted an affinity constant of 7.3±0.3 mg/mL between the

nanobiosystem and the sugar, and a detection sensitivity of 0.13 ± 0.06 a.u./mg mL^{-1}.

1. Introduction

Hydrophobins (HFBs) are small proteins of about 100 amino acid residues, produced by fungi, able

to self-assemble into an amphipathic membrane at interfaces such as water-air or solid-water. HFBs

have been classified into two groups, namely class I and class II. Class I HFB forms insoluble

assemblies and rodlets, which can only be dissolved in strong acids, i.e. 100% trifluoroacetic acid

(TFA). Assemblies of class II can be easily dissolved in ethanol or sodium dodecyl sulfate (SDS).

The intriguing properties of these proteins make them of great interest to biotechnologists, as they

have potentialities for many applications [1-3]. It has been observed that some class I HFBs interact

with sugars produced by the same fungus to stabilize small multimers in aqueous solution, or to

promote HFB interaction with interfaces. The HFB Vmh2 from *Pleurotus Ostreatus*, an edible

fungus common in Mediterranean diet, cannot be solubilized in polar acid solution. We have found

that when Vmh2 is mixed with sugars, its solubility increases: these proteins form complexes with

sugars, even if they seem to do not have a specific binding site for these small molecules, and this

bond strongly affects structure and behavior of Vmh2, both in solution and on solid surface [4].

Glucose plays a crucial role in life processesas a direct energy source facilitating various biological

activities [5]. The glucose detection in blood is commonly used as the marker in clinical diagnosis,

and its monitoring is important to evaluate the human health condition. In recent years,

determination of glucose with nanoparticles has attracted great interest because of their optical

properties [6]. However, most of these methods involving nanoparticles, are also based on enzymes, that can be easily denatured by environmental changes or digested proteases [7, 8], though some instrumental methods for the detection of glucose with non-enzymatic methods have been developed [9]. Metallic nanostructures have been studied extensively and are emerging as colorimetric reporters due to their high extinction coefficients, which are typically several orders of magnitude larger than those of organic dyes [10]. In particular, nanostructures made of noble metals, such as those of silver or gold, show strong plasmon resonance, which can be seen by naked eyes [11]. Gold nanoparticles display plasmon absorption bands that depend on their size and shape [12]. Cluster formation results in color changes of gold nanoparticle solutions due to mutually induced dipoles that depend on interparticle distance and aggregate size. Gold nanoparticle aggregation on exposure to several analytes has been demonstrated for DNA, metal ions and antibodies [13, 14].

Recently, we demonstrated a novel route to nanoparticles synthesis that takes advantage of using bioprobe during the production process together with stabilizers [15]. In this work, we exploited the peculiar properties of Vmh2 in order to use it both as stabilizer in one step synthesis and also as active biomolecular probe for glucose interaction monitoring. Synthesis and interaction monitoring were characterized by several analytical and imaging techniques such as Dynamic Light Scattering (DLS), Transmission Electron Microscopy (TEM), UltraViolet-Visible (UV-Vis) spectroscopy, Polarization-Modulated Infrared Reflection–Absorption Spectroscopy (PM-IRRAS) and X-ray Photoelectron Spectroscopy (XPS).

2. Experimental

2.1. Chemicals

All chemicals were reagent grade or higher and were used as received unless otherwise specified. Tetrachloroauric acid ($HAuCl_4$), sodium borohydride ($NaBH_4$), PolyEthyleneGlycol 600 Diacid (PEG), N-hydroxysuccinimide (NHS), 1-(3-dimethylaminopropyl)-N'-ethylcarbodiimide hydrochloride (EDC), PBS 0.1 M pH 7, trifluoroacetic acid (TFA), Sodium Dodecyl Sulfate (SDS),

methanol (CH_3OH), chloroform ($CHCl_3$) and ethanol (C_2H_5OH) were purchased from Sigma Aldrich.

2.2. Preparation of Vmh2

White-rot fungus, *P. ostreatus* (Jacq.: Fr.) Kummer (type: Florida; ATCC No. MYA-2306) was maintained through periodic transfer at 4 °C on potato dextrose agar (Difco) plates in the presence of 0.5% yeast extract. Mycelia were inoculated in 2 L flasks containing 500 mL of potato-dextrose broth (24 g/L) supplemented with 0.5% yeast extract, grown at 28 °C in shaken mode (150 rpm). After 10 days of fungal growth, mycelia were separated by filtration through gauze, treated twice with 2% SDS in a boiling water bath for 10 min, washed several times with water and once with 60% ethanol to completely remove the detergent. The residue was dried under nitrogen, grinded and treated with 100% trifluoroacetic acid (TFA) in a water bath sonicator (BandelinSonorexDigitec) for 10 min. The supernatant was dried, dissolved in 60% ethanol and centrifuged (10 min at 3200 g). The new supernatant was lyophilized, and lipids were extracted in a mixture of water-methanol-chloroform 4:4:1 v/v (5 min in bath sonicator). After centrifugation, proteins appeared as a solid aggregate at the interface. They were recovered by upper phase removal, methanol addition and centrifugation. The precipitate was again dried, treated with TFA for 30 min in bath sonicator, re-dried, dissolved in 60% ethanol and centrifuged (90 min at 12000g).

2.3. Synthesis of PEG-Gold Nanoparticles (PEG-AuNPs) and PEG-Hydrophobin-Gold Nanoparticles (PEG-HFB-AuNPs)

PEG-AuNPs synthesis was previously reported and discussed [16]. Briefly, 1mL of PEG 600 Diacid solution and 25 mLof 0.0001M aqueous $HAuCl_4$ solution were mixed under stirring at room temperature. After 10 min, 600μl of $NaBH_4$(0.01M) were added drop-wise followed by rapid stirring and kept without agitation for 2h. The solution obtained resulted red-rose. Details of PEG-HFB-AuNPs synthesis can be found in ref. [15]. Briefly, 2ml of Polyethylene glycol 600 Diacid (PEG) solution were mixed with 5 ml of HFB (150μg/mL) solution and 5 ml of 0.0001M aqueous $HAuCl_4$solution under stirring at room temperature. After 10 min, 1.2 ml of $NaBH_4$ (0.01M) were

added drop-wise followed by rapid stirring and kept without agitation for 2h. The solution obtained resulted purple.

2.4. Interaction monitoring of PEG-AuNPs and PEG-HFB-AuNPs with glucose aqueous solution

1 mL of PEG-AuNPs and PEG-HFB AuNPs was mixed to 50µL of glucose aqueous solution at concentrations of 0.3-0.6-1.2mg/mL and the Localised Surface Plasmon (LSP) change as function of time was monitored by UV-Vismeasurements until saturation was achieved. Further investigation was performed by PM-IRRAS measurementsas described in the following.

2.5. Instrumentations

2.5.1. Transmission electron microscopy (TEM)

Transmission electron microscopy measurements were recorded on a JEOL JEM 1011 microscope operating at an accelerating voltage of 100 KV. The TEM graphs were taken after separating the surfactant from the metal particles by centrifugation. Typically 1mL of the sample was centrifuged for 20 min at a speed of 14000 rpm/min. The upper part of the colorless solution was removed and the solid portion was re-dispersed in 1 ml of water. A droplet (10 µL) of the colloidal solution was deposited on a microscope grid and analyzed.

2.5.2. Dynamic light scattering (DLS)

The size evaluation of each kind of nanoparticles was performed by dynamic light scattering (DLS). A Zetasizer Nano ZS instrument (Malvern Instruments, Malvern, UK) equipped with a He-Ne laser (633 nm, fixed scattering angle of 173°, room temperature 25°C) was used.

2.5.3. UV-Vis spectroscopy

Absorption spectra were recorded using a Jasco V-570 UV/VIS/NIR Spectrophotometer from Jasco Int. Co. Ltd., Tokyo, Japan in the 200-800 nm range. Each solution wasanalyzed as synthesized and after interaction with glucose until the absorbance was stationary.

2.5.4. PM-IRRAS

PM-IRRAS spectra were recorded on a commercial Thermo (Les Ulis-France) Nexus spectrometer. The external beam was focused on the sample with a mirror, at an optimal incident angle of 80°. A ZnSe grid polarizer and a ZnSe photoelastic modulator, modulating the incident beam between *p*- and *s*-polarizations (HINDS Instruments, PEM 90, modulation frequency = 37 kHz), were placed prior to the sample. The light reflected at the sample was then focused onto a nitrogen-cooled MCT detector. The presented spectra result from the sum of 128 scans recorded at 8 cm^{-1} resolution. Chemical procedures, based on self-assembling monolayers (SAMs) of β-mercaptoethylamine (cysteamine) in absolute ethanol, have been described previously [17]. Briefly the freshly cleaned gold substrate was immersed in an unstirred 10 mM ethanol solution of cysteamine at room temperature, in the dark, for 6h. The gold substrate was then washed with ethanol and milli Q water to remove the excess of thiol. 2 ml of PEG-HFBAuNPs were dissolved in 2 ml of buffer solution (PBS pH 7), in which ½ eq of EDC/NHS was added, and stirred for 2h (pre-activation). The colloidal solution was deposited on cysteamine–gold-coated surface for 12h at room temperature under stirring condition, and finally the acquisition was performed. Each PM-IRRAS datapoint is the average of three measurements.

2.5.5. X-ray photoelectron spectroscopy (XPS)

XPS analyses were performed using a SPECS (Phoibos MCD 150) spectrometer (SPECS, Germany) equipped with a monochromatized Al X-ray source (*hv* = 1486.6 eV) and a Phoibos 150 hemispherical energy analyzer. Pass energies of 20 eV was used for the survey scan, and 10 eV for narrow scans.

3. Results and Discussions

It is well known by farthat PEG-derivedA uNPs have an increased stability in aqueous and biological media with respect to simple gold nanoparticles [18]. In our recent paper, we demonstrated an innovative synthesis of hybrid nanoparticle, which main aim was to improve AuNPs biocompatibility, by partially replacing PEG with Vmh2, but also add functionality to the nanocomplex, by exploiting properties of thishydrophobin [15]. The same scheme of the reaction

55

Bioconjugation of Enzymes and Proteins on Multifunctional and Nanostructured Solid Supports for Biomolecular Interactions Monitoring

Page 7 of 17   CONFIDENTIAL - AUTHOR SUBMITTED MANUSCRIPT draft

1
2
3
4
5
6
7
8
9
10
11
12
13
14
15
16
17
18
19
20
21
22
23
24
25
26
27
28
29
30
31
32
33
34
35
36
37
38
39
40
41
42
43
44
45
46
47
48
49
50
51
52
53
54
55
56
57
58
59
60

was adopted for both the systems: PEG-AuNPs and PEG-HFB-AuNPs were obtained by reducing tetrachloroauric acid ($HAuCl_4$) with sodium borohydride ($NaBH_4$) in presence of the organic stabilizers. Nanoparticles formation and growth can be schematized as follow (**Figure 1**): in case of PEG-AuNPs, gold clusters formation was facilitated by PEG stabilizer, since it promoted, as long as the reaction proceeded, the growth and the colloidal stabilizationof gold particles; while in case of PEG-HFB-AuNPs, there was firstly a pre-synthesis complex formation between PEG and HFBs, then gold clusters formation started and growth of nanoparticles could complete [15]. TEM and DLS characterizations (reported in **Figure 2**) revealed nanoparticles average sizes of about 8 ± 3 nm and 10 ± 5 nm with a polydispersion index of 0.2 ± 0.1 and 0.3 ± 0.1 for PEG AuNPs and PEG-HFB-AuNPs, respectively. The characterizations reported in ref. [15] demonstrated that the new metal-protein nanobiocomplex had really a hybrid nature, since the Vmh2 did not simply cover the gold core nor it was bound to polymer ends, but it was intimately engaged with both hard and soft phases (gold and PEG, respectively) in forming a single nanobiosystem.

On the other side, we recently studied the ability of Vmh2 to interact with glucose both in aqueous solution and after self-assembling onto nanostructured materials [19, 4], so that the aim of the present study concerned the evaluation of PEG-HFB-AuNPs ability to still interact with glucose molecules, even though the Vmh2 protein wasmerged with gold-PEG core.

Figure 3 (A, B and C) represents how UV-Vis spectra of PEG-HFB-AuNPs changed on exposure to different concentrations of glucose solutions (0.3-0.6-1.2 mg/mL, respectively). The absorbance of the localized surface plasmon (LSP) at 550nm decreased as function of time during the interaction with glucosefor all concentration tested. The LSP absorbance is stable after 360 minutes. The LSP signal was also normalizedto its value at 550nm, which took into account aggregation phenomena due to interaction with glucose molecules, and a dose-response behavioras function of glucose concentration (**Figure 3 D**) was detected. Theexperimental data points could be fitted by using OriginLab Software ™ Michaelis-Mentens exponential equation (1):

$$y = \Delta A_{max} \frac{[Glucose]}{K_m + [Glucose]} \ (1)$$

56

where ΔA_{max} is the saturation point; K_m is affinity constant; *[Glucose]* is glucose concentration. From this equation, we got a system affinity constant of 7.3 ± 0.3 mg/mL, which corresponded to about 40 mM, and a sensitivity in glucose monitoring ability of 0.13 ± 0.06 a.u./mg mL^{-1} (calculated in the linearity range of system response).

Figure 4 A shows the overlapped PM-IRRAS spectra of HFB, PEG AuNPs and PEG-HFB AuNPs. Vmh2 spectrum (**Figure 4 A black curve**) showed absorption band at 1670 cm^{-1} due to amide I (C=O) and 1550 cm^{-1}due to amide II. The peaks at 1460 and 1250 cm^{-1} are typical of the stretching mode of carboxylic groups (υC-O). PEG-AuNPs (**Figure 4 A blue curve**) revealed a band at 1115 cm^{-1} due to C–O–C of the PEG polymer. In PEG-HFB-AuNPs spectrum (**Figure 4 A red curve**) the presence of a peak in the region 1730 cm^{-1} due to carbonyl bonds was detected. It should be noted the PM-IRRAS signal was much stronger (about three times then HFB one) in case of PEG-HFB-AuNPs spectrum, due to the coupling of infrared radiation to the LSP of gold surface. On exposure to glucose, a variation of 1250 cm^{-1} peak area could be quantified for different concentration of the sugar. **Figure 4 B** shows the values of 1250cm^{-1} peak area of PEG-HFB-AuNPs PM-IRRAS spectrum at 0.3-0.6-1.2mg/mL glucose concentrations, fitted by OriginLab Software ™linear curve model. In this case, the sensitivity, calculated as the inverse of the slope, was equal to 0.14 ± 0.01 a.u./mgmL^{-1}, very close to that calculated by elaboration of UV-Vis data. These results demonstrated that PEG-HFB-AuNPs preserved the ability of Vmh2in glucose binding even if engaged in the formation of the hybrid nanosystem.

DLS measurements after interaction with glucose molecules shaded light on the mechanism of nanoparticle aggregationdue to sugar binding (**Figure 5 A and B**). The results highlighted again that only in case of PEG-HFB-AuNPs a size change occurred, revealing an aggregation behavior such as the one schematized in **Figure 5 C**: their size changed from 14 ± 2 nm to 47 ± 7 nm. Further investigations were performed using XPS measurements comparing PEG-HFB-AuNPs before and after interaction with glucose molecules (**Figure 6**). As showed by binding energy variation, the presence of glucose molecules partially fencedthe peak of N 1s @100eV, and also COOH and

Bioconjugation of Enzymes and Proteins on Multifunctional and Nanostructured Solid Supports for Biomolecular Interactions Monitoring

Page 9 of 17   CONFIDENTIAL - AUTHOR SUBMITTED MANUSCRIPT draft

O=C-N contribution @289.2 eV. On the other hand, CO signal @286.5eV showed an increasing in binding energy, confirming thePM-IRRAS data, so that Vmh2-glucose interaction was transduced in a CO peak increase. CH contribution @284.9eV was reasonably more intense after glucose molecules interaction, while Au 4f @83.9eVwas decreased probably due to a rearrangement of Vmh2 that produced a fencing of gold core.

4. Conclusion

In the present work, PEG-HFB-AuNPs were employed in preliminary study of glucose monitoring platforms development. Vmh2 class I HFB from *P.ostreatus* were used as both stabilizer and active biomolecular probe in glucose interaction monitoring nanobiosystem development. All experimental results highlighted thatVmh2 gave ability to PEG-HFB-AuNPs to bind glucose also if intrinsically engaged with gold core. Aggregation behaviour was proved by DLS measurements and glucose interaction, as CO and CH signal enhancing, was proved by PM-IRRAS and XPS spectroscopies. In conclusion, a novel hybrid bio/non-bio nanosystem was developed for both interface stabilization and biomolecular interaction monitoring applications.

Author Contributions

The manuscript was written through contributions of all authors. All authors have given approval to the final version of the manuscript.

References

[1]. Gravagnuolo, A. M.; Morales Narváez, E.; Matos, C. R. S.; Longobardi, S.; Giardina, P.; Merkoçi, A.; On the Spot Immobilization of Quantum Dots, Graphene Oxide, and Proteins via Hydrophobins. *Advanced Functional Materials*, **2015**, *25*, 6084-6092.

[2]. Gravagnuolo, A. M.; Morales-Narváez, E., Longobardi, S.; da Silva, E. T., Giardina, P.; Merkoçi, A.; In Situ Production of Biofunctionalized Few-Layer Defect-Free Microsheets of Graphene. *Advanced Functional Materials*, **2015**, *25*, 2771-2779.

[3]. Longobardi, S.; Gravagnuolo, A. M.; Funari, R.; Della Ventura, B.; Pane, F.; Galano, E.; Giardina, P; A simple MALDI plate functionalization by Vmh2 hydrophobin for serial multi-enzymatic protein digestions. *Analytical and Bioanalytical Chemistry*, **2015**, *407*, 487-496.

[4].   Armenante, A.; Longobardi, S.; Rea, I.; De Stefano, L, Giocondo, M; Silipo, A; Giardina, P.; The Pleurotusostreatus hydrophobin Vmh2 and its interaction with glucans. *Glycobiology* **2015**, 20, 594-602.

[5].   Quesada, I.; Tudurí, E.; Ripoll, C.; Nadal, Á; Physiology of the pancreatic α-cell and glucagon secretion: role in glucose homeostasis and diabetes. *Journal of Endocrinology* **2008**, 199, 5-19.

[6].   Kang, X.; Mai, Z.; Zou, X.; Cai, P.; Mo, J.; Glucose biosensors based on platinum nanoparticles-deposited carbon nanotubes in sol–gel chitosan/silica hybrid. *Talanta*, **2008**, *74*, 879-886.

[7].   Iyer, P. V.; Ananthanarayan, L.; Enzyme stability and stabilization—aqueous and non-aqueous environment. *Process Biochemistry* **2008**, 43, 1019-1032.

[8].   Moatsou, G.; Bakopanos, C.; Katharios, D.; Katsaros, G.; Kandarakis, I.; Taoukis, P.; Politis, I.; Effect of high-pressure treatment at various temperatures on indigenous proteolytic enzymes and whey protein denaturation in bovine milk. *Journal of dairyresearch* **2008**, 75, 262.

[9].   Adhikari, B.R.; Govindhan, M.; Chen, A.; Carbon Nanomaterials Based Electrochemical Sensors/Biosensors for the Sensitive Detection of Pharmaceutical and Biological Compounds *Sensors* **2015**, *15*, 22490-22508.

[10].   Labande, A.; Astrue, D.; Colloids as redox sensors: Recognition of H_2PO_4- and HSO_4 by amidoferrocenylalkylthiol-gold nanoparticles. *Chem. Commun.* **2000**, 12, 1007–1008.

[11].   Jin, X.; Li, M.; Wang, J; Marambio-Jones, C.; Peng, F.; Huang, X.; Damoiseaux, R.; Hoek E. M. V. High-Throughput Screening of Silver Nanoparticle Stability and Bacterial Inactivation in Aquatic Media: Influence of Specific Ions. *Environ. Sci. Technol.* **2010**, 44, 7321−7328.

[12].   Spadavecchia, J.; Perumal, R.; Barras, A.; Lyskawa, J.; Woisel, P.; Laure, W.; Pradier, C.-M.; Boukherroub, R.; Szunerits, S.; Amplified plasmonic detection of DNA hybridization using post-labeling with doxorubicin-capped gold particles. *Analyst* **2014**, 139, 157–164.

[13].   Reynolds, R.A.; Mirkinm, C.A.; Letsinger, R.L.; Homogeneous, Nanoparticle-Based Quantitative Colorimetric Detection of Oligonucleotides *J. Am. Chem. Soc.* **2000**, 122 3795.

[14].   Politi, J.; Spadavecchia, J.; Iodice, M.; De Stefano, L.; Oligopeptide-heavy metal interaction monitoring by hybrid gold nanoparticles based assay, *Analyst*, **2015**, 140, 149-155.

[15].   Politi, J., De Stefano, L.; Longobardi, S.; Giardina, P.; Rea, I.; Methivier, C.; Pradier, C.-M.; Casale, S.; Spadavecchia, J. The amphiphilic hydrophobin Vmh2 plays a key role in one step synthesis of hybrid protein–gold nanoparticles. *Colloids and Surfaces B: Biointerfaces* **2015**, 136, 214-221.

[16].   Spadavecchia, J.; Perumal, R.; Casale, S.;Kraftt, J.M.; Methivier, C.; Pradier, C.-M.; Polyethylene glycol Gold-Nanoparticles: Facile Nanostructuration of Doxorubicin and its complex with DNA molecules for SERS detection. *Chemical Physics Letters* **2015**.

[17].   Spadavecchia, J.; Moreau, J.; Hottin, J.; Canva, M., New cysteamine based functionalization for biochip applications. *Sensors and Actuators B: Chemical* **2009**, 143, 139-143.

[18].   Gee, N. K.; Kang, E. T.; Functionalization of inorganic nanoparticles with polymers for stealth biomedical applications. *Polymer Chemistry* **2011**, 2, 747-759.

[19].   Caliò, A.; Rea, I.; Politi, J.; Giardina, P.; Longobardi, S.; De Stefano, L.; Hybridbio/non-biointerfaces for protein-glucose interaction monitoring. *Journal of Applied Physics* **2013**, 114, 134904.

FIGURES
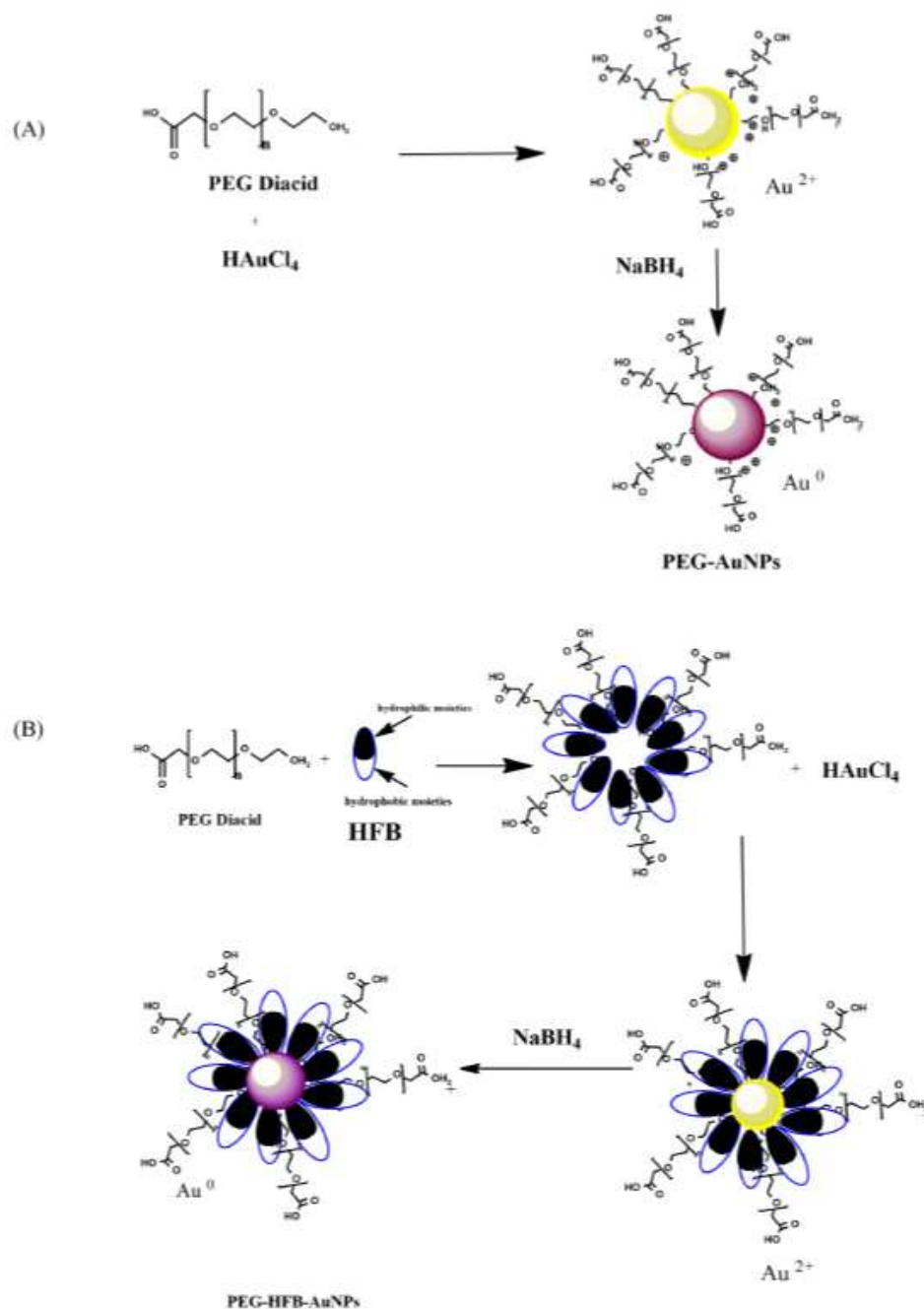
Figure 1. Schematization of gold nanoparticles synthesis in presence of only PEG diacid as surfactant (A) and in the presence of both PEG diacid and HFBs as surfactants (B).

Bioconjugation of Enzymes and Proteins on Multifunctional and Nanostructured Solid Supports for Biomolecular Interactions Monitoring

Page 13 of 17   CONFIDENTIAL - AUTHOR SUBMITTED MANUSCRIPT draft

1
2
3
4
5
6
7
8
9
10
11
12
13
14
15
16
17
18
19
20
21
22
23
24
25
26
27
28
29
30
31
32
33
34
35
36
37
38
39
40
41
42
43
44
45
46
47
48
49
50
51
52
53
54
55
56
57
58
59
60
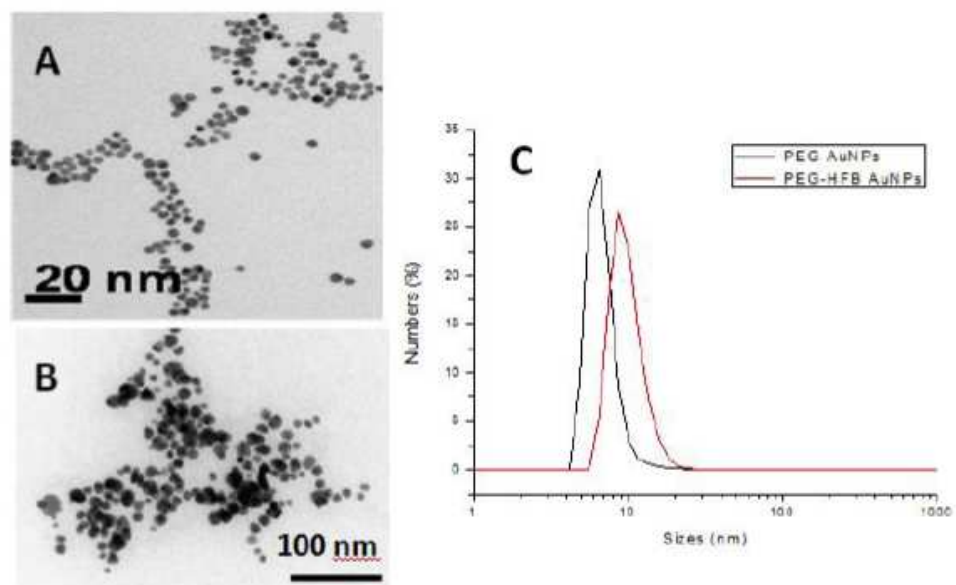
Figure 2.TEM images of PEG-AuNPs(A) andPEG-HFB-AuNPs(B)with correspondent size data obtained by DLS characterization(C).
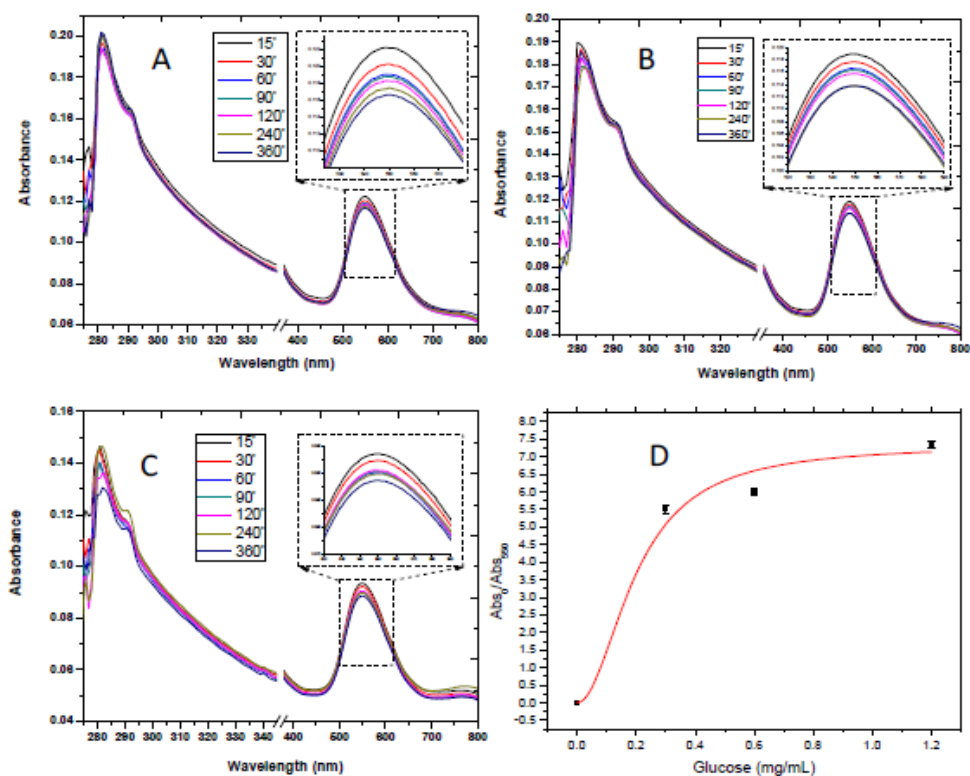
Figure 3. UV-Vis spectra of PEG-HFB-AuNPs interaction with glucose molecules at 0.3 mg/mL (A), 0.6 mg/mL (B), 1.2 mg/mL (C) as function of time and trend of PEG-HFB-AuNPs LSP at 550nm after 360minutes of interaction with glucose as function of solutions concentration normalized with respect to the same LSP before interaction (D).

Bioconjugation of Enzymes and Proteins on Multifunctional and Nanostructured Solid
Supports for Biomolecular Interactions Monitoring

Page 15 of 17
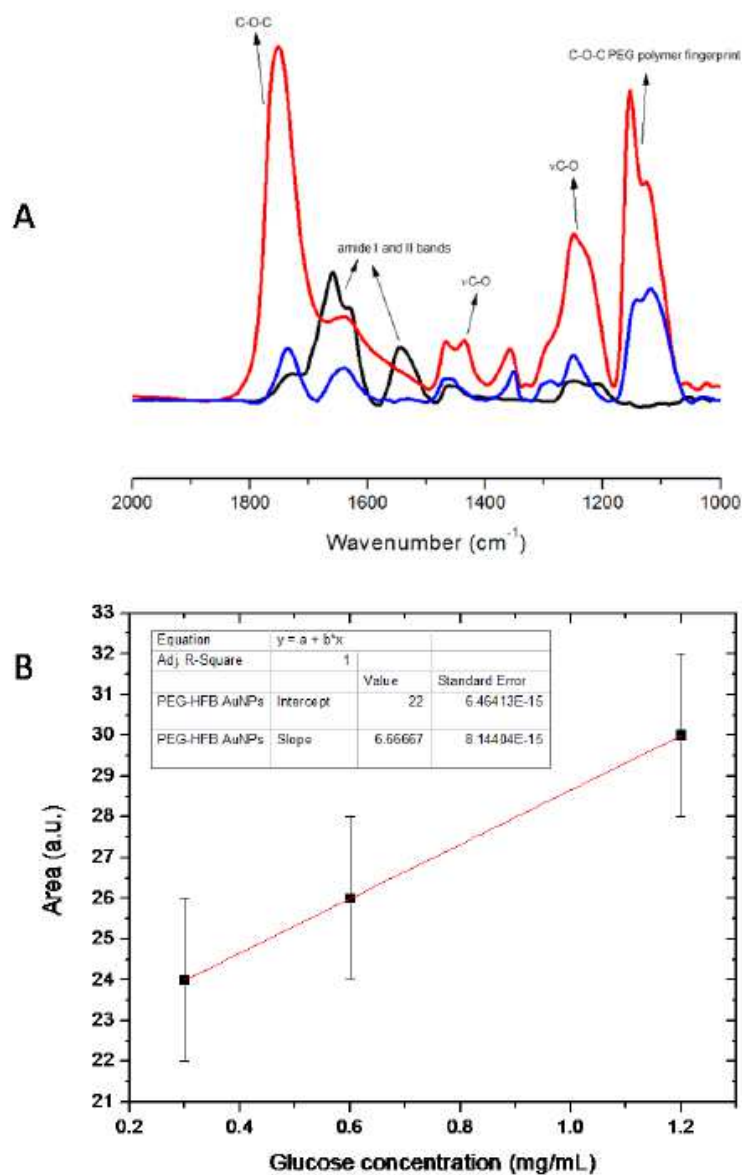
Figure 4. PM-IRRAS spectra of PEG-HFB-AuNPs (red line), PEG-AuNPs(blue line) and HFB
(black line) (A); area of peak @1250 cm^{-1} as a function of glucose concentration (B).
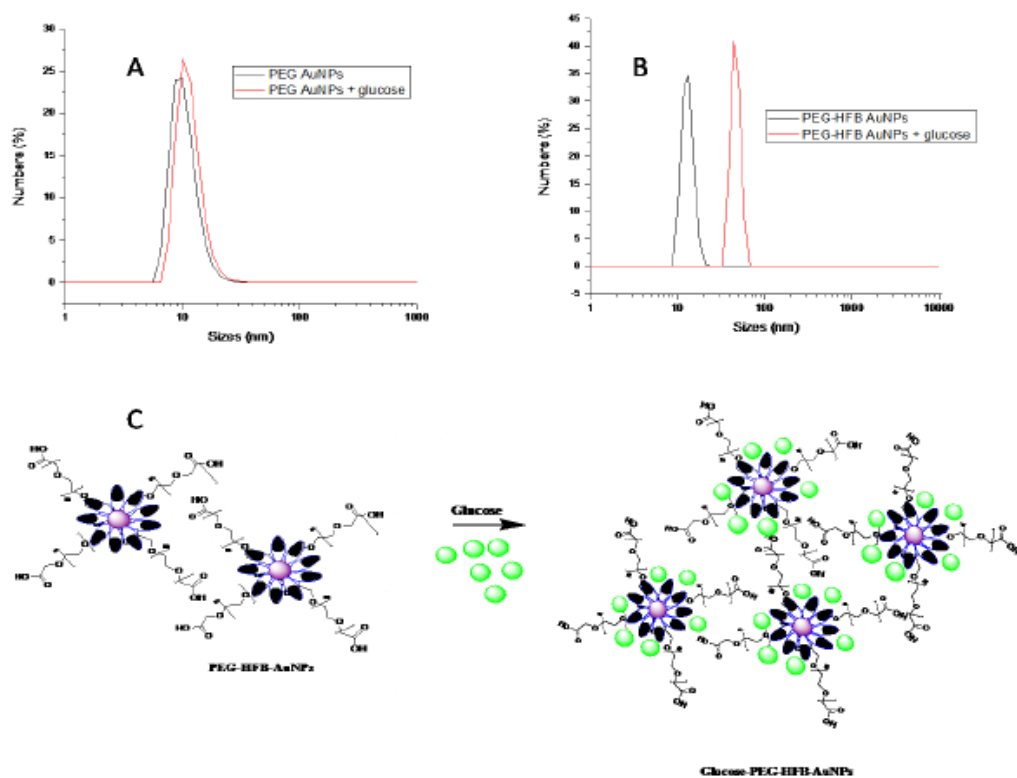
Figure 5. DLS measurements of PEG-AuNPs before and after glucose interaction (A), PEG-HFB-AuNPs before and after glucose interaction (B) and schematization proposed of nanoparticles-glucose interaction (C).

65
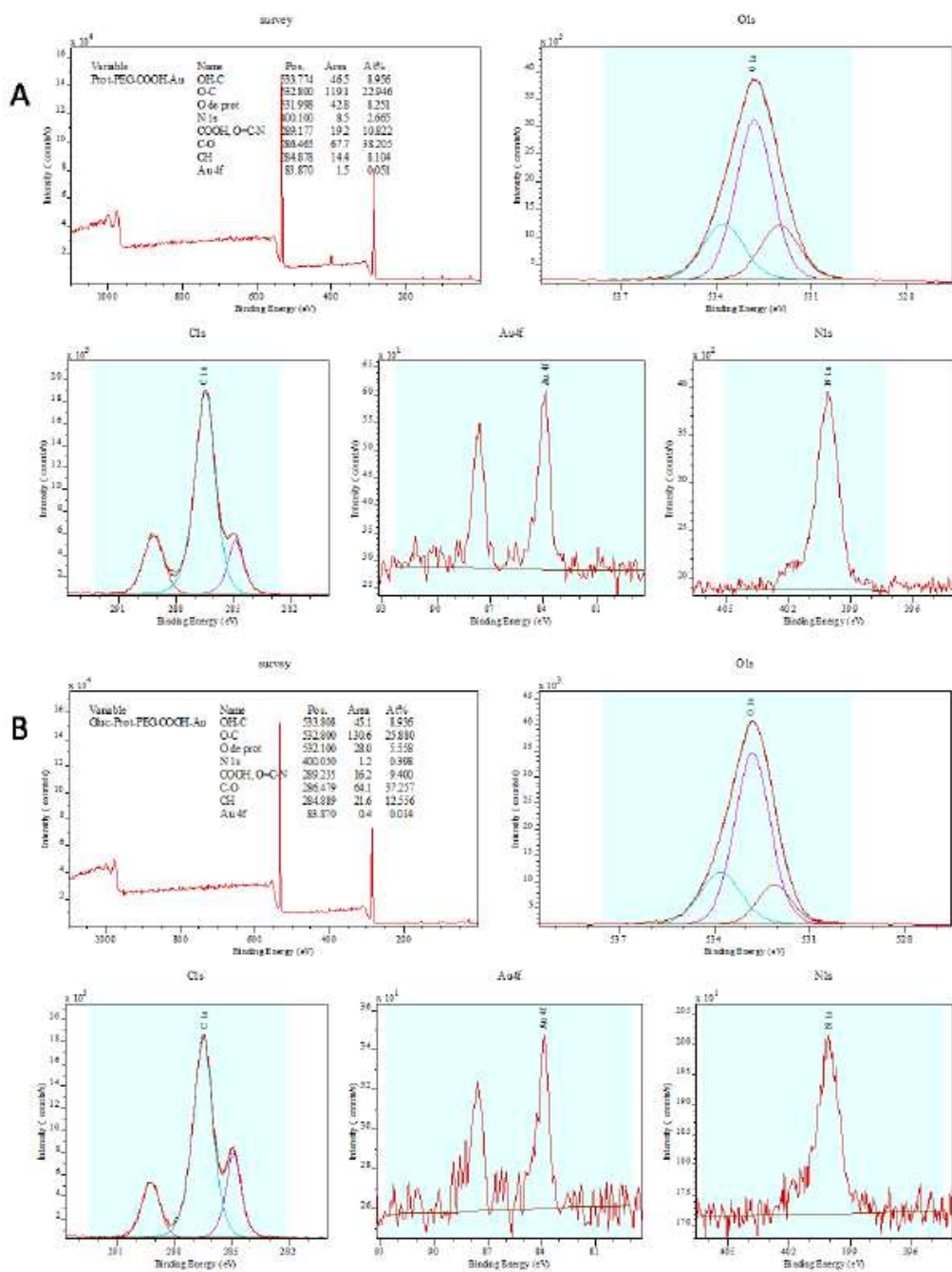
Figure 6. XPS spectra of PEG-HFB-AuNPs (A) and Glucose/PEG-HFB-AuNPs (B).

2.2.3 Synthesis and application of gold nanorods

Since their debut on the materials science scene, gold nanorods (AuNRs) attracted enormous interest in very different fields spanning from theoretical physics to applied medicine: AuNRs are actually powerful tools for probing plasmon propagation model in nano-optics; innovative elements in biomedical imaging, and even therapeutical agents in hyperthermia based therapies. The surface, for example an electrode or any other transducer material, receiving the nanoparticles can be prepared in order to enhance some specific properties with respect to others by a large amount of chemical or physical treatments such as wet functionalization, pre-patterning and any lithographic methods. The seeding-growth procedure is another popular technique that has been used for a century. Recent studies have successfully led to control of the size distribution (typically 10-15%) in the range 5-40 nm, whereas the sizes can be manipulated by varying the ratio of seed to metal salt. The step-by-step particle enlargement is more effective than a one-step seeding method to avoid secondary nucleation. Gold nanorods (AuNRs) have been conveniently fabricated using the seeding-growth method. Finally, sensing properties of AuNPs and AuNRs as as novel tools in perspective nanosciences and nanotechnology will be discussed.

Among others, the self-assembling monolayers (SAMs) offer the possibility to modify any kind of surface with a plethora of terminal functions, which can bind any type of ligands by covalent, ionic or hydrogen interactions (Lee et al. 2003). In the following paper, we have implemented, and evaluated for sensing application, a simple and reproducible chemical procedure for gold nanorods immobilization by an original functionalization of gold surface: the aim is obtaining a quasi-ordered surface of AuNRs covalently bound to a gold surface that could be used for antigen/antibody biorecognition by surface plasmon resonance (SPR) measurements.

In particular, will be showed the ability of novel hybrid nanobiosystem called PEG-HFB AuNPs to interact with BSA, antibodies and glucose molecules, and then AuNRs ability to interact with PSA and anti-PSA after a proper covalent organization onto gold planar surfaces.

Research Article   **Open Access**

Original Covalent Approach for Gold Nanorods Immobilization onto Acid-Terminated-Cysteamine Self-Assembled Monolayers for FT-SPR Biosensor Applications

Politi J[1,2], De Stefano L[2], Casale S[3] and Spadavecchia J[3,4*]

[1]Department of Chemical Sciences, University of Naples, Italy
[2]Institute for Microelectronics and Microsystems, Unit of Naples-National Research Council, Italy
[3]Laboratoire de Réactivité de Surface, UMR CNRS 7197, Université Pierre and Marie Curie-Paris VI, France
[4]CNRS, UMR 7244, CSPBAT, Laboratoire de Chimie, Structures et Propriétés de Biomateriaux et d'Agents Therapeutiques Université Paris 13, Sorbonne Paris Cité, Bobigny, France CNRS, Paris, France

Abstract

In this paper, we report an original method to immobilize gold nanorods onto mixed self-assembled monolayers (SAMs) of Mercaptoundecanoic Acid (MUA), Mercaptohexanol (MOH) and cysteamine (CYS) onto planar gold surface. Polarization modulation infrared reflection absorption spectroscopy (PM-IRRAS), scanning electron microscopy (SEM) and transmission electron microscopy (TEM) images revealed a remarkable shape and size narrow distribution on well functionalized gold surfaces, as well as a tendency to form linear assemblies after immobilization. The results highlight the good distribution of gold nanorods with an average length of 32.6 ± 0.9 nm and width of 13 ± 1.8 nm, the simplicity of the immobilization procedure of gold nanorods and the interest of using them as labels to enhance the sensitivity of FT-SPR-based sensors. gold nanostructured surface FT-SPR measurements of biorecognition using gold nanorods immobilized onto gold surfaces were performed at various prostatic antigen specific (PSA) concentrations, from 5 mg/L to 0.5 mg/L reaching a system sensitivity of 37 ± 2 cm^{-1}/mgL^{-1}.

Keywords: Gold nanorods; SAMs; FT-SPR; Biosensors

Introduction

Antibody immobilization is an important subject with a variety of purposes such as in diagnostic immunoassays. One of its applications is the immunosensor, a biosensor made by immobilizing an antibody monolayer onto a transducer, a support able to convert signals allowing specific antigen biorecognition, which helps to make the sensor more accurate, precise, and reproducible [1].

The formation of organized monolayers on surface by self-assembling is interesting in an increasing number of fields as surfaces nanostructuration, chemistry, biology and molecular engineering [2,3]. Self-assembling monolayers (SAMs) offer the possibility to modify the terminal functions of thiol-chains to bind any type of ligands by covalent, ionic or hydrogen interactions [4]. Various aspects of surface modification procedures, such as choice of surface material, types of assembling molecules, physical organic properties of the formed layers, have long been studied from pure scientific interest [5]. To date a number of strategies have been adopted to assemble metal/semiconductor nanospheres onto planar surfaces. Some methods include organization of nanospheres via simple solvent evaporation [6], attachment onto SAMs via covalent interactions and by Langmuir-Blodgett (LB) technique [7,8]. Immobilization of nanorods, surprisingly, has not received comparable attention. El Sayed [9] have demonstrated that simple solvent evaporation leads to the organization of gold nanorods into one, two, and three-dimensional structures. Others have recently demonstrated a spontaneous self-assembly of gold nanorods in concentrated solutions to produce liquid crystalline arrays [10]. Most of the above-mentioned methods use either nonspecific interactions [11,12] or specialized techniques for the organization of nanorods onto 2D surfaces. A simple method for programmed assembly of nanorods using covalent interactions is yet to be investigated.

SPR has the potential to be a useful technique due to real-time measurements, simplicity of measurement, and possible on-site testing. One of the most useful applications of AuNPs in SPR sensing is

the improved detection of small molecules. The improvement has been shown using both unlabelled and labelled techniques incorporating spherical AuNPs [13] or Au nanorods [14,15]. FT-SPR is an SPR-derivatized technique based on the coupling between the incident light and the gold surface Plasmon waves. Conversely to "classical" SPR, which measures changes in the angle of minimum reflectivity, FT-SPR is operated at constant angle, and measures changes in the wavenumber corresponding to the minimum of reflectivity [16]. The interface of a Fourier Transform infrared (FT-IR) spectrometer to an SPR setup provides the excitation light energy and readout detecting adsorption at the solid-liquid interface. Measuring changes in reflectivity as a function of the wavenumber, in the near-infrared (NIR) spectral region, the Fourier Transform Surface Plasmon resonance (FT-SPR) instruments provide quantitative information on the refractive index variation, and thus on molecular binding on a functionalized gold surface [17].

Prostate Specific Antigen (PSA) is prostate cancer marker [18]. In order to early diagnose the prostate cancer in men, studies on development of an ultra-sensitive diagnostic tool are currently performing [19]. Dedicated centralized laboratories use large, automated analyzers, requiring sample transportation, increasing

*Corresponding author: Spadavecchia J, Laboratoire de Réactivité de Surface, UMR CNRS 7197, Université Pierre and Marie Curie–Paris VI, Site d'Ivry–Le Raphaël, 94200 Ivry-sur-Seine, France, Tel : 33 4 37 42 35; E-mail: jolanda.spadavecchia@upmc.fr

waiting times and medical costs for PSA detection. Near-patient or point-of-care testing (POCT) are needed in order to reduce the number of clinic visits, decrease costs to the patient and the healthcare system, increase patient satisfaction and improve clinical outcome. Biosensor development, based on nanoparticles and nanostructures integrating on different devices, have brought POCT for PSA detection closer to reality. A PSA measurement above a cut-off value of 4.0 ng/ml is generally regarded as positive and might indicate the need for a biopsy [20]. Commercial SPR biochip with signal enhancement using a sandwich assay format are currently available and have a limit of detection of 18.1 ng/ml [21].

In this paper, we have evaluated a simple and reproducible method for labelling biomolecules with gold nanorods onto gold surface without utilizing organic solvents, but relying on electrostatic interactions between the positively charged end-groups of Cetyltrimethylammonium bromide (CTAB) and negatively charge of antibody. Gold nanorods synthesis and immobilization were furthermore investigated combining Transmission Electron Microscopy (TEM) and Scanning Electron Microscopy (SEM). Anti-PSA was then covalently grafted onto well immobilized gold nanorods and the recognition of PSA was essayed by Polarization modulation infrared reflection absorption spectroscopy (PM-IRRAS) and Fourier Transform Surface Plasmon Resonance (FT-SPR) measurements.
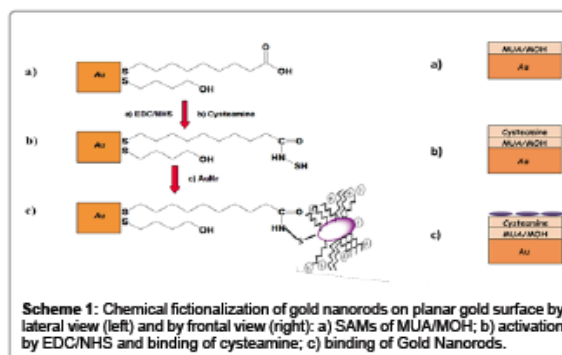
Materials and Methods

Reagents

Tetrachloroauric Acid (HAuCl$_4$), Cetyltrimethylammonium bromide (CTAB), sodium borohydride (NaBH$_4$), silver Nitrate (AgNO$_3$), Ascorbic Acid, 1-Mercapto-11-undecanoic acid (MUA), 1-mercapto-6hexanol (MOH), N-hydroxysuccinimide (NHS), 1-(3-dimethylaminopropyl)-N'-ethylcarbodiimidehydrochloride (EDC), DMF(Dimethylformammide for molecule biology 99%), cysteamine (CYS), ethanol (Normapur 99%), buffer solution (K+phthalate pH: 9; PBS pH: 7), Monoclonal Antibody-Prostatic (anti-PSA), Prostatic Antigen Specific (PSA) and Bovine Serum Albumine (BSA) were purchased from Sigma Aldrich (Saint-Quentin Fallavier, France). All chemicals were used as such without further purification. Milli Q water was used throughout the experiments. Gold substrates for FT-SPR measurements were deposited at the Institute IMM-CNR in Lecce (Italy).

Synthesis of Au nanorods (AuNr)

Nanorods were made and purified following the well-established seed-mediated procedure previously described [14]. Gold seeds solution stabilized by CTAB, were prepared by reduction of Au$_4^+$ (0.01 M; 5 mL) ions by ice–cooled NaBH$_4$ (0.01 M; 0.6 mL) in the presence of CTAB (0.20 M; 5 mL). After 4 h seed solution was added to growth solution containing CTAB (5 mL; 0.20 M), HAuCl4 (5 mL; 1×10^{-3} M), AgNO$_3$ (0.25 mL; 4×10^{-3} M) and Ascorbic Acid (70 µl; 8×10^{-3} M). The resultant solution was kept in dark for 24 h. The as-prepared solution was centrifuged at 11.000 rpm for 26 min for three times and then the supernatant was discarded and the residue was redispersed in an equivalent amount of buffer solution (PBS pH: 7). This was repeated twice principally to remove excess of CTAB. Stock solutions were stored at 27-29°C and characterized using UV-Vis spectroscopy and transmission electron microscopy (TEM).

Chemical immobilization procedure

The schematic representation of the chemical strategy is depicted in Scheme 1.

Scheme 1: Chemical fictionalization of gold nanorods on planar gold surface by lateral view (left) and by frontal view (right): a) SAMs of MUA/MOH; b) activation by EDC/NHS and binding of cysteamine; c) binding of Gold Nanorods.

SAMs formation: Chemistry procedures based on SAMs of thiol (MUA/MOH 1/3) in absolute ethanol have been described previously [22]. Briefly Au slides were immersed in 10^{-3} M ethanolic solution of MUA/MOH 1/3 for a period of 18 h under stirring. After this time, the slides were rinsed in ethanol, dried in flowing nitrogen, and characterized by PM-IRRAS spectroscopy.

EDC/NHS activation and cysteamine linkage onto SAMs film: For immobilization of ammine group of cysteamine (CYS) via carbodiimide binding method, the carboxyl groups of MUA on the surface were activated with a 50 mM NHS and 200 mM EDC solution. After 2 h under stirring the activating solution was removed, the substrates washed and dried under nitrogen and used immediately for CYS immobilization. For this purpose, the gold substrate was immersed in an unstirred 10 mM ethanol solution of CYS at room temperature, in the dark, for 6 h. The gold substrate was then washed with ethanol and milli Q water to remove the excess of thiol and characterized by PM-IRRAS spectroscopy.

Covalent Immobilization of gold nanorods onto cysteamine SAMs films: The SAMs coated gold slides were immersed into the gold nanorods solution for a period of 6 h under stirring. Thereafter, the films were rinsed in deionized water to remove unbound gold nanorods and dried in flowing nitrogen. These nanorods films were used for all further characterization.

Antibody interaction: Antibody anti-PSA (5 mg/L in buffer solution) was deposited on the nanostructured surface. After 1 h, the surface was rinsed with buffer solution then milliQ water for 10 min. To assure the specificity of interaction monitoring, a buffer solution of BSA (5 mg/L) was then used to block the potential residual reacting sites. After 40 min, BSA solution was removed by washing with buffer, pure H$_2$O and dried under nitrogen. Specific antigen interaction was then evaluated using a buffer solution containing PSA (5 mg/L) during 1 h followed by rinsing and drying with the same procedure. The as prepared nanostructured surfaces were analysed by PM-IRRAS and FT-SPR at each step of interaction and the showed results are the average of at least three measurements. As control test, a gold surface functionalized by SAMs and anti-PSA without step of gold nanorods coating was used for PSA biorecognition monitoring. In order to evaluate the sensitivity of the system, antigen interaction was then evaluated using a buffer solution containing PSA at different concentrations (0.5, 2.5, 5, 10, 20 mg/L) during 1 h followed by rinsing and drying with the same procedure. Each result here represented is the average of at least three measurements.

69

Instrumentation

UV-Vis spectrophotometer: All the absorption spectra reported in this work have been recorded by using a double-beam Varian Cary 500 UV-Vis spectrophotometer. UV absorption spectra of the solution of gold nanorods (AuNr), as synthesized, and after interaction with proteins in buffer solution, were recorded in the 400-1000 nm spectral range.

Transmission electron microscopy (TEM): TEM measurements were performed with a JEOL JEM 1011 microscope operating at an accelerating voltage of 100 kV. The TEM graphs were taken after separating the surfactant from the metal particles by centrifugation. Typically, 1 mL of the sample was centrifuged for 21 min at a speed of 11000 r/min. The upper part of the colourless solution was removed and the solid fraction was re-dispersed in 1 mL of buffer solution (PBS pH: 7). 2 μL of this re-dispersed particle suspension was placed on a carbon-coated copper grid and dried at room temperature.

Scanning electron microscopy (SEM): SEM images were obtained using a SEM FEG Hitachi SU-70 scanning electron microscope with a low voltage of 1 kV and distance of 1.5-2 mm; the secondary electron detector "in Lens" was used.

Polarization modulation infrared reflection absorption spectroscopy (PM-IRRAS): PM-IRRAS spectra were recorded on a commercial Thermo (Les Ulis- France) Nexus spectrometer. The external beam was focused on the sample with a mirror, at an optimal incident angle of 80°C. A ZnSe grid polarizer and a ZnSe photoelastic modulator, modulating the incident beam between p- and s-polarizations (HINDS Instruments, PEM 90, modulation frequency=37 kHz), were placed prior to the sample. The light reflected at the sample was then focused onto a nitrogen-cooled MCT detector. The presented spectra result from the sum of 128 scans recorded at a 8 cm−1 resolution.

Fourier transform surface plasmon resonance (FT-SPR): SPR substrates were prepared starting from 25 × 25 mm² SF10 slabs; then a Ti/Au (2 nm/50 nm) metallic multilayer was deposited on the slabs by e-beam evaporation. The presence of Ti layer was only for adhesion purposes. Then, the substrates were annealed in air at 200°C in order to obtain the optimum conditions for antigen immobilization in terms of the best surface roughness and proper (111) crystallographic orientation. As-prepared gold-coated substrates were first cleaned for 10 min in a boiling solution consisting of H_2O_2 (30%) and milliQ water (1:5 ratio). After cleaning, the chips were thoroughly washed with milliQ water, left in ethanol for 1 h and dried under a stream of nitrogen.

FT-SPR measurements were performed with an SPR 100 module from Thermo equipped with a flow cell mounted on a goniometer. It was inserted in a Thermo-scientific Nexus FT-IR spectrometer using a near-IR tungsten halogen light source. The incidence angle was adjusted to have the minimal reflectivity located at 9000 cm⁻¹, at the beginning of each experiment, so as to be in the best sensitivity region of the InGaAs detector. Immobilization of monoclonal mouse antibodies against rabbit PSA (anti-PSA; 5 mg/L), on the previously functionalized gold surface, was carried out in the test chamber (10 μl/min; T: 27°C).

Results and Discussion

The seed-mediated growth is the most popular method for the synthesis of colloidal AuNr due to the simplicity of the procedure, high quality and yield of nanorods, ease of controlling particle size, and flexibility for further chemical modifications [14,23]. Figure 1 displays the localised surface plasmon resonance (LSPR) bands of AuNr with a strong resonance band at around 708 nm corresponding to the longitudinal plasmon oscillation [24] and a weaker one at ca 510 nm corresponding to the transverse plasmon oscillation band confirming the presence of elongated AuNr isolated from each other. Figure 2 shows TEM investigation that reveals good dispersion in size and shape of nanorods with an average length of 32.6 ± 0.9 nm and width of 13 ± 1.8 nm, estimated from ca.100-350 rods. The immobilization of AuNr onto planar gold surface using by SAMs functionalization, was performed by PM-IRRAS providing to identification of chemical groups onto gold planar surface after each step of functionalization. Figure 3 (spectrum a) was obtained after acid-terminated thiolates MUA/MOH immobilization (scheme 1a) where it is observed the absorption bands of the symmetric υCOO and υCH₂ around 1543 cm⁻¹ and also the υCOOH at 1673 cm⁻¹. Figure 3 (spectrum b) shows the spectra of the surfaces modified by EDC/NHS (scheme 1b) that reveals a strong absorption at 1760 cm⁻¹ due to υ C=O in ester functions confirming the activation of ·COOH of MUA molecules. Figure 3 (spectrum c) after CYS modification (scheme 1b) exhibits C-N stretch and NH deformation modes at 1640 cm⁻¹, respectively and an intense NH deformation mode at 1550 cm⁻¹. Figure 3 (spectrum d) was obtained after AuNr immobilization (scheme 1c) highlighting the nature of interaction between AuNr and SAMs coated gold planar surfaces: a C-N⁺ absorption can be seen at 1230 cm⁻¹ close to the one
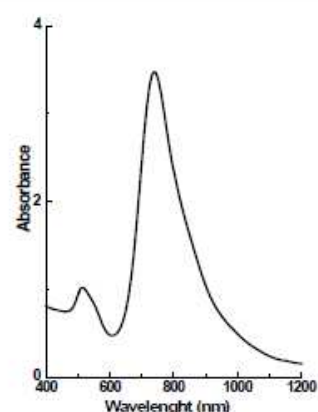

Figure 1: UV-Vis spectra of gold nanorods (λ max=708 nm, black line).
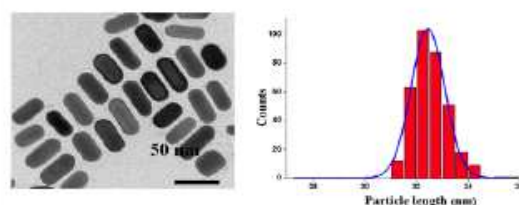

Figure 2: TEM images of gold nanorods (left)and particle size distribution (right).
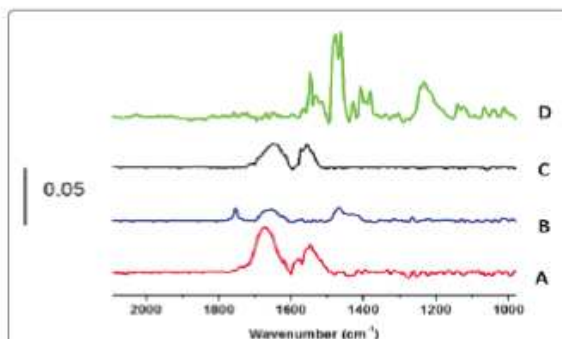
Figure 3: PM IRRAS spectra recorded after MUA/MOH treatment (a), EDC/NHS activation (b), Cys immobilization (c), gold nanorods incubation (d).
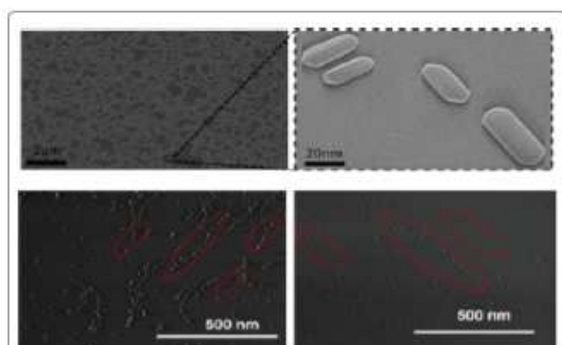

Figure 4: SEM images at three magnifications of gold nanorods, after immobilization on to a planar gold surface by SAMs approach.

reported by Nikobakht and El-Sayed, indicating the presence of CTAB-coated AuNr [25]. New bands centered at 1390 and 1468 cm⁻¹ and a very weaker peak at 1532 cm⁻¹ appear corresponding to the carboxylate asymmetric stretch modes [26]. These findings indicate formation of a binding between the ammonium head group of CTAB-coated gold nanorods with the cysteamine modified-carboxylic acid groups of the SAMs. Figure 4 shows SEM characterization where it is shown AuNr well aligned on the SAMs surface due to linkage descript above. Thanks to the findings, it is deducible that immobilization of AuNr via covalent interactions by SH of cysteamine layer induce order on nanorods immobilization on gold planar surfaces.

In order to investigate the ability of the as immobilized AuNr onto gold surface a set of PM-IRRAS data taken after proteins interaction where also acquired (Figure 5). After treatment by anti-PSA solution, the onset of intense amide I and II bands at 1650 and 1550 cm⁻¹, confirms the successful immobilization of antibody (Figure 5 spectrum a). When this antibody-terminated layer was submitted to BSA adsorption, its spectroscopic signature was unchanged (Figure 5 spectrum b) (amide band area equal to 14.8 ± 0.2 a.u. and 14.6 ± 0.2 a.u. for anti-PSA and anti-PSA + BSA, respectively), indicating that no significant amount of BSA molecules were adsorbed. Finally, the interaction with PSA solution led to a considerable increase of amide band area (Figure 5 spectrum c) evidencing the efficient recognition of the target by the

sensing layer (amide band area 20 ± 2 a.u for anti-PSA + BSA+ PSA).

Furthermore, PSA biorecognition was investigated using AuNr coated on gold surface by SAMs procedure tested in this work (Figure 6 A black line and B line II) in comparison with a gold surface not coated with AuNr (Figure 6 A red line and B line I), were then monitored by FT-SPR measurements. At time 20 min, a solution of anti-PSA (5 mg/L) was injected for 54 min; then a buffer solution (K+ phthalate pH 9) [14] was flowing to remove any weakly bound antibody yielding a FT-SPR wavenumber value of about 8395 cm⁻¹ (primary response). At time 55 min, a solution of bovine serum albumin (BSA; 5 mg/L) was injected
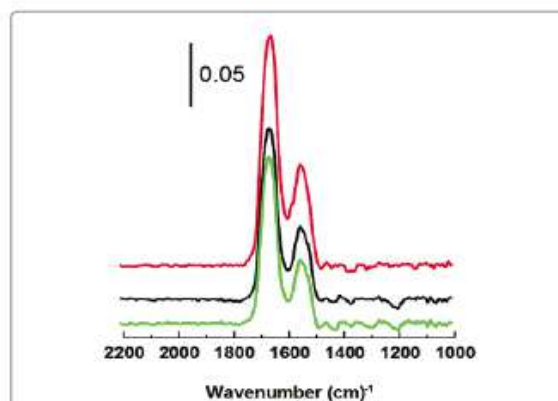

Figure 5: PM-IRRAS spectra obtained after adsorption of anti-PSA (green line), anti-PSA+BSA (black line) and PSA+BSA+anti-PSA (red line).
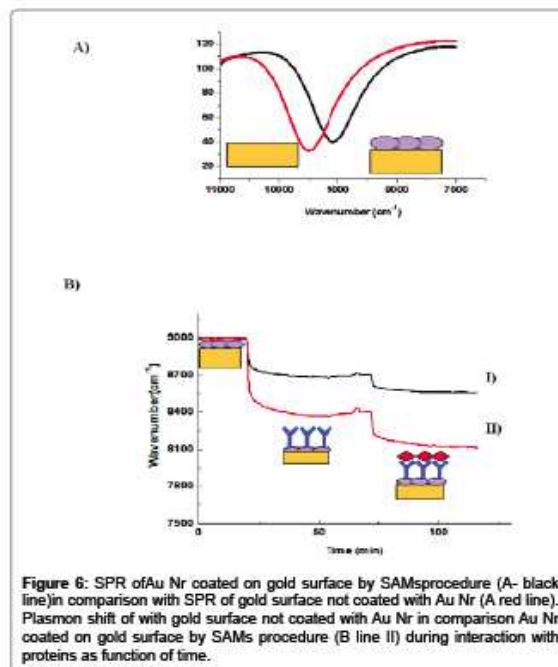

Figure 6: SPR ofAu Nr coated on gold surface by SAMsprocedure (A- black line)in comparison with SPR of gold surface not coated with Au Nr (A red line). Plasmon shift of with gold surface not coated with Au Nr in comparison Au Nr coated on gold surface by SAMs procedure (B line II) during interaction with proteins as function of time.

for 10 min without inducing any wavenumber change. After washing, the wavenumber value slightly decreased, likely due to desorption of weakly bound proteins (second response); then the wavenumber tended to an equilibrium value at 8164 cm^{-1}. These wavenumber shifts indicate that proteins, anti-PSA and PSA, significantly bind the surface. The shifts corresponding to each binding step are reported in Table 1.

It should be noted that, for identical concentrations, when the proteins are grafted to AuNr immobilized onto gold surface, the wavenumber shift is two times higher than PSA recognition by anti-PSA immobilized on the SAMs layer without AuNr immobilization. In order to determine the sensitivity reached by SAMs-AuNr based nanodevices, FT-SPR measurements of biorecognition were performed at various PSA concentrations, from 5 mg/L to 0.5 mg/L. Figure 7 shows on the left graph the dynamical responses as a function of time for each target concentrations and on the right graph the linearity of SPR shift response when the PSA concentration decreases. The calculated slope of linear response given by this set of experiments is 37 ± 2 cm^{-1}/mgL^{-1} that represents the sensitivity of the system. In conclusion, we successfully developed a novel simple covalent approach using mixed SAMs strategies to link AuNr on gold planar surfaces originating a well ordered active layer. Gold substrates were finally functionalized for interaction monitoring of anti-PSA with PSA. The findings highlighted AuNr coated gold surface as able to doubles the SPR interaction responses. Many authors, proved the assembling importance for biosensing applications: Jena [27] demonstrated that using a nanostructured material as gold nanoparticles integrated with a dehydrogenated enzyme well self-assembled it was originated a stable and fast response for electrochemical biosensing; Politi [15] highlighted that stable gold nanorods based nanobiosystem self-assembled on gold surfaces reveals an efficient detection of lead ions for environmental monitoring applications. On this path, an extraordinary variety of structures, properties, and applications is available for AuNPs motivating many studies and applications in interdisciplinary research involving chemistry, physics, biology, and medicine [28].

Conclusions

In this paper, we described a new concept of functionalization and self-organization of gold nanorods, bearing CTAB positively charged ligands, in order to bind proteins in an anisotropic way, and form linear chains after functionalization. The developed method does not require the use of organic solvent; the easy and versatile way, of forming such hybrid anisotropic nanostructures may have a wide range of applications, particularly using their optical properties to biosensors. Furthermore, ability of gold nanorods to enhance the interaction of SPR substrates with PSA molecules with an effective sensitivity (37 ± 2 cm^{-1}/mgL^{-1}) and specificity (no aspecific responses after BSA interaction were found neither by PM-IRRAS nor FT-SPR techniques) was finally proved. Further work will aim at optimizing the size and shape of gold nanostructures for biosensor signal enhancement.

References

1. Dai Z, Yan F, Yu H, Hu X, Ju H (2004) Novel amperometric immunosensor for rapid separation-free immunoassay of carcinoembryonic antigen. J Immunol Methods 287: 13-20.

2. Malem F, Mandler D (1993) Self-assembled monolayers in electroanalytical chemistry: application of O-mercapto carboxylic acid monolayers for the electrochemical detection of dopamine in the presence of a high concentration of ascorbic acid. Anal Chem 65: 37-41.

3. Lee W, Oh BK, Min Bae Y, Paek SH, Hong Lee W, et al. (2003) Fabrication of self-assembled protein A monolayer and its application as an immunosensor. Biosens Bioelectron 19: 185-192.

4. Kramer B, Rarey M, Lengauer T (1999) Evaluation of the FLEXX incremental construction algorithm for protein-ligand docking. Proteins: Structure, Function and Bioinformatics 37: 228-241.

5. Salloum DS, Schlenoff JB (2004) Protein adsorption modalities on polyelectrolyte multilayers. Biomacromolecules 5: 1089-1096.

6. Sau TK, Murphy CJ (2005) Self-Assembly Patterns Formed upon Solvent Evaporation of Aqueous Cetyltrimethylammonium Bromide-Coated Gold Nanoparticles of Various Shapes. Langmuir 21: 2923-2929.

7. Love JC, Estroff LA, Kriebel JK, Nuzzo RG, Whitesides GM (2005) Self-assembled monolayers of thiolates on metals as a form of nanotechnology. Chem Rev 105: 1103-1169.

8. Tao A, Kim F, Hess C, Goldberger J, He R, et al. (2003) Langmuir-Blodgett Silver Nanowire Monolayers for Molecular Sensing Using Surface-Enhanced Raman Spectroscopy. Nano Letters 3: 1229-1233.

9. Nikoobakht B, Wang ZL, El-Sayed MA (2000) Self-Assembly of Gold Nanorods. J Phys Chem B 104: 8635-8640.

10. Jana NR, Gearheart LA, Obare SO, Johnson CJ, Edler KJ, et al. (2002) Liquid crystalline assemblies of ordered gold nanorods. J Mater Chem 12: 2909-2912.

11. Yu C, Irudayaraj J (2007) Multiplex biosensor using gold nanorods. Anal Chem 79: 572-579.

12. Gole A, Orendorff CJ, Murphy CJ (2004) Immobilization of gold nanorods onto acid-terminated self-assembled monolayers via electrostatic interactions. Langmuir 20: 7117-7122.

13. Szunerits S, Spadavecchia J, Boukherroub R (2014) Surface plasmon resonance: colloidal gold nanoparticles-based amplification for enhanced sensitivity. Review Anal Chem 33: 153-164.

14. Spadavecchia J, Casale S, Boujday S, Pradier CM (2012) Bioconjugated gold nanorods to enhance the sensitivity of FT-SPR-based biosensors. Colloids Surf B Biointerfaces 100: 1-8.

15. Politi J, Spadavecchia J, Iodice M, de Stefano L (2015) Oligopeptide-heavy metal interaction monitoring by hybrid gold nanoparticle based assay. Analyst 140: 149-155.

16. Frutos AG, Weibel SC, Corn RM (1999) Near-infrared surface plasmon resonance measurements of ultrathin film and Fourier transform SPR spectroscopy. Anal Chem 71: 3935-3940.

17. Hanken DG, Corn RM (1995) Variable Index of Refraction Ultrathin Films Formed from Self-Assembled Zirconium Phosphonate Multilayers: Characterization by Surface Plasmon Resonance Measurements and Polarization/Modulation FT-IR Spectroscopy. Anal Chem 67: 3767-3774.

18. Csáki A, Kaplanek P, Möller R, Fritzsche W (2003) The optical detection of individual DNA-conjugated gold nanoparticle labels after metal enhancement. Nanotechnology 14: 1262-1268.

	Planar SAMs Gold surface (Δcm^{-1})	AuNr linked onto Planar SAMs Gold Surface (Δcm^{-1})
Anti-PSA (5 mg/L)	296	600
PSA (5 mg/L)	110	240

Table 1: FT–SPR shifts observed upon binding of anti-PSA, recognition of PSA.
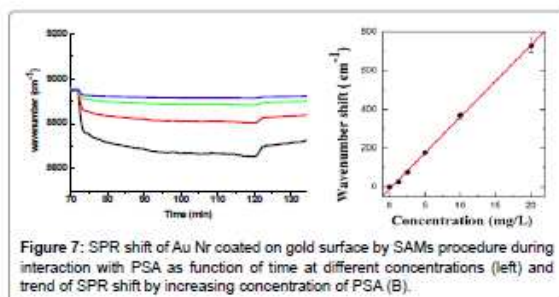

Figure 7: SPR shift of Au Nr coated on gold surface by SAMs procedure during interaction with PSA as function of time at different concentrations (left) and trend of SPR shift by increasing concentration of PSA (B).

72

19. Hayat Colloidal MA (1989) Gold: Principles, Methods and Applications. Academic Press Inc, CA.

20. Healy DA, Hayes CJ, Leonard P, McKenna L, O'Kennedy R (2007) Biosensor developments: application to prostate-specific antigen detection. Trends Biotechnol 25: 125-131.

21. Cao C, Kim JP, Kim BW, Chae H, Yoon HC, et al. (2006) A strategy for sensitivity and specificity enhancements in prostate-specific antigen-alpha-1-anti-chymotrypsin detection based on surface plasmon resonanceBiosens. Bioelectron 21: 2106-2113.

22. Thébault P, Boujday S, Sénéchal H, Pradier CM (2010) Investigation of an Allergen Adsorption on Amine- and Acid-Terminated Thiol Layers: Influence on Their Affinity to Specific Antibodies. J Phys Chem B 114: 10612-10619.

23. Jana NR, Gearheart L, Murphy CJ (2001) Seed-mediated growth approach for shape-controlled synthesis of spheroidal and rod-like gold nanoparticles using a surfactant template. Adv Mater 13: 1389-1393.

24. Jana NR, Gearheart I, Murphy CJ (2001) Seeding growth for size control of 5-40 nm diameter gold nanoparticle. Langmuir 17: 6782-6786.

25. Nikoobakht B, El-Sayed MA (2003) Preparation and Growth Mechanism of Gold Nanorods (NRs) Using Seed-Mediated Growth Method. Chem Mater 15: 1957-1962.

26. Chapo CJ, Paul JB, Provencal RA, Roth K, Saykally RJ (1998) Is Arginine Zwitterionic or Neutral in the Gas Phase? Results from IR Cavity Ringdown Spectroscopy. J Am Chem Soc 120: 12956-12957.

27. Jena BK, Raj CR (2006) Electrochemical biosensor based on integrated assembly of dehydrogenase enzymes and gold nanoparticles. Anal Chem 78: 6332-6339.

28. Daniel MC, Astruc D (2004) Gold Nanoparticles: Assembly, Supramolecular Chemistry, Quantum-Size-Related Properties, and Applications toward Biology, Catalysis, and Nanotechnology. Chem Rev 104: 293-346.

3. Heavy metal detection in aqueous solutions by Porous Silicon and Gold nanoparticles based devices

Environmental monitoring is fundamental theme of researches to investigate and to gain knowledge about natural processes as well as to regulate existing directives concerning chemical species in the environment. Portable, robust, accurate, specific, low-cost methods and devices to perform in situ analysis are hot topics to achieve efficient environmental monitoring. These enable results to be available faster minimizing the risk of contamination eliminating the samples transportation and degradation. The information obtained must be of sufficient quantity as well as quality in order to give high-resolution temporal and spatial data on environmental processes and portable devices for in situ assays (Bulusu et al. 2000).

Since nanostructured devices revealed an enhanced ability to interact with target molecules also using low quantity of samples, in the present section will be discussed the study performed to detect lead ions and arsenic ions in aqueous solutions by using porous silicon based devices (**section 3.1**) and gold nanoparticles based assays (**section 3.2**) developed.

3.1 Porous silicon based optical monitoring

3.1.1. Lead ions detection: optical vs gravimetric characterization

In the following section, it will be discussed oligopeptides bioconjugation onto porous silicon optical structure compared to quartz crystals bioconjugation. Then, the study was moved to lead ions interaction monitoring (Submitted Manuscript).

Quartz Crystal Microbalance (QCM) and spectroscopic reflectometry (SR) are label-free techniques very useful not only in biosensing measurements, but also for characterization of bioprobes conjugation on solid supports. The two techniques are completely different in both hardware frameworks and measurement protocols, but for this reason could be used in a very complementary way: QCM registered a continuum signal during all the steps of functionalization, QR has a planar surface of gold; while SR recorded the reflectivity spectra after each incubation step, PSi is characterized by a sponge-like matrix with a very large active surface area that allows the adsorption of a greater number of molecules inside the pores. The adsorption of substances into the PSi pores modifies its physical properties: in particular, since air is replaced by a denser layer of material, the average refractive index increases and the reflectivity spectrum red-shifts towards longer wavelengths, proportionally to the quantity of biological or chemical matter infiltrated into the pores. Since, the effectiveness study is crucial point in biosensors development, a comparative study between QR and PSi based devices functionalized up to phytochelatins oligopeptides was performed. The results highlighted the corrosive action due to phytochelatins and the reversibility of the interaction with lead ions for both devices.

Corresponding Author: Dr. Luca De Stefano, PhD

Corresponding Author's Institution: Institute for Microelectronics and
Microsystems - CNR

First Author: Jane Politi

Order of Authors: Jane Politi; Principia Dardano; Alessandro Caliò; Mario
Iodice; Ilaria Rea; Luca De Stefano, PhD

Lysine Modified Oligopeptides Allow Reversible Sensing of Lead (II) Ions on Chip

Jane Politi[1,2], Principia Dardano[1], Alessandro Caliò[1,3], Mario Iodice[1], Ilaria Rea[1] and Luca De Stefano[1*]

[1]Institute for Microelectronics and Microsystems, National Research Council, Via P. Castellino,111-80131 Naples, Italy

[2]Department of Chemistry, University of Naples "Federico II", Via Cynthia, 80126 Naples, Italy

[3]Department of Physical Sciences, University of Naples "Federico II", Via Cynthia, 80126 Naples, Italy

ABSTRACT

Phytochelatins (PCs), oligomers of glutathione, naturally chelate heavy metals in aqueous solution. Unfortunately, these small peptides cannot be used as covalently bound bioprobes on transducer surfaces since they promote corrosion of sensor standard supports, such as gold and porous silicon (PSi). In this work, we have chemically modified a commercial PC oligopeptide by a poly-lysine (Lys) chain, which turns the isoelectric point from 4.2 to 6.9. The PC-Lys bioprobes have been successfully immobilized on both porous silicon multilayer and flat gold surfaces. Interaction of PC-Lys and Lead (II) ions in aqueous solution has been quantified by optical spectroscopic reflectometry and quartz crystal microgravimetry. Both sensing systems are reversible and reveal an affinity between the molecular complex and its ligand in the range of 10^{-12} M and sensitivities of 0.18 ppb/nm (0.45 pM/nm) and 0.07 ppb/Hz (0.17 pM/Hz) for PSi based reflectometry and microgravimetry, respectively.

1. Introduction

Biosensors are generally constituted by a biological recognition element, the so-called bioprobe (which can be a DNA single strand, an enzyme, a protein, and so on) properly conjugated with a transducer component that converts biomolecular interactions into signals (optical, electrical, electrochemical, gravimetrical), providing final read out to users. In last twenty years, a silicon-derived material, namely the porous silicon (PSi), has been widely studied due to its peculiar properties (Cullis et al., 1997, Snow et al., 1999, Theißl, 1997, Lockwood, 1994). PSi is fabricated by electrochemical etching of doped crystalline silicon in hydrofluoridric acid (HF) water solutions (Sailor, 2012), and exhibits a sponge-like morphology characterized by a specific surface area up to $200 - 500 \text{ m}^2 \text{ cm}^{-3}$ (Laurell et al., 1996) so that it can be very sensitive to the presence of biological or chemical species which penetrate inside the pores. Moreover, since the dissolution of silicon is a charge-mediated self-stopping process, tuning the etching parameters (i.e. etch time, HF concentration, doping level, and so on) allows modulation of PSi porosity in each layer, which in turns permits the fabrication of multilayered structures. Due to high air content (up to 80-85 %), PSi is almost perfect electric insulator, while, from the optical point of view, the smoothness of interfaces between low porosity and high porosity layers is very high, so that good quality optical spectra can be obtained from visible to near infrared wavelength region (500-1600 nm), both in transmission and reflection. Several photonic multilayers devices have been demonstrated, such as optical microcavity, Bragg mirrors, rugate filters, and the Thue-Morse (T-M) sequences; all of them showing high quality factors and sharp optical resonances. Since on exposure to biochemical substances the average refractive index drastically changes, PSi can be thus used as smart optical transducer material (Rea et al., 2009). In particular, we demonstrated that T-M PSi optical structure, due to characteristic alternation of porosity layers, is more sensitive than symmetric multilayers (Moretti et al., 2007). Main drawback of this fascinating material is its chemical instability: as-etched PSi quickly ages on exposure to atmosphere since Si-H bonds tend to be substituted by Si-O-

Si ones, but also oxidized PSi is easily corroded in aqueous environments (Caliò et al., 2013). Chemical and biological passivation procedures have been published allowing functionalization and stability of PSi supports (Björkqvist et al., 2003, De Stefano et al., 2008).

Another quantitative measuring technique, commonly used in the development of biosensors, is the Quartz Crystal Microbalance (QCM) technology (Della Ventura et al., 2016, Nicolini et al., 2012, Spera et al., 2013a, Spera et al., 2013b). QCM is currently used to measure extremely small mass changes, down to nanograms, with high sensitivity, becoming a cost-effective tool in biosensing. Standard QCM exploits the piezoelectric quartz resonators (QRs) properties in quantifying the resonance frequency shift Δf when a mass m is adsorbed to or desorbed from their surface, according to Sauerbey's equation (1):

$$\Delta f/f_0 = -(\Delta m/A\rho l) \qquad (1)$$

where f_0 is the fundamental frequency of QR, A is the area of the gold layer partially covering the QR, Δm is the mass variation corresponding to frequency shift Δf and ρ and l are the quartz density and thickness, respectively (Nicolini et al., 1995).

The PSi and QR surfaces can be both functionalized with bioprobes in order to realize optical and nanogravimetric biosensors, respectively. Crucial point in biosensors development is bioprobes conjugation that can be used for immobilization onto the transducer surface. One of the most useful biomolecular probes for heavy metal ions detection is a family of oligopeptides able to bind them, named Phytochelatins (PCs). PCs are small, heavy metal-binding proteins with general structure of (γ-Glu-Cys)$_n$Gly (n=2-11) that complex with toxic metal ions: a well known mechanism developed in vegetal world to protect fungi and plants in nature (Grill et al., 1985, Piechalak et al., 2002, Salt and Rauser, 1995). Unfortunately, PCs cannot be easily covalently grafted to solid surface: in presence of ligands, molecular binding triggers charge-mediated corrosion of bioconjugated supports.

In this work, we describe synthesis of Phytochelatin 6 (PC$_6$) modified by Lysine chain (six amino-acid tail) and immobilization on PSi T-M and QR surfaces by a proper functionalization strategy.

The novel PC_6-Lys_6 synthetic oligopeptides fix supports corrosion and effectively detect lead ions in solutions. Spectroscopic reflectometry, gravimetric analysis and scanning electron microscopy were used as characterization techniques.

2. Materials and methods

2.1. Porous silicon fabrication

PSi structures were fabricated by electrochemical etching of crystalline Si (0.001Ωcm resistivity, <100> oriented, 500μm thick) in HF (50% in volume), water and ethanol solution (1:1:1) in dark and at room temperature (RT). PSi-based T-M realization and characterization was previously studied (Moretti et al., 2006). Briefly, starting from low porosity (high refractive index, H) - high porosity (low refractive index, L) bilayer, the 2^n layers T-M sequence was generated following the substitution rules H→HL and L→LH into the 2^{n-1} layers structure, so that the sequence of the 64 layers can be expressly written as LHHLHLLHHLLHLHHLHLLHLHHLLHHLHLLHHLLHLHHLLHHLHLLHLHHLHLLHHLHLLHHLLH LHHL. A current density equal to 100 mA/cm^2 was applied for 1.6s, to obtain the high refractive index (n_H=1.79 at λ=753 nm) layers with thickness d_H=120nm and a current density of 200 mA/cm^2 for 1.2 s for the low refractive index (n_L=1.53 at λ=753 nm) layers with thickness d_L=156 nm. Refractive indexes and thicknesses were determined by spectroscopic ellipsometry on single layer samples (data not showed here). For each layer, time breaks of 5s were used during etching process in order to recover HF concentration at dissolution edge and start next layer formation with zero current density, so that variation current is always the same for each layer. The etching area was 0.98 cm^2. After the electrochemical process, pores dimension was increased by rinsing the "as-etched" porous silicon structures in KOH-ethanol solution (1.5mM) for 15 min (Herino et al., 1987). Even if PSi stacks are made of several tenths of porous layers, the reflectivity spectra are of very good quality in a wide range of wavelengths, as shown in **Figure S1** in Supporting Materials. Then, the devices were thermally oxidized in order to prevent uncontrolled environmental aging and

limit corrosion in alkaline solutions (Charmad et al., 1998). Oxidation has been performed in oven on exposure to pure O_2, applying a two-step process: 30 min at 400° C followed by 15 min at 900 °C.

2.2 Modified peptides synthesis and characterization

PC_6-Lys_6 (4mg) was produced by Primm s.r.l. (Italy) following our indication on the position of Lysine chain with respect to PC_6 orientation by standard solid-state synthesis procedure. A solid sugar-like powder with a solubility of 1 mg/mL in H_2O was obtained and released. Molecular weight and purity were characterized by MALDI-TOF Spectrometry and HPLC, respectively. Mass spectrometry revealed a 2235.23 Da oligopeptides, while chromatogram highlighted purity higher than 95%.

2.3 Chemical biomodification

2.3.1. Porous silicon biomodification

PSi surfaces were biomodified by following a well-established method (Terracciano et al., 2013). **Figure S2-A** shows the functionalization procedure needed to obtain primary amine on PSi surfaces: the first passivation step is the oxidation of PSi in order to stabilize the surface against spontaneous aging due to the Si-H groups on its surface just after the fabrication. Thus, oxidized PSi was treated in piranha solution (H_2SO_4:H_2O, 4:2) at RT for 30 minutes in order to activate Si-O-Si in Si-OH groups. After several washes in distilled water (DI-H_2O) and drying under N_2, the samples were treated with a solution of 5% 3-(aminopropyl)triethoxysilane (APTES) (Sigma Aldrich) in anhydrous toluene for 30 minutes at RT, washed with anhydrous toluene three times, cured on a heater at 100°C for 10 minutes and washed again twice with anhydrous toluene. The silanized PSi samples were treated with the cross-linker Bis [sulfosuccinimidyl] suberate (BS[3] by Thermo scientific, USA) 1.7mM in PBS 1X at 4°C for 4h, washed three times with PBS 1X and once with DI-H_2O. BS[3] brings a sulfo-N-hydroxysulfosuccinimide (sulfo-NHS) group that reacts with primary amines at pH 7-9 to form stable, covalent amide bonds (Mattson et al. 1993). In this way the BS[3] binds from one side to the primary amines available on PSi silanized surface, and, on

the other side, to the primary amine exposed by PC_6. The PC_6 (AnaSpec IGT group) and PC_6-Lys_6 (Primm s.r.l.) were diluted in PBS 1X in order to obtain 2mM concentration. The samples were incubated at 4°C for 2h.

2.3.2. Quartz resonators biomodification

In **Figure S2-B** is reported the biomodification of QR using thiol-PEG-amine to obtain primary amines on QR surfaces. Thiol PEG Amine, (JenKem Technology USA) was flowed in the QCM cell at 2mM concentration in PBS 1X and leaved in incubation for 2h at RT. After extensive rising of PEGylated-QR (5 minutes at 5 rpm) in PBS solution, the functionalization was completed, as well as in the case of PSi, using BS^3 and PC_6 and PC_6-Lys_6.

2.4. Lead ions interaction monitoring

Interaction between as-described biomodified surfaces and lead (II) ions solutions was followed using spectroscopic reflectometry and QCM characterizations using 100 μL of lead (II) ions solutions at 100, 50, 25, 10, 5, 2 ppb concentration.

2.5. Spectroscopic reflectometry

The reflectivity spectra of PSi photonic structures have been acquired using a simple experimental setup: a Y optical reflection probe (Avantes) was used to guide the input white light on the PSi samples and the output signal to Optical Spectrum Analyzer (OSA by Ando AQ6315A) (see **Figure S1** in Supporting Materials, where the spectrum of the as-etched T-M sequence together with the schematic of 64 layers are reported). The spectra were acquired at normal incidence, with resolution of 0.2 nm, at least three times in order to have an average spectrum of each sample.

2.6. Quartz Crystal Microbalance measurements

The mass variations have been measured by a QCM (Novaetech S.r.l. Italy), connected to a computer by a producer-released software (see **Figure S3** in Supporting Materials). The QR (IEV S.r.l., Italy) has a fundamental nominal frequency of 10 MHz, a blank diameter of 8mm and a gold

lamina diameter of 4.5 mm. The fluidic apparatus consists of a GILSON peristaltic pump, two

Tygon® silicone tubes with diameters of 0.76 mm for the in and out flows. A microcell, with an

approximate volume of 30 μL, contains the QR.

2.7. Scanning electron microscopy

Morphology of PSi biochips, modified up to PC_6 and PC_6-Lys_6, were investigated by scanning

electron microscopy (SEM). SEM images have been performed at 5kV accelerating voltage and

30μm wide aperture by a Field Emission Scanning Electron Microscope (Carl Zeiss NTS GmbH

1500 Raith FESEM). Both secondary emission and in-lens detectors have been used.

3. Results and Discussion

It is well known from literature, and also from our previous experience, that PC_6 oligopeptides,

adsorbed on nanoparticle surface or electrodes, can be effective bioprobes for heavy metals

monitoring in aqueous solution (Politi et al., 2015, Adam et al., 2005). Nevertheless, the fabrication

of a PC_6 based biosensor requires a proper immobilization strategy of these biomolecules onto the

surface of transducer materials, i.e. porous silicon and gold, in the case considered. In particular, the

design of a device for quantitative determination of heavy metal concentration should be based on

covalent surface grafting since adsorption could be procedurally simpler, but also result in

disordered assembly and different amount of bioprobes on each surface; while a covalent binding

approach should guarantee better performances and less variability among different instruments.

Functionalization procedure depended on the nature of transducer surface: in case of porous silicon,

the chemical passivation, sketched in Figure S2 (A), was based on adding layer of materials that

expose specific reactive groups. Spectroscopic reflectometry was used to quickly asses the outcome

of functionalization steps: since multiple layers of chemical and biological matter were added to PSi

structure, a red-shift of the optical spectrum was expected due to the increase of average refractive

index. Quantitative results are presented in **Figure 1**: looking at the oxidised PSi T-M peak @944

nm, a red shift of about 30 nm after APTES deposition was achieved, and an additional one of about

20 nm was caused by the cross-linker BS^3, according to a thinner film formed on the PSi walls with respect to the self-assembled silane (Ouyang et al., 2006). Last functionalization step was incubation of PC_6 bioprobe: an unexpected blue shift of about 16nm was revealed. This effect suggested that the biofunctionalized T-M resulted optically less dense than before PC_6 incubation, which, in turns, meant that some matter (silicon, APTES, BS^3 or a combination of these three) was subtracted from chip surface. As it can be noted in **Figure 2**, PC_6 chemical structure is composed by seven carboxylic groups in lateral chain (due to glutamic acid presence) and just one amino group present in α position, with an isoelectric point (pI) equal to 4.2: these features could be both responsible of PSi corrosion through charge exchange and basic aggression (De Stefano et al., 2009). PC_6 engineering was thus needed in order to have a bioprobes with a final pI around 7, and a neutral solution during the bioconjugation of porous silicon devices. We designed a Phytochelatin-like oligopeptide (PC_6-Lys_6), whose chemical formula and ball-stick model are shown in **Figure 2**, including a carboxy-terminal chain of poly-Lysine (pI=6.9), and used it in the last step of functionalization: this time, we registered by spectroscopic reflectometry a further red-shift of about 3 nm (see **Figure 1 B**). This small spectrum shift was of the same order of that observed in case of small bioprobes bound on PSi surface in other published works (De Stefano et al., 2013, Lee and Fauchet, 2007). The corrosive effect of PC_6 with respect to PC_6-Lys_6 was well evident by SEM characterizations (**Figure 3**): after incubation of unmodified PC_6, PSi surface appeared highly irregular and partially dissolved, whereas a classic smooth and homogeneous image can be detected after immobilization of PC_6-Lys_6.

The bioconjugation procedure was also characterized by real-time monitoring each functionalization step of gold on QR resonators, by using the QCM technique. **Figure 4** (upper graph) shows a frequency decrease just after the BS^3 cross-linker, corresponding to a mass increase that demonstrated a successful binding of thiol-PEG-amine and BS^3. However, when PC_6 molecules interacted with QR, the data showed an increasing of frequency, corresponding to a mass decrease also in this case, again in qualitative agreement to the blue shift obtained by spectroscopic

reflectometry data. QCM experimental results underlined that the final oscillation frequency was even lower than Thiol-PEG-amine-QR frequency (see the inset in Figure 4, upper graph), according to the red shift between the spectra post APTES and PC_6 grafting steps on PSi surfaces. **Figure 4** (bottom graph) represents the results of PC_6-Lys_6 bioconjugation onto QR surface: the amino-modification of the oligopeptides was again successful since a decrease of about 11 Hz in QR frequency oscillation can be noted in inset of bottom graph, corresponding to the PC_6-Lys_6 mass covalently bound onto QR surface. Since the QCM balance had a sensitivity of 1.4 Hz/ngr (Della Ventura et. al., 2016), the PC_6-Lys_6 mass was quantified as about 7.9 ngr, corresponding to a surface density of 49 ngr/cm^2.

After successful bioprobes immobilization, optical and gravimetric monitoring of interaction with lead (II) were performed both by reflectometric spectroscopy and quartz crystal microbalance techniques. **Figure 5** reports optical measurements by spectroscopic reflectometry performed onto PC_6-Lys_6 modified-PSi devices. In particular, panel A shows the trend of reflectivity peak @944nm, that after aqueous solution infiltration (needed to obtain a proper blank) shifted to 1040nm, as a function of lead (II) ions concentration. Experimental data could be fitted by OriginLab Software ™ Hill model equation (2):

$$y = (\Delta\lambda_{max}[Lead])/(km+[Lead]) \ (2)$$

where $\Delta\lambda_{max}$ is the saturation point; K_m is affinity constant; [Lead] is Lead (II) ions concentration. The Hill model is a Langmuir-like equation, which assumes that just one site of reaction was present, and the affinity of the biomolecule for its ligand was not dependent on whether or not other ligand molecules were already bound. From data fit, we estimated system affinity constant of 3.5±0.6 ppb (8.8±1.5 pM), and system sensitivity, calculated in the linearity range of system response, of 0.18±0.03 ppb/nm (0.45±0.07 pM/nm). Even if the PC_6-Lys_6 modified-PSi system was highly affine to Pb II, the interaction between the oligopeptides and the metal ions is not stable and it can be neutralized by extensive rinsing of the sample. **Figure 5 B** shows measurement/regeneration cycles of PSi based device/lead (II) ions interaction as function of time

(each peak shift value is reported in **Table S1**), from which it could be noted that the biosensor was partially reversible, since after six cycles the signal could not be restored, probably due to partial occlusion of nanopores. The biomolecular interaction monitoring was also performed by PC_6-Lys_6 modified-QR surface (**Figure 6**), from which we got an affinity constant of 10 ± 2 ppb (25 ± 5 pM) and a sensitivity of 0.07 ± 0.03 ppb/Hz (0.17 ± 0.07 pM/nm). Moreover, also in this case reversible reactions were evidenced as reported in **Figure 6**, panel B. Even if the two sensing techniques, which used completely different measurement systems, revealed affinity constants of the same order, it should be noted that in case of the nanostructured biosensor, i.e. the PSi device, we quantified an almost three times higher affinity and an enhanced system sensitivity (around two times higher), which was due to higher surface area of PSi that allowed the immobilization of bioprobe greater amount.

4. Conclusions

Biosensors development critically depends on effective and affordable procedures for bioconjugating molecular probes onto transducer surfaces. In this study, the conjugation of heavy metal-binding proteins such as oligopeptides, known as Phytochelatins, has been monitored. Corrosion of transducers was evidenced on both porous silicon and quartz resonators surfaces in case of unmodified PC_6. A Phytochelatin-like oligopeptide was then designed and immobilized, fixing the corrosion and obtaining a final device useful for lead (II) ions interaction monitoring. A final sensitivity of 0.18 ± 0.03 ppb/nm and a system affinity constant of 3.5 ± 0.6 ppb was evidenced in case of porous silicon based device. The system was also found partially reversible, with a maximum of six regeneration cycles. Interaction optical monitoring results were confirmed by QCM microgravimetry measurements. Even if PC_6-Lys_6 is not a selective probe, i.e. it is not able to quantify any single heavy metal without suffering of the interference by any other, its great sensitivity to heavy metal low concentration can be considered a good starting point for the

development of a reversible nanostructured Lab-on-Chip low cost biosensor for in situ detection of these very diffuse dangerous inorganic pollutants.

Conflict of interest

All authors have declared that no competing interest exists.

References

Adam et al., 2005 V. Adam, J. Zehnalek, J. Petrlova, D. Potesil, B. Sures, L. Trnkova, R. Kizek Sensors, 5(2005), 70-84

Björkqvist et al., 2003 M. Björkqvist, J. Salonen, E. Laine, L. Niinistö, Phys. Status Solidi a 197 (2003), 374-377.

Caliò et al., 2013 A. Caliò, I. Rea, J. Politi, P. Giardina, S. Longobardi, L. De Stefano, J. Appl. Phys. 114 (2013), 134904.

Chamard et al., 1998 V. Chamard, G. Dolino, F. Muller, J. Appl. Phys. 84 (1998), 6659.

Cullis et al., 1997 A. G. Cullis, L. T. Canham, P. D. J. Calcott, J. Appl. Phys. 82 (1997), 909.

De Stefano et al., 2009 L. De Stefano, I. Rea, E. De Tommasi, P. Giardina, A. Armenante, S. Longobardi, I. Rendina, J. Nanophoton. 3 (2009), 031985-6.

De Stefano et al., 2013 L. De Stefano, G. Oliviero, J. Amato, N. Borbone, G. Piccialli, L. Mayol, I. Rea, J. R. Soc. Int., 10 (2013), 20130160.

De Stefano et al. 2008 L. De Stefano, I. Rea, P. Giardina, A. Armenante, I. Rendina, Adv. Mat., 20 (2008), 1529-1533.

Della Ventura et al., 2016 B. Della Ventura, I. Rea, A. Caliò, P. Giardina, A. M. Gravagnuolo, R. Funari, L. De Stefano, Appl. Surf. Sci. 364 (2016), 201-207.

Grill et al., 1985 E. Grill, E. L. Winnacker, M. H. Zenk, Science 230 (1985), 674–676.

Herino et al., 1987 R. Herino, G. Bomchil, K. Barla, C. Bertrand, J. L. Ginoux, J. Electrochem. Soc., 134 (1987), 1994.

Laurell et al., 1996 T. Laurell, J. Drott, L. Rosengren, K. Lindström, Sens. Act. B, 31 (1996), 161.

Lee and Fauchet, 2007 M. R. Lee, P. M. Fauchet, Optics express, 15(2007), 4530-4535.

Lockwood, 1994 D. J. Lockwood, Solid State Comm., 92 (1994), 101–112.

Mattson et al., 1993 G. Mattson, E. Conklin, S. Desai, G. Nielander, M. D. Savage, S. Morgensen, Mol. Biol. Rep., 17 (1993), 167-183.

Moretti et al., 2006 L. Moretti, I. Rea, L. Rotiroti, I. Rendina, G. Abbate, A. Marino, L. De Stefano, Optics Express, 14 (2006), 13, 6264-6272

Moretti et al., 2007 L. Moretti, I. Rea, L. De Stefano, I. Rendina, Appl. phys. lett., 90 (2007) 19.

Nicolini et al., 1995 C. Nicolini, M. Adami, T. Dubrovsky, V. Erokhin, P. Facci, P. Paschkevitsch, M. Sartore, Sens. Act. B., 24 (1995), 121–128.

Nicolini et al., 2012 C. Nicolini, M. Adami, M. Sartore, N. L. Bragazzi, V. Bavastrello, R. Spera, E. Pechkova, Sensors, 12 (2012), 17112-17127.

Ouyang et al., 2006 H. Ouyang, C. C. Striemer, P. M. Fauchet, , Appl. Phys. Lett. 88 (2006), 163108

Piechalak et al., 2002 A. Piechalak, B. Tomaszewska, A. Danuta, M. Baralkiewicz, Phytochem., 60, 2 (2002), 153–162.

Politi et al., 2015 J. Politi, J. Spadavecchia, M. Iodice, L. De Stefano, Analyst, 140 (2015), 149-155.

Rea et al., 2009 I. Rea, M. Iodice, G. Coppola, I. Rendina, A. Marino, L. De Stefano, Sens. Act. B: Chem., 139 (2009), 39-43.

Sailor, 2012 M. J. Sailor, Porous Silicon in Practice: Preparation, Characterization and Applications. 2012. Wiley-VCH Verlag GmbH & Co. KGaA.

Salt and Rauser, 1995 D. E. Salt, W. E. Rauser, Plant Physiol., 107 (1995), 1293–1301.

Snow et al., 1999 P. A. Snow, E. K. Squire, P. Russell, L. T. Canham, J. Appl. Phys. 86 (1999), 1781.

Spera et al., 2013a R. Spera, F. Festa, N. L. Bragazzi, E. Pechkova, J. LaBaer, C. Nicolini, J. Proteome Res., 12 (2013), 5535–5547.

Spera et al., 2013b R. Spera, T. T. Bezerra Correia, C. Nicolini, Sens. Act. B, 182 (2013) 682– 688.

Terracciano et al., 2013 M. Terracciano, I. Rea, J. Politi, L. De Stefano, , J. Europ. Opt. Soc., 8 (2013), 13075.

Theißl , 1997 B. Theißl, Science Reports 29 (1997), 91-192.
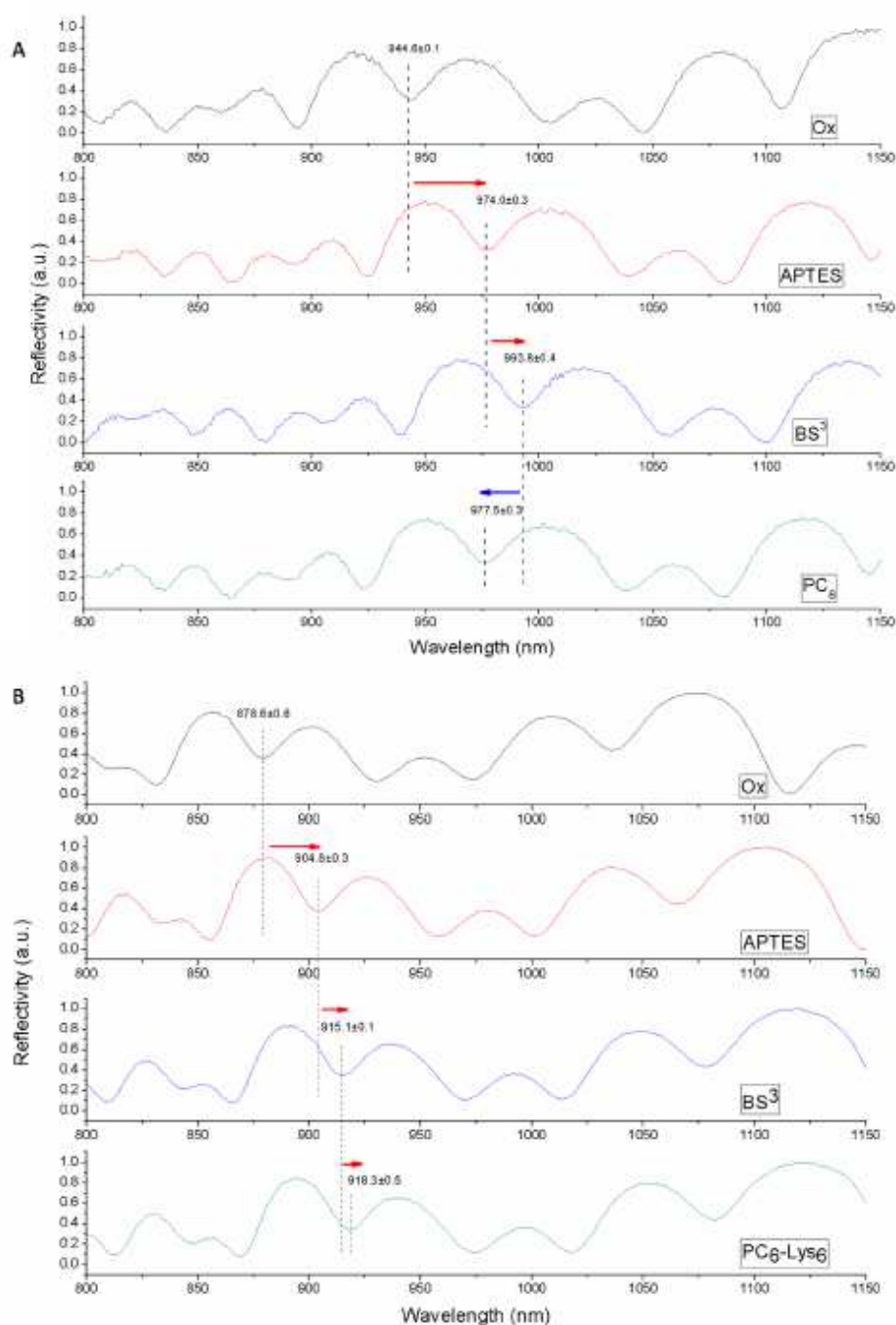
Figure(s)

Figure 1. PSi Thue-Morse reflectivity peak shifts after each step of biomodification from oxidized chip up to both PC$_6$ (A) and PC$_6$-Lys$_6$ (B) oligopeptides. Red arrows indicate optical red shift (mass adsorbed into the porous matrices); blue arrow indicates optical blue shift (mass subtracted by porous matrix).
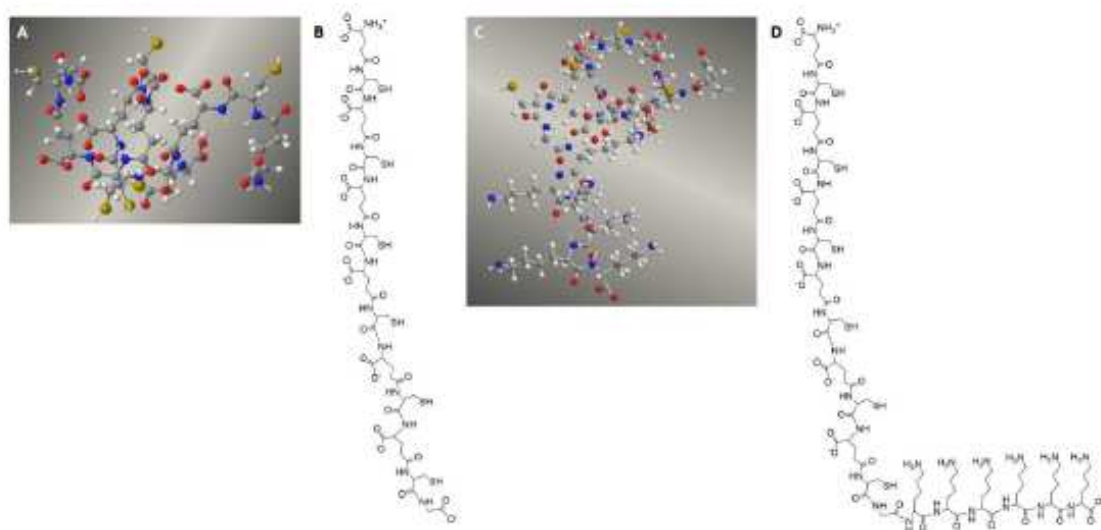
Figure 2. Schematic representation of oligopeptides used: PC_6 balls and stick model (A) and chemical structure representation (B); PC_6-Lys_6 balls and stick model (C) and chemical structure representation (D).
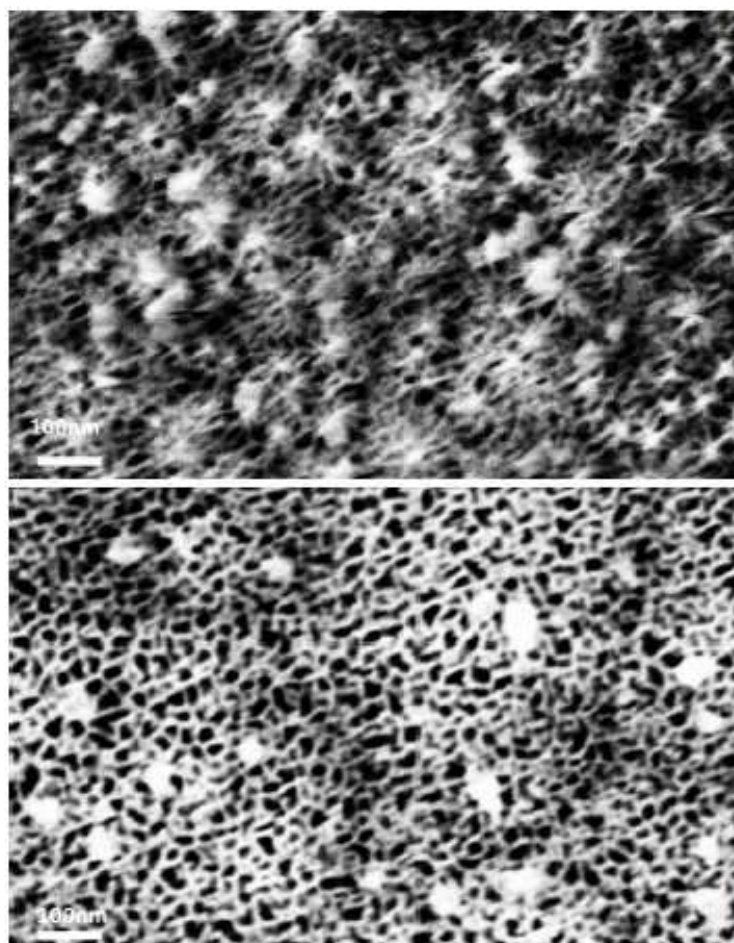
Figure 3. SEM images of PSi biochips biomodified up to PC_6 show evident corrosion (upper photo), while in case of PC_6-Lys_6 the surface is unaltered (bottom photo).
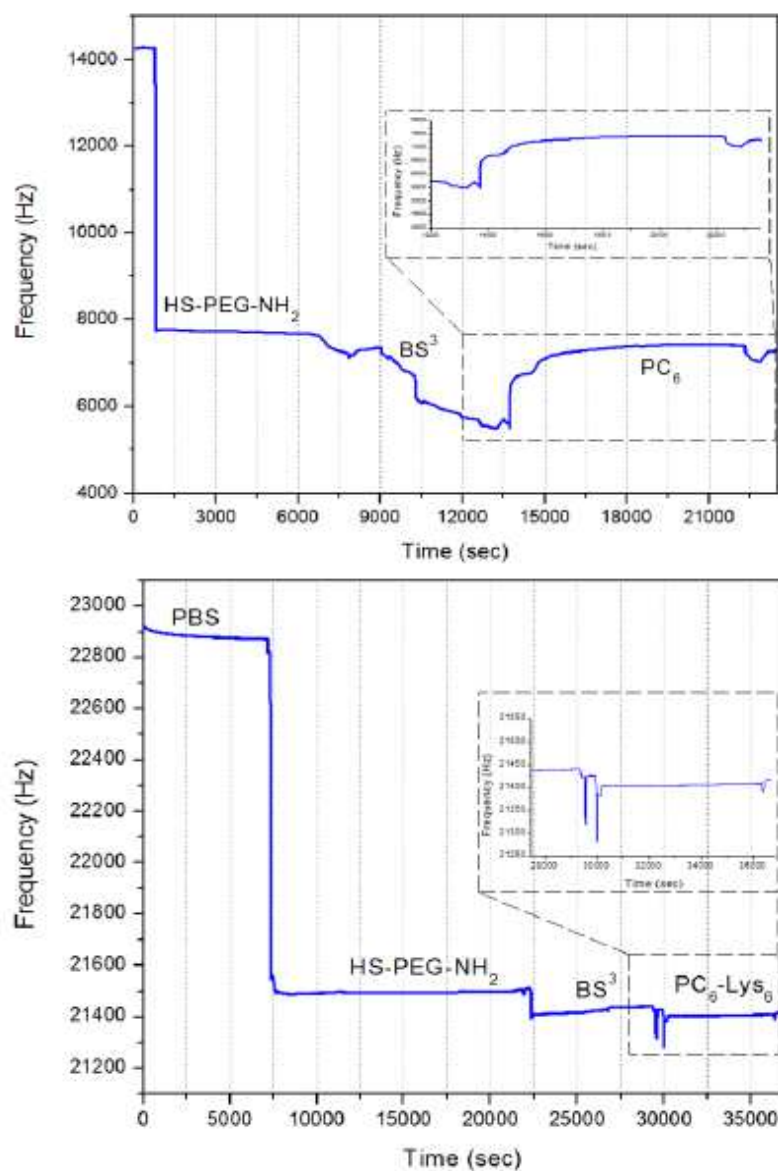
Figure 4. Real-time gravimetric monitoring of PC_6 (upper graph) and PC_6-Lys_6 (bottom graph) oligopeptides conjugation onto QRs surfaces.
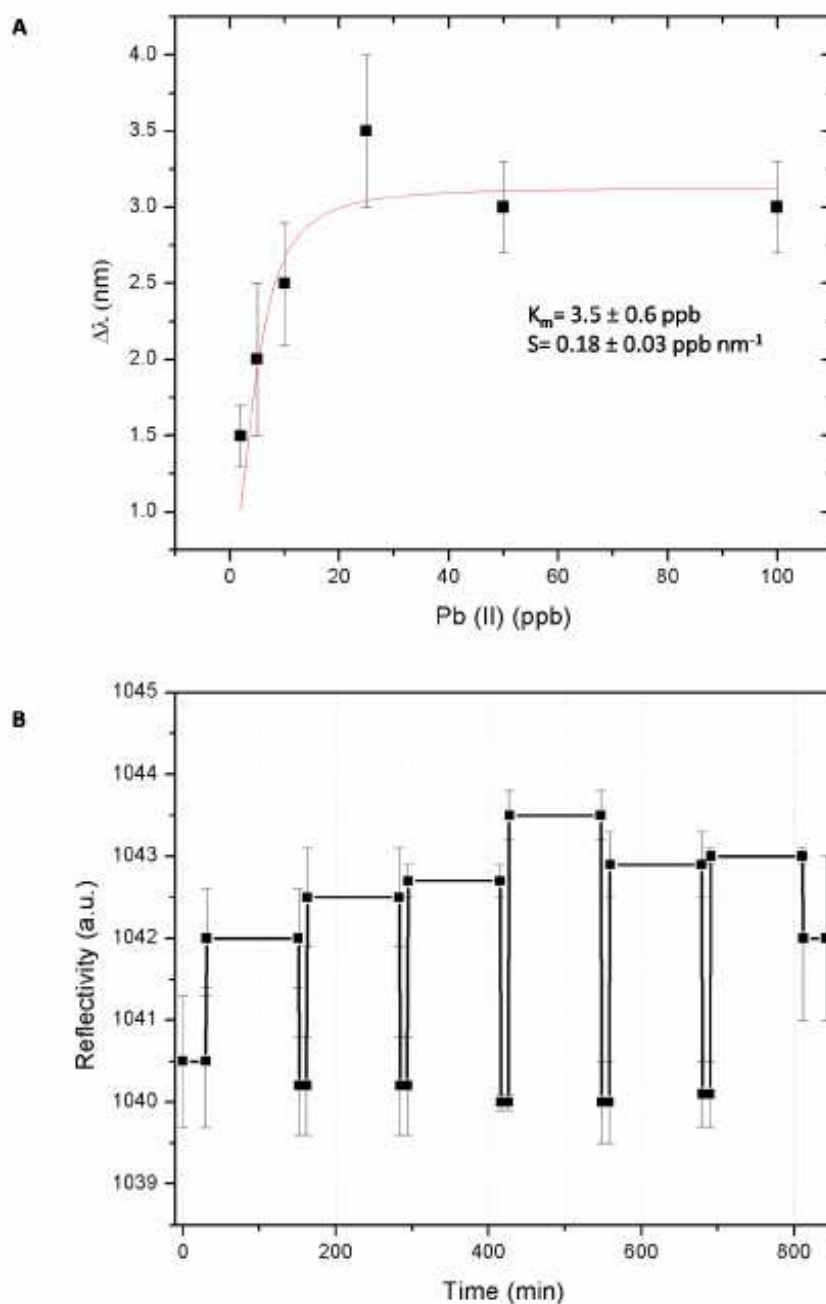
Figure 5. Lead (II) ions interaction monitoring optical measurements. Peak reflectivity shifts (at 1040nm) as function of lead (II) ions interaction monitoring (A); regeneration cycles: extensive water rinsing after each measurements restore signal line base (@1040nm) (B).
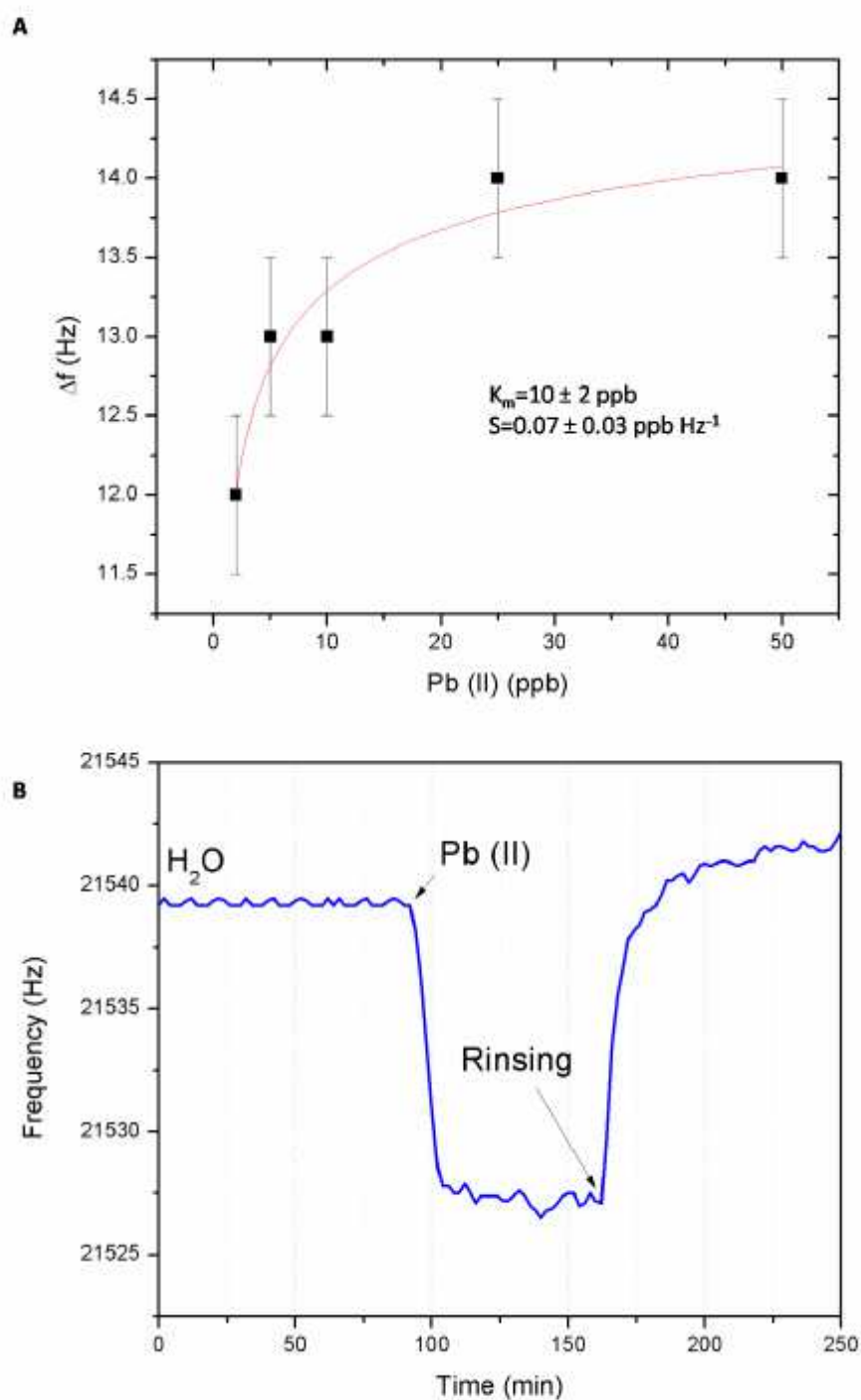
Figure 6. Lead (II) ions interaction monitoring by gravimetric measurements: trend of frequency change as function of lead (II) ions interaction monitoring (A);reversible binding cycle evidenced by QCM response (B).

3.2. Gold nanoparticles based monitoring

In the following sections, it will be discussed the enzyme and oligopeptides absorption onto peg diacid gold nanoparticles.

In particular, the enzyme called *TtArsC* from *Thermus thermophilus HB27* was used. This bacterium is an extremophile organism living in arsenic-rich geothermal environments that has developed ability in both oxidizing and reducing arsenic ions, thus playing an important role in its speciation and bioavailability. In the study reported in section 3.2.1, we report our results about adsorption of *TtArsC* enzyme on PEG-stabilized AuNPs (PEG-AuNPs) for monitoring its interaction with pentavalent arsenic ions (As (V)) and trivalent arsenic ions (As (III)). The nanobiosystem developed reveals the ability to speciate between arsenite and arsenate by a naked-eye visible change of color useful for in situ assays.

In section 3.2.2, the study of PEG-AuNPs biomodified by Phytochelatin oligopeptides for lead ions interaction monitoring is discussed. Also in this case, phytocelatins show an aggressive surface coverage that corroded PEG AuNPs, but not PEG AuNRs. The study conducted highlighted the good self-assembling of Phytochelatins onto nanostructured material and the characterization of Lead ions interaction monitoring with the novel and stable nanobiosystem.

3.2.1. Arsenic ions detection

Interaction of *Thermus thermophilus* ArsC enzyme and gold nanoparticles naked-eye assays speciation between As(III) and As(V)

Jane Politi[1,2], Jolanda Spadavecchia[3,4], Gabriella Fiorentino[5], Immacolata Antonucci[5], Sandra Casale[3] and Luca De Stefano[1]

[1] Institute for Microelectronics and Microsystems, Unit of Naples-National Research Council Via P. Castellino 111, 80127, Italy
[2] Department of Chemical Sciences, University of Naples 'Federico II', Via Cynthia, 80126 Naples Italy
[3] Sorbonne Universités, UPMC Univ Paris VI, Laboratoire de Réactivité de Surface, 4 place Jussieu, F-75005 Paris, France
[4] CNRS, UMR 7244, CSPBAT, Laboratoire de Chimie, Structures et Propriétés de Biomateriaux et d'Agents Therapeutiques Université Paris 13, Sorbonne Paris Cité, Bobigny, France CNRS, Paris, France
[5] Department of Biology, University of Naples 'Federico II', Via Cynthia, 80126 Naples, Italy

E-mail: jane.politi@na.imm.cnr.it and luca.destefano@na.imm.cnr.it

Abstract

The thermophilic bacterium *Thermus thermophilus HB27* encodes chromosomal arsenate reductase (*TtArsC*), the enzyme responsible for resistance to the harmful effects of arsenic. We report on adsorption of *TtArsC* onto gold nanoparticles for naked-eye monitoring of biomolecular interaction between the enzyme and arsenic species. Synthesis of hybrid biological–metallic nanoparticles has been characterized by transmission electron microscopy (TEM), ultraviolet-visible (UV–vis), dynamic light scattering (DLS) and phase modulated infrared reflection absorption (PM-IRRAS) spectroscopies. Molecular interactions have been monitored by UV–vis and Fourier transform-surface plasmon resonance (FT-SPR). Due to the nanoparticles' aggregation on exposure to metal salts, pentavalent and trivalent arsenic solutions can be clearly distinguished by naked-eye assay, even at 85 μM concentration. Moreover, the assay shows partial selectivity against other heavy metals.

S Online supplementary data available from stacks.iop.org/NANO/26/435703/mmedia

Keywords: arsenate reductase, gold nanoparticles, biorecognition, naked eye assay

(Some figures may appear in colour only in the online journal)

1. Introduction

Thermus thermophilus HB27 is an extremophile organism living in arsenic-rich geothermal environments: this bacterium has developed the ability to both oxidize and reduce arsenic, thus playing an important role in its speciation and bioavailability [1, 2]. Arsenate reduction mechanisms, apparently due to convergent evolution or originating in a common ancestor and then transferred to [3, 4], can be individuated into three families: the first family has been typified as *arsC* glutathione–glutaredoxin dependent (*arsC*-

GSH/Grx) and was identified in enteric bacteria (e.g. *Escherichia coli*); the second one is known as *arsC* tioredoxin dependent (*arsC-Trx*) and was found in Gram-positive bacteria (e.g. *Staphylococcus*). The last family, which includes the *ars2* gene, was amplified from *Saccharomyces cerevisiae* [5]. Microbial activities play critical roles in the geochemical cycling of arsenic because they can promote or inhibit its release from sediment material, mainly by redox reactions [6–8]. The reduction of pentavalent arsenate, As (V), to trivalent arsenite, As (III), is the major reaction causing the release of arsenic from the mineral surfaces into groundwater; in fact,

1

J Politi *et al*

besides being more toxic, arsenite is the most mobile and common form of arsenic found in anaerobic contaminated aquifers [9]. There is a worldwide demand to sense and quantify arsenic pollution, both natural and anthropogenic, in fresh water using low-cost and easy-to-use devices, especially in developing countries.

Nanostructured materials claim a range of exciting physical and chemical properties, which make them fundamental building blocks for the next generation of instruments and devices. In particular, gold nanoparticles (AuNPs) are among the most-used nano-objects, and are exploited in many applications ranging from medical to environment monitoring. The most popular method for preparing AuNPs in water uses citrate to reduce $HAuCl_4$ under boiling conditions [10]. Therefore, several approaches have been developed to reduce Au (III) salts in water using different ligands as colloid particle stabilizers [11]. Stabilizers, usually surfactant molecules, protect particles by avoiding aggregation mechanisms and controlling their physio-chemical properties [12, 13], but these molecules are mostly toxic. Dangerous organic molecules could be substituted by some biocompatible molecules, such as polyethylene glycol (PEG), in order to prepare biocompatible PEG-stabilized AuNPs [14, 15]. Recently, great advances have been made in the use of gold nanoparticles for signaling applications, owing to their stability, chemical reactivity, non-toxic nature, strong absorption and scattering properties, and electrostatic charges that allow strong interactions with proteins and enzymes [16, 17]. For instance, biomolecule- and/or biopolymer-conjugated AuNPs are largely used as biomarkers or biodelivery vehicles, as well as for cosmetics and as anti-aging components for skin protection [18, 19].

In the following study, we report our results on the adsorption of *TtArsC* enzyme onto PEG-stabilized AuNPs (PEG-AuNPs) for monitoring its interaction with pentavalent arsenic ions (As (V)) and trivalent arsenic ions (As (III)). Both the adsorption of enzyme onto PEG-AuNPs and its interaction with As (V) and As (III) salts can be followed easily by the naked eye, since solutions completely change their colors. UV–vis spectroscopy, polarization modulation infrared reflection/adsorption (PM-IRRAS) spectroscopy, dynamic light scattering (DLS) and Fourier transform-surface plasmon resonance (FT-SPR) were used as the main characterization techniques.

2. Experimental

2.1. Chemicals

Tetrachloroauric acid ($HAuCl_4$), sodium borohydride (NaBH4), polyethylene glycol 600 diacid (PEG diacid), β-Mercaptoethylamine (cysteamine), 1, 4-phenylenediisothiocyanate (PDC), ethanol (C_2H_5OH), pyridine, dimethylformamide (DMF), 15 mM Tris-HCl, potassium metarsenite ($NaAsO_2$), potassium arsenate (KH_2AsO_4), cadmium ions solution, lead (II) methanesulfonate ($C_2H_6O_6PbS_2$) and mercury (II) nitrate

solution (HgN_2O_6) were purchased from Sigma Aldrich. All chemicals were used without any further purification.

2.2. Purification and preparation of TtArsC enzyme

Recombinant *TtArsC* (*TtArsC*: protein arsenate reductase from the Gram-negative bacterium *Thermus thermophilus* HB27) was purified to homogeneity using the purification procedure already described, basically consisting of a thermo-precipitation of the *Escherichia coli* cell extract followed by anion exchange and gel filtration chromatography [20]. Fractions containing purified *TtArsC* were pooled, dialyzed against 15 mM Tris-HCl, 1 mM DTT, pH 7.5 and lyophilized in aliquots of 1 mg using a freeze dryer (HetoPowerDry PL6000, Thermo Scientific). Protein aliquots for nanoparticle interaction were prepared by resuspension of the protein in 1 ml of 15 mM Tris-HCl, pH 7.5.

2.3. Synthesis of PEG-stabilized Au nanospheres (PEG-AuNPs)

Li *et al* [10] have previously reported an easy method of synthesizing AuNPs from concentrated chloroauric acid solutions by adding sodium hydroxide as a reducer agent, citrate molecules as a stabilizer of colloidal solution. We modified this protocol using PEG-diacid as stabilizer molecules by the one-step method, using it inside the mixture reaction for AuNPs solution in spite of citrate molecules [21]. Briefly, 25 ml of chloroauric acid ($HAuCl_4$) aqueous solution (2.5×10^{-4} M) was added to 0.25 ml of PEG-diacid under stirring for 10 min at room temperature. After that, 20 ml of aqueous 0.01 M $NaBH_4$ was added at once. The formation of the PEG-AuNPs solution was observed by an instantaneous color change of the pale yellow solution to typical red/rose solution after addition of the $NaBH_4$ reducing agent. The PEG-AuNPs solution, prepared as described above, was centrifuged at 15 000 rpm for 26 min three times; then the supernatant was discarded while the residue was resuspended in an equivalent amount of buffer solution (PBS pH: 7). These procedures were repeated twice in order to remove the excess PEG-diacid.

2.4. Adsorption of TtArsC onto PEG-AuNPs

The enzyme *TtArsC* was adsorbed on PEG-AuNPs by using the following procedure: 1 ml of PEG-AuNPs was added into separate tubes containing 0.05 ml of *TtArsC* (1 mg ml^{-1} in 15 mM TrisHCl, pH 7). The resulting suspension of hybrid nanoparticles, reported in the following as *TtArsC*-AuNPs, was centrifuged twice at 6000 rpm for 20 min to remove excess protein, and then the pellets were re-dispersed in 1 ml MilliQ water. This colloidal solution was sonicated for 5 min and then stirred for 1 h at room temperature.

2.5. PM-IRRAS characterization

Polarization modulation infrared reflection absorption spectroscopy (PM-IRRAS) spectra were recorded on a commercial Thermo Nexus spectrometer (Les Ulis, France). The

device was set up by focusing the external beam, using an optimal incident angle of 80°, on the sample using a mirror. Prior to this, a ZnSe grid polarizer and a ZnSe photo-elastic modulator were placed on the sample, and the incident beam was tuned between p- and s-polarizations (HINDS Instruments, PEM 90, modulation frequency = 37 kHz). Finally, the light reflected by the sample was focused onto a nitrogen-cooled MCT detector. The presented spectra result from the sum of 128 scans recorded at 8 cm^{-1} resolution. Each spectrum reported represents the average of at least three measurements. The glass substrates (11 × 11 mm^2), coated by a 5 nm thick layer of chromium and a 200 nm thick layer of gold, were purchased from Arrandee (Werther, Germany). The gold-coated substrates were annealed on a butane flame to ensure a good crystallinity of the gold top layer and rinsed in a bath of absolute ethanol for 15 min before use.

Chemistry procedures based on a self-assembling monolayer of β-mercaptoethylamine (cysteamine) and a crosslinker have been described previously [22]. Briefly, the freshly cleaned gold substrates were immersed in an unstirred 10 mM ethanol solution of cysteamine at room temperature, in the dark, for 6 h. The gold substrates were then washed with ethanol and ultrapure water (Milli-Q, Millipore, France) to remove the excess thiols. The amino surface was treated following two strategies represented in scheme 1. Scheme S1 (A) shows that the amino surface was treated using 0.2% (w/v) of 1, 4-phenylenediisothio-cyanate (PDC) solution in a solution of 10% pyridine/90% dimethylformamide (DMF) for 2 h at room temperature. Then, the samples were successively washed in DMF and in ethanol and dried under a stream of nitrogen, leaving an isothiocyanate-derivatized surface. TtArsC was then chemically adsorbed to the isothiocyanate-covered slides by exposing the entire surface to the TtArsC solution for 40 min and then thoroughly rinsed twice in buffer and once in milliQ water. Scheme S1(B) shows how the amino surface was treated by EDC/NHS (80 mg/20 mg) and PEG-AuNPs modified with TtArsC solutions for 1 h and then rinsed with phosphate buffer solution and MilliQ water three times for 5 min. The resulting samples were used for PM-IRRAS investigations.

2.6. Transmission electron microscopy (TEM)

Transmission electron microscopy (TEM) measurements were recorded using a JEOL JEM 1011 microscope, which operates at an accelerating voltage of 100 KV. The TEM acquisitions were taken after separating the surfactant solution from the metal particles by centrifugation. Specifically, 1 ml of the nanoparticle solution was centrifuged at 14 000 rpm for 20 min. The supernatant was removed while the pellet was re-dispersed in 1 ml of water; then, a liquid droplet (10 μl) of the colloidal solution was deposited and dried on a microscope grid and finally analyzed.

2.7. Dynamic light scattering (DLS)

The size measurements were performed by dynamic light scattering (DLS) using a Zetasizer Nano ZS (Malvern

Instruments, Malvern, UK) equipped with a He-Ne laser (633 nm, fixed scattering angle of 173°, room temperature 25 °C).

2.8. UV/Vis measurements

The absorption spectra of each sample were recorded using a Jasco V-570 UV/VIS/NIR Spectrophotometer from Jasco Int. Co., Ltd, Tokyo, Japan, in the 200–800 nm range. The spectra were recorded after 30 min from the synthesis of PEG AuNPs, and from 2 min to 24 h after TtArsC enzyme adsorption. Finally, spectra were recorded after 10 min of TtArsC–AuNP interaction with each heavy metal solution.

2.9. FT-SPR

Fourier Transform-Surface Plasmon Resonance (FT-SPR) measurements were performed with an SPR 100 module from Thermo, equipped with a flow cell mounted on a goniometer. The setup was inserted in a Thermo-scientific Nexus FT-IR spectrometer, and a near-IR tungsten halogen light source was used. The incidence angle was adjusted at the beginning of each experiment with the minimal reflectivity located at 9000 cm^{-1}, in order to be in the highest sensitivity region of the InGaAs detector. Gold substrates for FT-SPR measurements were prepared at IMM-CNR in Lecce (Italy).

2.10. Heavy metals interaction monitoring

The interaction between TtArsC-AuNPs, As (V) and As (III) solutions was followed using UV–vis spectra of the TtArsC-AuNPs solution (50 μl of heavy metal solutions were added to 1 ml TtArsC-AuNPs solution) and the FT-SPR shifts of TtArsC-AuNPs–modified gold substrates using As (V) and As (III) at 750-325-170-85 μM. Furthermore, the interaction between TtArsC-AuNPs, Pb^{2+}, Cd^{2+} and Hg^{2+} solutions was followed using UV–vis spectra (50 μl of heavy metal solutions at 170 μM were added to 1 ml TtArsC-AuNPs solution).

3. Results and discussion

The interface properties of AuNPs are an interesting topic of study. In particular, the presence of chemical groups at the outer surfaces of AuNPs improves the ability of nanoparticles to interact with biological probes and consequently enhances the interaction of biosensing systems with target analytes. Coating AuNPs with a bifunctional PEG linker carrying two carboxylic groups using a one-step method [15–21] is one useful way to enhance the properties of interfaces: the so-called PEG-diacid can be used as a capping agent, an alternative approach with respect to the citrate-stabilized synthesis process [23, 24]. Furthermore, particle formation and growth can be tuned by exploiting the amphiphilic character of the PEG-diacid polymer in three steps: (1) reduction and stabilization of HAuCl$_4$ is facilitated by dicarboxylic acid-terminated PEG to form gold clusters through the exchange of electrons between them; (2) the presence of PEG-diacid molecules on gold surfaces shortens cluster dimensions and
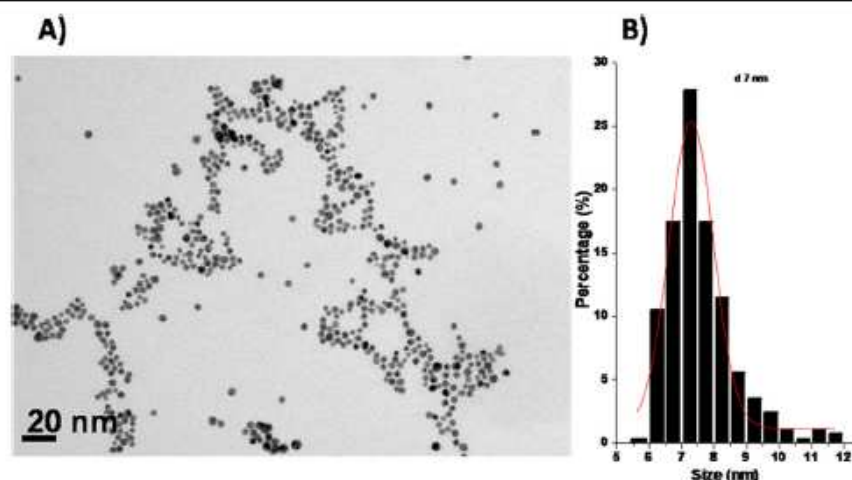
3

J Politi et al

Figure 1. TEM images of PEG AuNPs (A) and histogram of nanoparticle size distribution (B).
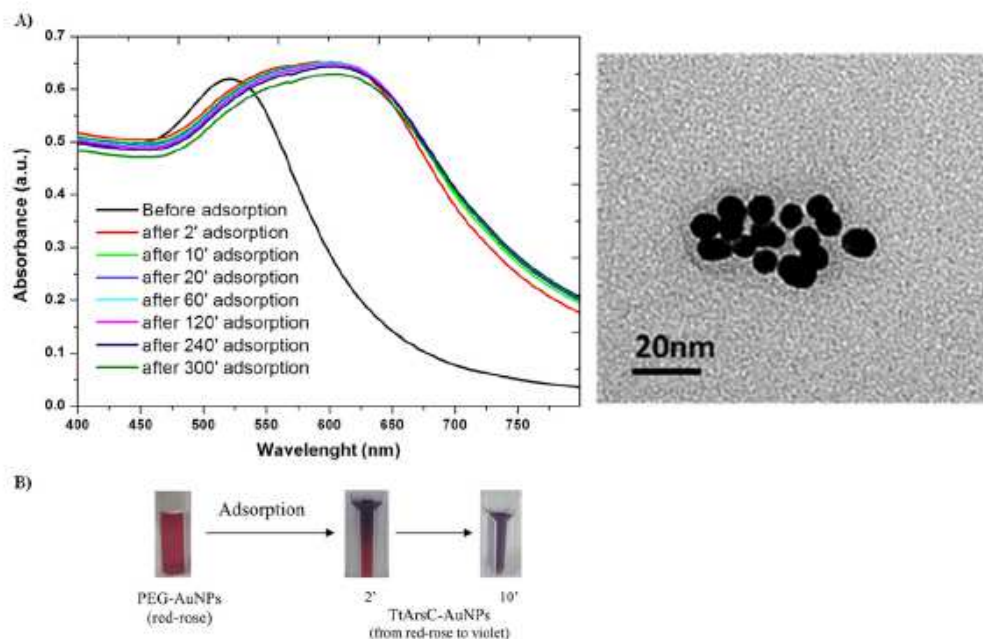

Figure 2. (A) UV–vis spectra of PEG AuNPs during adsorption of *TtArsC* enzyme as a function of time. (B) Schematic representation of nanoparticle solution change of color during adsorption of *TtArsC*.

(3) stabilizes the colloidal solution through electrostatic interactions between the carboxylic acid groups and the gold surface [15].

Figure 1(A) shows a TEM image of PEG-AuNPs after deposition on a microscope grid. The TEM picture of the PEG-AuNPs reveals fairly regular and monodispersed Au nanospheres. Figure 1(B) shows the histogram of 1623 particles: it can be fitted by a Gaussian curve with a mean size of 7 nm with a standard deviation of 2 nm. PEG-AuNPs were used as nanostructured supports for binding *TtArsC*

enzymes in the realization of an assay for biomolecular interaction. *TtArsC* enzyme adsorption onto PEG-AuNPs was monitored by the following methods: UV–Vis spectroscopy in order to monitor Localized Surface Plasmon (LSP) band shift; DLS characterizations in order to observe the aggregation/dispersion behavior of nanoparticles; TEM characterization in order to confirm the aggregation/dispersion behavior of nanoparticles; and PM-IRRAS characterizations in order to evaluate the chemical groups showed at the outer surfaces.
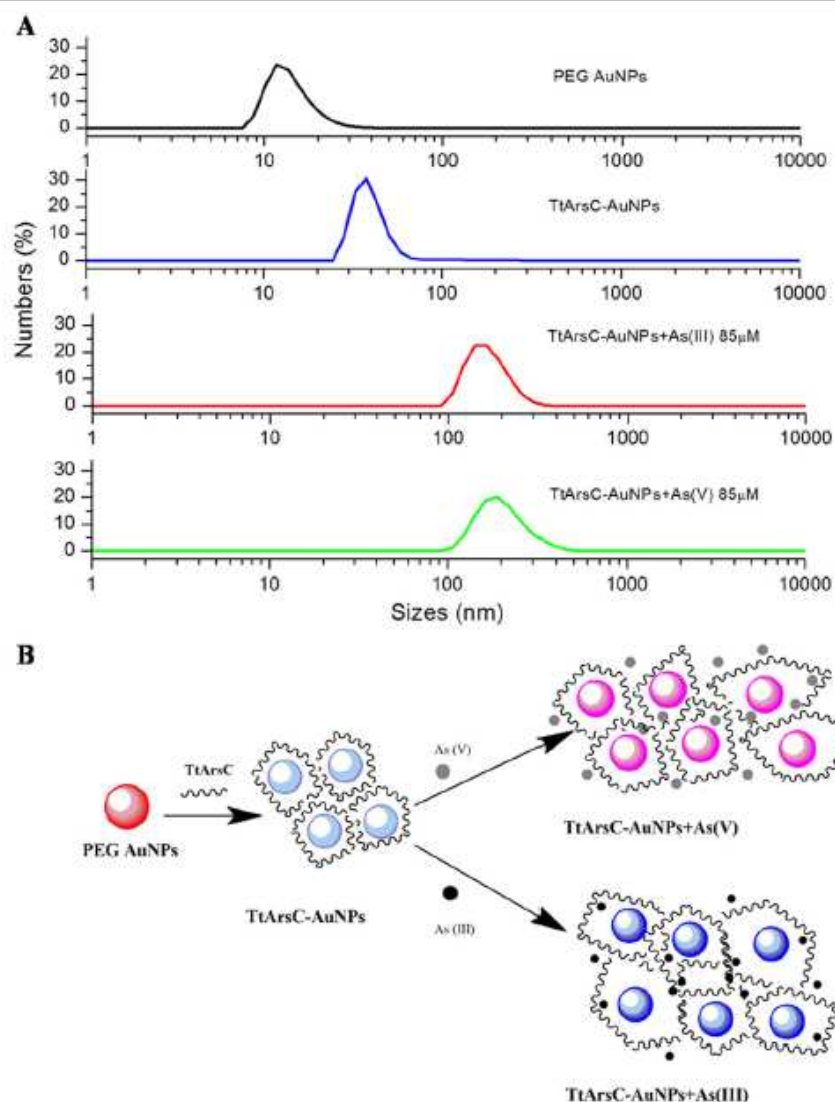
4

Figure 3. (A) Size change after each interaction step. (B) Schematization of aggregation process of PEG AuNPs with *TtArsC* enzyme and arsenate/arsenite ions.

Figure 2(A) (left graph) reports the LSP bands of PEG-AuNPs before and after the adsorption of enzyme molecules at equal concentrations of PEG-AuNPs in aqueous solution (10^{-4} M) as a function of time. Figure 2(A) (right image) reports the TEM image of PEG-AuNPs after adsorption to *TtArsC* (*TtArsC*-AuNPs), revealing an aggregation behavior of nanoparticles, while in figure 2(B) photographic images of the cuvettes containing the correspondent solutions are reported. The PEG-AuNP solution, before enzyme adsorption, shows an absorbance peak at 530 nm with a typical red/rose color, whereas, after mixing with the enzyme, in two minutes the color started changing and completed the reaction

in about 10 min, which corresponded to a shift of the LSP peak at around 640 nm. UV–vis spectra were recorded up to 24 h after *TtArsC* adsorption, although after 5 h the hybrid biological–metal nano-complex became stable, conferring a characteristic violet color to the solution. We estimated a hydrodynamic diameter of 14 ± 5 nm for PEG-AuNPs (figure 3(A)), while *TtArsC*-AuNPs have a hydrodynamic diameter of 39 ± 13 nm, which means that the enzyme aggregated three to four PEG-AuNPs on average. A more accurate evaluation of *TtArsC* adsorption on PEG-AuNPs was confirmed by PM-IRRAS, which is particularly useful to reveal the chemical groups exposed on nanoparticles' outer
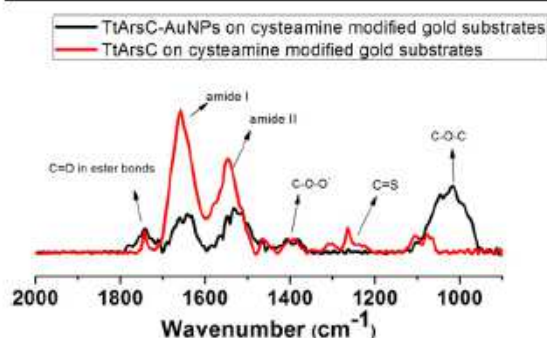
Figure 4. PM IRRAS spectra of *TtArsC* immobilized on cysteamine modified gold substrates (red line) and *TtArsC*-AuNPs on cysteamine-modified gold substrates (black line).

surfaces. Figure 4 reports, for comparison, a set of PM-IRRAS data from planar gold substrates where *TtArsC*-AuNPs (black line) and *TtArsC* alone (red line) have been covalently bonded. Figure 4 (black line) shows a peak at $1100\,cm^{-1}$ attributed to -COOH groups of PEG-diacid, and peaks at $1400\,cm^{-1}$ and $1450\,cm^{-1}$, typical of -COO- stretching vibrations.

Peaks at $1660\,cm^{-1}$ and $1530\,cm^{-1}$ are also present, representing amide II and I, respectively, which are characteristic of all proteins and enzymes. Peak at $1730\,cm^{-1}$ represent the C=O stretching mode of PEG-AuNPs immobilized onto a gold surface, thus endorsing an effective functionalization of the surface. The presence of a strong stretching band at $1100\,cm^{-1}$ together with peaks at $1450\,cm^{-1}$ and $1730\,cm^{-1}$ suggests the stabilization of the AuNPs with PEG molecules.

Figure 4 (red line) shows a peak at $1100\,cm^{-1}$ representing stretching of aliphatic ethers, a peak at $1240\,cm^{-1}$ characteristic of C=S stretching of the PDC crosslinker, and the amide I and II peaks at $1530\,cm^{-1}$ and $1660\,cm^{-1}$, respectively. The intensities of these peaks are higher with respect to the precedent case, due to rearrangement of *TtArsC* on AuNPs, where PEG-diacid functional groups interacting with the enzyme can partially mask the amide bonds. In this paper, we investigate a versatile chemistry modification that uses homobifunctional crosslinker PDC in order to achieve covalent binding of TtArsC before and after interaction with PEG-AuNPs. The isothiocyanate group present in PDC crosslinker generally act as electrophiles with a carbon atom as the electrophilic center. Electrophilic substitutions with the amino group of cysteamine lead to a stable ligand with a crosslinker that allows covalent binding of TtArsC and TtArsC-AuNPs.

Since the *TtArsC* enzyme is specialized in binding and transforming arsenic compounds, FT-SPR measurements were used to monitor the interaction between *TtArsC*-AuNPs and arsenate (As(V))/arsenite (As(III)) ions; four different concentrations were used for each salt and the details of the results are reported in figure 5. Figure S2 represents a typical shift of surface plasmon resonance from $9000\,cm^{-1}$ before interaction (black line in left graph) to $8600\,cm^{-1}$ after ion

detection (red line in left graph), and the shift of peak position as a function of time during the binding cycle followed by rinsing (right graph).

Figure 5 clearly shows that the interaction between *TtArsC*-AuNPs and arsenate/arsenite ions is concentration dependent (panels **A** and **C**); in both panels, each point reported represents the value of plasmon stabilization after interaction with arsenate/arsenite ions as a function of different concentration. The linear regression parameters obtained by OriginLab Software™ for both arsenite/arsenate ion interaction monitoring are reported in tables S1 and S2 in supplementary data. Moreover, the absolute position of the plasmon absorbance peak changes as a function of different concentrations for both arsenate and arsenite (panels B and D, respectively). Experimental data points in figures 5(B) and (D) were fitted using OriginLab Software™ by Michaelis-Mentens dose-response exponential equation:

$$y(x) = A^* e^{(x/C)} + y_0 \qquad (1)$$

where A represents the amplitude and C a growth constant. The first derivative of equation (1) is

$$y^1(x) = (A/C)^* e^{(x/C)} \qquad (2)$$

By equation (2), the sensitivity of the nanosystem in ion biorecognition can be obtained as $y^1(x_M)$ where x_M is the middle point of each data set:

$$S_{AsV} = 1.6 \pm 0.2\ cm^{-1}\,\mu M^{-1}$$

$$S_{AsIII} = 2.82 \pm 0.02\ cm^{-1}\,\mu M^{-1}$$

where S_{AsV} is the sensitivity of the system against arsenate and S_{AsIII} is the sensitivity of the system against arsenite. The estimated sensitivities reveal that the nanobiocomplexes have a higher sensitivity for As (III) ions with respect to As (V) ions, even if the natural substrates of *TtArsC* enzyme are arsenate ions. As is already known [19], the *TtArsC* enzyme has a redox system, able to link the reduction of arsenate to the consumption of dihydronicotinamide adenine dinucleotide phosphate, the so-called NADPH, by using the thioredoxin reductase/thioredoxin (Tr/Trx) system for the redox recycling with a catalytic mechanism that involves the thiol group of the N-terminal cysteine residue (Cys7). In view of our results, we can deduce that these amino acid residues, essential in redox reactions, are partially or totally masked, due to the adsorption of the enzyme onto the PEG-AuNPs' surface.

Further investigations on biorecognition at 85 μM concentrations of both arsenite and arsenate have been performed by UV–vis measurements (see curves in figure 6). The LSP bands and the images reported also showed that, at the lowest concentration tested, a change of LSP band position and of the color of the solutions is clearly observable, thus confirming the biomolecular interaction quantified by FT-SPR measurements. Furthermore, the photographic images reported on the left of figure 6 highlight how the solution color change is a function of the arsenic ions' oxidation state: the solution of *TtArsC*-AuNPs became violet/pink on exposure to As(V), while in the case of As(III) it turned to blue. In both cases, it was clearly visible to the naked eye. Again, we
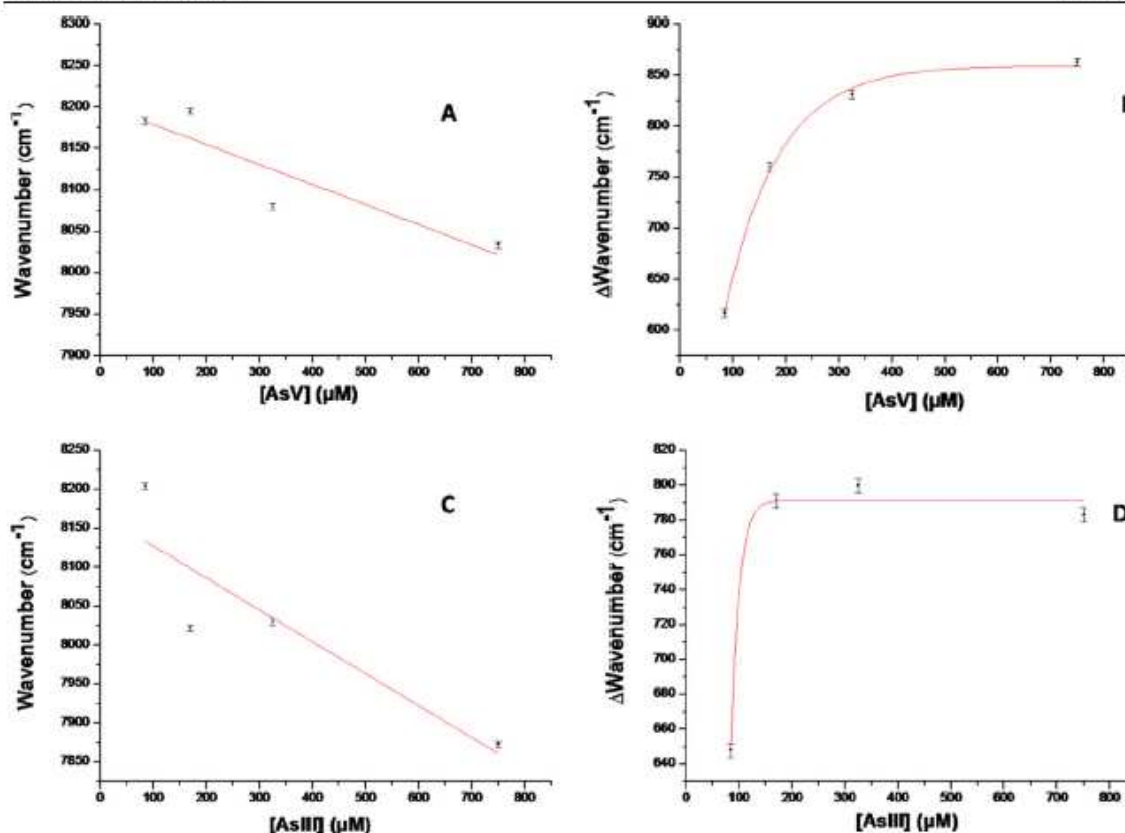
Figure 5. Trasmittance of SPR trend by increasing concentration of As V (A) and As III (C) solutions; shift of SPR trasmittance as a function of increasing concentration (85–170–325–750 μM) of As V (B) and As III (D) solutions.
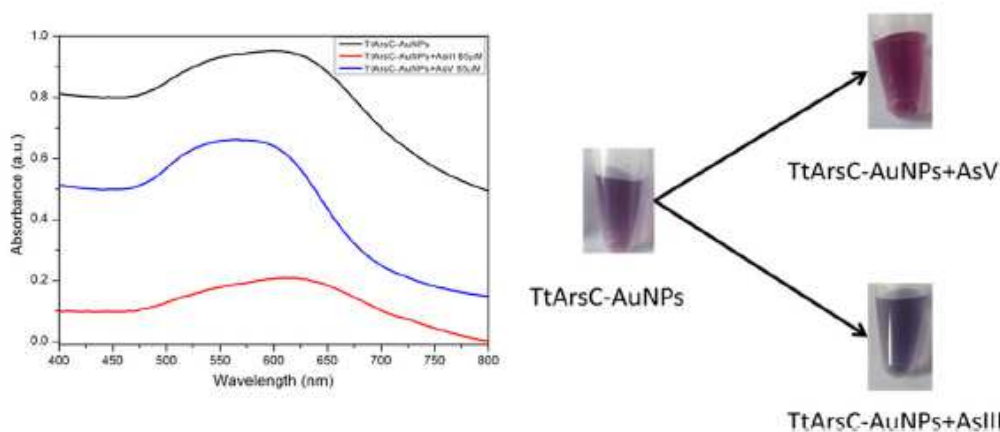

Figure 6. UV–vis spectra (vertically shifted for clarity) of *TtArsC*-AuNPs before and after interaction with arsenate and arsenite ions (right graph). Images of *TtArsC*-AuNPs color change after interaction with arsenate and arsenite ions (left scheme).

attributed this macroscopic evidence of biomolecular interaction to the nanoparticle clustering process; this is also confirmed by the DLS data in figure 3(A), specifically the fourth (red) and fifth (green) curves.

We sketched the interaction mechanism in the scheme reported in figure 3(B). Enzyme biosensing was achieved using gold nanoparticles [25]. These peptides lead to the assembly of nanoparticles due to their crosslinking by long-
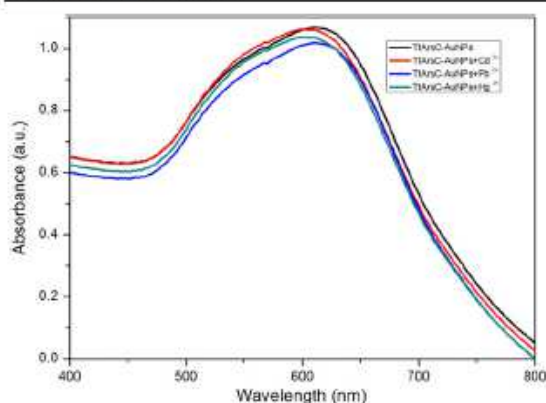
7

Figure 7. UV–vis spectra of TtArsC adsorbed on PEG AuNPs after interaction with cadmium, mercury and lead ions.

chain molecules. This aggregation–dispersion process leads to the colorimetric changes in the nanoparticle solution. Aggregation of gold nanoparticles leads to red shift in the plasmon band due to the electric dipole–dipole interaction, which in turn leads to a coupling between the plasmon oscillations of different particles [26]. The color of the gold nanoparticle solution turns from red to blue/purple due to red shift in the plasmon band. Aggregated or assembled nanoparticles display red shift in the plasmon band when compared to the isolated gold nanoparticles. This phenomenon is attributed to the coupling between the dipole modes of plasmons of different particles. As the interparticle distance is decreased, more red shift in the plasmon band is observed due to an increase in the extent of coupling.

In order to verify the interference of other heavy metal ions that are not natural substrates for the enzyme in the recognition of arsenic ions, UV–vis measurements have been performed in the presence of single ion species (Cd^{2+}, Pb^{2+} and Hg^{2+}) at a concentration of 170 μM. Figure 7 shows that in the presence of such heavy metals, there are not relevant changes in LSP position or intensity, indicating that the assay is highly specific against arsenic compounds. In order to verify whether the nanobiocomplex was also selective for As (III) and As (V), we measured the UV–vis spectra in the presence of a mixture of heavy metals. The results are reported in figure S3. We found that, despite the apparent insensitivity to other heavy metal ions that can be conjectured by data in figure 6, on exposure to a complex mix, the LSP in UV–vis spectra is quite different from the reference ones, i.e. the spectra obtained for As (III) and As(V) alone. This behavior demonstrates a lack of selectivity and prevents the use of the assay for a quantitative measurement of arsenic ions in a complex mixture. Nevertheless, since the solution always changes color in the presence of As(III) and As(V), the assay can be simply and usefully used in fast and cheap screening of water quality.

4. Conclusions

In this work, we used a novel chromosomal arsenate reductase (*TtArsC*) as biomolecular probe to screen for the presence of arsenic in water. Using optical, label-free techniques, we have characterized the interaction between *TtArsC* and arsenic ions, quantitatively evaluating interaction and biorecognition with pentavalent arsenic, As(V), and trivalent arsenic, As(III). The novel and original nanobiocomplexes demonstrated stability and the capacity to strongly bind the toxic ions. Experimental data demonstrated relevant signal changes, i.e. variation of the FT-SPR peak position (about 200 cm^{-1} also at low concentrations). *TtArsC*-AuNPs showed greater sensitivity for arsenite ions, as opposed to what happens in nature, where arsenate ions are the main substrate of *TtArsC* enzymes. On these bases, *TtArsC*-AuNP nanobiocomplexes were found to be able to interact with arsenite ions solutions, veering to blue solutions, and arsenate ions solutions, veering to violet/pink solutions, at all concentrations tested. These phenomena were confirmed quantitatively by LSP shifts in UV–vis spectra, and DLS characterization reveals that the nanobiocomplex aggregates in the presence of arsenic ions. Finally, LSP band study in the presence of metal ions that are not enzyme substrates (Cd^{2+}, Pb^{2+} and Hg^{2+}) indicated that the biorecognition is highly specific but not completely selective. A straightforward application in fast and low-cost screening of water can be envisaged.

Acknowledgments

Supplementary data

Scheme of immobilization on gold support for PM-IRRAS analysis; working principle of FT-SPR; further investigation of LSP band in UV–vis spectrum and naked-eye response of the *TtArsC*-AuNPs in the presence of complex mixtures of heavy metals are reported.

References

[1] Espino D P, Tamames J, de Lorenzo V and Cánovas D 2009 Microbial responses to environmental arsenic *Biometals* **22** 117–30

[2] Gihring T M and Banfield J F 2001 Arsenite oxidation and arsenate respiration by a new Thermus isolate *Microbiol. Lett.* **204** 335–40

[3] Jackson C R and Dugas S L 2003 Phylogenetic analysis of bacterial and archaealarsC gene sequences suggests an ancient, common origin for arsenate reductase *BMC Evol. Biol.* **3** 18

[4] Macy J M, Santini J M, Pauling B V, O'Neill A H and Sly L I 2000 Two new arsenate/sulfate-reducing bacteria: mechanisms of arsenate reduction *Arch. Microbiol.* **173** 49–57

[5] Mukhopadhyay R and Rosen B P 2002 Arsenate reductases in prokaryotes and eukaryotes *Environ. Health Perspect.* **5** 745–8

[6] Reyes C, Lloyd J R and Saltikov C W 2008 *Arsenic Contamination of Groundwater: Mechanism, Analysis, and Remediation* (Hoboken, NJ: Wiley) pp 123–46

[7] Oremland R S and Stolz J F 2005 Arsenic, microbes and contaminated aquifers *Trends Microbiol.* **13** 45–9

[8] Bartolucci S, Contursi P, Fiorentino G, Limauro D and Pedone E 2013 Responding to toxic compounds: a genomic and functional overview of Archaea *Front. Biosci.* **18** 165–89

[9] Murphy J N and Saltikov C W 2009 The ArsR repressor mediates arsenite-dependent regulation of arsenate respiration and detoxification operons of Shewanella sp. Strain ANA-3 *J. Bacteriol.* **191** 6722–31

[10] Li C, Li D, Wan G, Xu J and Hou W 2011 Facile synthesis of concentrated gold nanoparticles with low size-distribution in water: temperature and pH controls *Nanoscale Res. Lett.* **6** 1–10

[11] Huo Z, Tsung C, Huang W, Zhang X and Yang P 2008 Sub-Two Nanometer Single Crystal Au Nanowires *Nano Lett.* **7** 2041–4

[12] Li N, Zhao P, Liu N, Echeverria M, Moya S, Salmon L, Ruiz J and Astruc D 2014 'Click' chemistry mildly stabilizes bifunctional gold nanoparticles for sensing and catalysis *Chem. Eur. J.* **20** 8363–9

[13] Spadavecchia J, Apchain E, Albéric M, Fontan E and Reiche I 2014 One-step synthesis of collagen hybrid gold nanoparticles and formation on Egyptian-like gold-plated archaeological ivory *Angew. Chem. Int. Ed.* **53** 1756–89

[14] Doane T L, Cheng Y, Babar A, Hill R J and Burda C 2010 Electrophoretic mobilities of PEGylated Gold NPs *J. Am. Chem. Soc.* **132** 15624–31

[15] Spadavecchia J, Perumal R, Barras A, Lyskawa J, Woisel P, Laure W, Pradier C-M, Boukherroub R and Szunerits S 2014 Amplified plasmonic detection of DNA hybridization using doxorubicin-capped gold particles *Analyst* **139** 157–64

[16] Manson J, Kumar D, Meenan B and Dixon D 2011 Polyethylene glycol functionalized gold nanoparticles: the influence of capping density on stability in various media *Gold Bulletin* **44** 99–105

[17] Tian L, Gandra N and Singamaneni S 2013 Monitoring controlled release of payload from gold nanocages using surface enhanced Raman scattering *ACS Nano* **7** 4252–60

[18] Zhenhai G, Jianhui J, Ting Z and Daocheng W J 2011 Preparation of rhodamine B fluorescent poly(methacrylic acid) coated gelatin nanoparticles *Nanomaterials* **1** 753705

[19] Huang H J *et al* 2011 Biocompatible transferrin-conjugated sodium hexametaphosphate-stabilized gold nanoparticles: synthesis, characterization, cytotoxicity and cellular uptake *Nanotechnology* **22** 395706

[20] Del Giudice I, Limauro D, Pedone E, Bartolucci S and Fiorentino G 2013 A novel arsenate reductase from the bacterium Thermusthermophilus HB27: its role in arsenic detoxification *Biochim. Biophys. Acta* **1834** 2071–9

[21] Politi J, Spadavecchia J, Iodice M and De Stefano L 2015 Oligopeptide–heavy metal interaction monitoring by hybrid gold nanoparticle based assay *Analyst* **140** 149–55

[22] Spadavecchia J, Moreau J, Hottin J and Canva M 2009 Newcysteamine based functionalization for biochip applications *Sensors Actuators* B **143** 139–43

[23] Neoh K G and Kang E T 2011 Functionalization of inorganic nanoparticles with polymers for stealth biomedical applications *Polym. Chem.* **2** 747–59

[24] Pernodet N, Fang X, Sun Y, Bakhtina A, Ramakrishnan A, Sokolov J, Ulman A and Rafailovich M 2006 Adverse effects of citrate/gold nanoparticles on human dermal fibroblasts *Small* **2** 766–73

[25] Liu J and Lu Y 2004 Adenosine-dependent assembly of aptazyme-functionalized gold nanoparticles and its application as a colorimetric biosensor *Anal. Chem.* **76** 1627–32

[26] Mirkin C A, Storhoff J J, Lazarides A A, Macic R C, Letsinger R L and Schatz G C 2000 What controls optical properties of DNA-linked gold nanoparticle assemblies? *J. Am. Chem. Soc.* **122** 4640–50

3.2.2. Lead ions detection

Oligopeptide–heavy metal interaction monitoring by hybrid gold nanoparticle based assay

Jane Politi,†[abd] Jolanda Spadavecchia,†*[bc] Mario Iodice†[a] and Luca de Stefano†[a]

Phytochelatins are small peptides that can be found in several organisms, which use these oligopeptides to handle heavy metal elements. Here, we report a method for monitoring interactions between lead(II) ions in aqueous solutions and phytochelatin 6 oligopeptide bioconjugated onto pegylated gold nanorods (PEG-AuNrs). This study is the first step towards a high sensitive label free optical biosensor to quantify heavy metal pollution in water.

1. Introduction

Nanostructured materials have become increasingly popular due to their unique properties as well as their promising breakthrough in the development of novel biosensors for medical diagnostics and environmental monitoring.[1–3] In recent years, gold nanoparticles have been widely applied in biosensor devices due to their unique size-dependent optical properties.[4–6] Therefore, more attention should be paid to find efficient synthesis methods to match the enlarging demand for gold nanoparticles (AuNPs). Several different solution synthesis methods have been employed to prepare gold nanoparticles, including biomolecule reduction of $HAuCl_4$,[7] seed mediated synthesis at room temperature[8] and polymer-assisted synthesis.[9] Recently, the utility of nanomaterials for any application has been strongly dependent upon their physicochemical characteristics and their interactions with surface modifiers. Let us recall the importance of stabilizers, used in the synthesis of nanoparticles, not only to protect particles against aggregation but also to control their functional properties. Biver et al.[10] synthesized Au nanoparticles using thio-alkylated oligoethylene glycols and functionalized them with various fluorescent Acridine Orange derivatives.[11] Exchange of organic molecules on Au nanoparticles with PEG can indeed be performed to prepare biocompatible PEG-stabilized Au nanoparticles.[12] Wang et al. synthesized a polyethylene glycol (PEG)-modified gold nanoparticle complex by a one-step reaction synchrotron X-ray irradiation method.[13] A low concentration of unmodified PEG macromolecules is very important to control the particle size and stabilize gold nanoparticles to demonstrate high stability under realistic biomedical conditions.[14] Other approaches were applied to stabilize gold nanoparticles using sulfur-containing polymers, with a possible limitation of their suitability for specific biomedical application. Self-assembly of biomolecular probes with free thiol groups on gold nanoparticle surface is allowed by well-known specific interactions, such as the Au–SH bond, thus avoiding complex chemical procedures for covalent conjugation.[15,16] Some studies[17–19] showed that gold nanoparticles can interact with specifically sequenced peptides that can self-assemble on their surface. The polypeptides could induce or prevent aggregation of nanoparticles causing consequently the change of absorbance and, moreover, allow them to interact with other metal ions i.e. Cd^{2+}, Ni^{2+}, Co^{2+}, Zn^{2+}, etc. Lead is a widely used heavy metal and has a large number of industrial applications, such as battery manufacturing, paint, gasoline, alloys, radiation shielding, piping and so on. The lead content in paints and gasoline represents a severe risk of environmental pollution and, consequently, for human health. Lead is toxic by ingestion and inhalation, and can seriously affect the gut and the central nervous system, and it can also cause anemia.[20,21] Furthermore, overexposure to lead can also cause birth defects, mental retardation, behavioral disorders, and death in fetuses and young children.[22,23] Beside social impacts, detection and quantization of lead contamination is not an easy task since water is a complex matrix and any method proposed should be not only sensitive but also highly selective: the lead content should be determined in the presence of lot of interference substances, without any pre-treatment of the collected sample. This is the reason why bioprobes having high specific affinity with this metal must be used. Some oligopeptides, named phytochelatins (PCs), with a structural relationship to glutathione (γ-Glu–Cys–Gly) have been widely studied because of their ability to chelate heavy metal ions in plants and fungi for detoxification mechanisms.[24,25] PCs are formed by dipeptide γ-Glu–Cys repeated from 2 to 11 times followed by a final Gly, so that their general structure is (γ-Glu–Cys)$_n$Gly. We report here

[a]Institute for Microelectronics and Microsystems, Unit of Naples-National Research Council, Via P. Castellino 111, 80127, Italy
[b]Sorbonne Université, UPMC Univ Paris 06, Laboratoire de Réactivité de Surface, 4 place Jussieu, F-75005 Paris, France. E-mail: jolanda.spadavecchia@upmc.fr
[c]CNRS, UMR 7197, Laboratoire de Réactivité de Surface, F-75005, Paris, France
[d]Department of Chemical Sciences, University of Naples, Federico II, Via Cintia, 80126 Naples, Italy

† All authors contributed equally to this work.

the synthesis to prepare polymer-modified gold nanoparticles and gold nanorods using dicarboxylic PEG (DPEG) as the stabilizer. We have thus implemented and evaluated a simple and reproducible method for labeling biomolecules with PEG gold nanostructures without utilizing organic solvents and surfactants. A new kind of pegylated gold nanorod based assay to quantify lead–phytochelatin 6 (PC6) interactions in aqueous solutions by using oligopeptides as bioprobes was developed. Ultraviolet-visible (UV-Vis) spectroscopy and Fourier transform surface plasmon resonance (FT-SPR) have been used for monitoring the formation of metal–biological complexes at different concentrations of lead.

2. Experimental

2.1. Materials

Tetrachloroauric acid (HAuCl$_4$), sodium borohydride (NaBH4), ethanol (C$_2$H$_5$OH), polyethylene glycol 600 Diacid (DPEG; $M_w =$ 600 Da), cetyl-trimethyl ammonium bromide (CTAB), β-mercaptoethylamine (cysteamine), N-hydroxysuccinimide (NHS), 1-(3-dimethylaminopropyl)-N′-ethylcarbodiimide hydrochloride (EDC), PBS (phosphate buffer solution, pH 7.2), and lead(II) methanesulfonate solution were purchased from Sigma Aldrich. Phytochelatin 6 (PC6) was purchased from the Anaspec IGT group. All chemicals were used without any further purification. Gold substrates for FT-SPR measurements were deposited at IMM-CNR in Lecce (Italy).

2.2. Synthesis of pegylated Au nanorods (PEG-AuNRs)

The synthesis of pegylated gold nanorods (PEG-AuNRs) was performed following the well established seed-mediated procedure, in the presence of CTAB and DPEG in growth solution. Seed solution (S): seed particles were prepared following the method described elsewhere.[26,27] Briefly, 5 mL of CTAB (0.20 mol L^{-1}) were added to 5 mL of an aqueous solution containing HAuCl$_4$ (2.5×10^{-4} mol L^{-1}) under stirring conditions at room temperature. 0.6 mL of ice-cooled NaBH$_4$ (0.01 mol L^{-1}) was then added. Growth solution (G): growth solution was prepared by adding 5 mL of CTAB (0.02 mol L^{-1}) to a solution of 0.75 mL of DPEG and under stirring for 10 min at room temperature. After 10 min 0.25 mL AgNO3 (4×10^{-3} mol L^{-1}) and 5 mL of HAuCl$_4$ (1×10^{-3} mol L^{-1}) were transferred to the mixture for 5 min. After this time, 70 μl of ascorbic acid (8×10^{-3} M) was added. The synthesis of PEG hybrid gold nanorods (AuNrs) was achieved as follows: 12 μl of gold seed solution (S) was transferred to the growth solution (G) under room temperature conditions.

2.2.1. Synthesis of pegylated Au nanoparticles (PEG-AuNPs).
Li et al.[28] have reported a facile method to synthesize AuNPs from concentrated chloroauric acid by adding sodium hydroxide in the presence of citrate as the stabilizer. We modified this protocol by adding dicarboxylic PEG as the surfactant, in the mixture reaction. Briefly, 25 mL of chloroauric acid (HAuCl$_4$) aqueous solution (2.5×10^{-4} M) was added to 0.25 mL of dicarboxylic PEG and mixed under magnetic stirring for 10 min at room temperature. To this solution, 20 mL of aqueous 0.01 M NaBH$_4$ was added at once. The formation of the

PEG-AuNPs was observed as an instantaneous color change of the solution from pale yellow to bright red after addition of the reducing agent. The as-prepared PEG-AuNP solution was centrifuged at 15 000 rpm for 26 min three times and then the supernatant was discarded and the residue was redispersed in an equivalent amount of buffer solution (PBS pH: 7). This was repeated twice principally to remove the excess dicarboxylic PEG. Stock solutions were stored at 27–29 °C and characterized using UV-Vis spectroscopy and transmission electron microscopy (TEM).

2.2.2. Bioconjugation of PEG-AuNrs and PEG-AuNPs with PC6.
The gold nanorod surface was modified with PC6 peptides according to the following procedure (see Scheme 2). 0.5 mL of the PEG-AuNrs and PEG-AuNPs in a buffered solution (PBS, pH: 7.2) were added into separate tubes containing 0.5 mL of PC6 (0.7 μM). Next, the AuNr–AuNP/PC6 suspension was centrifuged twice at 6000 rpm for 20 min to remove the excess protein and then the pellets were redispersed in 1 mL MilliQ water. The resultant colloidal solution was sonicated for 5 min and then stirred for 1 h at room temperature. Scheme 1 depicts the bioconjugation of gold nanospheres and nanorods.

2.2.3. PC6 immobilization on gold substrates.
For PM-IRRAS analyses, glass substrates (11 × 11 mm^2), successively coated with a 5 nm thick layer of chromium and a 200 nm thick layer of gold, were purchased from Arrandee (Werther, Germany). The gold-coated substrates were annealed in a butane flame to ensure good crystallinity of the topmost layers and rinsed in a bath of absolute ethanol for 15 min before use. Chemistry procedures based on SAMs of β-mercaptoethylamine (cysteamine) in absolute ethanol have been described previously.[29] Briefly, the freshly cleaned gold substrate was immersed in an unstirred 10 mM ethanol cysteamine solution at room temperature, in the dark, for 6 h. The gold substrate was then washed with ethanol and ultrapure water (Milli-Q, Millipore, France) to remove the excess thiols. The cysteamine-modified gold substrates were immersed in EDC/NHS (80 mg/20 mg)-PC6 and PC6-AuNr solutions for 1 h and then rinsed with phosphate buffer solution and MilliQ water three times for 5 minutes.

2.2.4. Lead(II) detection.
The interaction between PC6-AuNrs and lead(II) solutions was followed using UV-Vis spectra (50 μL lead solution added to 1 mL PC6-AuNr solution to obtain final lead concentrations of 100, 50 and 25 ppb) and FT-SPR shifts of PC6-modified gold substrates.
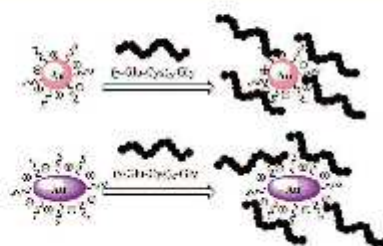
Scheme 1 Ionic interaction mechanism of PC6 protein grafting onto gold nanospheres (above) and gold nanorods (below).

2.3. Instrumentation

2.3.1. UV/Vis measurements. Absorption spectra were recorded using a Jasco V-570 UV/VIS/NIR Spectrophotometer from Jasco Int. Co. Ltd., Tokyo, Japan in the 200–800 nm range.

2.3.2. TEM imaging. Transmission electron microscopy measurements were recorded on a JEOL JEM 1011 microscope operating at an accelerating voltage of 100 KV. The TEM graphs were taken after separating the surfactant from the metal particles by centrifugation. Typically 1 mL of the sample was centrifuged for 20 min at a speed of 14 000 rpm min^{-1}. The upper part of the colourless solution was removed and the solid portion was re-dispersed in 1 ml of water. 2 μL of this redispersed particle suspension was placed on a carbon coated copper grid and dried at room temperature.

2.3.3. PM-IRRAS. PM-IRRAS spectra were recorded on a commercial Thermo (Les Ulis-France) Nexus spectrometer. The external beam was focused on the sample with a mirror, at an optimal incident angle of 80°. A ZnSe grid polarizer and a ZnSe photoelastic modulator, modulating the incident beam between p- and s-polarizations (HINDS Instruments, PEM 90, modulation frequency = 37 kHz), were placed prior to the sample. The light reflected at the sample was then focused onto a nitrogen-cooled MCT detector. The presented spectra resulted from the sum of 128 scans recorded at a 8 cm^{-1} resolution.

2.3.4. FT-SPR. FT-SPR measurements were performed with an SPR 100 module from thermo equipped with a flow cell mounted on a goniometer. It was inserted in a Thermo-scientific Nexus FT-IR spectrometer using a near-IR tungsten halogen light source. The incidence angle was adjusted to have minimal reflectivity located at 9500 cm^{-1}, at the beginning of each experiment, so as to be in the best sensitivity region of the InGaAs detector. Interactions between nanostructured surfaces and lead solution were carried out in the test chamber (10 μL min^{-1}; $T = 27$ °C).

3. Results and discussion

3.1. Synthesis of PEG-AuNps and PEG-AuNrs

It is well established that PEG-functionalized AuNPs have an increased stability in aqueous and biological media with respect to simple gold nanoparticles.[20,21] In order to improve the biointerfacial properties of AuNPs, we coated them with a bifunctional PEG linker carrying two carboxylic groups. The synthesis of PEG-capped gold nanoparticles (DPEG-AuNPs) was achieved by reducing tetrachloroauric acid (HAuCl₄) with sodium borohydride (NaBH₄) in the presence of PEG-diacid as a capping agent. The main difference with other synthesis procedures of DPEG-AuNPs is that PEG-diacid is used in the same way as the citrate for the stabilization of the particles through electrostatic interactions between the carboxylic acid groups and the gold surface.[22] Particle formation and growth were tuned by the amphiphilic character of the PEG-diacid polymer and include three steps: (1) reduction of HAuCl₄ facilitated by dicarboxylic acid-terminated PEG to form gold clusters; (2) adsorption of PEG diacid molecules on the surface of the gold clusters and reduction of metal ions in that vicinity; and (3) growth of gold
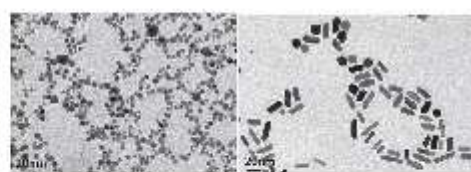
particles and colloidal stabilization by PEG polymers. The TEM picture of PEG-AuNPs highlights well and monodisperse Au nanospheres with a mean size of 7.2 nm and with a standard deviation of 2 nm (Fig. 1 (left)). The growth of gold nanostructures, synthesized by a seed-mediated procedure, is known to be strongly dependent on the seed nanocrystal structure, the latter being influenced by the nature of surfactants.[21] In the present study, the influence of PEG diacid molecules on the growth nanostructures was investigated. Based on the literature, the protocol conducted in the absence of PEG diacid at any step is expected to lead to the formation of gold nanorods.[20,22]

Fig. 1 (right) reports TEM images which confirm the morphology and the remarkable dispersion of the nanorods, with a typical diameter of *ca.* 5 nm and a length of *ca.* 20 nm. Fig. 2 displays the LSPR bands of AuNrs: the UV-Vis spectrum shows a strong resonance band at around 780 nm corresponding to the longitudinal plasmon oscillation, and a weaker one at *ca.* 530 nm corresponding to the transverse plasmon oscillation band confirming the presence of elongated gold nanorods, well isolated from each other, which is in agreement with previous published findings.[23] In a remarkable review, Pérez-Juste *et al*, have clarified the role of CTAB concentration and temperature upon the nanoparticle aspect ratio, based on a large set of experimental results.[23] In particular, these authors proposed that the binding of Au ions, and thus the growth of Au nanorods in aqueous surfactant solution, is controlled by the electric field around the CTAB micelles.[24] In the present study, CTAB present in the seed solution is supposed to be in the micellized form, as the concentration used is significantly higher than the critical micelle concentration, reported to be equal to 0.92 mM.[25] When PEG diacid is added in the growth solution, leading to the formation of a presumable CTAB–PEG diacid complexes, the same reduction process involving ascorbic acid may occur. Further reduction of Au can then proceed *via* an electron transfer at the surface of electron-rich, CTAB–PEG diacid capped, seed particles. The rate of hybrid NP formation depends in this case on the reaction of the AuCl₂⁻–CTAB–PEG diacid complex with CTAB–PEG diacid capped seed particles that confer more stability in aqueous medium.

3.2. PC6 adsorption onto pegylated gold nanostructures (PEG-AuNPs and PEG AuNrs)

Interactions of PC6 biomolecules with gold nanoparticles (PEG-AuNPs) or nanorods (PEG-AuNrs) were monitored by observing the Localized Surface Plasmon (LSP) band in the UV-Vis

Fig. 1 Transmission Electronic Microscopy images of AuNPs (left) and AuNrs (right).
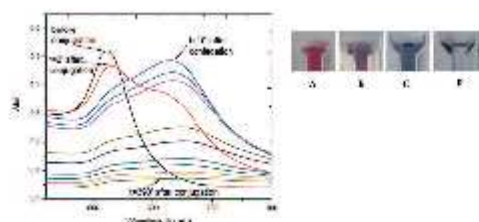
Analyst

Fig. 2 On the left: UV-Vis spectra of PC6-modified AuNPs as a function of time; on the right: images of AuNPs color changing during bioconjugation.

spectrum. Fig. 2 displays the LSP bands of AuNPs before and during interactions with PC6 molecules at equal concentrations of AuNPs in aqueous solution (10^{-4} M). It is well visible that AuNPs before adsorption show one peak at 530 nm and their water solution has a typical red-rose color (Fig. 2A), while after 2 minutes of mixing with PC6 peptides, a strong color change can be clearly observed (Fig. 2B and C), which corresponds to the appearance of a second LSP peak around 650 nm. UV-Vis spectra were recorded up to 390 minutes after PC6 molecule interactions but just after 120 minutes when the hybrid biological–metal complex becomes unstable, since the solution turns transparent (Fig. 2D), due to agglomeration and sedimentation of nanoparticles. Fig. 3 shows the variation of absorption peaks of PEG-AuNrs before and after binding with PC6.

These measurements were carried out at room temperature for 18 h. The violet color of PEG-AuNr solution resulting after the interaction of PC6 did not change any more. A decrease of the plasmon absorption can be attributed to the change of localized refractive index near the AuNr surface indicating that PC6 was attached to the AuNr surface. From UV-Vis recorded

spectra, it is clear that AuNrs bind PC6 molecules and the resulting complexes are stable since there is not any degradation of the absorption peak. We remark that the stability of PEG-AuNrs is due to the presence of two different capping agents, such as DPEG and CTAB, respectively. After their synthesis, gold nanorods carry positive and negative charges on their surfaces due to strongly adsorbed CTA$^+$–PEG–COO$^-$ ions, preferentially along the side surfaces. PC6 may adsorb to the PEG-AuNr sides via electrostatic attractions. As a matter of fact, with positively charged CTAB, PC6 likely interacts via its negative charges, thus exposing neutral, or positively charged, groups towards the external sides. Conversely, on PC6 interacting with the end of nanorods, charges are evenly distributed thus favoring classical Van der Waals inter-phytochelatin interactions. We do not exclude the interaction of COO$^-$ groups of DPEG with positive charges of PC6 onto gold nanorods: the mechanism for peptide assembly is probably triggered by electrostatic interactions between the deprotonated DPEG and the positively charged CTAB surfactant bilayer on the surface of gold nanorods, as a consequence of the improvement of AuNr stability. A better stability and evaluation of PEG-AuNr bioconjugation was confirmed by PM-IRRAS, which is particularly useful in the case of a very thin layer of modified materials. Planar gold surfaces were functionalized by a cysteamine self-assembled monolayer, which could strongly bound, under EDC/NHS chemistry activation, PC6 in one sample, and PC6-AuNr in another sample, for comparison purposes (see Scheme 2).

Fig. 3 shows a set of PM-IRRAS data taken after protein immobilization on the gold surface (Fig. 3 black line) and after PC6 conjugated PEG-AuNr immobilization on the gold surface (Fig. 4 redline). The PEG spectral pattern is confirmed by the vibration band of the (C–O–C) at 1020 cm^{-1}; the C=O stretching mode of the carboxylic group expected at 1725 cm^{-1} is evidenced. The peaks at 1420 cm^{-1} were attributed to the asymmetric and symmetric C–H scissoring vibrations of CH$_2$–
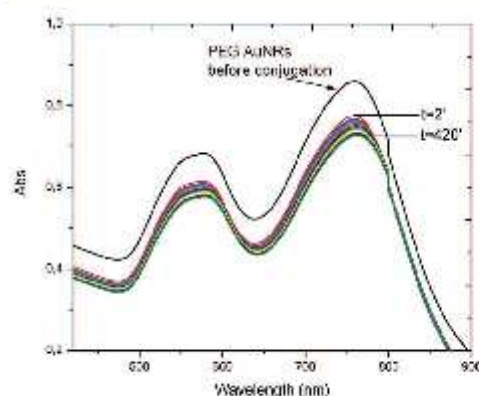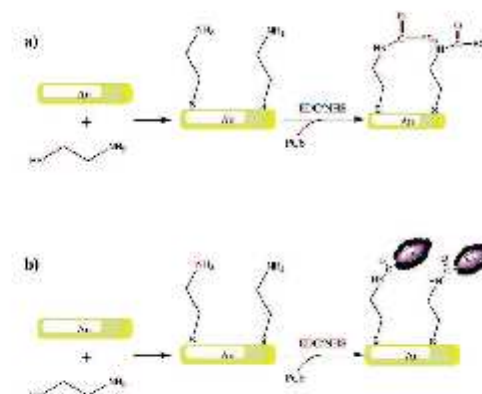

Fig. 3 UV-Vis spectra of AuNrs before and after bio-conjugation with PC6 protein.

Scheme 2 Schematic representation of the biosensor elaboration strategy: Au surface modification with cysteamine self-assembled monolayer and PC6 (a) or PC6-modified gold nanorods (b).
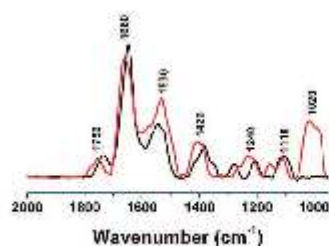
Fig. 4   PM-IRRAS spectra of PC6-modified gold substrates (black line) and PC6-AuNR-modified gold substrates (red line).

N^+ moieties and to the CH_2 scissoring mode, respectively. In PM-IRRAS spectra, the peak at 1750 cm^{-1} is assigned to ester bonds, as a consequence of EDC/NHS activation, the peak at 1660 cm^{-1} is assigned to the amide II bonds and the one at 1530 cm^{-1} is assigned to the amide I bonds: in both cases all the peaks are comparable, except the peak at 1020 cm^{-1}, characteristic of the C–O–C chain of PEG that confirms a good interaction between PC6 and PEG-AuNrs.

3.3.   Interaction of PC6-AuNRs with lead(ɪɪ) ions

FT-SPR measurements were used in monitoring interactions between PC6-AuNRs and lead(ɪɪ) ions. Fig. 5A shows the real-time monitoring of all Pb(ɪɪ) solutions with different concentrations tested. At the instant $t = 64$ min, a solution of lead ions with 100 ppb concentration was injected into the test flow chamber, producing a shift of the FT-SPR peak absorption to 8650 cm^{-1}; then an aqueous solution was flown in order to wash the SPR surface, and the FT-SPR signal was restored to its starting value at 9320 cm^{-1}. At $t = 93$ min, a solution of lead ions at 50 ppb concentration was injected, producing a shift of FT-SPR up to 9050 cm^{-1}; then aqueous solution was flown again to rinse the surface. At $t = 115$ min, a solution of lead ions at 25 ppb concentration was injected yielding a FT-SPR wavenumber

value of about 9100 cm^{-1}; finally aqueous solution was flown to rinse the surface. It is of particular interest that after rinsing the signal restores its initial value since this means that the interaction between nanocomplexes and metal ions is reversible. These wavenumber shifts indicate that lead(ɪɪ) ions in solution significantly bind to phytochelatin modified AuNrs even if the hybrid probes are conjugated to the analysis surface of FT-SPR. Fig. 5B reports how the absolute position of the plasmon absorbance peak changes as a function of different concentrations of lead ion solution, while Fig. 5C shows data obtained from relative shifts of the plasmon peak during exposition to Pb(ɪɪ) ion solutions. These data could be fitted using OriginLab Software™ by the following equation (Boltzmann model):

$$y = A_2 + ((A_1 - A_2)/(1 + [e]^{\wedge}((x - x_0)/dx)))$$

where A_1 is the initial value, A_2 is the final value, x_0 is the inflection point and dx is the lead concentration constant. The inflection point is useful for the evaluation of the affinity which quantifies how strong is the biomolecular interaction between PC6-AuNrs and lead(ɪɪ) ions in aqueous solutions: in our case, the x_0 value is 73.6 ± 0.9 cm^{-1} ppb^{-1} corresponding to $1.8 \times 10^{-10} \pm 2 \times 10^{-12}$ cm^{-1} mol L^{-1}.

Conclusions

In this work, we have characterized by optical, label free techniques the interaction between small peptides, namely PC6, and Pb(ɪɪ) in aqueous solutions based on peptide adsorbed gold nanorods. These hybrid nanocomplexes are stable and biologically active: even if linked by adsorbed-gold interactions on the nanorod surface, the peptides are able to strongly bind the heavy metal ions with an affinity constant in the range of picomolars. The signal changes, i.e. variation of the FT-SPR peak position, are important (more than 200 cm^{-1}) even at a very low concentration (25 ppb) of metal ions: this result is very promising for the development of sensitive and effective nanoparticle-based biosensors for quantifying the Pb(ɪɪ) ion concentration in water.

Author Contributions

The manuscript was written through contributions from all authors. All authors have given approval to the final version of the manuscript.
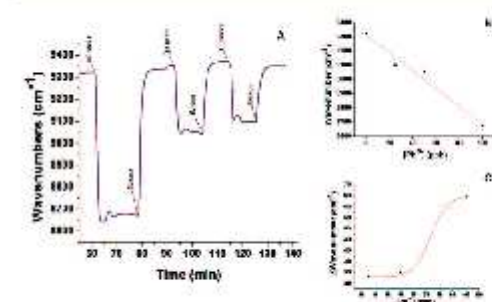
Funding Sources

Fig. 5   (A) FT-SPR response as a function of lead(ii) solution concentrations (respectively 100, 50 and 25 ppb) during 3 cycles of binding followed by rinsing; (B) SPR transmittance peak position by increasing concentrations of lead solutions; (C) SPR transmittance peak shift as a function of lead(ii) solution concentrations.

References

1 M. S. Yavuz, Y. Cheng, J. Chen, C. M. Cobley, Q. Zhang, M. Rycenga, J. Xie, C. Kim, K. H. Song, A. G. Schwartz, L. V. Wang and Y. Xia, Gold nanocages covered by smart

polymers for controlled release with near-infrared light, *Nat. Mater.*, 2009, **8**, 935–939.

2 D. A. Giljohann, D. S. Seferos, W. L. Daniel, M. D. Massich, P. C. Patel and C. A. Mirkin, Gold nanoparticle in Biologie und Medizin, *Angew. Chem.*, 2010, **122**, 3352–3366.

3 E. E. Bedford, J. Spadavecchia, C.-M. Pradier and F. X. Gu, Surface Plasmon Resonance Biosensors Incorporating Gold Nanoparticles, *Macromol. Biosci.*, 2012, **12**, 724–739.

4 E. T. Castellana, R. C. Gamez and D. H. J. Russell, Label-Free Biosensing with Lipid-Functionalized Gold Nanorods, *J. Am. Chem. Soc.*, 2011, **133**(12), 4182–4185.

5 N. Xia, Y. Shi, R. Zhang, F. Zhao, F. Liu and L. Liu, Simple, rapid and label-free colorimetric assay for arsenic based on unmodified gold nanoparticles and a phytochelatin-like peptide, *Anal. Methods*, 2012, **4**, 3937–3941.

6 L. Rodríguez-Lorenzo, R. De la Rica, R. A. Álvarez-Puebla, L. M. Liz-Marzán and M. M. Stevens, Plasmonic nanosensors with inverse sensitivity by means of enzyme-guided crystal growth, *Nat. Mater.*, 2012, **11**, 604–607.

7 G. Zhenhai, J. Jianhui, Z. Ting and W. J. Daocheng, Preparation of Rhodamine B Fluorescent Poly(methacrylic acid) Coated Gelatin Nanoparticles, *Nanomaterials*, 2011, **1**, 753705.

8 R. J. Nikhil, L. Gearheart and C. J. Murphy, Seed-Mediated Growth Approach for Shape-Controlled Synthesis of Spheroidal and Rod-like Gold Nanoparticles Using a Surfactant Template, *Adv. Mater.*, 2001, **13**(18), 1389–1393.

9 H. J. Parab, J-H. Huang, T-C. Lai, Y-H. Jan, R-S. Liu, J-L. Wang, M. Hsiao, C-H. Chen, Y-K. Hwu, D. P. Tsai, S-Y. Chuang and J-H. S. Pang, Biocompatible transferrin-conjugated sodium hexametaphosphate-stabilized gold nanoparticles: synthesis, characterization, cytotoxicity and cellular uptake, *Nanotechnology*, 2011, **22**, 395706.

10 T. Biver, N. Eltugral, A. Pucci, G. Ruggeri, A. Schena, F. Secco and M. Venturini, Synthesis, characterization, DNA interaction and potential applications of gold nanoparticles functionalized with Acridine Orange fluorophores, *Dalton Trans.*, 2011, **40**, 4190.

11 J. Manson, D. Kumar, B. Meenan and D. Dixon, Polyethylene glycol functionalized gold nanoparticles: the influence of capping density on stability in various media, *Gold Bull.*, 2011, **44**, 99.

12 H. Zhao, S. Q. Wu, Q.-H. Yao, G. Xu and Q. Xu, Nanocomposites containing gold nanorods and porphyrin-doped mesoporous silica with dual capability of two-photon imaging and photosensitization, *Langmuir*, 2010, **26**, 14937.

13 C.-J. L. Chang-HaiWang, C.-L. Wang, T.-E. Hua, K. H. L. J. M. Obliosca, Y. Hwu, C.-S. Yang, H.-M. L. Ru-Shi Liu, J.-H. Je and G. Margaritondo, *J. Phys. D: Appl. Phys.*, 2008, **41**, 195301.

14 Q. Shen, Z. Nie, M. Guo, C. Zhong, B. Lin, W. Li and S. Yao, Simple and rapid colorimetric sensing of enzymatic cleavage and oxidative damage of single-stranded DNA with unmodified gold nanoparticles as indicator, *Chem. Commun.*, 2009, 929–931.

15 Y. L. Tang, F. D. Feng, S. F. He, Y. L. Wang Li and D. B. Zhu, Direct Visualization of Enzymatic Cleavage and Oxidative Damage by Hydroxyl Radicals of Single-Stranded DNA with a CationicPolythiophene Derivative, *J. Am. Chem. Soc.*, 2006, **128**, 14972–14976.

16 W. Li, Z. Nie, K. He, X. Xu, Y. Li, Y. Huang and S. Yao, Simple, rapid and label-free colorimetric assay for Zn^{2+} based on unmodified gold nanoparticles and specific Zn^{2+} binding peptide, *Chem. Commun.*, 2011, **47**, 4412–4414.

17 Y. Guo, Z. Wang, W. Qu, H. Shao and X. Jiang, Colorimetric detection of mercury, lead and copper ions simultaneously using protein-functionalized gold nanoparticles, *Biosens. Bioelectron.*, 2011, **26**, 4064–4069.

18 M. Zhang, Y.-Q. Liu and B.-C. Ye, Attomolar ultrasensitive microRNA detection by DNA-scaffolded silver-nanocluster probe based on isothermal amplification, *Analyst*, 2012, **137**, 601–607.

19 S. Tong, Lead exposure and cognitive development: Persistence and a dynamic pattern, *J. Paediatr. Child Health*, 1998, **34**, 114–118.

20 H. Lilienthal, G. Winneke and T. Ewert, Effects of lead on neurophysiological and performance measures: animal and human data, *Environ. Health Perspect.*, 1990, **89**, 21–25.

21 CDC, *Surveillance for elevated blood lead levels among children-United States, 1997–2001*, Centers for Disease Control and Prevention MMWR Morb Mortal Wkly Rep., 2003, vol. 53, pp. 1–21.

22 S. J. Rothenberg, A. Poblano and L. Schnaas, Neurodegenerative Diseases and Metal Ions, *Met. Ions Life Sci.*, 2000, **22**, 503–510.

23 M. Orita, H. Iwahana, H. Kanazawa, K. Hayashi and T. Sekiya, Detection of polymorphisms of human DNA by gel electrophoresis as single-strand conformation polymorphisms., *Proc. Natl. Acad. Sci. U. S. A.*, 1989, **86**, 2766–2770.

24 C. S. Cobbett, Phytochelatin biosynthesis and function in heavy-metal detoxification, *Curr. Opin. Plant Biol.*, 2000, **3**, 211–216.

25 J. Manson, D. Kumar, B. J. Meenan and D. Dixon, Polyethylene glycol functionalized gold nanoparticles: the influence of capping density on stability in various media, *Gold Bull.*, 2011, **44**, 99–105.

26 N. R. Jana, L. Gearheart and C. J. Murphy, Seed-Mediated Growth Approach for Shape-Controlled Synthesis of Spheroidal and Rod-like Gold Nanoparticles Using a Surfactant Template, *Adv. Mater.*, 2001, **13**, 1389.

27 H. J. Parab, J.-H. Huang, T.-C. Lai, Y.-H. Jan, R.-S. Liu, J.-L. Wang, M. Hsiao, C.-H. Chen, Y.-K. Hwu, D. P. Tsai, S.-Y. Chuang and J.-H. S. Pang, Biocompatible transferrin-conjugated sodium hexametaphosphate-stabilized gold nanoparticles: synthesis, characterization, cytotoxicity and cellular uptake, *Nanotechnology*, 2011, **22**, 395706.

28 C. Li, D. Li, G. Wan, J. Xu and W. Hou, Facile synthesis of concentrated gold nanoparticles with low size-distribution in water: temperature and pH controls, *Nanoscale Res. Lett.*, 2011, **6**, 440.

29 J. Spadavecchia, J. Moreau, J. Hottin and M. Canva, New cysteamine based functionalization for biochip applications, *Sens. Actuators, B*, 2009, **143**, 139.

Paper

30 K. G. Neoh and E. T. Kang, Functionalization of inorganic nanoparticles with polymers for stealth biomedical applications, *Polym. Chem.*, 2011, **2**, 747.

31 A. Gole and C. J. Murphy, Seed-Mediated Synthesis of Gold Nanorods: Role of the Size and Nature of the Seed, *Chem. Mater.*, 2004, **16**, 3633.

32 B. D. Busbee, S. O. Obare and C. J. Murphy, An Improved Synthesis of High-Aspect-Ratio Gold Nanorods, *Adv. Mater.*, 2003, **15**, 414.

33 J. Pérez-Juste, I. Pastoriza-Santos, L. M. Liz-Marzan and P. Mul-vaney, Gold nanorods: synthesis, characterization and applications Coord, *Chem. Rev.*, 2005, **249**, 1870.

34 C. Li, F. Fan, B. Yin, L. Chen, T. Ganguly and Z. Tian, Au⁺-cetyltrimethylammonium bromide solution: A novel precursor for seed-mediated growth of gold nanoparticles in aqueous solution, *Nano Res.*, 2013, **6**, 29–37.

35 J. Mattay, Photochemistry in Microheterogeneous Systems. Von K. Kalyanasundaram, *Angew. Chem.*, 1988, **100**, 744.

4. Conclusions

The PhD entitled "BIOCONJUGATION OF ENZYMES AND PROTEINS ON MULTIFUNCTIONAL AND NANOSTRUCTURED SOLID SUPPORTS FOR BIOMOLECULAR INTERACTIONS MONITORING" performed at National Research Council - Institute for Microelectronics and Microsystems, in collaboration with Department of Chemical Sciences, University of Naples under the co-tutoring of Dr. Luca De Stefano and Prof. Paola Giardina, was focused on the study and development of innovative devices for biomedical and environmental monitoring applications. Nanostructured materials such as porous silicon and gold nanoparticles were used as transducer elements in order to develop sensible label-free biosensors.

The first aim of the present work was the optimization of covalent biomodification of silicon derived materials for bioprobes conjugation. It was studied how the layer of bioprobe can be affected by incubation time, solvents and different aminosilanes during chemical procedure. Quantitative measurements based on Spectroscopic Ellipsometry, sessile drop and Atomic Force Microscopy reveal that smoother and homogeneous film can be obtained using the APDMES aminosilane in toluene incubated for 30 min. Anyway, all other samples show good functionalization degree proved by fluorescence characterization. The covalent approach was fundamental topic in porous silicon devices development for lead ions detection. The interaction monitoring of the lead ions in aqueous solutions have been completed by optical and gravimetric methods. In particular, affinity constants of 3.5 ± 0.6 ppb and 10 ± 2 ppb with a sensitivity 0.07 ± 0.03 ppb / Hz and 0.18 ± 0.03 ppb / nm and in the case of PSi and quartz resonators, respectively was evidenced. It was also verified that this system is reversible, with a maximum of six cycles of regeneration. The work provides a good starting point for the development of a biosensor nanostructured and reversible to achieve a future Lab-on-chip (LoC) device for the in situ detection of heavy metals. Concerning porous silicon based devices, it was studied also the possibility to passivate porous silicon optical structures by using Hydrophobins proteins as active layer that both passivate the device and interact with outer environment. In particular, interaction with glucose molecules was investigated after self-assembling onto porous silicon devices. Different optical techniques have been used in monitoring interaction between the self-assembled biofilm of Hydrophobin proteins and glucose molecules. The stability of compact protein biofilm penetrate into the intricate, sponge-like matrix of different PSi multilayers was proved by exposing them to diluted HF (1% V/V) solution showing the device protection. Furthermore, spectroscopic reflectometry does not reveal any red shift ($\Delta\lambda < 1$ nm) of HFB-PSi optical spectra on exposure to glucose solution

(1.2mg/ml), but water contact angle measurements and fluorescence microscopy highlight the presence of oligosaccharides in HFB-PSi without any doubts.

The second aim of the present work was focused on the gold nanoparticles based devices development. Firstly, the use of Hydrophobins as co-stabilizers in gold nanoparticles synthesis was characterized. It was showed that hybrid HFB–AuNPs can be synthesized via a simple one step method. The key role of the HFB molecules during the growth process of nanoparticles was investigated by mixing it with dicarboxylic acid-terminated polyethylene-glycol (PEG), as standard surfactants in the synthesis. Stable nanometric hybrid protein–organic–metal NPs have been obtained, with average diameter of 12 nm. XPS showed that Vmh2 strongly bind to Au core whereas surfactants act as outer shells. PEG-HFB-AuNPs were then employed as possible glucose monitoring platforms. All experimental results highlighted that Vmh2 gave ability to PEG-HFB-AuNPs to bind glucose also if intrinsically engaged with gold core. Aggregation behaviour was proved by DLS measurements and glucose interaction, as CO and CH signal enhancing, was proved by PM-IRRAS and XPS spectroscopies. In conclusion, a novel hybrid bio/non-bionanosystem was developed for both interface stabilization and biomolecular interaction monitoring applications. A binding affinity of 7.3 ± 0.3 mg / mL and a sensitivity of 0.13 ± 0.06 au / mg mL^{-1} were calculated. PEG-Gold nanospheres were also studied for arsenic ions and lead ions detection. In arsenic ions interaction monitoring, it was used a novel chromosomal arsenate reductase (*TtArsC*) as biomolecular probe to screen for the presence of arsenic in water. The novel and original nanobiocomplexes demonstrated stability and capacity to strongly bind the toxic ions. *TtArsC*-AuNPs showed greater sensitivity for arsenite ions, as opposed to what happens in nature, where arsenate ions are the main substrate of *TtArsC* enzymes. On these bases, *TtArsC*-AuNP nanobiocomplexes were found to be able to interact with arsenite ions solutions, veering to blue solutions, and arsenate ions solutions, veering to violet/pink solutions, at all concentrations tested. These phenomena were confirmed quantitatively by LSP shifts in UV–vis spectra, and DLS characterization reveals that the nanobiocomplex aggregates in the presence of arsenic ions. Finally, LSP band study in the presence of metal ions that are not enzyme substrates (Cd^{2+}, Pb^{2+} and Hg^{2+}) indicated that the biorecognition is highly specific but not completely selective. In the case of lead ions interaction monitoring, the study started by PEG gold nanospheres biomodification by Phytochelatin oligopeptides, but a corrosive behavior in neutral pH conditions was evidenced. Then, the study was moved to PEG gold nanorods biomodification with Phytochelatins. These hybrid nanocomplexes are stable and biologically active: even if linked on the gold nanorod surface, the peptides are able to strongly bind the heavy metal ions with an affinity constant in the range of picomolars. The signal changes, i.e. variation of the FT-SPR peak position, are important (more than 200 cm^{-1}) even at a very low concentration (25 ppb) of metal ions: this result is very promising for the development of sensitive and effective nanoparticle-based biosensors.

5. References/Bibliografia

Adhikari, B.R.; Govindhan, M.; Chen, A.; Carbon Nanomaterials Based Electrochemical Sensors/Biosensors for the Sensitive Detection of Pharmaceutical and Biological Compounds. *Sensors* **2015**, 15, 22490-22508

Alivisatos, P. "The use of nanocrystals in biological detection." *Nature biotechnology* **2004**, 22, 47-52.

Bartolucci, S.; Contursi, P.;Fiorentino, G.; Limauro, D.;Pedone, E.; Responding to toxic compounds: a genomic and functional overview of Archaea, *Front Biosci*, **2013**,18 165-89.

Bauer, L. A.; Birenbaum, N. S.; Meyer, G. J. Biological applications of high aspect ratio nanoparticles. *Journal of Materials Chemistry*, **2004**, 14.4: 517-526.

Boisselier E. and Astruc D., "Gold nanoparticles in nanomedicine: preparations, imaging, diagnostics, therapies and toxicity.," *Chem. Soc. Rev.*, 38, **2009**, 1759–1782.

Bradt, J. H., Mertig, M., Teresiak, A., & Pompe, W. Biomimetic mineralization of collagen by combined fibril assembly and calcium phosphate formation. *Chemistry of Materials*, **1999**, 11, 2694-2701.

Cobbett C.S., Phytochelatin biosynthesis and function in heavy-metal detoxification. *Current opinion in plant biology*, **2000**, 3, 211–216.

Cui, D., and Huajian G. "Advance and prospect of bionanomaterials." *Biotechnology progress* 19.3, **2003**, 683-683.

Cui, R., et al., Gold Nanoparticle–Colloidal Carbon Nanosphere Hybrid Material: Preparation, Characterization, and Application for an Amplified Electrochemical Immunoassay. *Advanced Functional Materials*, **2008**. 18, p. 2197-2204.

Daglar B. and Aydogan N., "Fluorocarbon–hydrocarbon hybrid gold NPs synthesized by bulk exchange reactions and surface coatings of fluorocarbon coated gold NPs are increased," *Colloids Surfaces A Physicochem. Eng. Asp.,* 419, **2013**, 257–262,.

Daniel M. C. and Astruc D., "Gold nanoparticles: assembly, supramolecular chemistry, quantum-size-related properties, and applications toward biology, catalysis, and nanotechnology," *Chem. Rev.*, 104, **2004**, 293–346.

De Stefano L, Rea I, Armenante A, Giardina P, Giocondo M, Rendina I. Self assembled biofilm of hydrophobins protects the silicon surface in the KOH wet etch process. *Langmuir* **2007**, 23, 7920–2.

De Stefano L, Rea I, Giardina P, Armenante A, Rendina I. Protein-modified porous silicon nanostructures. *Adv Mater.* 20, **2008**, 1529

Doane T. L., Cheng Y., Babar A., Hill R. J., Burda C., Electrophoretic Mobilities of PEGylated Gold NPs, *J. Am. Chem. Soc.* **2010**, 132, 15624 – 15631.

Drummond, T. Gregory, Michael G. Hill, and Jacqueline K. Barton. "Electrochemical DNA sensors." *Nature biotechnology* 21.10 (**2003**): 1192-1199.

Espino, D. P.; Tamames, J.; de Lorenzo, V.;Cánovas, D.; Microbial responses to environmental arsenic, *Biometals* **2009**, 22, 117–130.

Gentilini L., Evangelista, F.; Rudolf, P.; Franchi, P.; Lucarini, M.; Pasquato, "Water-Soluble Gold Nanoparticles Protected by Fluorinated Amphiphilic Thiolates," *J. Chem. Soc.*, 130, **2008**, 15678–15682.

Ghosh S. K. and Pal T., "Interparticle Coupling Effect on the Surface Plasmon Resonance of Gold Nanoparticles : From Theory to Applications," **2007**.

Gihring, T.M.; Banfield, J.F.; Arsenite oxidation and arsenate respiration by a new Thermus isolate, *Microbiol. Lett.* **2001**, 204 335–340.

Hou, S., Li, X., Li, X., & Feng, X.. Coating of hydrophobins on three-dimensional electrospun poly (lactic-co-glycolic acid) scaffolds for cell adhesion. *Biofabrication*, **2009**, *1*(3), 035004.

Huo Z., Tsung C. , Huang W., Zhang X., Yang P.,Sub-Two Nanometer Single Crystal Au Nanowires, *Nano Lett.*, **2008**, 8, 2041–2044

Jackson, C. R.; Dugas, S. L.; Phylogenetic analysis of bacterial and archaealarsC gene sequences suggests an ancient, common origin for arsenate reductase, *BMC Evolutionary Biology*, **2003**, 3, 18.

Jenison, R. D., Gill, S. C., Pardi, A., & Polisky, B. High-resolution molecular discrimination by RNA. *Science*, **1994**, 263, 1425-1429.

Jerius, H., Beall, A., Woodrum, D., Epstein, A., & Brophy, C. Thrombin-induced vasospasm: cellular signaling mechanisms. *Surgery*, **1998**, 123, 46-50.

Kang, X.; Mai, Z.; Zou, X.; Cai, P.; Mo, J.; Glucose biosensors based on platinum nanoparticles-deposited carbon nanotubes in sol–gel chitosan/silica hybrid. *Talanta*, **2008**, 74, 879-886.

Kikuchi, M., Ikoma, T., Itoh, S., Matsumoto, H. N., Koyama, Y., Takakuda, K., Tanaka, J. Biomimetic synthesis of bone-like nanocomposites using the self-organization mechanism of hydroxyapatite and collagen. *Composites Science and Technology*, **2004**, *64*(6), 819-825.

Kong Y.C., Yu D.P. Zhang, B. Fang, W.S.Q. Feng, Ultraviolet-emitting ZnO nanowires synthesized by a physical vapor deposition approach, *Appl. Phys.Lett.* **2001,** 78, 407.

Kumar S.A., Chen S.M., Nanostructured zinc oxide particles in chemi-cally modified electrodes for biosensor applications, *Anal. Lett.* **2008**, 41, 141–158.

Laurell, T. Drott, J., Rosengren, L., Lindstrom, K. Enhanced enzyme activity in silicon integrated enzyme reactors utilizing porous silicon as the coupling matrix, *Sens. Actuators B*, **1996**, 31, 161.

Lee W., Oh B.-K., Bae Y.M., Paek S.H., Lee W. H., Choi J.-W., Fabrication of self-assembled protein A monolayer and its application as an immunosensor, **2003**, 19, 185-192

Letant S. and Sailor M. J., Detection of HF gas with a porous silicon interferometer. *Adv. Mater.* **2000**, 12, 355.

Li, C., Li, D., Wan, G.; Xu, J.; Hou, W. ; Facile synthesis of concentrated gold nanoparticles with low size-distribution in water: temperature and pH controls, *Nanoscale Res. Lett.* **2011**, 6,1 – 10.

Li, N., Zhao P., Liu N., Echeverria M., Moya S., Salmon L., Ruiz J., Astruc D., "Click" Chemistry Mildly Stabilizes Bifunctional Gold Nanoparticles for Sensing and Catalysis. *Chem. Eur. J.,* **2014**, 20 8363–8369.

Ligler, F.S. and Rowe, C.A., Optical Biosensors, Eds. Taitt, Elsevier, Amsterdam, The Netherlands, **2004**.

Link S. and El-Sayed M., "Size and Temperature Dependence of the Plasmon Absorption of Colloidal Gold Nanoparticles," *J. Phys. Chem. B*, 103, **1999**, 21, 4212–4217.

Macy, J. M.; Santini, J. M.; Pauling, B. V.; O'Neill, A. H.; Sly, L. I.; Two new arsenate/sulfate-reducing bacteria: mechanisms of arsenate reduction, *Arch Microbiol* 173, **2000**, 49–57

Mannironi, C., Di Nardo, A., Fruscoloni, P., & Tocchini-Valentini, G. P.. In vitro selection of dopamine RNA ligands. *Biochemistry*, **1997**, 36, 9726-9734.

Manson J., Kumar D., Meenan B., Dixon D., Polyethylene glycol functionalized gold nanoparticles: the influence of capping density on stability in various media*, Gold Bulletin,* **2011**, 44, 99-105.

Marle, L.; Greenway, G. M. Microfluidic devices for environmental monitoring. *TrAC Trends in Analytical Chemistry*, **2005**, 24.9: 795-802.

Moatsou, G.; Bakopanos, C.; Katharios, D.; Katsaros, G.; Kandarakis, I.; Taoukis, P.; Politis, I.; Effect of high-pressure treatment at various temperatures on indigenous proteolytic enzymes and whey protein denaturation in bovine milk. *Journal of dairy research* **2008**, 75, 262.

Moghimi, S. M., & Szebeni, J. Stealth liposomes and long circulating nanoparticles: critical issues in pharmacokinetics, opsonization and protein-binding properties. *Progress in lipid research*, **2003**, *42*, 463-478.

Moretti, L., Rea, I., Rotiroti, L., Rendina, I., Abbate, G., Marino, A., De Stefano, L. Photonic band gaps analysis of Thue-Morse multilayers made of porous silicon. *Optics express*, **2006**, *14*, 6264-6272.

Mukhopadhyay, R.; Rosen, B.P.; Arsenate reductases in prokaryotes and eukaryotes, *Environ. Health Perspect.*, **2002**, 5, 745–748.

Müller, R. H., Jacobs, C., & Kayser, O. (**2001**). Nanosuspensions as particulate drug formulations in therapy: rationale for development and what we can expect for the future. *Advanced drug delivery reviews*, *47*(1), 3-19.

Murphy, J.N.; Saltikov, C.W.; The ArsR repressor mediates arsenite-dependent regulation of arsenate respiration and detoxification operons of Shewanella sp. Strain ANA-3, *J. Bacteriol.,* **2009**, 191, 6722–6731.

Niemeyer, C.M. Nanoparticles, proteins, and nucleic acids: biotechnology meets materials science. *Angewandte Chemie International Edition*, **2001**, 40.22: 4128-4158.

Oremland, R.S.; Stolz, J.F.; Arsenic, microbes and contaminated aquifers, *Trends Microbiol.*, **2005**, 13, 45–49.

Ouyang, H., Christophersen, M., Viard, R., Miller, B. L., & Fauchet, P. M.. Macroporous silicon microcavities for macromolecule detection. *Advanced Functional Materials*, **2005**, 15, 1851-1859.

Özgür, Ü., Alivov, Y. I., Liu, C., Teke, A., Reshchikov, M. A., Doğan, S., & Morkoçd, H. Applied Physics Reviews. *Journal of Applied Physics*, **2005**, 98, 041301.

Parab H. J., Huang J-H., Lai T-C., Jan Y-H., Liu R-S., Wang J-L., Hsiao M., Chen C-H., Hwu Y-K., Tsai D. P., Chuang S-Y., Pang J-H.S., Biocompatible transferrin-conjugated sodium hexametaphosphate-stabilized gold nanoparticles: synthesis, characterization, cytotoxicity and cellular uptake, *Nanotechnology*, **2011**, 22, 395706

Páez-Espino, D., Tamames, J., de Lorenzo, V., & Cánovas, D. Microbial responses to environmental arsenic. *Biometals*, **2009**, *22*(1), 117-130.

Pengo P., Polizzi S., Battagliarin M., Pasquato L., and Scrimin P., "Synthesis, characterization and properties of water-soluble gold nanoparticles with tunable core size, 2002.," *J. Mater. Chem.,* 13, **2003,** 10, 2471.

Penn, S. G., He, L., & Natan, M. J. (**2003**). Nanoparticles for bioanalysis. *Current opinion in chemical biology, 7*(5), 609-615.

Rea, I., Giardina, P., Longobardi, S., Porro, F., Casuscelli, V., Rendina, I., & De Stefano, L.. Hydrophobin Vmh2–glucose complexes self-assemble in nanometric biofilms. *Journal of The Royal Society Interface, 9,* **2012**, 2450-2456.

Reyes, C.; Lloyd, J.R.;Saltikov, C.W.; Arsenic Contamination of Groundwater: Mechanism, Analysis, and Remediation, John Wiley & Sons Inc., New Jersey, **2008**, 123–146.

Safarik, I., and Safarikova M. "Magnetic nano-and microparticles in biotechnology." *Chemical Papers* 63.5 (**2009**): 497-505.

Sailor, M. J., Porous Silicon in Practice: Preparation, Characterization and Applications, Wiley-VCH Verlag GmbH & Co. KGaA, **2012**.

Sassanfar, M., and Szostak J. W. "An RNA motif that binds ATP." *Nature* **1993**, 364, 550-553.

Sigel, A., H. Sigel, and Sigel, R. K. O.. "Metallothioneins and related chelators. metal ions in life sciences. 5." **2009**, RSC Publishing.

Simard J., Briggs C., Boal A. K., Rotello V. M., "Formation and pH-controlled assembly of amphiphilic gold nanoparticles," *Chem. Commun.*, 19, **2000**, 1943–1944.

Song, C.X., et al., Formulation and characterization of biodegradable nanoparticles for intravascular local drug delivery. *Journal of Controlled Release*, **1997**. 43: p. 197-212.

Song, S., Wang, L., Li, J., Fan, C., & Zhao, J. Aptamer-based biosensors. TrAC *Trends in Analytical Chemistry*, **2008**, 27(2), 108-117.

Spadavecchia J., Apchain E., Albéric M., Fontan E., Reiche I., One-Step Synthesis of Collagen Hybrid Gold Nanoparticles and Formation on Egyptian-like Gold-Plated Archaeological Ivory, *Angew. Chem. Int. Ed.* **2014**, 53, 1756 – 1789.

Sun, C, Han, Q., Wang, D., Xu, W., Wang, W., Zhao, W., & Zhou, M. "A label-free and high sensitive aptamer biosensor based on hyperbranched polyester microspheres for thrombin detection." *Analytica chimica acta* **2014**, 850, 33-40.

Takeuchi, H., Yamamoto, H., & Kawashima, Y.. Mucoadhesive nanoparticulate systems for peptide drug delivery. *Advanced drug delivery reviews, 47,* **2001**, 39-54.

Tian L., Gandra N., Singamaneni S., Monitoring controlled release of payload from gold nanocages using surface enhanced Raman scattering, *ACS Nano*, **2013**, 7, 4252-4260.

Turkevich J., Stevenson P. C., and Hillier J., "A study of the nucleation and growth processes in the synthesis of colloidal gold," *Discuss. Faraday Soc.,* **1951**, 55.

Vayssieres, L. Growth of Arrayed Nanorods and Nanowires of ZnO from Aqueous Solutions. *Adv. Mater.*, **2003**, 15, 464–466.

Walt, D. R., and Agayn V. I.. "The chemistry of enzyme and protein immobilization with glutaraldehyde." *Trends in Analytical Chemistry* **1994**, 13, 425-430.

Whitesides, G. M. The 'right' size in nanobiotechnology. *Nature biotechnology*, **2003**, 21.10: 1161-1165.

Wösten HA. Hydrophobins: multipurpose proteins. *Annu Rev Microbiol.* **2001**, 55, 625-46.

Zampieri F, Wösten HAB, Scholtmeijer K. Creating surface properties using a palette of hydrophobins. *Materials.* **2010**, 3, 4607-25.

Zhang F, Sautter K, Larsen AM , Findley D A, Davis R C, Samah H, Linford M R, Chemical Vapor Deposition of Three Aminosilanes on Silicon Dioxide: Surface Characterization, Stability, Effects of Silane Concentration, and Cyanine Dye Adsorption, *Langmuir* **2010**, 26, 14648–14654

Zheng J., Zhang C., and Dickson R. M., "Highly fluorescent, water-soluble, size-tunable gold quantum dots," *Phys. Rev. Lett.*, 93, **2004**, 5–8.

Zhenhai G., Jianhui J., Ting Z., Daocheng W. J., Preparation of Rhodamine B Fluorescent Poly(methacrylic acid) Coated Gelatin Nanoparticles, *Nanomaterials*, **2011**, 1, 753705

APPENDIX I. Publications, communications, experiences in foreign laboratories, courses and workshop

Scientific Pubblications

J9. **J. Politi**, L. De Stefano, I. Rea, A. M. Gravagnuol4, P. Giardina, C. Methivier,S. Casale, J. Spadavecchia, One-Pot Synthesis of Gold Nanoparticles-Vmh2 Hydrophobin Nanobiocomplex for Glucose Monitoring, Submitted to Nanotechnology

J8. P. Dardano, A. Caliò, **J. Politi**, I. Rea, I. Rendina, Luca De Stefano, Optically monitored drug delivery patch based on porous silicon and polymer microneedles, Accepted paper to Biomedical Optics Express

J7. **J. Politi**, J. Spadavecchia, G. Fiorentino, I. Antonucci, S. Casale, L. De Stefano, Interaction of Thermus thermophilus ArsC enzyme and gold nanoparticles naked-eye assays speciation between As(III) and As(V), *Nanotechnology*, 26 (2015) 435703, doi:10.1088/0957-4484/26/43/435703

J6. **J. Politi**, L. De Stefano, S. Longobardi, P. Giardina, I. Rea, C. Methivier, C. M. Pradier, S. Casale, J. Spadavecchia, The Amphiphilic Hydrophobin Vmh2 Plays a Key Role in One Step Synthesis of Hybrid Protein–Gold Nanoparticles, *Colloids and Surfaces B: Biointerfaces*, 136, 214-221 (2015), doi:10.1016/j.colsurfb.2015.09.021

J5. **J. Politi**, L. De Stefano, S. Casale, J. Spadavecchia, "Original Covalent Approach for Gold Nanorods Immobilization onto Acid-Terminated-Cysteamine Self-Assembled Monolayers for FT-SPR Biosensor Applications." *J Biosens Bioelectron* 6, 167 (2015). doi:10.4172/2155-6210.1000167

J4. **J. Politi**, I. Rea, P. Dardano, L. De Stefano, M. Gioffrè, Versatile Synthesis of ZnO Nanowires for Quantitative Optical Sensing of Molecular Biorecognition, *Sensors and Actuators B: Chemical*, 220, 705-711 (2015), doi:10.1016/j.snb.2015.05.135

J3. **J. Politi**, J. Spadavecchia, M. Iodice, L. De Stefano, Oligopeptide-heavy metal interaction monitoring by hybrid gold nanoparticles based assay, *Analyst*, 140, 149-155 (2015), doi: 10.1039/c4an01491j

J2. M. Terracciano, I. Rea, **J. Politi**, L. De Stefano, Optical characterization of aminosilane-modified silicon dioxide surface for biosensing, *Journal of European Optical Society*, 8, 13075 (2013), doi: 10.2971/jeos.2013.13075

J1. A. Caliò, I. Rea, **J. Politi**, P. Giardina, S. Longobardi and L. De Stefano, Hybrid bio/non-bio interfaces for protein-glucose interaction monitoring, *Journal of Applied Physics*, 114, 134904 (2013), doi: 10.1063/1.4824379

Submitted Scientific Pubblications

- **J. Politi**, I. Rea, F. Nici, P. Dardano, M. Terracciano, G. Oliviero, N. Borbone, G. Piccialli, L. De Stefano, Nanogravimetric and Optical Characterizations of Thrombin Interaction with a Self-assembled Thiolated Aptamer, Submitted to Journal of Sensors

- **J. Politi**, P. Dardano, A. Caliò, M. Iodice, I. Rea, L. De Stefano, Lysine Modified Oligopeptides Allow Reversible Sensing of Lead (II) Ions on Chip, Submitted to Biosensors and Bioelectronics

Proceedings

P9. P. Dardano, A. Caliò, **J. Politi**, V. Di Palma, M. F. Bevilacqua, I. Rea, M. Casalino, A. Di Matteo, I. Rendina, L. De Stefano, "Hybrid microneedles devices for diagnostic and therapeutic applications: fabrication and preliminary results" Proc. SPIE 9518, Bio-MEMS and Medical Microdevices II, 2015; doi:10.1117/12.2178919

P8. A. Calio, A. Cassinese, M. Casalino, **J. Politi**, M. Barra, L. De Stefano, "Hybrid organic-inorganic semiconductor transducer for optical and electrical sensing" SPIE Optics + Optoelectronics, 2015, 95061R-6

P7. **J. Politi,** M. Gioffrè, I. Rea, L. De Stefano, I. Rendina, "Photoluminescence characterization of ZnO nanowires functionalization" SPIE Optics+ Optoelectronics, 2015, 95061Z-7

P6. P. Dardano, A. Calio, **J.Politi,** I. Rea, L. De Stefano,V.Di Palma, M.F. Bevilacqua, A. Di Matteo, "Diagnostic and therapeutic devices based on polymeric microneedles: fabrication and preliminary results", AISEM Annual Conference, 2015 XVIII, 1 - 4doi: 10.1109/AISEM.2015.7066782

P5. **J. Politi**, A. Caliò, P. Dardano, M. Iodice, I. Rea and L. De Stefano, "Bioconjugation of heavy metal-binding proteins on surface: an optical and gravimetric characterization", Procedia Engineering, 2014, 87, 292–295

P4. A. Calio, **J. Politi**, I. Rea, L. De Stefano, "Hydrophobin-glucose interaction monitored by porous silicon optical multi-layers hybrid interfaces for sugar-proteins interaction monitoring"
Photonics Technologies, 2014 Fotonica AEIT Italian Conference on doi: 10.1109/Fotonica.2014.6843956, 2014, 1-4 IEEE CONFERENCE PUBLICATIONS

P3. **J. Politi**, P. Dardano, M. Iodice, I. Rea, L. De Stefano, "Nanostructured photonic biosensor for heavy metal detection. Design and development of porous silicon optical biosensors Photonics Technologies, 2014 Fotonica AEIT Italian Conference on doi: 10.1109/Fotonica.2014.6843953, 2014 , 1 - 3, IEEE CONFERENCE PUBLICATIONS

P2. I. Rea, A. Caliò, M. Terracciano, **J. Politi**, L. De Stefano, I. Rendina, "Porous silicon based photonic structures for optical monitoring of biochemical interactions", Fotonica 2013, AEIT ISBN 9788887237160 (ISBN-A 10.978.8887237/160).

P1. L. De Stefano, A. Caliò, **J. Politi**, P. Giardina, I. Rendina, I. Rea, "Hybrid interfaces for a new class of optical biosensors", Proc. SPIE 8774, Optical Sensors 2013, 87741G (May 3, 2013), doi:10.1117/12.2017615;

Communications at Conferences and Workshops

C38. **J. Politi**, J. Spadavecchia, P. Giardina, I. Rea, M. Terracciano, M. Gioffrè, P. Dardano, L. De Stefano, "Nanostructured Optical Transducers For Biosensing Applications" CNS 2016, 23-25 February 2016, Rome (Italy)

C37. **J.Politi**, P.Dardano, A. Caliò, I.Rea, L.De Stefano, Hybrid polymeric microneedles and porous silicon based device for biosensing and therapeautic applications, NanotechITALY 2015, 25-27 Novembre 2015, Bologna (Italy).

C36. F. Nici, G. Oliviero, **J. Politi**, L. De Stefano, N. Borbone, B. Pinto, S. D'Errico, G. Piccialli, Real time and label free detection of TBA-thrombin interactions using Quartz Crystal Microbalance, Convegno Nazionale della Chimica dei Sistemi Biologici, 24-25 September 2015, Siracusa (Italy).

C35. **J. Politi**, I. Rea, P. Dardano, I. Rendina, F. Nici, G. Oliviero, G. Piccialli, L. De Stefano, Thrombin Recognition by Self-assembledThiolated-TBA: QCM and ellipsometric characterizations, The 6th EOS Topical Meeting on Optical Microsystems (OµS'15), 17-19 September, Capri (NA), Italy.

C34. **J. Politi**, I. Rea, P. Dardano, L. De Stefano, M. Gioffrè, Photoluminescent ZnO Nanowires as quantitative tool for biosensing applications, The 6th EOS Topical Meeting on Optical Microsystems (OµS'15), 17-19 September, Capri (NA), Italy.

C33. A. Caliò, P. Dardano, **J. Politi**, I. Rea, Luca De Stefano, Optically controlled release of biomolecules by porous silicon and microneedle based device: fabrication and characterization, The 6th EOS Topical Meeting on Optical Microsystems (OµS'15), 17-19 September, Capri (NA), Italy.

C32. **J. Politi**, J. Spadavecchia, M. Iodice, G. Fiorentino, P. Giardina, I. Rea and L. De Stefano, Study Of Hybrid Gold Nanoparticles Surface Plasmon Resonance For Quantitative Biomolecular Interaction Monitoring, The 6th EOS Topical Meeting on Optical Microsystems (OµS'15), 17-19 September, Capri (NA), Italy.

C31. P. Dardano, I. Rea, L. De Stefano, A. Caliò, **J. Politi,** "Optically controlled drug delivery system based on Porous Silicon and Microneedles patch" Nanofim 2015, Lecce , Italy, July 24 – 25, 2015

C30. L. De Stefano, M. Terracciano, **J. Politi**, A. Caliò, P. Dardano, M. Casalino, M. Gioffrè, I. Rea, "Synthetic and natural nanostructured materials for innovative optical biosensors " MiNaB-ICT International Workshop on Micro-Nano-Bio-ICT Converge, Otranto (Lecce), Italy, July 13-15, 2015

C29. **J. Politi**, M. Iodice, J. Spadavecchia, I. Rendina, G. Fiorentino, I. Antonucci, L. De Stefano "Heavy metal ions plasmonic detection using hybrid gold nanoparticles-based biosensors" Plasmonica 2015, Padova, Italy, July 1-3, 2015

C28. **J. Politi**, J. Spadavecchia, M. Iodice and L. De Stefano "Hybrid gold nanoparticles modified by oligopeptides for lead (II) ions interaction monitoring" Nanotech France 2015, Parigi, 15-17 June 2015

C27. A. Caliò, A. Cassinese, **J. Politi**, M. Casalino, L. De Stefano "PDIF-CN2 modified porous silicon optical and electrical transducer for biochemical sensing" GS, Parma, 15-17 June 2015

C26. P. Dardano, **J. Politi**, A. Caliò, I. Rea, L. De Stefano "Drugs delivery microneedles patch controlled by porous silicon membrane" GS, Parma, 15-17 June 2015

C25. **J. Politi**, M. Gioffrè, I. Rea, P. Dardano, L. De Stefano "Photoluminescence ZnO NWs as a quantitative sensing tool for molecular biorecognition" GS, Parma, 15-17 June 2015

C24. **J. Politi**, P. Dardano, M. Iodice, A. Caliò, I. Rea, L. De Stefano, "Optical and nanogravimetric characterization of heavy metal-binding proteins bioconjugation for heavy metals detection" E-MRS Spring 2015, Lille, 11 – 15 May 2015

C23. P. Dardano, A. Caliò, **J. Politi**, L. De Stefano, "Microneedles patch for drug delivery applications: fabbrication and characterization" E-MRS Spring 2015, Lille, 11 – 15 May 2015

C22. **J. Politi**, M. Iodice, J. Spadavecchia, G. Fiorentino, I. Antonucci, L. De Stefano "Hybrid Gold Nanoparticles-Based Optical Biosensors for Heavy Metals Detection", Fotonica 2015, Torino, May 6-8 2015

C21. P. Dardano, A. Caliò, L. De Stefano, **J. Politi**, M. Casalino, I. Rendina "Hybrid microneedles devices for diagnostic and therapeutic applications: fabrication and preliminary results" SPIE Microtechnologies, Baercelona, 2-6 May 2015

C20. A. Caliò, A. Cassinese, M. Casalino, **J. Politi**, M. Barra, L. De Stefano, "PDIF-CN2 modified porous silicon optical and electrical transducer for biochemical sensing" SPIE optics+Optoelectronics, Prague, 12-16 April 2015

C19. **J. Politi**, M. Gioffrè, I. Rea, L. De Stefano, I. Rendina "Photoluminescence characterization of ZnO Nanowires functionalization", SPIE optics+Optoelectronics, Prague, 12-16 April 2015

C18. **J. Politi**, L. De Stefano, S. Longobardi, P. Giardina, I. Rea, C. Methivier, C. M. Pradier, J. Spadavecchia, "New synthetic probes for biological applications based on hybrid Hydrophobin/Gold Nanoparticles" Multifunctional, Hybrid and Nanomaterials, Sitges (Spain), 9-13 March 2015.

C17. P. Dardano, A. Caliò, **J. Politi**, V. Di Palma, M. F. Bevilacqua, A. Di Matteo, L. De Stefano, "Diagnostic and therapeutic devices based on polymeric microneedles: fabrication and preliminary results" AISEM, Trento, 3-5 February, 2015.

C16. **J. Politi**, A. Caliò, M. Terracciano, M. Iodice, I. Rea, P. Dardano, M. Gioffrè, L. De Stefano, "Nanostructured transducers as sensing platforms for biomedical applications" Workshop INBB 2014, Roma, 14 November 2014

C15. **J. Politi**, A. Caliò, P. Dardano, M. Iodice, I. Rea and L. De Stefano, "Bioconjugation of heavy metal-binding proteins on surface: an optical and gravimetric characterization" Eurosensors 2014, Brescia 7-10 September 2014.

C14. M. Gioffrè, I.Rea, **J. Politi** and L. De Stefano, "Photoluminescent nanomaterial for optical biosensing" Fotonica 2014, 12-14 May 2014, Naples (Italy);

C13. A. Caliò, **J.Politi**, I. Rea, and L. De Stefano, "Hydrophobin-glucose interaction monitored by porous silicon optical multi-layers" Fotonica 2014, 12-14 May 2014, Naples (Italy);

C12. **J.Politi**, P. Dardano, I. Rea, M. Iodice and L. De Stefano "Nanostructured photonic biosensor for heavy metal detection", Fotonica 2014, 12-14 May 2014, Naples (Italy);

C11. A. Caliò, I. Rea, **J. Politi**, P. Giardina, S. Longobardi and L. De Stefano, "Hydrophobin-glucose interaction monitored by porous silicon optical multi-layers" Porous semiconductors science and technology, 9-14 March 2014, Alicante (Spain);

C10. M. Gioffrè, I. Rea, **J. Politi** and L. De Stefano, "Functionalization of zinc oxide hydrothermal nanowire for optical biosensing" Porous semiconductors science and technology, 9-14 March 2014, Alicante (Spain);

C9. I. Rea, A. Caliò, M. Terracciano, **J. Politi** and L. De Stefano, "Porous silicon based microsystems for optical monitoring of molecular interactions" Aptamers in medicine and perspectives, 4-5 October 2013, Napoli (Italy).

C8. A. Caliò, I. Rea, **J. Politi**, P. Giardina, S. Longobardi and L. De Stefano, "Optical monitoring of proteins-glucose interaction using hybrid bio/non-bio interfaces" Secondo Workshop del Gruppo Biosensori Ottici e Biofotonica, 19-20 September 2013, Sestri Levante (Italy);

C7. A. Caliò, I. Rea, **J. Politi**, P. Giardina, S. Longobardi and L. De Stefano, "Optical monitoring of proteins-glucose interaction using hybrid bio/non-bio interfaces" Optical Microsystems, 12-14 September 2013, Capri (Italy);

C6. M. Terracciano, **J. Politi**, A. Caliò, L. De Stefano, N. Borbone and I. Rea, "Functionalization of porous silicon optical devices for biosensing and drug delivery studies" Nanostructured Materials in Biomedical Applications, 2-5 September 2013, Turku (Finland);

C5. "Silicon and porous silicon-based biosensors by covalent and non-covalent functionalization" **J. Politi**, M. Terracciano, A. Caliò, I. Rea, P. Giardina and L. De Stefano, Nanostructured Materials in Biomedical Applications, 2-5 September 2013, Turku (Finland);

C4. "Porous silicon based photonic structures for optical monitoring of biochemical interactions", I. Rea, A. Caliò, M. Terracciano, **J. Politi**, L. De Stefano, I. Rendina, Photonic 2013, 21-23 May 2013, Milano (Italy);

C3. L. De Stefano, **J. Politi**, A. Caliò, I. Rea, "Hybrid interfaces for a new class of optical biosensors", SPIE Optics and Optoelectronics, 15-18 April 2013, Prague (Czech Republic);

C2. I. Rea, A. Caliò, **J. Politi**, M. Terracciano, L. De Stefano, P. Giardina, "Hybrid bio/non-bio interfaces based on protein-saccharides complexes" Hybrid Materials, 3-7 March 2013 Sorrento (Italy);

C1. I. Rea, A. Caliò, M. Terracciano, **J. Politi**, I. Rendina, L. De Stefano and A. Lamberti, "Porous silicon based biosensors and nanopowders", Hybrid Materials, 3-7 March 2013 Sorrento (Italy);

Book Chapters

B2. L. De Stefano, I. Rea, A.Caliò, **J. Politi**, M. Terracciano, G.Korotcenkov, Porous Silicon-Based Optical Chemical Sensors, Chapter 3, pp 69-94, in Porous Silicon: From Formation to Application: Biomedical and Sensor Applications, Volume Two, Ed. G.Korotcenkov, 2015, ISBN 9781482264562, CRC Press, Taylor & Francis Group, Boca Raton, FL, USA;

B1. **J. Politi**, P. Dardano, M. Iodice, I. Rea, L. De Stefano, Optical Characterization of Heavy Metal-Binding Proteins Bioconjugation on Porous Silicon Devices, Sensors, 319, 2015, 53-58, doi: 10.1007/978-3-319-09617-9_10.

Courses, conferences and seminars

- International Autumn school on "Nanostructured materials for biomedical applicaions" Turku, Finland – 2/5 September 2013
- Seminar about "Quartz crystal microbalance biosensors:results and future perspectives", 21/03/2014
- Seminar about "Fuctionalization of porous materials for transition elements in catalysis application", 07/04/2014

- Seminar about "Spectroscopic approaches to live cell microscopy", 24/07/2014
- "XXVIII Eurosensors" Conference, 7-10/09/2014
- Second School on Optical Biosensors and Biophotonic, 15-20/09/2014
- Corso di Europrogettazione, 15 ore, 7/11/2014
- B2 Level of CEFR certificate, 11/11/2014
- Workshop "Biosensori Innovativi per l'ambiente e la salute" 14/11/2014
- "Luce e Futuro" Conference, 1/12/2014
- Seminar about "Synthesis and optical properties of Silicon nanocrystal for biosensing applications", 17/12/2014
- Fourth International Conference on Multifunctional, Hybrid and Nanomaterials (Hybrid Materials 2015), 9 - 13 March 2015
- Conference "Nanotech France 2015 International Conference", 15-17 June 2015, Paris, France
- Conference EOS Topical Meetings at Capri 2015, 17-19 September 2015, Capri
- Conference "NanoItaly", 21-23 September 2015, Roma
- Seminar about "Engineering electromagnetic fields at the nanoscale", 26/10/2015
- Seminar about "The biological hallmarks of nanomaterials: from behaviour to genes", 01/12/2015

Visiting in Foreign Laboratories

3rd year

8th April 2015 to 8th May 2015 at Laboratory "Chimie, Structures, Propriétés de Biomatériaux et d'Agents Thérapeutiques" (CSPBAT), under the supervision of Dr. Jolanda Spadavecchia.

2nd year

1st April 2014 to 30th June 2014 at Laboratoire de réactivité de surface (LRS)-Sorbonne University, UPMC - University Pierre and Marie, Paris (France), under the supervision of Dr. Jolanda Spadavecchia.

Organized Conferences

- "BIOtecnologie Industriali: UNIone tra uniVERsità e impreSE", BIO-UNIVERSE 2015, January 30th, Università degli studi di Napoli "Federico II", Naples, Italy.

- 6th EOS Topical Meeting on Optical Microsystems (OμS'15), 17-19 September, Capri (NA), Italy.

APPENDIX II. Research article

Versatile synthesis of ZnO nanowires for quantitative optical sensing of molecular biorecognition

Jane Politi [a,b], Ilaria Rea [a], Principia Dardano [a], Luca De Stefano [a,*], Mariano Gioffrè [a]

[a] Institute for Microelectronics and Microsystems, National Research Council, Naples 80127, Italy
[b] Department of Chemical Sciences, University of Naples « Federico II », Naples 80126, Italy

ARTICLE INFO

ABSTRACT

A zinc oxide nanowires (ZnO NWs) forest has been grown by a versatile hydrothermal method on solid supports of very different nature, such as flat crystalline silicon, glass fiber and polymer surface. ZnO NWs shown a characteristic photoluminescence (PL) spectrum that has been used for optical transduction of molecular interactions. In this study, ZnO NWs were chemically modified in order to bind a proper bioprobe for selective protein–protein biorecognition. Techniques such as scanning electron microscopy (SEM), water contact angle (WCA), fluorescence microscopy and Fourier transform infrared (FTIR) spectroscopy were used for characterization of nanostructures bioconjugation, demonstrating that ZnO NWs can be easily and efficiently functionalized. Quantitative and label-free sensing of protein–protein interaction was obtained by monitoring PL emission of ZnO NWs under laser irradiation.

© 2015 Elsevier B.V. All rights reserved.

1. Introduction

Optical transduction, as alternative to electrochemical and amperometric analytical methods, is an attractive technique for biosensing due to high sensitivity and specificity, real-time monitoring, high throughput, and no sample pretreatment. When a molecular probe (i.e. a protein, an enzyme, a DNA strand, and so on) is conjugated to an optical transducer, an optical biosensor is created, adding natural, high selectivity to the other listed features. Optical biosensors could be integrated in small device and used in applications of social interest such as medical diagnostic, therapeutics, health care, monitoring of environmental pollutants, home and defense security [1–3]. Fluorescence is one of the most used signals in optical transduction, even if the labeling of the probe is often a limiting step in biological sensing [4]. Label free optical biosensors can be realized integrating biomolecular probes on a signaling material which directly transduces the molecular recognition into an optical signal without any external manipulation [5].

Zinc Oxide (ZnO) is one of the most interesting transducer materials for chemical and biological sensing applications: it has a very reactive surface; it is biocompatible and very stable from the chemical point of view; it shows an intense photoluminescence (PL) emission at room temperature under laser irradiation [6]. ZnO is a well-known n-type, direct wide-band-gap II–VI semiconductor with a band gap of 3.37 eV and a large excitonic binding energy of 60 meV, which allows an efficient excitonic emission even at room temperature [7,8]. Moreover, ZnO exhibits the richest family of nanostructures (nanoribbons, tetrapods, nanorods and nanowires) among semiconductor oxides and different methods are available in literature of ZnO nano-objects fabrication, including Vapor–Liquid–Solid growth (VLS), Metal Organic Chemical Vapor Deposition (MOCVD), High Pressure Pulsed Laser Deposition (HP-PLD) [9,10]. However, these technologies always require high temperatures, sometimes the presence of a catalyst, and, in general, complex equipments that make very expensive and energy-consuming the production of ZnO nanowires (NWs).

An alternative approach in ZnO NWs production is the hydrothermal synthesis, an aqueous mediated growth of ZnO nanostructures, which presents several advantages with respect to those aforementioned: it requires not very high temperatures (60–95 °C), simple equipment and low cost reagents. The best asset of hydrothermal synthesis is that different morphologies of nano-objects can be obtained on large surfaces, i.e. tenths of centimeters squares, whereas other nanotechnologies are strongly limited in dimensions of the structured surface. Moreover, the hydrothermal method is not dependent on the nature of the support material: it can be indifferently used on different hard surfaces, such as glasses, metals (gold, aluminum, and so on) thick or thin layers, and other semiconductors (silicon, germanium and other

(A) (B) (C) (D)
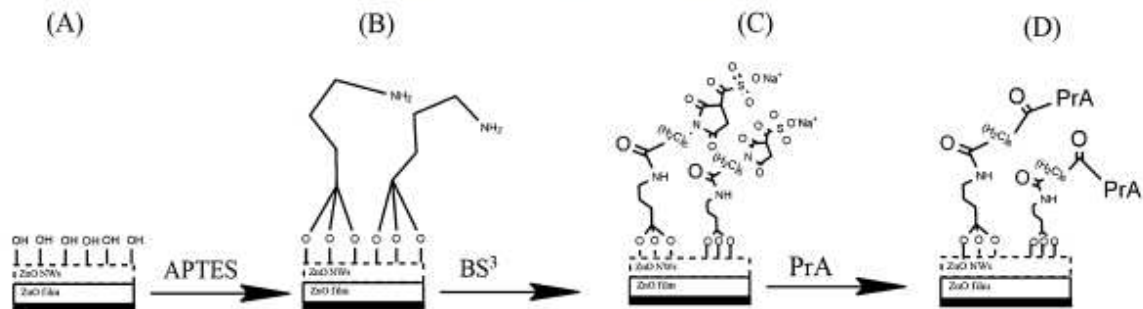
Scheme 1. Schematic representation of ZnO NWs bio-modification: the nanostructured surface of ZnO is highly hydrolyzed (A) and can be silanized by APTES (B). After silanization, the surface exposes ammine groups that bind the cross-linker BS³ (C). The cross-linker is used to bind the protein A (D).

of electronic industry interest); or on soft, flexible substrates, such as plastics or polymers, of any shape, not necessarily planar, but also curved or even more complicate. Changing the process parameters, it is also possible to modulate the NWs order, density and height [11]. Under laser irradiation, the ZnO NWs show a characteristic photoluminescence (PL) spectrum, which presents a very intense near-band-edge ultraviolet peak at about 380 nm, due to free excitonic emission, and one or two broad bands in the visible-near infrared range related to Zn vacancies, interstitial Zn atoms and lattice defects related to O and Zn, i.e. strongly depending on the preparation conditions. The morphological (such as large surface-to-volume ratio) and physico–chemical (biocompatibility and the PL emission) characteristics of ZnO NWs make this material a good candidate for optical biosensing application [12,13].

In this work, we tested the hydrothermal growth process on different substrates: a flat crystalline silicon wafer, the glassy clad of an optical fiber, and a film of Polyethylene Naphthalate (PEN). ZnO NWs grown on crystalline silicon have been characterized by several techniques such as scanning electron microscopy (SEM), Fourier transform infrared (FTIR) spectroscopy, fluorescence microscopy and water contact angle (WCA). The ZnO NWs surface has been functionalized with a biotinylated-protein A and its interaction with different concentrations of Avidin-Horseradish peroxidase (Avidin-HRP) has been label-free monitored by ZnO NWs PL emissions.

2. Materials and methods

2.1. ZnO NWs hydrothermal synthesis

A uniform ZnO seed layer was deposited on different support materials using a radio frequency (RF) magnetron sputtering equipment from a 99.999% pure ceramic ZnO target. The substrate was placed on the substrate holder and the deposition chamber was pumped down to a base pressure of 3×10^{-6} mbar before introducing the process gases (Ar). A 150 nm ZnO thin film was then deposited at room temperature, with 150 W RF power, 2.5×10^{-2} mbar pressure, 40 sccm Ar flux and 30 min deposition time. The solution for hydrothermal process was prepared by dissolving in 200 mL D.I. water an equimolar (0.5 M) solution of alkaline reagent hexamethylenetetramine ($C_6H_{12}N_4$) and the Zn^{2+} salt ($Zn(NO_3)_2$) that act as a precursor. The solution was then heated at 90 °C for 4 h on a P.I.D. controlled hot plate with an immersion thermal sensor and the substrate, with the sputtered ZnO thin film, was immersed upside down. All of the resultant NWs were rinsed with de-ionized water and dried with nitrogen.

2.2. Substrates

The hydrothermal growth method was performed on different substrates with different morphologies to investigate the possibility of using different material like platform for biosensing sensor. In particular we tested a standard optical glass fiber, a plastic film of Polyethylene Naphthalate (PEN) and a silicon wafer. In any case a ZnO seed layer was deposited by sputtering process and the substrate was immersed in the hydrothermal solution.

2.3. ZnO NWs biomodification and biorecognition

Naturally hydrolyzed ZnO NWs (Scheme 1A) grown on silicon were treated with a solution of 5% APTES ((3-aminopropyl)triethoxysilane) (Sigma–Aldrich) in toluene anhydrous for 30 min at room temperature (RT), cured on heater at 100 °C for 10 min. Amino-modified ZnO NWs (Scheme 1B) were then treated by cross-linker BS³ (Bis[sulfosuccinimidyl] suberate) (Thermo Scientific) 1.7 mM in PBS 1X pH 7.4 at 4 °C for 5 h. The sulfo-NHS-terminated samples (Scheme 1C) were then incubated at 4 °C overnight (ON) with FITC-labeled Protein A (Sigma–Aldrich) 48 μM in PBS 1X pH 7.4 for preliminary bioconjugation evaluation (Scheme 1D) by fluorescence microscopy. ZnO NWs as synthesized, and APTES-modified ZnO NWs were ON incubated with FITC-labeled protein A (48 μM in PBS 1X pH 7.4) as control samples against aspecific adsorption. Protein A modified samples have been reacted with biotin (Sigma–Aldrich) 48 μM in PBS 1X pH 7.4 at RT for 1 h. Avidin-HRP (BioLegend) at 8-4-2-1 μg/mL concentrations (PBS 1X pH 7.4 at RT for 1 h) was drop-deposited onto samples for biorecognition monitoring. The process was carried out in triplicate.

2.4. Scanning electron microscopy

The morphology of ZnO NWs, for each substrate, was investigated by scanning electron microscopy (SEM). SEM images have been collected at 5 kV accelerating voltage and 30 μm wide aperture by a Field Emission Scanning Electron Microscope (Carl Zeiss NTS GmbH 1500 Raith FESEM). Secondary emission and in-lens detectors have been used for imaging.

2.5. Fluorescence microscopy

Fluorescence measurements were made by a Leica Z16 APO fluorescence macroscope equipped with a camera Leica DFC300 and I3 filter (450–490 nm band-pass excitation filter plus a 510 nm dichromatic mirror and a 515 nm suppression filter). Fluorescence intensity values reported in the paper are averaged on three independent determinations.
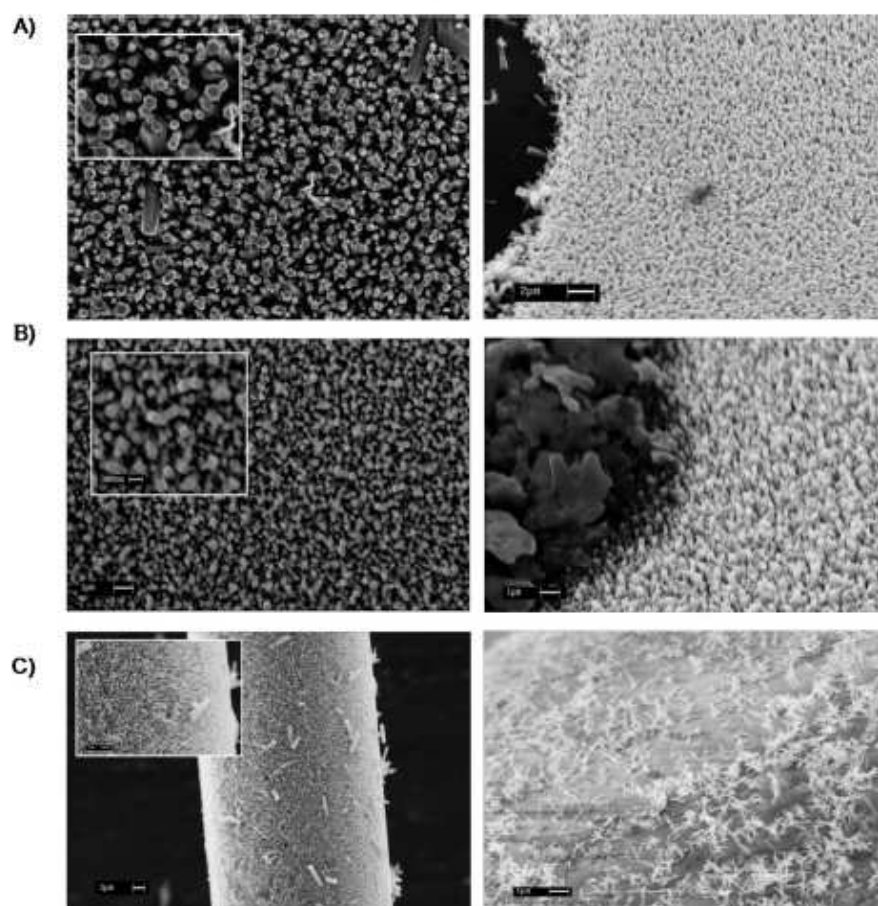
Fig. 1. Scanning electron microscopy (SEM) images of ZnO NWs grown with (left column) and without (right column) ZnO seed layer: flat crystalline silicon wafer (A); plastic film of PEN (B); glassy cladding of optical fiber (C). In left column, insets are magnification of the different surfaces.

2.6. Water contact angle measurements

Sessile drop technique has been used for Water contact angle (WCA) measurements using a First Ten Angstroms FTA 1000 C Class instrument coupled with drop shape analysis software. The WCA values reported are average of three measurements at least.

2.7. Fourier transform infrared spectroscopy

Surface chemical biomodification has been investigated by FTIR spectroscopy. FTIR spectra have been recorded by a Nicolet Continum XL (Thermo Scientific); measurements have been performed in transmission mode. Spectra were collected in air (32 scans per spectrum) in the range of 4000–400 cm^{-1} with a resolution of 2 cm^{-1}.
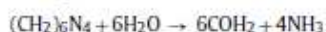
2.8. Steady-state photoluminescence

Steady-state photoluminescence (PL) spectra were excited by a diode-pumped solid-state laser at 325 nm. PL was collected at normal incidence to the surface of samples through a fiber, dispersed in a spectrometer (Princeton Instruments, SpectraPro 300i), and detected using a Peltier cooled charge coupled device (CCD)

camera (PIXIS 100F). A long pass filter (Thorlabs) with a nominal cut-on wavelength of 365 nm was used to remove the laser line at monochromator inlet. Three measures for each sample were collected.

3. Results and discussion

Hydrothermal growth of ZnO NWs consists in hydrolysis of zinc nitrate in presence of an amine [14]. During this process, $ZnO(NO_3)_2$, a water soluble salt, dissociates to form free Zn^{2+} ions and the HTMA hydrolyzes into formaldehyde and ammonia. OH^- ions are supplied from the dissociation of NH_3 into NH_4^+ and OH^-, i.e. the OH^- ions are supplied by the HTMA that acts as a pH buffer. Finally, Zn^{2+} reacts with OH^- to form $Zn(OH)_2$ which leads to $ZnO + H_2O$. The hydrothermal process is summarized by the following reactions:

$$(CH_2)_6N_4 + 6H_2O \rightarrow 6COH_2 + 4NH_3$$

$$NH_3 + H_2O \leftrightarrow NH_4^+ + OH^-$$

$$2OH^- + Zn^{2+} \rightarrow Zn(OH)_2$$

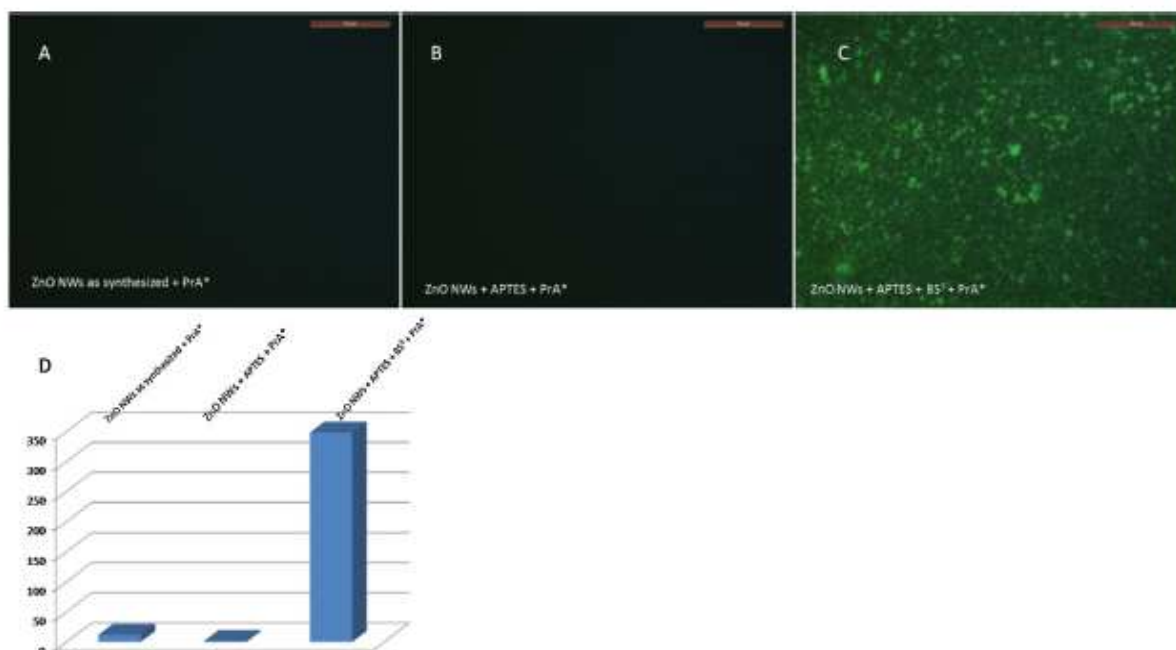$$Zn(OH)_2 \rightarrow ZnO + H_2O$$
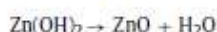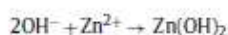
Fig. 2. Fluorescence images of ZnO NWs as synthesized incubated with FITC-labeled protein A (A), ZnO NWs modified by aminosilane and then incubated by FITC-labeled protein A (B) as control samples and ZnO NWs modified by aminosilane, BS³ crosslinker and then incubated by FITC-labeled protein A biomodified (C). Histogram of fluorescence intensity after FITC-labeled protein A incubation (D).

Even if the hydrothermal method is actually a bulk solution, multi-steps reaction, substrate independent, the NW assemblies directly grown on the surfaces of different materials could be very disordered and irregular with poor adhesion. In Fig. 1 SEM images of ZnO NWs grown with (left column) and without (right column) the ZnO seed layer are reported. It can be immediately observed that without the ZnO seed layer the quality of nanostructured surface is unacceptable: in case of flat silicon (Fig. 1A, right) the dark zone is that without seed layer and only residues of ZnO NWs can be seen, whereas the adjacent surface crowded of NWs has been coated by sputtered ZnO. A very similar observation holds for PEN surface: the naked polymer surface is covered by irregular structures, while the sputtered PEN has an ordered forest of NWs on top (Fig. 1B, right). Again, in case of fiber bare glass, the ZnO NWS are sparse on the surface (Fig. 1C, right). It is always true that, during the growth process, there could be a solid phase precipitation of large crystallites in solution due to the exceeding of the minimum critical super saturation concentration of Zn^{2+}. However, most of these crystallites can be removed by rinsing and the few macro-aggregates that rest do not affect the overall NWs density and morphology. From the discussion of these results, it emerges the need of ZnO seed layer by sputtering deposition, if a good quality nanostructured surface is desired: the zinc seed layer promotes the growth of a uniform forest. Among the plethora of thin film deposition techniques, sputtering is one of the most simple and economic one; it only requires a solid target, a neutral gas (i.e. argon) a plasma generation power supply and it works in medium vacuum. Using a sputtered ZnO seed layer, good quality ZnO NWs can be grown practically everywhere [15,16].

In Fig. 1 left column some details of ZnO NWs can be appreciated: the diameter of NWs is around 200 nm and the height is about 1 μm and on all the support surfaces exploited, despite their different nature, the ZnO NWs are quite perpendicular to the plane

and high density of nanostructures can be obtained (Fig. 1A–C, left). Moreover, the adhesion of NWs on the surfaces is strong enough to clean the devices in standard ultrasonic bath (35 kHz, 150 W, for 15 min) since mechanical properties are assured by the ZnO sputtered film. High power sonication could longitudinally break the NWs, thus producing a nanometric powder.

A standard silanization chemistry (see Scheme 1) has been used for ZnO NWs passivation. The aim is to obtain a homogeneous functional surface that covalently binds the crosslinker spacer (BS³) and the bioprobe, which in the case under study is a biotinylated-protein A. Such a biomolecular complex is able to specifically interact with IgG, through protein A, and with avidin, through biotin. In our study, we monitored the interaction between the biotinylated protein A and an avidin-IgG like biomolecule as avidin-HRP, which is commonly used as a second step for detection of biotinylated antibodies by ELISA assay and western blot. Between the pairs avidin–biotin and PrA-HRP, the first one has the strongest specific interaction, i.e. greatest affinity constant, and thus is responsible of results in biomolecular interaction quantitative monitoring. For a first characterization of functionalization process, we used a fluorescein labeled-protein A (PrA*). Fig. 2 reports fluorescence microscopy images (A–C) and counts (D) of differently functionalized ZnO NWs after ON incubation with FITC labeled-protein A. Images showed that only when the complete multistep immobilization procedure is used, the fluorescence emission from PrA* is evident (Fig. 2C), while control samples against aspecific adsorption are completely black (Fig. 2A and B). The functionalization of ZnO surface and the molecular biorecognition experiment have been monitored by FTIR (whole spectra are reported in Fig. S1 of Supporting Information) and WCA measurements as reported in Fig. 3A and B, respectively. Each curve of Fig. 3A shows the following peaks: at 410 cm^{-1} for ZnO stretching vibration, 900–560 cm^{-1} for R_xSiH_x stretching vibration, 1100 cm^{-1} for Si–O

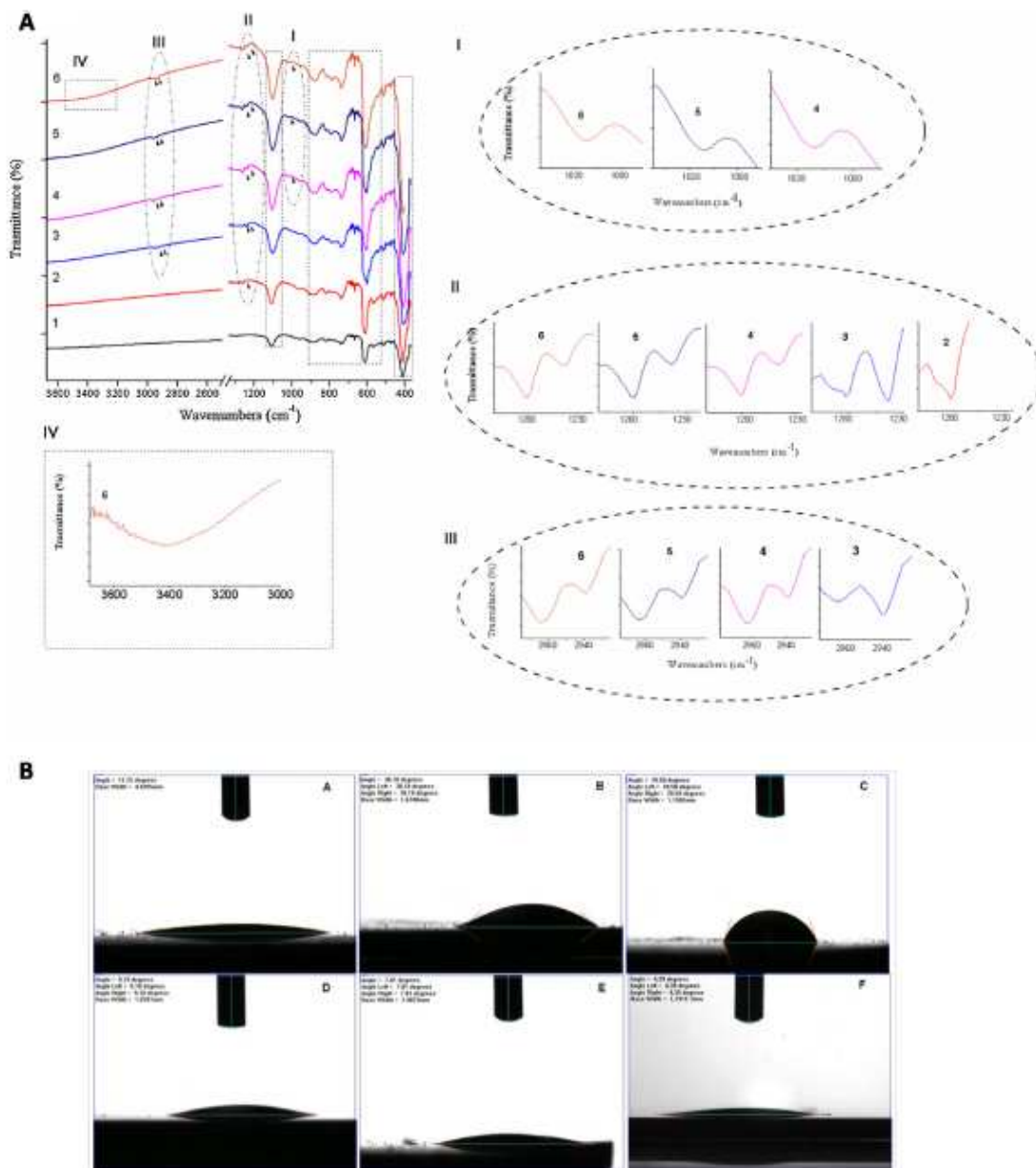**Fig. 3.** (A) FTIR spectra of ZnO NWs after each step of biomodification: after synthesis (1), after amino-silanization (2), after BS³ cross-linker (C), after protein A (4), after biotin (5), after avidin-HRP at 4 μg/mL (6). I–IV are magnification of portion of FTIR spectra, as indicated in (A). (B) Images of wettability changes during biomodification: before biomodification (1), after amino-silanization (2), after BS³ cross-linker (3), after protein A (4), after biotin (5), after avidin-HRP at 0.004 mg/mL (6).

stretching vibration (evidenced by dashed rectangles, well evident in Fig. 3A curve 1) due to hydroxylation and silanization steps. The wettability of ZnO NWs surface before the chemical passivation is very high (see Fig. 3B, image (A)) with a WCA = $10 \pm 4°$, since the surface is almost completely hydrolyzed, as a consequence of the fabrication process. After samples silanization by APTES a peak at $1260\,cm^{-1}$ due to $-CH_2/NH_2$ twisting vibrations (Fig. 3A curve 2) is present and a decrease of surface wettability due to the same residues is evidenced (Fig. 3B image (B), WCA = $43 \pm 5°$). After BS³ immobilization (Fig. 3A curve 3), the FTIR signal highlights peaks at

$1240\,cm^{-1}$ for S=O stretch and peaks at $2932\,cm^{-1}$ and $2940\,cm^{-1}$ for asymmetric stretch and asymmetric vibration of $-CH_2$ groups, respectively, and at $2960\,cm^{-1}$ due to BS³ antisymmetrical and symmetrical stretching of $-CH_3$. Moreover, the hydrophobic portion of BS³ results in a further reduction of surface wettability (Fig. 3B image (C), WCA = $76 \pm 5°$). After protein A immobilization, FTIR spectrum reported in Fig. 3A curve 4 shows peaks at $1014\,cm^{-1}$ due to symmetrical stretches of protein A C—N—C bond and $1260\,cm^{-1}$ due to amide III band of protein A. Fig. 3A curve 5, measured after biotin binding, shows a characteristic
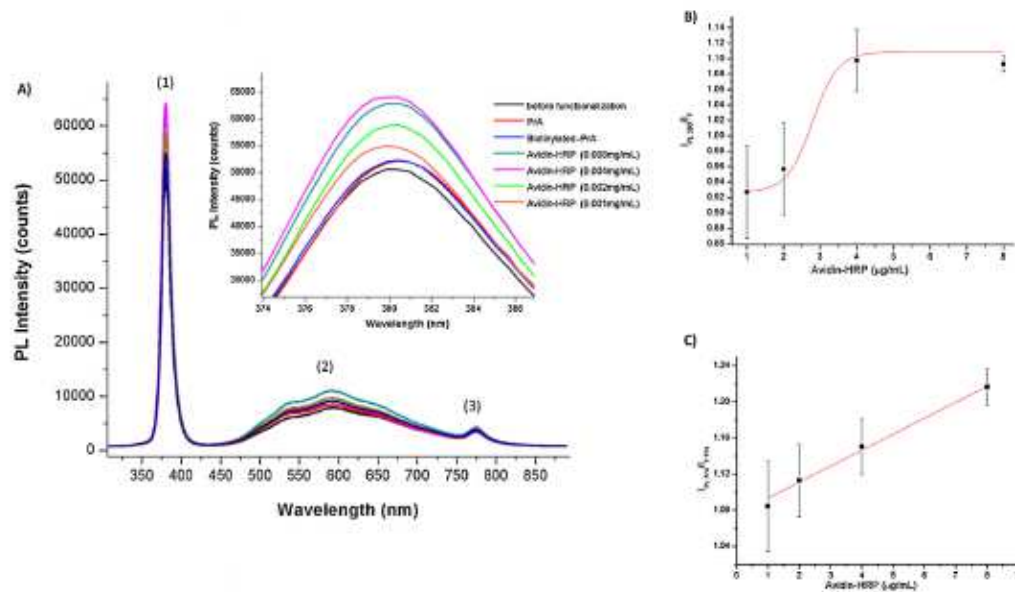
Fig. 4. PL spectra variations of functionalized ZnO NWs after avidin-HRP interaction (A); normalized PL intensity of peak at 380 nm for different concentrations of avidin-HRP (B); normalized PL intensity of peak at 774 nm for different concentrations of avidin-HRP (C).

peak at 1280 cm⁻¹ due to C—O stretching vibrations of carboxylic acids, while Fig. 3A curve 6, registered after avidin-HRP (4 μg/mL) interaction, shows a strong band at 3580–3230 cm⁻¹ due to O—H stretching vibration. The large number of hydrophilic domains, characteristic of protein structures, implies that the surface wettability of ZnO NWs after protein A, biotin and avidin-HRP strongly increased (WCA = 10 ± 5°; 11 ± 4°; 8 ± 4°, respectively) as shown in Fig. 3B images (D)–(F), respectively.

The PL emission of ZnO is highly stable and intense and for these reasons it has been extensively studied for its potential optical applications [16–18]. We have monitored all the functionalization steps of ZnO NWs and the biorecognition between biotinylated-protein A and solutions at different concentrations (8-4-2-1 μg/mL) of avidin-HRP by measuring the PL changes. Fig. 4A shows the PL spectra before any modification, which has been used as reference intensity in normalization calculations, and after interaction with avidin-HRP at different concentrations. In the ZnO NWs PL spectrum the three contributions are due to different physical phenomena: the ultraviolet intense emission at 380 nm is ascribed to near band edge excitonic transitions; while the visible peaks, at 590 nm and 774 nm, to interstitial Zn atoms and oxygen vacancies [19,20]. After biofunctionalization of ZnO NWs surface, the PL emission increases since the molecular complexes can supply extra free electrons which can participate to transitions between surface energy levels available: this phenomenon is the well known adsorption assisted increase of exciton–phonon interaction, which of course is more evident in case of the peak at 380 nm [21]. After the interaction between the bioprobes, the biotin molecules and the avidin-HRP complexes, the PL signals slightly decrease since some electrons are now engaged in the molecular binding between them. It is very interesting to note that the normalized peak intensities, i.e. the ratio between the PL emission of a peak before any modification and the PL intensity recorded for each solutions, have quite different behaviors on exposure to different concentration solutions. The normalized intensities of peaks at 380 nm and 774 nm, as function of avidin-HRP concentration are reported in Fig. 4B and C, respectively. In case of peak at 590 nm, the

plot of the experimental data shows a general tendency to increase when the target concentration rises, but with large fluctuations, probably due to absorption phenomena which are inherently non-linear, and it cannot be usefully fitted (data not shown here).

The experimental data relative to peak at 380 nm (each point is an average of three independent measurements and the errors are the statistical standard deviations) in Fig. 4B were fitted by Origin-Lab Software™ by Eq. (1), which represents a typical dose-response curve (Boltzmann model), i.e. a classic saturation behavior expected when all the available sites for target accommodation are occupied:

$$y = A2 + ((A1 - A2)/(1 + [e]^{\wedge}((x - x0)/dx)))$$ (1)

where $A1$ is an initial value, $A2$ the final value, $x0$ the inflection point and dx is the avidin-HRP concentration constant. The inflection point is useful for evaluation of the affinity [22], which quantifies how strong is the interaction between the biomodified ZnO NWs and the target avidin-HRP. In this case, the $x0$ value is 2.8 ± 0.1 μg/mL per counts.

The data relative to peak 774 nm in Fig. 4C can be fitted, using the proper routine of OriginLab Software™, by a simple linear equation, which, again, it can be used to determine the molecular recognition. The slope of the linear fit, in fact, quantifies the sensitivity of the system, as 18 ± 5 ng/mL per normalized counts, since it represents how the optical response changes as the target concentration changes too. From these measurements, we cannot estimate the resolution and the limit of detection of our optical device, which are both conditioned by the noise of the optical system, and should both be measured at very low concentration of the target analyte. The different curves obtained depend on how the electronic properties, in particular energy levels distribution and surface bands bending, of the biomodified ZnO NWs are sensible to biomolecular interactions. Even if a detailed study of these phenomena is beyond the scope of the present paper, it is important to note that these results confirm that the synthesized ZnO NWs forest is a quite sensitive, robust and versatile optical transducer.

4. Conclusion

In this work, we have characterized by optical, label free techniques the interaction between biomodified ZnO NWs, obtained by hydrothermal process, and avidin-HRP. The ZnO nanostructuration was studied by scanning electron microscopy and the biomodification was extensively characterized by fluorescence microscopy, Fourier transform infrared spectroscopy and wettability change evaluation. Finally, photoluminescence of ZnO NWs was used in monitoring the biomolecular recognition of avidin-HRP at different concentrations. The results show that the photoluminescence intensity is very sensitive to target concentration changes. A simple normalization of the emission peaks provided a quantitative monitoring of the biomolecular interaction, revealing an affinity constant in the range of µg/mL per counts and sensitivity in the range of tenths of ng/mL per counts, at least for wavelengths at 380 nm and 774 nm. These results, which are representative of a proof-of-concept device, open an alternative route in development of a useful optical device for label-free bio-medical diagnostic and environmental monitoring based on ZnO NWs.

Appendix A. Supplementary data

Supplementary data associated with this article can be found, in the online version, at http://dx.doi.org/10.1016/j.snb.2015.05.135

References

[1] F.S. Ligler, C.A. Rowe Taitt (Eds.), Optical Biosensors, Elsevier, Amsterdam, The Netherlands, 2004.
[2] A. Heitzer, K. Malachowsky, J.E. Thonnard, P.R. Bienkowski, D.C. White, G.S. Sayler, Optical biosensor for environmental on-line monitoring of naphthalene and salicylate bioavailability with an immobilized bioluminescent catabolic reporter bacterium, Appl. Environ. Microbiol. 60 (5) (1994) 1487–1494.
[3] D. Frense, A. Muller, D. Beckmann, Detection of environmental pollutants using optical biosensor with immobilized algae cells, Sens. Actuators B: Chem. 51 (1998) 256–260.
[4] S.S. Saliterman, Fundamentals of BioMEMS and Medical Microdevices, Wiley-Interscience, SPIE PRESS, Bellingham, WA, USA, 2006.
[5] L. De Stefano, P. Arcari, A. Lamberti, C. Sanges, L. Rotiroti, I. Rea, I. Rendina, DNA optical detection based on porous silicon technology: from biosensors to biochips, Sensors 7 (2007) 214–221.
[6] S.A. Kumar, S.M. Chen, Nanostructured zinc oxide particles in chemically modified electrodes for biosensor applications, Anal. Lett. 41 (2008) 141–158.
[7] W.I. Park, Y.H. Jun, S.W. Jung, Y. Gyu-Chul, Excitonic emissions observed in ZnO single crystal nanorods, Appl. Phys. Lett. 82 (2003) 6.
[8] KongY.C. Yu, D.P. Zhang, B. Fang, W.S.Q. Feng, Ultraviolet-emitting ZnO nanowires synthesized by a physical vapor deposition approach, Appl. Phys. Lett. 78 (2001) 407.
[9] T. Okada, B.H. Agung, Y. Nakata, ZnO nano-rods synthesized by nano-particle-assisted pulsed-laser deposition, Appl. Phys. A 79 (4–6) (2004) 1417–1419.
[10] W.I. Park, G.C. Yi, M. Kim, S.J. Pennycook, ZnO nanoneedles grown vertically on Si substrates by non-catalytic vapor-phase epitaxy, Adv. Mater. 14 (2002) 1841–1843.
[11] C.H. Liu, J.A. Zapien, Y. Yao, X.M. Meng, C.S. Lee, S.S. Fan, Y. Lifshitz, S.T. Lee, High-density, ordered ultraviolet light-emitting ZnO nanowire arrays, Adv. Mater. 15 (2003) 838.
[12] T. Kong, Y. Chen, Y. Ye, K. Zhang, Z. Wang, X. Wang, An amperometric glucose biosensor based on the immobilization of glucose oxidase on the ZnO nanotubes, Sens. Actuators B: Chem. 138 (2009) 344–350.
[13] A. Choi, K. Kim, H.-I. Jung, S.Y. Lee, ZnO nanowire biosensors for detection of biomolecular interactions in enhancement mode, Sens. Actuators B: Chem. 148 (2) (2010) 577–582.
[14] Y. Sun, N.G. Ndifor-Angwafor, D.J. Riley, M.N.R. Ashfold, Synthesis and photoluminescence of ultrathin ZnO nanowire/nanotube arrays formed by hydrothermal growth, Chem. Phys. Lett. 431 (2006) 352–357.
[15] L.E. Greene, M. Law, J. Goldberger, F. Kim, J.C. Johnson, Y. Zhang, R.J. Saykally, P. Yang, Low-temperature wafer-scale production of ZnO nanowire arrays, Angew. Chem. Int. Ed. 42 (2003) 3031–3034.
[16] Y.Q. Chang, D.B. Wang, X.H. Luo, X.Y. Xu, X.H. Chen, L. Li, C.P. Chen, R.M. Wang, J. Xu, D.P. Yu, Synthesis, optical, and magnetic properties of diluted magnetic semiconductor Zn1-xMnxO nanowires via vapor phase growth, Appl. Phys. Lett 83 (2003) 4020–4022.
[17] P. Yang, H. Yan, S. Mao, R. Russo, J. Johnson, R. Saykally, N. Morris, J. Pham, R. He, H.-J. Choi, Controlled growth of ZnO nanowires and their optical properties, Adv. Funct. Mater. 12 (5) (2002) 303–305.
[18] C.H. Liu, J.A. Zapien, Y. Yao, X.M. Meng, C.S. Lee, S.S. Fan, Y. Lifshitz, S.T. Lee, High-Density, Ordered ultraviolet light-emitting ZnO nanowire arrays, Adv. Mater. 15 (2003) 838–841.
[19] S.C. Lyu, Y. Zhang, H. Ruh, H.-J. Lee, H.-W. Shim, E.-K. Suh, C.J. Lee, Low temperature growth and photoluminescence of well-aligned zinc oxide nanowires, Chem. Phys. Lett. 363 (2002) 134–138.
[20] I. Shalish, H. Temkin, V. Narayanamurti, Size-dependent surface luminescence in ZnO nanowires, Phys. Rev. B 69 (2004) 245401.
[21] H.-C. Hsu, Y.-K. Tseng, H.-M. Cheng, J.-H. Kuo, W.-F. Hsieh, Selective growth of ZnO nanorods on pre-coated ZnO buffer layer, J. Cryst. Grow. 261 (2004) 520–525.
[22] J. Politi, J. Spadavecchia, M. Iodice, L. De Stefano, Oligopeptide–heavy metal interaction monitoring by hybrid gold nanoparticle based assay, Analyst 140 (2015) 149–155.

Biographies

Jane Politi is graduated (106/110) in 2011 in Pharmaceutical Chemistry and Technology at University of Calabria. Now, she is a Ph.D. student in Molecular and Industrial Biotechnologies at University of Naples "Federico II" working on functionalization of nanostructured materials for biomedical and environmental applications. She published three papers on peer reviewed journals, and presented her work at more than 10 international conferences.

Ilaria Rea graduated in physics at "Federico II" University of Naples in July 2003. She worked in ENEA, Portici Research Center, Italy, on porous silicon based sensors up to December 2004. In 2005 she worked at Institute for Microelectronics and Microsystems of National Council of Research in Naples. Her activity was the design and the realization of resonant optical microstructures based on porous silicon. These structures, used as all optical sensor devices, have given very interesting results both in the quantitative determinations of toxic and harmful volatile substances and in DNA and proteins recognition. In 2008 she got the PhD degree at "Federico II" University of Naples defending a thesis on "Porous silicon based optical devices for biochemical sensing". At the present time she is a researcher at Institute for Microelectronics and Microsystems in Naples. Her current research interests are in the fields of silicon optoelectronics and optical sensors. She is reviewer for some international scientific journals. She is author or co-author of more than 50 scientific papers published on international journals and conference proceedings.

Principia Dardano is responsible for the design, fabrication and optical characterization of optoelectronic silicon devices. She graduated in Physics at the University of Studies of Naples "Federico II" in March 2004 and received his Ph.D. in Fundamental and Applied Physics at the same university in January 2008, with thesis on negative refractive index 2D photonic crystals in silicon. Since December 2004 she has worked at the Institute for Microelectronics and Microsystems (IMM-CNR) in Naples, where she is the head of the laboratory of electron beam lithography since February 2006. She is the author and co-author of about 30 publications in international journals

Luca De Stefano graduated cum laude in Physics at University of Naples "Federico II" in 1992 and received the Ph.D. in Physics in 1996. He is senior scientist at the Institute for Microelectronic and Microsystems of National Research Council in Naples, where he heads a small research group in the fields of biophotonics and optical microsystems for biochemical sensing. He presented his work to more than 170 national and international conferences, many of which he has been invited to. He is author or co-author of more than 115 scientific articles published on peer reviewed journals, more than 70 conference proceedings, and eight books. He holds one European patent, and eight Italian patents. He is reviewer for many high impact factors scientific journals.

Mariano Gioffrè received the M.Sc. degree and the Ph.D. degree in Electronic Engineering from the University "Mediterranea" of Reggio Calabria in 2003 and 2006, respectively. In December 2006 he obtained a fellowship at the Institute of Microelectronic and Microsystems of National Council of Research (IMM-CNR) and, from December 2011, he works as researcher, permanent position. His research activity concerns the deposition and characterization of thin films obtained by PVD and CVD technologies. He has a remarkable experience in the basic technologies for microelectronic application like lithography, thermal oxidation of silicon, wet and dry etching.

AKNOWLEDGMENTS